

# **Non-invasive monitoring of key hemodynamical and cardiac parameters using physics-based modelling and artificial intelligence**

THIS IS A TEMPORARY TITLE PAGE  
It will be replaced for the final print by a version  
provided by the registrar's office.

Thèse n. 1234 2021  
présentée le 3 novembre 2021  
à la Faculté des sciences et techniques de l'ingénieur  
laboratoire d'hémodynamique et de technologie cardiovasculaire  
programme doctoral en Biotechnologie et génie biologique  
École polytechnique fédérale de Lausanne  
pour l'obtention du grade de Docteur ès Sciences  
par



**Vasiliki BIKIA**

acceptée sur proposition du jury :

Prof. Stéphanie Lacour, président du jury  
Prof. Nikolaos Stergiopoulos, directeur de thèse  
Prof. Leontios Hadjileontiadis, rapporteur  
Prof. Patrick Segers, rapporteur  
Dr. Jean-Marc Vesin, rapporteur

Lausanne, EPFL, 2021

---

---

"All our knowledge begins with the senses, proceeds then to the understanding, and ends with reason. There is nothing higher than reason."

— Immanuel Kant (1724-1804)

"La souffrance physique on la subit, la souffrance morale on la choisit."

— Éric-Emmanuel Schmitt, *Oscar et la dame rose* (2002)

"Παιδεία ευτυχούσι μεν εστί κόσμος, ατυχούσι δε καταφύγιον."

— Ισοκράτης (436-338 π.Χ.)

This thesis is dedicated to

*Miltos, Mary, Thomas, and Philippos.*

---

## Acknowledgements

I am grateful to many people who have supported and encouraged me in several ways throughout this work.

Firstly, I would like to express my sincere gratitude to my supervisor, Professor Nikolaos Stergiopoulos, for the opportunity to pursue a Ph.D. in his laboratory and for constantly providing valuable advice. Most importantly, thank you for your trust and for a wonderful collaboration over the years.

Next, I would like to thank the members of the jury committee: Professor Leontios Hadjileontiadis who was the first to introduce me to biomedical engineering, through the example of his own determination and leadership - I learnt so much from you; Professor Patrick Segers for always generously sharing his valuable insights and expertise; and Dr. Jean-Marc Vesin for following and supporting my research path from the very beginning.

I would also like to thank Professor Theodore Papaioannou for vigorously supporting my research and for sharing his sharp view on the clinical implications of our work.

To my beloved labmates: Adan, Bram, Sylvia, Rodrigo, Matina, Maiia, Lydia, George, Seb, Constantinos, Augusto, Stéphane, Fabiana, Mauro, Stefanie, Natália, Valeria, Pedro, Allancer, a heartfelt thank you for creating an enjoyable and positive ambiance inside and outside of the lab. A special thanks to Adan for his advice and for offering me my first adventurous and fun ski excursions on the Swiss Alps, to Bram for his valuable professional and personal advice during our endless bus trips in the depths of Ireland (and not only), and to Sylvia for her constant availability and support in administrative matters. I would also like to thank my students: Marie, Thibaut, Emma, Julian, Marija, Méline, Deborah, and Mary-Lou, for their genuine motivation, contribution, and hard work.

I am grateful to my friends who have been a great support throughout the years. Αθηνά, Νατάσα, Κωνσταντίνε, Δημήτρη, Δέσποινα, thank you for your friendship and for always being beside me in both my happiest and most challenging moments. Η φίλια δε γνωρίζει από αποστάσεις. Moreover, I'm very fortunate for the friends I made along this journey. Some honorable mentions to Έλενα, Ειρήνη, Lorenzo, Elena, Charlotte, Wissem: thank you for all

## Acknowledgements

---

the laughs, excursions, and unforgettable moments we shared together, and for the moments that will come in the future. You have made Lausanne feel like home, and nothing would have been the same without you.

A sincere thank you to Σωτήρης for his unwavering love and for constantly supporting me with valuable remarks and all his might along this long pathway. This work would not have been possible without you.

Finally, I would like to express my deepest gratitude to my parents, Μίλτο and Μαίρη, for teaching me the value of knowledge and contribution, and for always encouraging me to aim for the moon - "*we aim above the mark to hit the mark*"; and, certainly, to my loving brothers, Θωμά and Φίλιππο-Άγγελο, for supporting me every day with their unconditional love, brilliant ideas, reason, and affection. Σας ευχαριστώ για όλα!

Vasiliki Bikia

*Lausanne, November 3, 2021*

## Abstract

In a progressively aging population, it is of utmost importance to develop reliable, non-invasive, and cost-effective tools to estimate biomarkers that can be indicative of cardiovascular risk. Clinical parameters directly measured in the heart or the aorta are crucial for the diagnosis and management of disease. However, their clinical use is severely hampered by their invasive nature, cost, or need for special equipment. Aortic systolic blood pressure (aSBP), cardiac output (CO), end-systolic elastance ( $E_{es}$ ), and arterial stiffness provide valuable information about the cardiovascular state in humans, and are strongly associated with clinical outcomes. This thesis presents original predictive algorithms suitable for estimating such cardiovascular biomarkers from commonly measured non-invasive clinical data.

The first aim of this thesis is to develop and validate methods to estimate central hemodynamics, such as aSBP and CO. Firstly, a novel inverse problem-solving method is introduced to estimate aSBP and CO from non-invasive measurements of cuff pressure and carotid-femoral pulse wave velocity (cfPWV). The method relies on the adjustment of a previously validated one-dimensional arterial tree model. Assessment of the accuracy is achieved by implementing the algorithm, initially, on a small cohort ( $n = 20$ ), and, thereafter, using a large cohort with a wide range of age groups from the Anglo-Cardiff Collaborative Trial ( $n = 144$ ). The second approach involves the machine learning-based estimation of aSBP and CO using again cuff pressure and cfPWV. Validation of the method on *in silico* data shows that machine learning offers a greatly accurate alternative for monitoring aSBP and CO. Moreover, transfer learning allows for evaluating the performance of the aSBP estimator *in vivo*, with results showing satisfactory agreement between the predicted and the reference data.

The second objective of this thesis entails the development and validation of a gamut of different machine learning frameworks for the non-invasive prediction of  $E_{es}$ . First, a machine learning model is trained and tested using as inputs cuff pressure and cfPWV. The importance of incorporating ejection fraction (EF) as additional input for estimating  $E_{es}$  is also assessed. Results indicate that  $E_{es}$  cannot be predicted from pressure-based data alone. The addition of the EF information greatly improves the estimated  $E_{es}$ . Alternatively, we propose a novel artificial intelligence-based approach to estimate  $E_{es}$  using the information embedded in clinically relevant systolic time intervals. A training/testing scheme is developed using virtual subjects ( $n = 4,645$ ) from a previously validated *in silico* model. The evaluation provides

## Abstract

---

very promising results which permit to deduce that this approach constitutes a step towards the development of an easy and clinically applicable method for assessing left ventricular systolic function. Furthermore, this work aims to provide evidence on the potential in using the morphology of the brachial blood pressure waveform and convolution neural networks for predicting  $E_{es}$  using 3,748 in silico subjects. The arterial blood pressure wave appears to be a promising source of information for assessing  $E_{es}$ . Predictions are found to be in good agreement with the reference  $E_{es}$  values over an extensive range of left ventricular contractility values and loading conditions.

The third objective is to improve in vivo assessment of aortic characteristic impedance ( $Z_{ao}$ ) and total arterial compliance ( $C_T$ ). Given that regional PWV measurements are non-invasive and clinically available, we present a non-invasive method for estimating  $Z_{ao}$  and  $C_T$  using cuff pressure, cfPWV, and carotid-radial PWV via regression analysis. In silico validation using 3,818 subjects yields high accuracy for both  $Z_{ao}$  and  $C_T$  estimators, verifying that the method may offer a valuable tool for assessing arterial stiffness, while reducing the cost and the complexity of the existing techniques.

As a step forward, we introduce a non-invasive method to estimate  $C_T$  from a single carotid waveform using artificial neural networks. The proposed methodology is appraised using the large human cohort ( $n = 2,256$ ) of the Asklepios study. Precise estimates of  $C_T$  are yielded, indicating that such an approach could offer promising applications, ranging from fast and cost-efficient hemodynamical monitoring by the physician to integration in wearable technologies.

Finally, in view of the conflicting clinical and experimental evidence regarding the influence of heart rate (HR) on arterial stiffness and its surrogate marker cfPWV, the last stride of this research is to evaluate and quantify the effect of HR on cfPWV measurement under controlled hemodynamic conditions, and especially with respect to blood pressure (BP) that is a strong determinant of arterial stiffness. The findings conclude that large variations of HR may have a clinically significant impact on cfPWV, and correction of PWV measurement with respect to BP may be considered.

In conclusion, this dissertation shows that physics-based modelling and machine learning are valuable for developing and validating novel, non-invasive health monitoring algorithms. The high performance of the proposed algorithms for predicting hemodynamical and cardiac parameters from routinely collected non-invasive data suggests that it is feasible to improve the current state of the art of monitoring tools for cardiovascular events, while reducing complexity and cost.

Keywords: non-invasive monitoring, central hemodynamics, cardiac contractility, aortic pres-



sure, cardiac output, end-systolic elastance, arterial compliance, aortic impedance, pulse wave velocity, computational modelling, predictive modelling, inverse problem-solving, machine learning, regression analysis, artificial neural networks, random forests, gradient boosting



## Résumé

Dans une société avec une population vieillissante, il est primordial de développer des outils fiables, non-invasifs et rentables afin d'identifier les biomarqueurs révélateurs d'un risque cardiovasculaire. Les paramètres cliniques mesurés directement dans le cœur ou l'aorte sont cruciaux pour le diagnostic et la gestion de la maladie. Cependant, leur utilisation clinique est gravement entravée par leur nature invasive, leur coût ou la nécessité d'un équipement spécial. La pression artérielle systolique aortique (aSBP), le débit cardiaque (CO), l'élastance télésystolique ( $E_{es}$ ) et les indices de rigidité artérielle fournissent des informations précieuses sur l'état cardiovasculaire du sujet, et sont fortement corrélés aux résultats cliniques. Cette thèse propose des algorithmes prédictifs originaux afin d'estimer ces biomarqueurs cardiovasculaires tout en utilisant des données cliniques non-invasives simples.

Le premier objectif de cette thèse est de développer et de valider des méthodes pour estimer l'hémodynamique centrale, telles que la aSBP et le CO. Dans ce but, une nouvelle méthode de résolution de problèmes inverses est introduite afin d'estimer la aSBP et le CO à partir de mesures non-invasives comme la pression du brassard et la vitesse d'onde de pouls carotide-fémorale (cfPWV). La méthode repose sur l'ajustement d'un modèle d'arbre artériel unidimensionnel préalablement validé. L'évaluation de l'exactitude est réalisée en mettant en œuvre l'algorithme, initialement sur une petite cohorte ( $n = 20$ ), et, par la suite, en utilisant une grande cohorte comprenant divers groupes d'âge provenant de l'essai collaboratif Anglo-Cardiff ( $n = 144$ ). La deuxième approche implique l'estimation basée sur l'apprentissage automatique de l'aSBP et du CO en utilisant à nouveau la pression du brassard et le cfPWV. La validation de la méthode sur des données *in silico* montre que l'apprentissage automatique offre une alternative très précise pour la surveillance des aSBP et CO. L'apprentissage par transfert (transfer learning) permet d'évaluer les performances de l'aSBP *in vivo*, avec des résultats significatifs démontrant la vraisemblance entre les données prédites et les données de référence.

Le second objectif est le développement et la validation d'une gamme de différents cadres d'apprentissage automatique pour la prédiction non-invasive de  $E_{es}$ . Pour cela, un modèle d'apprentissage automatique est formé et testé en utilisant comme entrées la pression du brassard et le cfPWV. L'importance d'incorporer la fraction d'éjection (EF) comme entrée supplémentaire pour estimer  $E_{es}$  est également évaluée. Les résultats indiquent que  $E_{es}$  ne peut

pas être prédit à partir des seules données basées sur des données liées à la pression. L'ajout de l'information EF grandement améliore la  $E_{es}$  estimé. Alternativement, une nouvelle approche basée sur l'intelligence artificielle pour estimer  $E_{es}$  en utilisant les informations intégrées dans des intervalles de temps systoliques cliniquement pertinents est proposée. Un schéma d'entraînement/test est développé en utilisant des sujets virtuels ( $n = 4,645$ ) à partir d'un modèle précédemment validé *in silico*. Cette évaluation fournit des résultats très encourageants permettant de déduire que cette approche est une première étape vers le développement d'une méthode facile et cliniquement applicable pour évaluer la fonction systolique ventriculaire gauche. Enfin, ce travail fournit des preuves du potentiel de l'utilisation de la morphologie de l'onde de la pression artérielle brachiale et des réseaux neuronaux à convolution pour prédire  $E_{es}$  en utilisant 3,748 sujets *in silico*. En effet, l'onde de pression artérielle apparaît comme une source d'information prometteuse pour évaluer  $E_{es}$ . Les prédictions faites se sont avérées proches des valeurs de référence  $E_{es}$  sur une large gamme de valeurs de contractilité ventriculaire gauche et de conditions de charge.

Le troisième objectif est d'améliorer l'évaluation *in vivo* de l'impédance caractéristique aortique ( $Z_{ao}$ ) et de la compliance artérielle totale ( $C_T$ ). Étant donné que les mesures régionales de la PWV sont non-invasives et disponibles en clinique, nous présentons une méthode non-invasive pour estimer  $Z_{ao}$  et  $C_T$  en utilisant la pression du brassard, la cfPWV et la PWV carotide-radiale via une analyse de régression. La validation *in silico* utilisant 3,818 sujets donne une grande précision pour les estimateurs  $Z_{ao}$  et  $C_T$ , démontrant que la méthode peut offrir un outil précieux pour évaluer la rigidité artérielle tout en réduisant le coût et la complexité des techniques existantes.

En outre, nous introduisons une méthode non-invasive pour estimer  $C_T$  à partir d'une seule signal d'onde de la pression artérielle carotidienne en utilisant des réseaux de neurones artificiels. La méthodologie proposée est évaluée en utilisant la grande cohorte ( $n = 2,256$ ) de l'étude Asklepios. Des estimations précises de  $C_T$  sont produites indiquant qu'une telle approche peut être applicable à de nombreuses fins allant de la surveillance hémodynamique rapide et rentable par le médecin jusqu'à son intégration dans des technologies portables.

Finalement, compte tenu des preuves cliniques et expérimentales contradictoires concernant l'influence de la HR sur la rigidité artérielle et de son marqueur de substitution cfPWV, la dernière étape de cette recherche est d'évaluer l'effet de la HR sur la mesure de la cfPWV dans des conditions hémodynamiques contrôlées, et en particulier, en ce qui concerne la pression artérielle, déterminante pour l'évaluation de la rigidité artérielle. Les résultats concluent que de grandes variations de la fréquence cardiaque peuvent avoir un impact cliniquement significatif sur la cfPWV, et une correction de la mesure de la PWV par rapport à la pression artérielle doit probablement être envisagée.

En conclusion, cette thèse démontre que la modélisation basée sur la physique et l'apprentissage automatique peuvent servir à développer et valider de nouveaux algorithmes à des fins de surveillance non-invasives de la santé. Les performances des algorithmes pour prédire les paramètres hémodynamiques et cardiaques, à partir de données non-invasives collectées périodiquement, suggèrent qu'il est possible d'améliorer l'état de l'art actuel des outils de surveillance des événements cardiovasculaires tout en réduisant leur complexité et leur coût.

Mots clés : surveillance non-invasive, hémodynamique centrale, contractilité cardiaque, pression aortique, débit cardiaque, élastance télésystolique, compliance artérielle, impédance aortique, vitesse de l'onde de pouls, modélisation informatique, modélisation prédictive, résolution de problèmes inverse, apprentissage automatique, analyse de régression, réseaux de neurones artificiels, forêt d'arbres décisionnels, gradient boosting



## Περίληψη

Σε έναν προοδευτικά γηράσκοντα πληθυσμό, η ανάπτυξη αξιόπιστων, μη επεμβατικών και οικονομικά προσιτών εργαλείων για την εκτίμηση βιοδεικτών του καρδιαγγειακού κινδύνου είναι υψίστης σημασίας. Συγκεκριμένα, μελέτες έχουν δείξει πως οι κλινικές παράμετροι που μετρώνται απευθείας στην καρδιά ή την αορτή συμβάλλουν εξαιρετικά στην αποτελεσματικότερη διάγνωση και διαχείριση της καρδιαγγειακής νόσου. Ωστόσο, η κλινική υιοθέτηση των παραμέτρων αυτών υποβαθμίζεται σημαντικά εξαιτίας της παρεμβατικής τους φύσης, του κόστους ή της ανάγκης για ακριβό και εξειδικευμένο εξοπλισμό. Η αορτική συστολική αρτηριακή πίεση (aSBP), η καρδιακή παροχή (CO), η τελική συστολική ελαστικότητα ( $E_{es}$ ) και οι δείκτες αρτηριακής δυσκαμψίας παρέχουν πολύτιμες πληροφορίες σχετικά με την κατάσταση του καρδιαγγειακού συστήματος στον άνθρωπο, ενώ συνδέονται ισχυρά με κλινικά περιστατικά. Η παρούσα διδακτορική διατριβή προτείνει πρωτότυπους προγνωστικούς αλγόριθμους κατάλληλους για την εκτίμηση τέτοιων καρδιαγγειακών βιοδεικτών χρησιμοποιώντας ευρέως διαθέσιμα δεδομένα τα οποία μπορούν να συλλεχθούν με εύκολο και μη επεμβατικό τρόπο στο κλινικό περιβάλλον.

Ο πρώτος στόχος της παρούσας εργασίας είναι η ανάπτυξη και επικύρωση μεθόδων για την εκτίμηση κεντρικών αιμοδυναμικών παραμέτρων, και συγκεκριμένα, της aSBP και της CO. Καταρχάς, παρουσιάζουμε μια καινοτόμα μέθοδο αντίστροφης επίλυσης προβλημάτων με σκοπό την εκτίμηση της aSBP και της CO από μη επεμβατικές μετρήσεις πίεσης μανσέτας και ταχύτητας παλμικού κύματος (cfPWV). Ειδικότερα, η μέθοδος βασίζεται στην προσαρμογή ενός προηγουμένως επικυρωμένου μονοδιάστατου μοντέλου αρτηριακού δέντρου. Η αξιολόγηση της ακρίβειας της μεθόδου πραγματοποιείται με την εφαρμογή του αλγορίθμου, αρχικά, σε μια μικρή ομάδα ενήλικων εθελοντών ( $n = 20$ ) και, στη συνέχεια, χρησιμοποιώντας μια μεγάλη ομάδα υποκειμένων ( $n = 144$ ) ενός ευρέους φάσματος ηλικιακών ομάδων. Η δεύτερη προτεινόμενη μέθοδος περιλαμβάνει την εκτίμηση της aSBP και της CO μέσω μηχανικής μάθησης χρησιμοποιώντας, ομοίως με προηγουμένως, δεδομένα πίεσης μανσέτας και cfPWV. Η *in silico* επικύρωση της μεθόδου δείχνει ότι η μηχανική μάθηση προσφέρει μια αξιόπιστη εναλλακτική για την παρακολούθηση της aSBP και της CO. Παράλληλα, η μεταφορά μάθησης (transfer learning) επιτρέπει την αξιολόγηση της απόδοσης του εκτιμητή της aSBP σε *in vivo* κλινικά δεδομένα, με τα αποτελέσματα να δείχνουν εξαιρετική συμφωνία και ακρίβεια μεταξύ των εκτιμώμενων τιμών και των πραγματικών τιμών αναφοράς.

Ο δεύτερος στόχος της εργασίας αφορά την ανάπτυξη και εφαρμογή μιας γκάμας διαφορετικών πλαισίων μηχανικής μάθησης για τη μη επεμβατική πρόβλεψη της  $E_{es}$ . Αρχικά, ένα μοντέλο μηχανικής μάθησης εκπαιδεύεται και δοκιμάζεται χρησιμοποιώντας ως στοιχεία εισόδου μετρήσεις πίεσης μανσέτας στο βραχίονα και cfPWV. Στο πλαίσιο της εργασίας, εκτιμάται, επίσης, η σημαντικότητα της ενσωμάτωσης του κλάσματος εξώθησης (EF) ως πρόσθετης εισόδου για τον υπολογισμό της  $E_{es}$ . Τα αποτελέσματα δείχνουν πως τα δεδομένα από μετρήσεις αρτηριακής πίεσης δεν επαρκούν για την ακριβή εκτίμηση της  $E_{es}$ . Εντούτοις, η επιπρόσθετη πληροφορία που εισάγει το EF βελτιώνει σημαντικά τις εκτιμήσεις της  $E_{es}$ . Εναλλακτικά σε αυτήν την τεχνική, προτείνεται μια τρίτη προσέγγιση βασισμένη, εκ νέου, σε τεχνητή νοημοσύνη για τον υπολογισμό της  $E_{es}$  χρησιμοποιώντας, αυτήν τη φορά, την πληροφορία που εμπεριέχεται σε κλινικά συναφή συστολικά χρονικά διαστήματα. Ένα μοντέλο εκπαίδευσης/δοκιμών αναπτύσσεται χρησιμοποιώντας *in silico* υποκείμενα ( $n = 4,645$ ) που παράγονται από ένα προηγούμενος επικυρωμένο υπολογιστικό μοντέλο ρευστών. Τα ευρήματα της αξιολόγησης υποδεικνύουν εξαιρετική συνάφεια μεταξύ των εκτιμήσεων και των πραγματικών τιμών και, έτσι, συνάδεται πως η προσέγγιση αυτή αποτελεί ένα βήμα μπροστά προς την ανάπτυξη μιας απλής και κλινικά εφαρμόσιμης μεθόδου για την αξιολόγηση της συστολικής λειτουργίας της αριστερής κοιλίας. Τέλος, μια διαφορετική τεχνική επιδιώκει να ερευνήσει την δυνατότητα πρόβλεψης της  $E_{es}$  από ολόκληρη τη μορφολογία της κυματομορφής της βραχιόνιας πίεσης, σε συνδυασμό με την υπολογιστική ισχύ που παρέχουν τα ευρέως γνωστά νευρωνικά δίκτυα. Το κύμα αρτηριακής πίεσης αποδεικνύεται μία πλούσια πηγή πληροφοριών για την αξιολόγηση της συσταλτικότητας της αριστερής κοιλίας. Ειδικότερα, διαπιστώνεται ότι οι προβλέψεις της  $E_{es}$  είναι ιδιαίτερα ακριβείς για ένα ευρύ φάσμα τιμών συσταλτικότητας της αριστερής κοιλίας, καθώς και διαφορετικών φορτίων.

Επιπλέον, ως τρίτος στόχος ορίζεται η βελτίωση της κλινικής αξιολόγησης της σύνθετης αντίστασης της αορτής ( $Z_{ao}$ ) και της συνολικής αρτηριακής συμμόρφωσης ( $C_T$ ). Δεδομένου ότι οι τοπικές μετρήσεις της PWV είναι μη επεμβατικές και κλινικά άμεσα διαθέσιμες, εφάρμοσαμε μια μη επεμβατική μέθοδο για την εκτίμηση της  $Z_{ao}$  και της  $C_T$  χρησιμοποιώντας πίεση μανσέτας, cfPWV και καρωτιδοακτινική PWV και εφαρμόζοντας ανάλυση παλινδρόμησης. Η *in silico* επικύρωση της μεθόδου χρησιμοποιώντας 3,818 εικονικά υποκείμενα αποδίδει υψηλή ακρίβεια για τις εκτιμώμενες τιμές τόσο της  $Z_{ao}$  όσο και της  $C_T$ . Τα αποτελέσματα συνηγορούν στο γεγονός ότι η παρούσα μέθοδος ενδέχεται να αποτελέσει ένα πολύτιμο εργαλείο για την εκτίμηση της αρτηριακής δυσκαμψίας, μειώνοντας ταυτόχρονα το κόστος και την πολυπλοκότητα των υφιστάμενων τεχνικών.

Στη συνέχεια, παρουσιάζουμε μια μη επεμβατική μέθοδο για την εκτίμηση της  $C_T$  από μια μεμονωμένη κυματομορφή αρτηριακής πίεσης καρωτίδας χρησιμοποιώντας τεχνητά νευρωνικά δίκτυα. Η προτεινόμενη μεθοδολογία αξιολογείται αξιοποιώντας ένα μεγάλο πληθυσμό υγιών ενηλίκων ( $n = 2,256$ ) από τη μελέτη του Asklepios. Συγκεκριμένα, παρατηρείται υψηλή ακρίβεια στις εκτιμήσεις της  $C_T$ , γεγονός που υποδεικνύει πως μια τέτοια προσέγγιση θα



μπορούσε να προσφέρει πολλά υποσχόμενες τεχνολογικές εφαρμογές. Τέτοιες εφαρμογές θα μπορούσαν να συμπεριλάβουν τεχνολογίες γρήγορης και οικονομικής αιμοδυναμικής παρακολούθησης από τον ίδιο το γιατρό, αλλά και εφαρμογές που ενσωματώνουν αντίστοιχες μεθόδους σε φορητές τεχνολογίες, όπως έξυπνα ρολόγια ή άλλες συσκευές.

Τέλος, εν όψει των αντικρουόμενων κλινικών και πειραματικών στοιχείων σχετικά με την επίδραση του HP στην αρτηριακή δυσκαμψία και τον υποκατάστατο δείκτη του cfPWV, το τελευταίο βήμα αυτής της έρευνας πραγματεύεται την αξιολόγηση και ποσοτικοποίηση της επίδρασης του HP στη μέτρηση της cfPWV υπό ελεγχόμενες αιμοδυναμικές συνθήκες, και ιδιαίτερα σε σχέση με αρτηριακή πίεση που αποτελεί έναν ισχυρό καθοριστικό παράγοντα της αρτηριακής δυσκαμψίας. Βάσει των ευρημάτων μας, συμπεραίνουμε ότι οι μεγάλες διακυμάνσεις του HP μπορεί να έχουν κλινικά σημαντική επίδραση στην cfPWV και, άρα, η διόρθωση της μέτρησης της PWV ως προς την αρτηριακή πίεση μπορεί να κριθεί αναγκαία σε τέτοιες περιπτώσεις.

Εν κατακλείδι, αυτή η διατριβή δείχνει ότι τα μοντέλα φυσικής και η μηχανική εκμάθηση αποτελούν πολύτιμα εργαλεία για την ανάπτυξη και την επικύρωση νέων, μη επεμβατικών αλγορίθμων παρακολούθησης της υγείας. Εκείνο που αξίζει να σημειωθεί είναι πως τα εργαλεία αυτά εισάγονται για πρώτη φορά στην παρακολούθηση καρδιαγγειακών στοιχείων και παρέχουν σημαντικές δυνατότητες ως προς τη βελτίωση του συγκεκριμένου τομέα. Πιο ειδικά, οι επιδόσεις των αλγορίθμων για την πρόβλεψη των αιμοδυναμικών και καρδιακών παραμέτρων από τα μη επεμβατικά δεδομένα υποδηλώνουν ότι είναι εφικτό να βελτιώσουμε τις τρέχουσες τεχνολογίες παρακολούθησης των καρδιαγγειακών συμβάντων, ενώ μειώνοντας ταυτόχρονα την πολυπλοκότητα και το κόστος τους.

Λέξεις-κλειδιά: μη επεμβατική παρακολούθηση, κεντρικά αιμοδυναμικά στοιχεία, καρδιακή συσταλτικότητα, αρτηριακή πίεση, καρδιακή παροχή, τελική συστολική ελαστικότητα, αρτηριακή συμμόρφωση, αρτηριακή σύνθετη αντίσταση, ταχύτητας παλμικού κύματος, υπολογιστική μοντελοποίηση, προγνωστική μοντελοποίηση, αντίστροφη επίλυση προβλημάτων, μηχανική μάθηση, ανάλυση παλινδρόμησης, τεχνητά νευρωνικά δίκτυα, τυχαία δάση, **gradient boosting**

## **Licence**

This work is licensed under the Creative Commons Attribution 4.0 International (CC BY 4.0) Licence. For further information see: <http://creativecommons.org/licenses/by/4.0/>

## List of tables

2.1	Input and output parameters of the 1-D arterial tree model. . . . .	44
2.2	Description of the $\Delta\theta_j$ and $SC_i$ parameters. . . . .	45
2.3	List of the input model parameters' importance ranking. . . . .	45
2.4	Descriptive hemodynamical parameters and clinical characteristics of the study population (n = 20). . . . .	53
2.5	Parameters of accuracy, correlation and agreement of CO estimation by the model in comparison to the reference method. . . . .	54
2.6	Parameters of accuracy, correlation and agreement of aSBP estimation by the model in comparison to the reference method. . . . .	54
2.7	Estimates of relative errors in CO and aSBP after introducing: (i) a $\pm 10$ % error in the brachial SBP measurement and (ii) a $\pm 10$ % error in the cfPWV measurement. . . . .	59
3.1	Subject characteristics and hemodynamic parameters according to the age group. . . . .	86
3.2	Real and estimated aortic flow characteristics according to age group. . . . .	89
3.3	Overall comparison between the SV estimates and the reference MRI SV. . . . .	91
4.1	List of the hyperparameters which were chosen to be optimized and their corresponding values. . . . .	106
4.2	Distributions of the parameters of the in silico population (n = 4,018). . . . .	109
4.3	Regression statistics between the model predicted aSBP and the reference aSBP. The input features include brSBP, brDBP, HR, and cfPWV. . . . .	110
4.4	Regression statistics between the model predicted CO and the reference CO. The input features include brSBP, brDBP, HR, and cfPWV. . . . .	110
4.5	Regression statistics between the model predicted $E_{es}$ and the reference $E_{es}$ . The input features include brSBP, brDBP, HR, and cfPWV. . . . .	110
4.6	Regression statistics between the model predicted $E_{es}$ and the reference $E_{es}$ . The input features include brSBP, brDBP, HR, cfPWV, and EF. . . . .	111
4.7	Statistical results in percentage of times that the hyperparameter value was selected during the hyperparameter tuning with ten-fold cross validation process. Values selected consistently are presented in bold. . . . .	112
4.8	Average feature importances for the prediction of aSBP, CO, and $E_{es}$ . . . . .	112

**List of tables**

---

4.9 Model performance for the best performing configurations (SVR) using different subsets of the input features. . . . . 113

4.10  $t$ -statistics for the OLS regression coefficients. . . . . 113

4.11 Distributions of the parameters of the in vivo population (n = 783). . . . . 114

4.12 Regression statistics between the model predicted aSBP and the reference aSBP. The input features include brSBP, brDBP, HR, and cfPWV. The testing set consists of in vivo data only. . . . . 115

4.13  $t$ -statistics for the OLS regression coefficients. . . . . 115

5.1 List of the hyperparameters which were chosen to be optimized and their corresponding values. . . . . 140

5.2 List of the selected hyperparameters for all the predictive models. . . . . 140

5.3 Summary of the cardiovascular characteristics of the virtual study cohort (n = 4,645). . . . . 144

5.4 Regression statistics between the model-predicted  $E_{es}$  and the reference  $E_{es}$ . . . 145

5.5 Feature importances for the prediction of  $E_{es}$ . . . . . 146

5.6 Regression statistics between the model-predicted  $E_{es}$  and the reference  $E_{es}$  when artificial noise is considered. . . . . 151

6.1 List of the inputs and outputs of the 1-D cardiovascular model. . . . . 165

6.2 Selected distributions of the model’s input parameters based on the literature . 167

6.3 Number of filters per each convolutional layer for the two CNN models. . . . . 169

6.4 Summary of the virtual study cohort (n = 3,748) cardiovascular characteristics. 172

6.5 Regression statistics between the model-predicted and the reference elastance values. . . . . 173

7.1 List of the selected hyperparameters for the predictive models. . . . . 190

7.2 Summary of the cardiovascular characteristics of the virtual study cohort (n = 3,818). . . . . 196

7.3 Correlation between the input features and the target outputs. . . . . 197

7.4 Regression statistics between model predictions and reference values. . . . . 198

7.5 Feature importances for the prediction of  $Z_{ao}$  and  $C_T$  using RFR. . . . . 198

7.6 Comparison of the proposed machine learning-based  $Z_{ao}$  and  $C_T$  estimators to prior art. . . . . 204

8.1 Asklepios study inclusion and exclusion criteria. . . . . 221

8.2 Summary of all the machine learning models trained/tested in this study. . . . 225

8.3 Optimal number of epochs for every ANN configuration. . . . . 225

8.4 Description of the cardiovascular characteristics and parameters of the study cohort (n = 2,256). . . . . 227

8.5 Regression statistics between the model-predicted and the reference  $C_T$  data. . 227

8.6 Permutation feature importances for the ANN1. . . . . 228

8.7	Correlation coefficients and nRMSE values as a function of the artificial noise level in the distorted carotid pressure waves for the ANN1 and ANN3. . . . .	233
9.1	Cardiovascular parameters of the virtual study population (n = 59). . . . .	245
9.2	Hemodynamical parameters of the two groups with different levels of compliance at baseline (HR = 60 bpm). . . . .	247
9.3	Hemodynamical characteristics of the entire population with increasing heart rate (from 60 to 100 bpm). . . . .	248
9.4	Relative changes in hemodynamical variables at 100 bpm with respect to their baseline values at 60 bpm for the two groups with different levels of arterial compliance. . . . .	249

## List of tables

---

## List of figures

1.1	Schematic representation of the basic principle of applanation tonometry. . . . .	5
1.2	Conventional automated sphygmomanometer. . . . .	6
1.3	Imaging methods for measuring cross-sectional area or diameter waveforms and flow or mean velocity waveforms. . . . .	7
1.4	Concept of left ventricular elastance: (A) A heart cycle is presented as a ventricular pressure-volume graph. Instantaneous elastance, end-systolic elastance ( $E_{es}$ ) and end-diastolic elastance ( $E_{ed}$ ) are also presented. $E_{es}$ intersects the left ventricular (LV) volume axis at the dead volume abscissa ( $V_0$ ). (B) Normalized time varying elastance ( $E_N, E_N^*$ ) as a function of normalized time. . . . .	10
1.5	Graphical representation of the concept of compliance being the ability of the arterial walls to distend, $dA$ , under a given increase in transmural pressure, $dP$ . . . . .	11
1.6	Graphical representation of the magnitude and the phase of arterial input impedance. . . . .	13
1.7	Conventional foot-to-foot computation of the carotid-femoral pulse wave velocity (PWV). . . . .	15
1.8	Evolution of 1-D arterial tree models over the passage of time. . . . .	18
1.9	Machine learning applications in the assessment of vascular ageing. . . . .	21
2.1	Schematic representation of the 1-D model of the systemic circulation. . . . .	43
2.2	Scaled sensitivity matrix for the entire set of input parameters of the 1-D arterial tree model. . . . .	46
2.3	Variation of the proximal scaling factor with respect to age for adjusting the relative distensibility of the proximal aorta. . . . .	47
2.4	Schematic representation of the optimization process for predicting non-invasive cardiac output and central systolic blood pressure. . . . .	49
2.5	Uncalibrated generic aortic flow waveform that is used as input to the 1-D arterial tree solver. . . . .	50
2.6	Comparison between the estimated CO values and the reference in vivo data (using the Mobil-O-Graph pressure data). . . . .	55
2.7	Comparison between the estimated CO values and the reference in vivo data (using the SphygmoCor pressure data). . . . .	56

## List of figures

---

2.8	Comparison between the estimated aSBP values and the reference in vivo data (using the Mobil-O-Graph pressure data). . . . .	57
2.9	Comparison between the estimated aSBP values and the reference in vivo data (using the SphygmoCor pressure data). . . . .	58
2.10	Arbitrary aortic pressure waveform that was yielded from the 1-D arterial tree solver. . . . .	63
3.1	Schematic representation of the optimization process for predicting non-invasive stroke volume. . . . .	84
3.2	Comparison between the estimated SV values and the reference in vivo data. . . . .	87
3.3	Variation of the mean absolute error in the stroke volume estimation across the age groups. . . . .	88
3.4	Comparison between the estimated SV values and the reference in vivo data. . . . .	90
4.1	Schematic illustration of the regression pipeline for predicting aSBP, CO, and $E_{es}$ . . . . .	103
4.2	Experimental design for the evaluation of the regression models. The model evaluation was done using ten-fold cross validation (CV) (external CV). In every external fold, we performed hyperparameter tuning with ten-fold CV (internal CV). . . . .	107
4.3	Experimental design for the evaluation of the synthetically trained model against the in vivo data. . . . .	108
4.4	Comparison between the estimated and the reference aSBP data. . . . .	116
4.5	Comparison between the estimated and the reference CO data. . . . .	117
4.6	Comparison between the estimated and the reference $E_{es}$ data. . . . .	118
4.7	Sensitivity of RMSE to changes in the training size for the aortic systolic blood pressure (aSBP) estimator. . . . .	119
4.8	Sensitivity of RMSE to changes in the training size for the cardiac output (CO) estimator. . . . .	120
4.9	Sensitivity of RMSE to changes in the training size for the end-systolic elastance ( $E_{es}$ ) estimator. . . . .	121
4.10	Correlation matrix for the in silico dataset. . . . .	122
4.11	Correlation matrix for the in vivo dataset. . . . .	123
5.1	Representative elastance curve $E(t)$ with the indicated $t_{ed}$ (early time point of isovolumic contraction), $t_{ad}$ (ending time point of isovolumic contraction), and $t_{es}$ (end-systolic time point). . . . .	139
5.2	Learning curve visualizing the effect of the number of training data instances on the model's performance. . . . .	143
5.3	Comparison between the estimated $E_{es}$ values and the reference $E_{es}$ for the $XGB_{E_{es}}$ M1 model. . . . .	147



5.4	Comparison between the estimated and the reference $E_{es}$ data for the XGB $_{E_{es}}$ M2 model. . . . .	148
5.5	Comparison between the estimated and the reference $E_{es}$ data for the XGB $_{E_{es}}$ M3 model. . . . .	149
5.6	Comparison between the estimated and the reference $V_d$ data for the XGB $_{V_d}$ M3 model. . . . .	150
5.7	Representation of the aortic pressure waveform, the left ventricular pressure, the ECG including the timing components of pre-ejection period (PEP), ejection time (ET), and the newly introduced Q-aoClos interval. The Q-aoClos interval is the time period from the initial trace of Q-wave (point 1) (as measured via ECG) until the closure of the aortic valve (point 2) (as recorded via a phonographic device). . . . .	152
6.1	Schematic representation of the cardiovascular model developed by [?]. . . . .	166
6.2	Representation of the architecture of the CNN model configurations. The two CNN models are shown in different colors (CNN $_1$ in blue and CNN $_2$ in green) and the number of the in_channels and out_channels for each convolutional layer is reported. . . . .	169
6.3	Brachial blood pressure waves after adding artificial noise. The noisy data are presented in red solid lines and the original noise-free data in black dashed lines. . . . .	171
6.4	Comparison between the predicted $E_{es}$ and the reference $E_{es}$ data for CNN $_1$ . . . . .	174
6.5	Comparison between the predicted $E_{es}$ and the reference $E_{es}$ data for CNN $_2$ . . . . .	175
7.1	Schematic representation of the training/testing pipeline for predicting aortic characteristic impedance ( $Z_{ao}$ ), and total arterial compliance ( $C_T$ ). . . . .	187
7.2	The 1-D cardiovascular model that was used for the data generation. . . . .	188
7.3	Typical representation of a random forest regression model. . . . .	191
7.4	Typical representation of an artificial neural network. . . . .	192
7.5	Learning curves presenting the impact of the number of training data instances on the RFR's performance for $Z_{ao}$ (A) and $C_T$ (B). . . . .	193
7.6	Comparison between the estimated and the reference $Z_{ao}$ data using RFR. . . . .	199
7.7	Comparison between the estimated and the reference $C_T$ data using RFR. . . . .	200
7.8	Comparison between the estimated and the reference $Z_{ao}$ data using ANN. . . . .	201
7.9	Comparison between the estimated and the reference $C_T$ data using ANN. . . . .	202
7.10	Sensitivity of precision in terms of nRMSE to the number of the training data. The 100 % of the training size corresponds to 2,290 cases. . . . .	203
8.1	Indication of features on the carotid pressure waveform and the time-derivative. . . . .	224
8.2	Comparison between the predicted and the reference $C_T$ data using LR1. . . . .	229
8.3	Comparison between the predicted and the reference $C_T$ data using ANN1. . . . .	230
8.4	Comparison between the predicted and the reference $C_T$ data using ANN3. . . . .	231

## List of figures

---

8.5	Carotid blood pressure waves after adding artificial noise. The noisy data are presented in red solid lines and the original noise-free data in black dashed lines.	232
9.1	Schematic representation of the optimization algorithm that corrects blood pressure. . . . .	246
9.2	Changes in the carotid-femoral pulse wave velocity with increasing heart rate under two scenarios: (1) with free-varying blood pressure (solid line) and (2) with fixed DBP (dashed line). . . . .	250

# Contents

<b>Acknowledgements</b>	<b>v</b>
<b>Abstracts (English\Français\Ελληνικά)</b>	<b>vii</b>
<b>List of tables</b>	<b>xxi</b>
<b>List of figures</b>	<b>xxvi</b>
<b>Chapter 1 Introduction</b>	<b>1</b>
1.1 Motivation . . . . .	1
1.2 Cardiovascular monitoring . . . . .	2
1.2.1 Aortic systolic blood pressure . . . . .	6
1.2.2 Cardiac output . . . . .	7
1.2.3 End-systolic elastance . . . . .	9
1.2.4 Total arterial compliance . . . . .	10
1.2.5 Aortic characteristic impedance . . . . .	12
1.2.6 Arterial stiffness . . . . .	14
1.3 Numerical models of the cardiovascular system . . . . .	16
1.4 Machine learning framework . . . . .	18
1.4.1 Supervised learning . . . . .	18
1.4.2 Application in cardiovascular medicine . . . . .	20
1.5 Thesis aims . . . . .	21
1.6 Thesis outline . . . . .	22
Bibliography . . . . .	23
<b>Chapter 2 Non-invasive cardiac output and central systolic pressure from cuff pressure and pulse wave velocity</b>	<b>39</b>
Abstract . . . . .	40
2.1 Introduction . . . . .	41
2.2 Methods & materials . . . . .	42
2.3 Results . . . . .	52
2.4 Discussion . . . . .	57
Bibliography . . . . .	65

<b>Chapter 3</b>	<b>Validation of a non-invasive inverse problem-solving method for stroke volume: do physics-based models add to the traditional statistical approaches?</b>	<b>77</b>
	Abstract . . . . .	78
	3.1 Introduction . . . . .	79
	3.2 Methods & materials . . . . .	80
	3.3 Results . . . . .	85
	3.4 Discussion . . . . .	90
	Bibliography . . . . .	94
<b>Chapter 4</b>	<b>Non-invasive estimation of aortic hemodynamics and cardiac contractility using machine learning</b>	<b>99</b>
	Abstract . . . . .	100
	4.1 Introduction . . . . .	101
	4.2 Methods & materials . . . . .	102
	4.3 Results . . . . .	109
	4.4 Discussion . . . . .	114
	Bibliography . . . . .	124
<b>Chapter 5</b>	<b>Artificial intelligence-based estimation of end-systolic elastance from arm pressure and systolic timing intervals</b>	<b>135</b>
	Abstract . . . . .	136
	5.1 Introduction . . . . .	137
	5.2 Methods & materials . . . . .	138
	5.3 Results . . . . .	143
	5.4 Discussion . . . . .	146
	Bibliography . . . . .	155
<b>Chapter 6</b>	<b>Estimation of cardiac contractility from brachial pressure waveform via deep learning</b>	<b>161</b>
	Abstract . . . . .	162
	6.1 Introduction . . . . .	163
	6.2 Methods & materials . . . . .	164
	6.3 Results . . . . .	170
	6.4 Discussion . . . . .	174
	Bibliography . . . . .	177
<b>Chapter 7</b>	<b>Determination of aortic characteristic impedance and total arterial compliance from regional pulse wave velocities using machine learning</b>	<b>185</b>
	Abstract . . . . .	185
	7.1 Introduction . . . . .	186
	7.2 Methods & materials . . . . .	187

## Contents

---

7.3 Results . . . . .	195
7.4 Discussion . . . . .	197
Bibliography . . . . .	206
<b>Chapter 8 On the assessment of arterial compliance from carotid pressure wave- form</b>	<b>217</b>
Abstract . . . . .	218
8.1 Introduction . . . . .	219
8.2 Methods & materials . . . . .	220
8.3 Results . . . . .	226
8.4 Discussion . . . . .	229
Bibliography . . . . .	235
<b>Chapter 9 The impact of heart rate on pulse wave velocity: an in silico evaluation</b>	<b>241</b>
Abstract . . . . .	242
9.1 Introduction . . . . .	243
9.2 Methods & materials . . . . .	243
9.3 Results . . . . .	247
9.4 Discussion . . . . .	250
Bibliography . . . . .	254
<b>Chapter 10 Conclusions</b>	<b>261</b>
10.1 Summary of thesis achievements . . . . .	261
10.1.1 Non-invasive estimation of aortic hemodynamics from readily available clinical data . . . . .	261
10.1.2 Machine learning for the prediction of left ventricular contractility . . .	263
10.1.3 Can machine learning improve the assessment of arterial elasticity? . . .	264
10.1.4 Disentangling the mystery behind heart rate's effect on pulse wave veloc- ity measurement . . . . .	265
10.2 Future perspectives . . . . .	265
<b>Curriculum vitae</b>	<b>268</b>
<b>List of publications</b>	<b>271</b>

# Chapter 1

---

## Introduction

### 1.1 Motivation

Maintaining a healthy vascular state is the cornerstone of human longevity. Cardiac and vascular diseases remain among the leading causes of hospitalization and morbidity in the western world (approximately 18 million deaths per year, representing 30 % of all global deaths) [1]. Cardiovascular diseases constitute a group of disorders of the heart and blood vessels among which are coronary heart disease, cerebrovascular disease, and peripheral arterial disease. Adverse conditions such as these are detrimental to patients as they increase morbidity and mortality, and prolong hospital stay [2; 3; 4]. In addition, adverse events have a significant impact on healthcare costs and resources.

Chronological age is a major risk factor for cardiovascular disease. While age-related arterial damage occurs predominantly in later life, there is high inter-individual variability, with some displaying early vascular ageing [5]. This has led to the development of the concept of vascular age, which may be better linked to the prognosis of cardiovascular disease [6]. Whereas chronological aging is related to the passage of time, vascular aging relates to the decline in arterial function.

In a progressively aging world population, it is of utmost importance to define the biomarkers that accurately reflect the state of vascular ageing in order to improve the detection and assessment of cardiovascular disease. Clinical parameters directly measured in the heart or at the root of the aorta are crucial for early detection of vascular age, diagnosis, prognosis, treatment, and management of the disease. But despite their diagnostic importance, their clinical use is severely hampered by their invasive nature, cost, or need for special equipment. Therefore, there is an unmet need for reliable, convenient, non-invasive, and cost-efficient

predictive technologies to assist the clinician with cardiovascular monitoring.

The overall goal of this thesis is to establish biomedical predictive models for cardiovascular monitoring and assessment in order to aid clinical decision-making for cardiovascular disease. Our vision is to transform the clinical monitoring environment and offer solutions to facilitate the acquisition of valuable but, until now, difficult to obtain biomarkers. Precisely, this work focuses on major cardiovascular biomarkers, including aortic systolic blood pressure, cardiac output, end-systolic elastance, total arterial compliance, aortic characteristic impedance, and arterial stiffness, given the wealth of evidence that they can capture age-related changes and pathologies and predict clinical outcomes.

### 1.2 Cardiovascular monitoring

In recent years, cardiovascular risk assessment has been developed into a prominent area of research and has risen to the forefront of efficient management of patients at risk of developing cardiovascular disease. Monitoring of biomarkers for the vascular and cardiac function is crucial for cardiovascular disease identification, treatment planning, and assessment of therapy response.

Although many factors contribute to the incidence and progression of cardiovascular disease, adverse outcomes are ultimately associated with a failure or ineffectiveness of the biomechanical system to deliver oxygenated blood to organs and tissues. It is to be noted that the key biomechanical properties of the heart and the circulatory system, including cardiac contraction, arterio-ventricular coupling, large artery stiffness, and microvasculature, influence the morphology of pressure and flow waves in blood vessels [7].

An arterial wave can be termed as a time-wise change in pressure or flow that propagates along a blood vessel. Pressure and flow waveforms result from the superposition of waves that pass by an arterial location, with each wave causing an increment or decrement in the resulted waveform. Arterial waves of pressure and flow contain a wealth of information on the cardiovascular system and their measurement has become the cornerstone of current advancements in research and technology. Importantly, pressure and flow waveforms allow for the derivation of numerous cardiovascular parameters, such as heart rate, systolic blood pressure, cardiac output, peripheral resistance, arterial stiffness, respiration, and many more, which can be informative of disease initiation or/and progression.

Pulse wave analysis has introduced a multitude of new invasive and non-invasive biomarkers which have been tested in order to determine their clinical utility in the stratification of cardiovascular risk. Several pulse wave analysis techniques rely solely on the pressure wave, while others harness both the pressure and flow information. Circulating markers of endothelial function and inflammation have been identified as useful markers in the diagnosis

of disease, as well as disease monitoring, progression, and risk assessment [8; 9; 10]. In addition, technologies assessing structural and functional parameters have been evaluated with regard to their clinical value in risk assessment [10]. However, less attention has been given to other equally important parameters like total systemic compliance and aortic characteristic impedance, which are major determinants of cardiac afterload and, in consequence, arterial blood pressure [11].

Moreover, central hemodynamical quantities, such as cardiac output and central (aortic) pressure, have been generally shown to be more powerful predictors of clinical outcomes than corresponding measurements obtained in the peripheral arteries such as the radial, femoral or brachial arteries [12; 13]. Critically ill or intensive care unit patients often require continuous assessment of cardiac output for diagnostic purposes or for guiding therapeutic interventions [14; 15; 16], whereas several studies have shown the pathophysiological importance of central systolic blood pressure as the critical index for diagnosis and preventing cardiovascular diseases [17; 18; 19].

Although a great number of the monitoring methods are currently established in the clinical setting, their use is severely hampered by their invasive nature, cost, need for special equipment and training, or inapplicability to sensitive age groups [20]. In addition, the majority of the existing techniques cannot be used outside the clinic rendering cardiovascular monitoring unfeasible after hospital discharge.

Therefore, there is a demand for a new generation of non-invasive methods and corresponding devices that will provide clinical insights on cardiovascular health, inside and outside of the clinical setting. Such efforts should focus on non-invasive technologies which have the potential to transform cardiovascular assessment enabling monitoring feasible outside the hospital, reducing hospitalization periods, and essentially decreasing the staff-to-patient ratio [21; 22].

In the next section, we briefly review current techniques for measuring blood pressure and flow/velocity waveforms. Subsequently, we cover some of the most well-established techniques that use the measured pressure or/and flow waves for estimating key cardiovascular parameters. The section concludes with some considerations with respect to the effect of cardiac frequency on the assessment of arterial stiffness.

### **Measurement of blood pressure**

The gold-standard measurement for acquiring the blood pressure waveform is invasive, and it is performed either with a micromanometer-tipped catheter or fluid-filled catheter and external manometer [7; 23]. Micromanometer-tipped catheters have an excellent frequency response and provide a high fidelity waveform, but they are expensive. Fluid-filled catheter configurations are less expensive; however, their performance can be poor and should be



## Chapter 1. Introduction

---

tested to ensure that the waveform is faithfully captured [7]. A common drawback of such systems pertains to damping which can often occur in the case of an improperly flushed catheter. Importantly, the clinical use of these catheter-based systems is severely limited in the routine examination due to its invasive nature and its associated complications of bleeding, thrombosis, and infection.

Applanation tonometry and sphygmomanometry offer non-invasive alternatives for measuring the arterial blood pressure waveform. Applanation tonometry involves slightly compressing against bone over a superficial artery with a pen-like pressure transducer (Figure 1.1) [24; 25]. Although the technique is relatively easy to learn, it requires some experience from the operator for attaining the correct sensor position during the measurement. Applanation tonometry is commonly applied on the radial artery, as well as in other locations, including carotid or femoral arteries, but with less adequate performance [7]. The acquired signal is typically calibrated using the conventional brachial cuff pressures, which, however, may involve errors due to cuff pressure inaccuracies and pulse amplification from the brachial site to the radial site [26; 27]. A sphygmomanometer is a device that composes of an inflatable rubber cuff, which is wrapped around the arm (brachial artery) (Figure 1.2). A bulb inflates the cuff and a valve releases pressure. Currently, digital sphygmomanometers are automated, providing blood pressure readings without needing someone to operate the device. However, convenience comes at the expense of accuracy in the pressure measurement. The newest technologies have introduced cuff-based devices for other arterial locations, such as carotid and femoral arteries (e.g. SphygmoCor EXCEL). While being fully non-invasive and cost-efficient, it should be noted that both applanation tonometry and sphygmomanometry cannot be applied to every arterial location, such as locations which are covered by thick layers of tissue or bones (e.g. the aorta).

### Measurement of blood flow/velocity

The gold-standard for invasive flow measurement is perivascular flow probes which use transit-time ultrasound methods. In humans, the use of flow probe is limited to the clinical assessment of bypass grafts [28], whereas invasive arterial wave analysis is usually performed using blood velocity measurements from Doppler flow wires which measure velocity, rather than flow (e.g. Philips Volcano ComboWire) [29].

Phase-contrast magnetic resonance imaging (PC-MRI) is considered as the gold-standard non-invasive method for measuring flow. PC-MRI involves the motion of magnetic spins through a magnetic field gradient which enables velocity encoding in a specified direction [30]. Arterial flow is obtained by setting a two-dimensional acquisition plane through the selected vessel cross-section, encoding velocity through-plane, and integrating velocities over the cross-section [Figure 1.3 (left panel)]. The signal-to-noise ratio (SNR) is determined by the encoding velocity (VENC), which must be set properly in order to avoid aliasing (SNR is

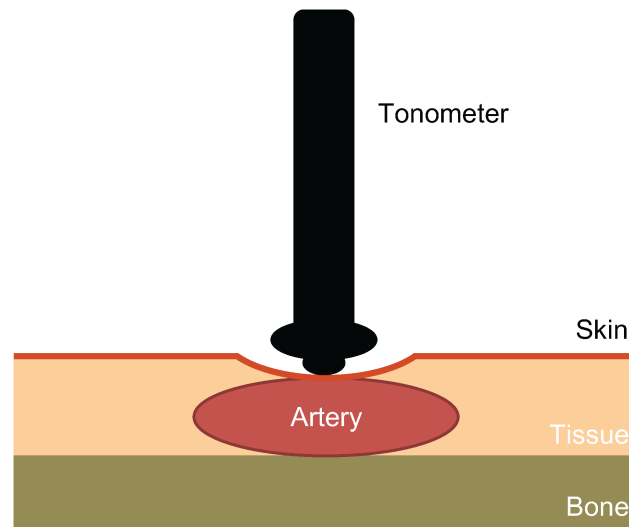


Figure 1.1 – Schematic representation of the basic principle of applanation tonometry.

set too low) or insufficient contrast (SNR is set too high) [29]. Despite the advantages offered by the method, PC-MRI is expensive and most suited to imaging central vessels.

Doppler ultrasound is less expensive and can be more easily employed for imaging peripheral arteries. Pulsed Doppler relies on the acquisition of a velocity spectrum over time inside a sample volume that is positioned by the operator, typically in the center of the vessel [Figure 1.3 (right panel)]. The intensities of pixels in each vertical line of the spectrum essentially represent a histogram of velocities within the sample volume at the given time instance. Therefore, the spectrum can indicate whether "the velocity profile is relatively flat (narrow spectrum) or contains a range of velocities due to a more parabolic, skewed, or turbulent profile (broad-spectrum)" [29]. Potential problems with this technique include the assumption of a circular left ventricular outflow tract (LVOT) and the requirement of parallel alignment of the pulsed Doppler signal.

Having provided an overview of techniques for measuring pressure and flow/velocity waveforms, the following subsections review the most commonly applied techniques that harness the measured pressure and/or flow waves for acquiring some major cardiovascular parameters. In particular, this section presents the current state of the art for the following cardiovascular biomarkers: aortic systolic blood pressure, cardiac output, end-systolic elastance, total arterial compliance, and aortic characteristic impedance.



Figure 1.2 – Conventional automated sphygmomanometer.

### 1.2.1 Aortic systolic blood pressure

#### Definition and clinical relevance

Arterial pressure varies continuously over the cardiac cycle, but in clinical practice, only systolic and diastolic pressures are routinely reported. These are usually measured in the brachial artery using cuff sphygmomanometry. However, the shape of the pressure waveform changes continuously throughout the arterial tree. Although diastolic and mean arterial pressures are relatively constant, systolic pressure may be up to 40 mmHg higher in the brachial artery than in the aorta [31; 32; 33]. Aortic blood pressure is of great importance, as it represents the direct pressure load faced by the ejecting left ventricle. Aortic systolic blood pressure (aSBP) represents the cardiac and cerebral burden more directly than office systolic blood pressure. Overall, it has been shown to be an important biomarker for the diagnosis and prevention of cardiovascular disease [17].

#### State of the art

Direct measurement of aSBP is done via catheterization, which constitutes the clinical reference method for blood pressure monitoring in high-risk surgical patients and critically ill patients. However, invasive monitoring is not feasible for routine examination or continuous monitoring. This inherent limitation has led to the development of numerous methods for deriving central aortic pressure waveform from a peripheral pressure wave via generalized transfer functions [34; 35; 36], or parameter-estimation techniques from pooled clinical data

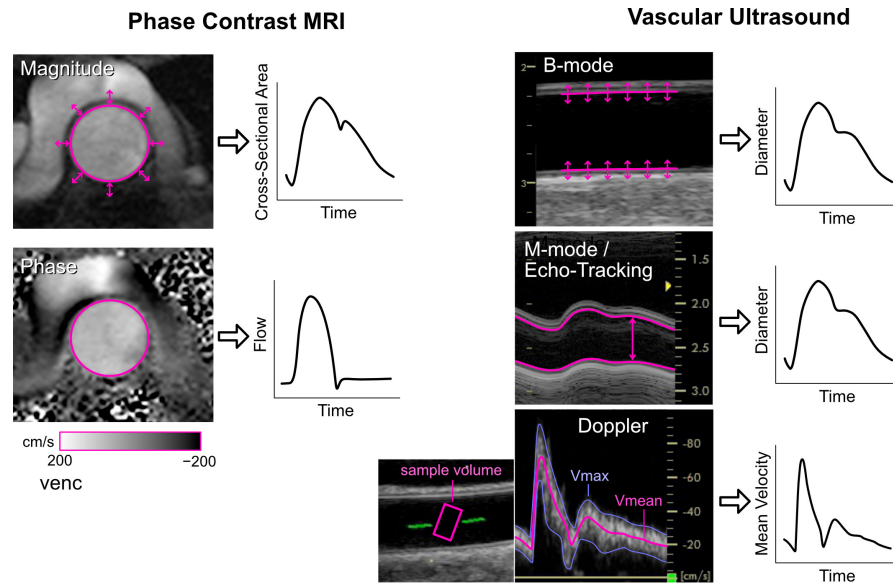


Figure 1.3 – Imaging methods for measuring cross-sectional area or diameter waveforms and flow or mean velocity waveforms. Taken from [29].

[37; 38]. The generalized transfer function constitutes a popular technique for deriving aortic pressure from non-invasively measured peripheral pressure waves, and is employed in several commercial devices. In essence, a transfer function is computed from the ratio of the Fourier transform of the peripheral pressure wave,  $P_p$ , to the Fourier transform of the aortic pressure wave,  $P_{ao}$ , in the frequency domain. For every harmonic, the amplitude of the transfer function is defined as the ratio of amplitudes of the peripheral and aortic pressure wave and the phase of the transfer function as the difference in the phase between the peripheral and aortic pressure. The generalized transfer function is derived from the average of a (large) number of transfer functions measured in a group of human subjects. Importantly, these techniques rely on simplified assumptions which reduce accuracy in predictions, whereas they do not account for the specific arterial tree properties of the subject under consideration [39; 40].

### 1.2.2 Cardiac output

#### Definition and clinical relevance

Cardiac output (CO) is defined as the volume of blood expelled by the heart per unit time. For a healthy adult at rest, CO is approximately 5 liters per minute (L/min). CO, being the main determinant of oxygen transport to the different body regions, must be adapted to the needs of the body at all times; CO exceeds 30 L/min during intense exercise or it can be less than 2 L/min for a patient in circulatory shock. Critically ill patients generally have abnormal oxygen demands as a result of the underlying disease triggering process. Thus, CO monitoring is essential for patient management in the operating room and the intensive care unit (ICU). The

dynamic range suggests that CO is a major indicator of one's hemodynamic state. As a result, the determination of CO in a non-invasive, accurate, and reliable way is of utmost importance.

### State of the art

The most direct and accurate way of measuring CO is to use a flowmeter, which, however, is impractical to perform in humans only for diagnostic purposes. Other methods for acquiring CO include invasive approaches, such as the Fick method and the thermodilution method. The Fick method utilizes a pulmonary artery catheter to measure oxygen consumption by the lungs and the arteriovenous difference in oxygen concentration. CO is calculated by dividing the oxygen consumption of the lungs by the arteriovenous difference in oxygen. The thermodilution method uses a pulmonary artery catheter having a thermistor to measure a decrease in temperature that results from an injection of a bolus of cold fluid into the right atrium. The Stewart-Hamilton conservation of heat equation is then used to compute CO [41]. Although the Fick method and thermodilution are both clinically feasible, they are limited in use due to their invasive nature, as well as their association with increased risk and morbidity in critically ill patients [42].

Other methods of measuring CO include minimally invasive methods such as pulse contour analysis and oesophageal Doppler monitoring [43]. Pulse contour analysis requires the insertion of an arterial catheter at an arterial location, allowing a continuous pulse waveform contour analysis to be performed. Several methods for obtaining CO from a peripheral pressure pulse have been reported in the literature [44; 45; 46]. The oesophageal Doppler technique measures blood flow velocity in the descending aorta utilizing a Doppler transducer placed at the tip of a flexible probe. The probe is introduced into the oesophagus of sedated, mechanically ventilated patients and then rotated so the transducer faces the descending aorta and a characteristic aortic velocity signal is obtained. The CO is calculated as the heart rate multiplied by the stroke volume, where the stroke volume is calculated as a function of the flow velocity and the cross-sectional area of the aorta. The convenience of previously known minimally invasive methods of measuring CO is limited by their invasive nature (catheterization is required), high cost, and the need for specialized equipment or training.

Finally, the most commonly used non-invasive methods for CO are based on pulse wave analysis from the cross-sectional area and blood velocities in the LVOT [47] or directly from MRI-derived aortic flow-time signals [48]. PC-MRI has been considered to be the most precise non-invasive technique for measuring CO [30]. Doppler ultrasound and MRI, while completely non-invasive and reasonably accurate, require the allocation of expensive resources. Importantly, none of the aforementioned methods are practical for continuous bedside monitoring of a patient's CO or routine examination.

### 1.2.3 End-systolic elastance

#### Definition and clinical relevance

Evaluation of systolic left ventricular (LV) performance is of high importance in physiological investigation and clinical practice. An ideal parameter of LV contractility should assess the inotropic state independently of preload, afterload, heart rate, and LV remodelling.

The concept of end-systolic elastance ( $E_{es}$ ), first introduced by Suga and Sagawa in 1974 [49], has become widely accepted. The  $E_{es}$ , i.e. the slope of the end-systolic pressure-volume relationship (ESPVR), constitutes a pivotal determinant of LV systolic performance and is now considered an established index of contractility [49; 50; 51]. Modelling of time-varying elastance can be described using the relationship between the LV pressure,  $P_{LV}$ , and volume,  $V_{LV}$ , namely:

$$E(t) = \frac{P_{LV}(t)}{V_{LV}(t) - V_d}, \quad (1.1)$$

where  $V_d$  indicates the dead volume of the left ventricle [49; 51].

Being an index of the contractility and systolic stiffness of the left ventricle,  $E_{es}$  is affected by the inotropic state of the myocardium and, in the long-term, by geometric remodelling and biophysical myocardial tissue properties (which in turn depend on the stiffness of myocardial cells, fibrosis, and other factors) [52; 53]. The effective matching between  $E_{es}$  and vascular load leads to optimal mechanical function. Age-related arterial stiffening [54] and hypertension [55] are related to the stiffening of the left ventricle, which is accompanied by an increased value of  $E_{es}$ . It has also been shown that anti-hypertensive treatment reduces  $E_{es}$  and enhances arterial-ventricular coupling [56]. Furthermore, the intercept of the ESPVR (namely  $V_d$ ) has been linked with prognosis in chronic heart failure [57].

#### State of the art

Derivation of  $E_{es}$  requires the measurement of multiple invasive pressure-volume loops under various loading conditions [59] which limits its use in the routine clinical setting. Echocardiography is commonly used in the evaluation of LV systolic function and thus in the evaluation of  $E_{es}$ . More recently, new techniques such as tissue Doppler imaging, three-dimensional evaluation, and speckle tracking echocardiography have been proposed for more precisely quantifying LV systolic function [60; 61; 62; 63]. Yet, these methods are technically complex, time-consuming, and user-dependent.

Research has been directed towards the development of methods for deriving  $E_{es}$  from non-invasive single-beat measurements [64; 65]. First, Chen et al. [64] proposed a simple equation

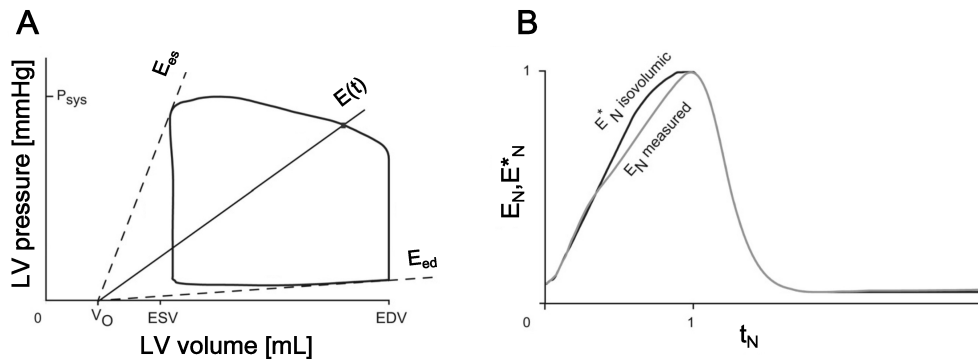


Figure 1.4 – Concept of left ventricular elastance: (A) A heart cycle is presented as a ventricular pressure-volume graph. Instantaneous elastance, end-systolic elastance ( $E_{es}$ ) and end-diastolic elastance ( $E_{ed}$ ) are also presented.  $E_{es}$  intersects the left ventricular (LV) volume axis at the dead volume abscissa ( $V_0$ ). (B) Normalized time varying elastance ( $E_N, E_N^*$ ) as a function of normalized time. EDV: end-diastolic volume, ESV: end systolic volume,  $E(t)$ : time varying elastance,  $P_{sys}$ : systolic pressure. Adapted from [58].

for estimating  $E_{es}$  from arm cuff pressure, stroke volume, and ejection fraction. Their proposed method incorporates an estimated normalized ventricular elastance at arterial end-diastole which was derived from regression on previously recorded studies. Moreover, Shishido et al. [65] suggested the estimation of  $E_{es}$  from pressure values, systolic time intervals, and stroke volume. Their analysis relies on the approximation of the time-varying elastance curve by two linear functions corresponding to the isovolumic contraction phase and the ejection phase. The slope ratio of these functions is calculated and used for estimating  $E_{es}$  by the employment of a simple equation. This methodology evidences the utility of systolic time intervals on the estimation of  $E_{es}$ , while Reant et al. have also emphasized the importance of leveraging the valuable information of systolic time intervals for assessing LV function [66]. Finally, other clinical indices for evaluating the contractile state of the heart include the use of simple equations involving additional quantities, such as arterial elastance, end-systolic volume, or ejection fraction [67]. However, the calculation of ejection fraction as assessed by echocardiography can be rather sensitive to errors and derived approximately. Removal (and replacement) of ejection fraction from the calculation equation could potentially reduce the error imposed by such an approximation.

## 1.2.4 Total arterial compliance

### Definition and clinical relevance

The total arterial compliance ( $C_T$ ) is a biomechanical property of the arterial tree with great physiological and pathological importance [68; 69; 70].  $C_T$  and peripheral resistance constitute

a major part of the arterial load on the heart [11]. Arterial compliance expresses the ability of the arterial system to store blood during systole without excessive pressure rise (Figure 1.5) and influences central blood pressure [47] and stroke volume [71].  $C_T$  is becoming a promising parameter for evaluating the relationship between structural and functional changes in the vascular system with respect to its elasticity [72; 73]. Alterations in arterial compliance are associated with various physiological (aging) [74] or pathological (hypertension) conditions [75], which cannot be necessarily assessed by current biomarkers. Importantly,  $C_T$  has been found to be superior over traditional evaluation techniques including pulse pressure and echocardiography [73; 75]. In addition, other studies have shown that  $C_T$  was proven capable of differentiating among diseased, elderly, and healthy individuals [75; 76; 74]. In view of the emerging evidence on the importance of  $C_T$  [72], the development of an accurate and simple method for its estimation may be valuable.

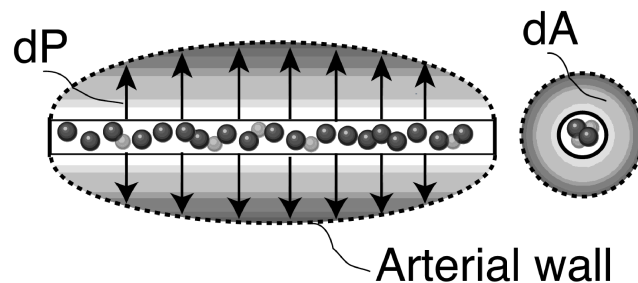


Figure 1.5 – Graphical representation of the concept of compliance being the ability of the arterial walls to distend,  $dA$ , under a given increase in transmural pressure,  $dP$ .

### State of the art

The direct, non-invasive measurement of the  $C_T$  is not feasible due to two inherent difficulties: (i) the absence of no simple way to compute the changes in blood volume in the systemic arterial tree, and (ii) the strong pressure-dependency of arterial compliance that does not allow for the derivation of a single value that can characterize arterial compliance over the whole physiological pressure range. Some direct but traumatic methods for estimating arterial compliance in animals have been reported in the literature [77].

To overcome these limitations, several methods have been proposed for indirect estimation of  $C_T$  [78; 79; 80; 81]. Most commonly, these methods require simultaneous recordings of the invasive aortic pressure and flow waves or cardiac output. Still, the complexity of these methods has limited the assessment of  $C_T$  in everyday clinical practice, while other surrogates of local or regional arterial stiffness [82; 83] have been used more often.

Some well-established methods for estimating  $C_T$  include the diastolic decay method, the area method, and the pulse pressure method [81; 78]. The decay time method is based on the



two-element Windkessel model of systemic circulation. Its principle is that during diastole there is no inflow from the heart, and thus, the decrease of aortic pressure, is characterized by the decay time. This decay can be fitted mono-exponentially to any portion of the diastole to yield the characteristic time or time constant, which is  $RC_T$ . The  $C_T$  can be then calculated for a known value of peripheral resistance ( $R$ ).

The area method was introduced by Randall [84]. It essentially represents an integral variation of the exponential decay method. The advantage is that no exponential fit is necessary. Compliance is calculated from

$$RC_T = \int_{t_1}^{t_2} P dx / (P_1 - P_2), \quad (1.2)$$

where  $P_1$  and  $P_2$  are diastolic pressure at time points  $t_1$  and  $t_2$ , respectively.

Moreover, the pulse pressure method (PPM) [80] is based on the fact that the modulus of the input impedance of the arterial system is represented very well by the two-element Windkessel model for the low frequencies (1<sup>st</sup> to 5<sup>th</sup> harmonic). Therefore, the pulse pressure will be similar in the true arterial system and the two-element Windkessel model. The PPM uses an iterative process that yields the value of  $C_T$  that gives the best fit between the measured pulse pressure and the pulse pressure predicted by the two-element Windkessels model.

### 1.2.5 Aortic characteristic impedance

#### Definition and clinical relevance

The impedance can be defined as the ratio of the pulsatile components of pressure and flow (Figure 1.6). The impedance computed in the ascending aorta is termed input impedance ( $Z_{in}$ ) and is a global systemic parameter, which encompasses all effects of wave travel and reflections of all contributions of the distal parts of the arterial tree. The aortic  $Z_{in}$  constitutes the afterload of the heart. In the special case that the system is free of reflections,  $Z_{in}$  reduces to  $Z_{ao}$ . The  $Z_{ao}$  is a cardinal parameter related to aortic stiffness and geometry. The prior art has included invasive [85; 86; 87; 88; 89; 90; 91; 92; 93; 94] and non-invasive [47; 93; 95] techniques for estimating  $Z_{ao}$  in the frequency domain, whereby  $Z_{ao}$  is approximated as the average  $Z_{in}$  in the mid-to-high frequency range, the underlying assumption being that in those frequencies the effects of reflected waves are minimal. Other approaches have proposed time-domain calculations of the  $Z_{ao}$  based on the early systolic part of pressure and flow waveforms [91; 94; 96; 97; 98], when reflections are considered negligible. All of the above frequency and time domain methods require simultaneous recordings of pressure and flow in the aorta, which are invasive (pressure) or inconvenient and expensive (flow).

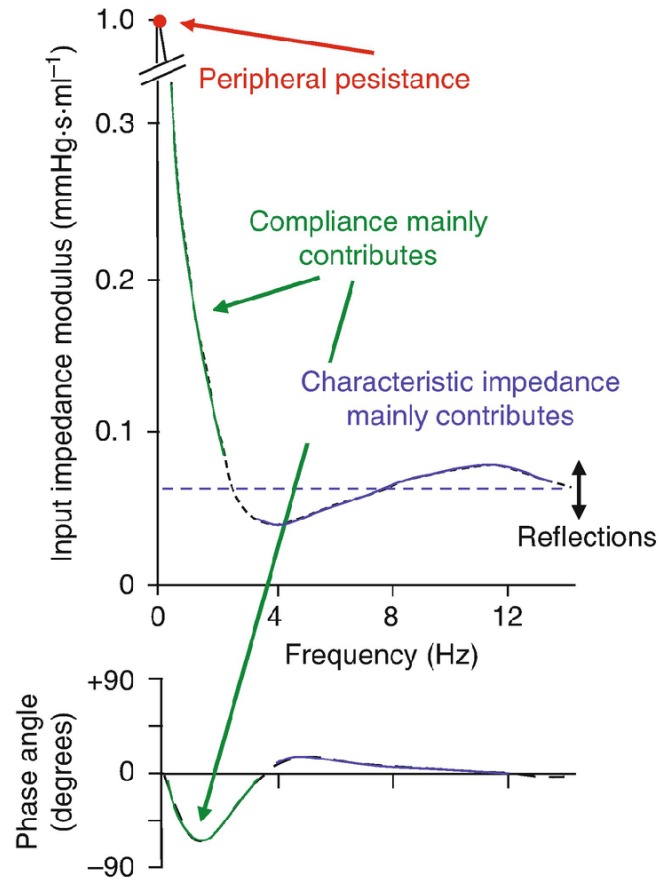


Figure 1.6 – Graphical representation of the magnitude and phase of arterial input impedance. Taken from [99].

**State of the art**

Existing non-invasive methods for estimating  $Z_{ao}$  rely on pressure, flow, and geometry measurements. Following the area compliance and geometry method, the characteristic impedance at the root of the ascending aorta is calculated analytically using the area compliance and the geometry of the ascending aorta, namely:

$$Z_{ao} = \sqrt{\frac{\rho}{A} \frac{1}{C_A}} \tag{1.3}$$

where  $\rho$  is the blood density equal to  $1050 \text{ kg/m}^3$ ,  $A$  is the cross-sectional area of the ascending aorta, and  $C_A$  is the area compliance of the ascending aorta, respectively. Another method relies on the wave speed and geometry, and calculate  $Z_{ao}$  as follows:

$$Z_{ao} = \frac{\rho c}{A} \tag{1.4}$$

## Chapter 1. Introduction

---

with  $\rho$  blood density,  $c$  the local pulse wave velocity, and  $A$  the luminal cross-sectional area.

Another commonly used approach is the frequency-based method which computes the characteristic impedance of large vessels by averaging the modulus of the input impedance between the fourth and tenth harmonic. The  $Z_{ao}$  can also be determined by taking the slopes of the aortic pressure and flow waves during the early part of the ejection period,  $\Delta P$  and  $\Delta Q$ , and calculating their ratio:

$$Z_{ao} = \frac{\Delta P}{\Delta t} \frac{\Delta Q}{\Delta t}. \quad (1.5)$$

Both methods rely on the fact that characteristic impedance is a pressure-flow relation in the absence of reflections (as reflections are small in early systole and at high frequencies).

Finally, some simplified formulas have been introduced for estimating  $Z_{ao}$ . The time-derivative peaks method suggests the following:

$$Z_{ao} = \frac{P'_{max}}{Q'_{max}}, \quad (1.6)$$

where  $P'_{max}$  and  $Q'_{max}$  are the maximum values of the pressure and flow time derivatives, respectively. Finally, the peak flow method estimates  $Z_{ao}$  as follows:

$$Z_{ao} = \frac{(P_{Qmax} - aDBP)}{Q_{max}}, \quad (1.7)$$

where  $aDBP$  is the aortic DBP,  $Q_{max}$  is the maximum flow value, and  $P_{Qmax}$  is the aortic pressure magnitude at the maximum flow value [91].

The use of all aforementioned methods is hampered by the need for either invasive or inconvenient and expensive methods to access simultaneous recordings of aortic pressure and flow, wall thickness, and cross-sectional area.

### 1.2.6 Arterial stiffness

The beating heart is the powerhouse of the cardiovascular system. With each heartbeat, the vasculature dilates to accommodate the additional blood volume that is ejected from the ventricles into the aorta and the pulmonary artery. The increase in pressure associated with vascular dilation is determined by the tension in the arterial wall, which in turn is determined by the properties affecting the distensibility of the vessel [100]. The proximal pressure pulse generated by ventricular ejection travels across the vasculature, at a velocity determined by arterial geometry and mechanical properties, but also by blood pressure and vascular tone.

Pulse wave velocity (PWV), defined as the propagation speed of the pulse wave through the circulatory system, is gaining increasing interest in the clinical assessment of arterial stiffness [101]. This is mainly attributed to a huge body of clinical evidence that has recognized PWV being an independent predictor of cardiovascular and all-cause mortality as well as a pivotal factor on the prognosis of hypertension [101; 102; 103; 104]. Measurement of carotid-femoral PWV (cfPWV) is considered as the gold-standard non-invasive method for the assessment of aortic stiffness [101], and can be readily performed by several non-invasive techniques and devices. Its acquisition requires the distance between the two arterial sites and the time lag between the two pulses (as assessed via the foot-to-foot methods) [105], as illustrated in Figure 1.7.

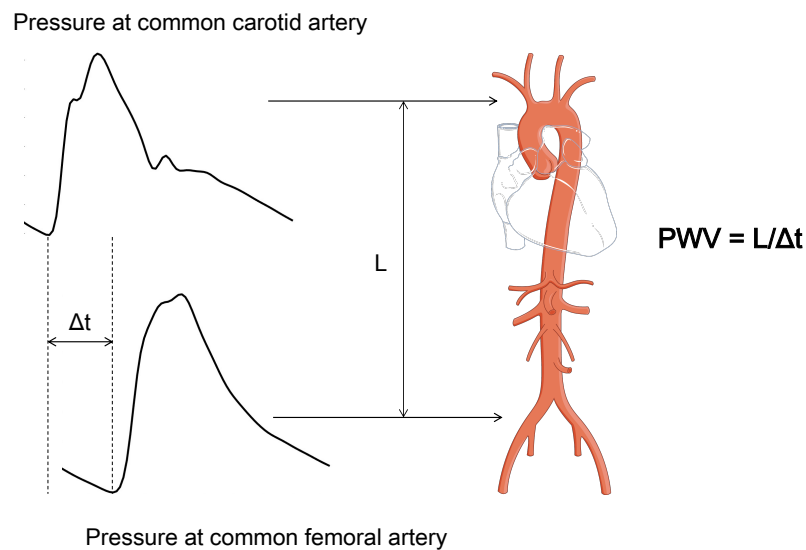


Figure 1.7 – Conventional foot-to-foot computation of the carotid-femoral pulse wave velocity (PWV).  $\Delta t$ : the pulse transition time between the two arterial sites,  $L$ : pulse wave travel distance between the two arterial sites.

An increased variation in sequential cfPWV measurements may be often observed [106], due to inherent physiological vascular and hemodynamic variations or/and measurement errors. Although age and blood pressure are two well-established determinants of PWV, the influence of heart rate (HR) on PWV remains controversial with conflicting results being observed in both acute and epidemiological studies [107].

Cross-sectional population studies have demonstrated either no significant correlation [108] or a positive correlation between cfPWV and resting HR [109; 110]. Albaladejo et al. [108] reported that there is no significant rise in cfPWV when HR is increased. On the contrary, Lantelme et al. [110] demonstrated that HR is an important factor of the intra-patient cfPWV changes in the elderly. Nevertheless, those studies have investigated the potential effect of

HR on cfPWV without isolating the effect of the concurrent increase in blood pressure with increasing HR. Arterial stiffness is known to increase with increasing blood pressure [111]. In particular, foot-to-foot cfPWV has been theoretically and empirically shown to vary with diastolic blood pressure [7; 112; 113].

In addition, results from existing acute experimental studies have been also inconclusive [110]. Further to the lack of consensus on the effects of HR on PWV, the possible mechanisms contributing to observed PWV changes with HR need to be fully elucidated; yet, many investigators have attributed HR-related changes in arterial stiffness to the viscoelasticity of the arterial wall. With elevated HR being associated with hypertension as well as being an independent prognostic factor of cardiovascular disease, the interaction between HR and PWV continues to be relevant in assessing cardiovascular risk.

The aforementioned evidence concludes that it is critical to investigate more thoroughly the blood pressure-independent cfPWV-HR relation; especially, now, that the clinical use of cfPWV is increasing [114; 115; 116].

### 1.3 Numerical models of the cardiovascular system

Models of the cardiovascular system aim to disentangle the functioning of the cardiovascular system via the mathematical analysis and computational simulations of pulsatile hemodynamics (i.e. the dynamics of pulsatile blood flow). Cardiovascular models can be used to understand the physiological basis underlying measured outcomes, predict the effect of vascular ageing and pathophysiology on cardiovascular properties, and study the effect of treatment and interventions to address vascular ageing.

There exist three main modelling approaches: three-dimensional (3-D), one-dimensional (1-D), and zero-dimensional (0-D) models. They can all describe time-varying blood pressure and flow in the cardiovascular system, but with a different degree of precision in space. More specifically, 3-D models consider changes in pressure and flow in the three-dimensional space, 1-D models account for the variation of pressure and flow only along the axial direction of the arteries, and 0-D models are space-independent. The choice of dimensionality in modelling the cardiovascular system is dictated by the scope and the precision required in the performed study.

Lumped parameter (0-D) models involve the assumption of uniform distributions of pressure, flow, and volume within any compartment of the model (vessel or part of vessel) at any instant in time, while in higher dimensional models these parameters can vary spatially [117]. The Windkessel models [118] offer an overall description of the arterial network, but they do not allow for studying pressure and flow wave propagation phenomena in the arterial tree. On the other hand, such an aim can be fulfilled by distributed models which take into account the

### 1.3. Numerical models of the cardiovascular system

---

arterial geometry. The principle behind distributed models is that they discretize the arterial vasculature in small segments with known mechanical and geometrical properties. The wave transmission characteristics of each arterial segment can be described using Womersley's oscillatory flow theory [119].

In distributed models of the arterial tree, the 1-D form of the blood flow equations describing the conservation of mass and momentum is given as:

$$\frac{\partial Q}{\partial x} + \frac{\partial A}{\partial t} = 0 \quad (1.8)$$

$$\frac{\partial Q}{\partial t} + \frac{\partial(Q^2/A)}{\partial x} = -\frac{1}{\rho} A \cdot \frac{\partial P}{\partial x} - 2\pi r_i \cdot \frac{\tau}{\rho} \quad (1.9)$$

where  $A$  is the vessel cross-sectional area and  $\tau$  is wall shear stress, usually estimated using Poiseuille's law. The two equations above have three variables: pressure  $P$ , flow  $Q$ , and area  $A$ . Therefore a constitutive law relating cross-sectional area,  $A$ , to pressure,  $P$ , is needed to form a system of three equations with three unknowns, which can be then easily solved using different numerical techniques (e.g. finite differences).

Distributed 1-D models of the arterial tree have attracted great interest due to the increasing impact of cardiovascular disease. They have provided a valuable alternative for simulating wave propagation either in parts or the entire human arterial network, under various physiological or pathological conditions [120; 121; 122; 58; 123] which are difficult to study *in vivo*. These models are fairly accurate and compare well to human measurements of flow and pressure. Moreover, they allow for the preliminary evaluation of predictive models across a wide range of cardiovascular parameters [117] in a quick and cost-efficient way, while their results can be rather informative of the design of clinical studies [124; 125].

Previous works have introduced a plethora of 1-D models with substantial variations in many aspects such as the incorporation (or not) of a heart left ventricular (LV) model (essential for grasping ventricular-vascular coupling effects), inclusion (or not) of cerebral and/or coronary circulation, formulations for the viscoelasticity of the aortic wall, approximations for wall shear stress and convective acceleration term and boundary conditions at terminal sites [58].

In this thesis, we used the model previously developed and validated by Reymond et al. [58; 127]. This valuable computational tool permitted the development and validation of monitoring methods designed in this thesis, by providing a controlled *in silico* environment where the actual entire hemodynamical profile is known. In addition, it allowed us to generate large datasets which are particularly useful for the training and testing of machine learning algorithms.

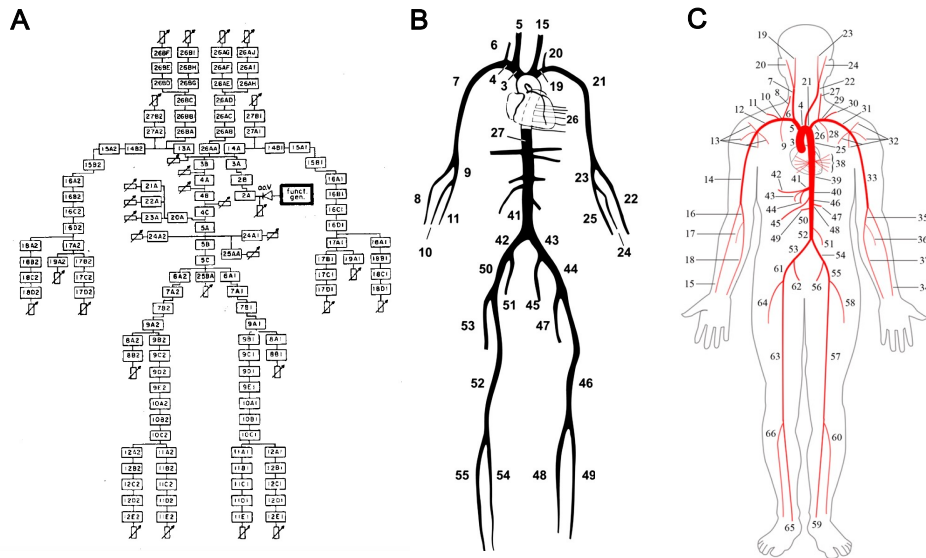


Figure 1.8 – Evolution of 1-D arterial tree models over the passage of time: (A) Westerhof's model in 1969 [126], (B) Reymond's model in 2009 [58], (C) Mynard's model in 2015 [123].

## 1.4 Machine learning framework

### 1.4.1 Supervised learning

In clinical practice, diagnosis of disease or pathology is performed by means of tests, examinations or other procedures that can be applied rapidly and easily to the target population. Sensu lato, these tests can be formulated as a form of mapping  $f: X \rightarrow Y$ , where  $X$  is an input information space and  $Y$  is the output of the test. Importantly, when a clinician conducts an examination, he/she uses the available or measured data and performs the mapping based on the knowledge that he/she has acquired from domain expertise and experience. This process allows him/her for reaching a clinical decision regarding the medical state of the subject under consideration. Nevertheless, in the majority of medical cases, determining the mapping function  $f$  for achieving effective diagnosis is not a trivial task.

Recent advancements in computer systems and measurement techniques have allowed for the acquisition and analysis of high-fidelity data. In addition, the increase in computational power, storage, memory, and the generation of staggering volumes of data have permitted computers to perform a wide-range of complex tasks with impressive accuracy [128]. All the above have created an area full of promise for the development of novel biomedical tools which can assist clinical decision-making.

Supervised learning refers to methods in which a model is trained on a range of inputs (or features) which are associated with a known outcome. Once the model is successfully trained,

it is capable of making outcome predictions when applied to new data. Predictions which are made by models trained using supervised learning can be either discrete (e.g. positive or negative, benign or malignant) or continuous (e.g. a score from 0 to 100). The supervised learning techniques that yield a discrete prediction are known as classification techniques, whereas those techniques that predict a continuous outcome are called regression techniques.

The methods developed in this thesis employ regression models. In regression analysis, we assume a training dataset of  $N$  examples  $(x_1, y_1), \dots, (x_N, y_N)$ . We consider some particular regression problems for which we need to relate some specific parameters (input features) to a clinical continuous variable (output). A loss function  $L(\hat{y}, y)$ , that measures the discrepancy between the model predictions [namely  $\hat{y}_i = f(x_i)$ ] and the actual outcome instance ( $y_i$ ) is selected. The most common loss function in a regression setting is the (squared) difference between the target and the predicted value, namely  $L(\hat{y}, y) = (\hat{y} - y)^2$ .

In supervised learning, the aim is to find the function  $f^*$  that minimizes the expected loss over the data generating distribution  $D$ . Therefore, the learned mapping allows for establishing a system which can be used to map de novo elements of  $X$  to  $Y$ . The expected loss can be approximated by averaging the loss over the available training data:

$$f \approx \operatorname{argmin} \frac{1}{N} \sum L(f(x_i), y_i) \quad (1.10)$$

The performance of a regression model is usually assessed using either cross-validation or external validation methods. Cross-validation, or  $k$ -fold cross-validation, refers to the validation technique where the dataset is partitioned in  $k$  subsets. The  $k-1$  subsets are used for the training and the remaining left-out subset is used for the testing [129]. This technique helps overcome issues, such as selection bias or overfitting with the model. However, the model performance needs to be tested for heterogeneity, which is followed through with external validation. The use of independent datasets allows proper assessment of whether a model can be generalised to populations outside of the study data [130].

Learning curves are a well-established diagnostic tool for regression methods that learn from a training dataset incrementally. The model can be evaluated on the training dataset and on a hold-out validation dataset after each update during training and plots of the measured performance can be created to show learning curves. Reviewing learning curves of models during training can be used to diagnose problems with learning, such as an underfit or overfit model, as well as whether the training and validation datasets are suitably representative.

In regression problems, the performance of machine learning methods is often assessed using the correlation between estimated and reference parameter values. The limits of agreement technique (also known as Bland-Altman analysis [131]) is also used. This technique quantifies the accuracy of the predictive model in comparison to the reference method using the bias



(mean error) and limits of agreement (twice the standard deviation of the errors). The limits of agreement technique is preferred for assessing agreement between two methods since correlation coefficients can be misleading in this context. Additional measures include the root mean square error (RMSE), normalized RMSE, mean absolute error (MAE) or others.

This thesis uses a multitude of regression pipelines (different combinations of regression models and features) as well as evaluation metrics. The detailed description of the machine learning methods can be found in the literature [132; 133; 134; 135; 136; 137; 138].

### 1.4.2 Application in cardiovascular medicine

The booming of data has led to efforts of developing new biomedical tools using artificial intelligence. Artificial intelligence plays a major role in the revolution in medicine by providing systems with the capacity to learn and improve from experience without explicit human intercession. In addition, recent technological advances have spurred an abundance of “big data” in healthcare [139]. Machine learning algorithms, including deep learning algorithms [140], are being used increasingly due to their flexible nature in evaluating large datasets without the need for specified assumptions.

A large amount of biomedical and clinical data is routinely collected which is suitable for training machine learning models to assess health in humans. In relation to pathophysiology, the advancement in measuring and imaging techniques has encouraged the employment of machine learning for estimating clinical pathophysiological indices and validating their results. This promising area of research could not exclude applications on cardiovascular health [141; 142; 143; 144]. A multitude of previous examples exists in the literature, including applications of multiple linear regression for estimating PWV from age and routine blood pressure measurements [145; 146], and neural networks to estimate aortic blood pressure from radial blood pressure [142].

Arterial pulse wave signals can be acquired in the clinical setting using, for instance, applanation tonometry and ultrasound systems. Concurrently, signals such as the electrocardiogram (ECG) and photoplethysmogram (PPG) can be obtained using consumer devices such as smartphones and fitness trackers. In addition, images of the cardiovascular system and affected organs can be acquired by ultrasound, MRI, and computed tomography, resulting in improved visual assessment of functional and structural changes associated with disease and pathology. Importantly, the complexity of the new, available data often renders traditional statistical methods insufficient to efficiently develop predictive tools to assist clinical decision-making. In contrast, machine learning offers promise for developing methods to improve and automate cardiovascular health assessment, and to guide therapeutic interventions.

Moreover, machine learning-based techniques for assessing vascular age have the potential to improve the accessibility of vascular age assessment. Currently, blood pressure is the only

biomarker of vascular age that is routinely measured in primary care. A notable number of issues limit the use of other markers of vascular ageing [147]. Machine learning-based techniques are now being developed which could be used in primary care with the minimal additional workload, such as using routinely collected clinical data to estimate central hemodynamical quantities and cardiac indices. Thus, machine learning-based techniques have potential to improve the accessibility of vascular age assessment (Figure 1.9).

This thesis emphasizes on the clinical utility of machine learning for assessing vascular ageing via its application for estimating key cardiovascular parameters.

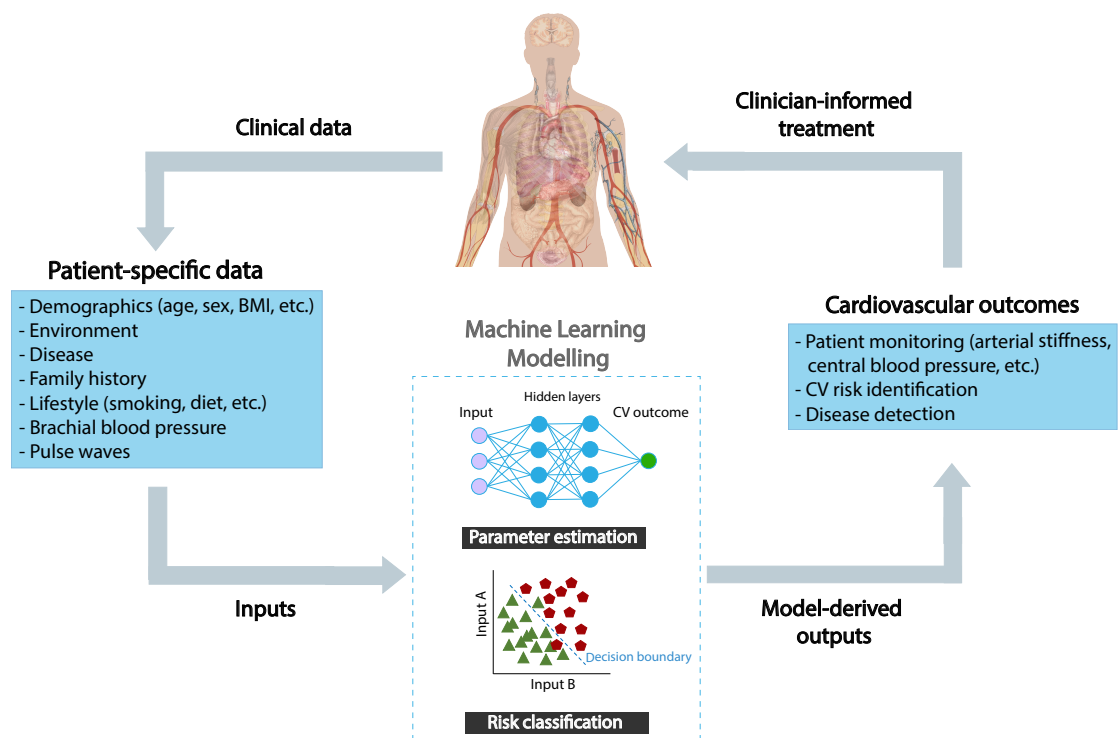


Figure 1.9 – Machine learning applications in the assessment of vascular ageing. Adapted from [148].

## 1.5 Thesis aims

The overall objective of this thesis was to develop and validate original non-invasive methods for the estimation of cardiovascular biomarkers by leveraging the simulation capacity of a physics-based model of the cardiovascular system and artificial intelligence. The research presented in this thesis aims to achieve the following:

- To develop novel monitoring tools for central hemodynamics (i.e. aSBP and CO) and cardiac contractility (i.e. LV  $E_{e,s}$ ) using easily obtained non-invasive measurements.

## Chapter 1. Introduction

---

- To improve assessment of local and global arterial elasticity (i.e.  $Z_{ao}$  and  $C_T$ ) via the development of machine learning-based estimation methods.
- To study the intrinsic effect of heart rate on arterial stiffness as assessed by the cfPWV measurement.
- To evaluate the performance of the methods on large sets of both clinical and in silico data.

### 1.6 Thesis outline

This thesis is structured as follows. Chapter 2 introduces a novel inverse problem-solving method for estimating aSBP and CO. Chapter 3 presents a study of the performance of the inverse method for estimating SV using an MRI protocol, culminating in the conclusion that our algorithm performs well in a large cohort of healthy individuals. Moreover, in Chapter 3, we wish to verify whether physics-based models provide an additional value over the traditional statistical approaches. In Chapter 4, an alternative predictive model is adopted for the estimation of central hemodynamics and cardiac contractility using machine learning. Chapter 5 presents an artificial intelligence-based technique for LV  $E_{es}$  using non-invasive systolic timing features. Chapter 6 aims to investigate the utility of peripheral blood pressure waves in the prediction of the contractile state of the heart by deciphering relevant hidden morphology-based information in the waves using deep learning. The next goal arises from the need to monitor the hemodynamic condition in humans is the evaluation of the arterial elastic properties. In Chapter 7, we develop machine learning models for predicting  $Z_{ao}$  and  $C_T$  by leveraging the informative and easily obtained regional pulse wave velocity measurements. We additionally investigate the accuracy in determining  $C_T$  by exploiting the entire peripheral blood pressure wave (Chapter 8). To complement the research for the assessment of arterial stiffness, in Chapter 9 we aim to answer the research question that emerged in the Introduction of this thesis (section 1.2.6): *Is the PWV measurement independent on changes in HR?*. Consequently, we evaluate the effect of HR on PWV under controlled hemodynamic conditions and especially with respect to blood pressure that is a strong determinant of arterial stiffness. Finally, Chapter 10 presents a summary of the achievements of this thesis, and directions for future work.

The chapters of this dissertation are written as manuscripts that are either published or in preparation for publication.

## Bibliography

- [1] W. H. Organization, "Global action plan for the prevention and control of noncommunicable diseases 2013–2020," 2013.
- [2] P. McAleese and W. Odling-Smee, "The effect of complications on length of stay," *Annals of Surgery*, vol. 220, no. 6, pp. 740–744, Dec. 1994.
- [3] N. A. Khan, H. Quan, J. M. Bugar, J. B. Lemaire, R. Brant, and W. A. Ghali, "Association of postoperative complications with hospital costs and length of stay in a tertiary care center," *Journal of General Internal Medicine*, vol. 21, no. 2, pp. 177–180, Feb. 2006.
- [4] R. J. Lagoe, P. E. Johnson, and M. P. Murphy, "Inpatient hospital complications and lengths of stay: a short report," *BMC research notes*, vol. 4, p. 135, May 2011.
- [5] N. Savji, C. B. Rockman, A. H. Skolnick, Y. Guo, M. A. Adelman, T. Riles, and J. S. Berger, "Association between advanced age and vascular disease in different arterial territories: a population database of over 3.6 million subjects," *Journal of the American College of Cardiology*, vol. 61, no. 16, pp. 1736–1743, Apr. 2013.
- [6] M. R. Hamczyk, R. M. Nevado, A. Baretino, V. Fuster, and V. Andrés, "Biological versus chronological aging," *Journal of the American College of Cardiology*, vol. 75, no. 8, pp. 919–930, Mar. 2020. [Online]. Available: <https://linkinghub.elsevier.com/retrieve/pii/S0735109720300711>
- [7] W. W. Nichols, M. F. O'Rourke, and C. Vlachopoulos, *McDonald's blood flow In arteries*, 6th ed. London: Arnold, 2011.
- [8] H.-K. Yip, C.-J. Wu, H.-W. Chang, C.-H. Yang, T.-H. Yu, Y.-H. Chen, and C.-L. Hang, "Prognostic value of circulating levels of endothelin-1 in patients after acute myocardial infarction undergoing primary coronary angioplasty," *Chest*, vol. 127, no. 5, pp. 1491–1497, May 2005.
- [9] C. Di Gennaro, A. Biggi, A. L. Barilli, E. Fasoli, N. Carra, A. Novarini, R. Delsignore, and A. Montanari, "Endothelial dysfunction and cardiovascular risk profile in long-term withdrawing alcoholics," *Journal of Hypertension*, vol. 25, no. 2, pp. 367–373, Feb. 2007.

## Bibliography

---

- [10] W. Koenig, "Update on integrated biomarkers for assessment of long-term risk of cardiovascular complications in initially healthy subjects and patients with manifest atherosclerosis," *Annals of Medicine*, vol. 41, no. 5, pp. 332–343, 2009.
- [11] G. Elzinga and N. Westerhof, "Pressure and flow generated by the left ventricle against different impedances," *Circulation Research*, vol. 32, no. 2, pp. 178–186, Feb. 1973. [Online]. Available: <https://www.ahajournals.org/doi/10.1161/01.RES.32.2.178>
- [12] T. K. Waddell, A. M. Dart, T. L. Medley, J. D. Cameron, and B. A. Kingwell, "Carotid pressure is a better predictor of coronary artery disease severity than brachial pressure," *Hypertension (Dallas, Tex.: 1979)*, vol. 38, no. 4, pp. 927–931, Oct. 2001.
- [13] M. E. Safar, J. Blacher, B. Pannier, A. P. Guerin, S. J. Marchais, P.-M. Guyonvarc'h, and G. M. London, "Central pulse pressure and mortality in end-stage renal disease," *Hypertension (Dallas, Tex.: 1979)*, vol. 39, no. 3, pp. 735–738, Mar. 2002.
- [14] H. Berkenstadt, N. Margalit, M. Hadani, Z. Friedman, E. Segal, Y. Villa, and A. Perel, "Stroke volume variation as a predictor of fluid responsiveness in patients undergoing brain surgery," *Anesthesia & Analgesia*, vol. 92, no. 4, pp. 984–989, Apr. 2001. [Online]. Available: <https://insights.ovid.com/crossref?an=00000539-200104000-00034>
- [15] M. McKendry, H. McGloin, D. Saberi, L. Caudwell, A. R. Brady, and M. Singer, "Randomised controlled trial assessing the impact of a nurse delivered, flow monitored protocol for optimisation of circulatory status after cardiac surgery," *BMJ*, vol. 329, no. 7460, p. 258, Jul. 2004. [Online]. Available: <http://www.bmj.com/lookup/doi/10.1136/bmj.38156.767118.7C>
- [16] N. Lees, M. Hamilton, and A. Rhodes, "Clinical review: goal-directed therapy in high risk surgical patients," *Critical Care*, vol. 13, no. 5, p. 231, 2009. [Online]. Available: <https://www.ncbi.nlm.nih.gov/pmc/articles/PMC2784362/>
- [17] A. Avolio, "Central aortic blood pressure and cardiovascular risk: a paradigm shift?" *Hypertension (Dallas, Tex.: 1979)*, vol. 51, no. 6, pp. 1470–1471, Jun. 2008.
- [18] L. Yang, B. Qin, X. Zhang, Y. Chen, and J. Hou, "Association of central blood pressure and cardiovascular diseases in diabetic patients with hypertension," *Medicine*, vol. 96, no. 42, Oct. 2017. [Online]. Available: <https://www.ncbi.nlm.nih.gov/pmc/articles/PMC5662393/>
- [19] A. Song-Tao, Q. Yan-Yan, and W. Li-Xia, "The severity of coronary artery disease evaluated by central systolic pressure and fractional diastolic pressure," *North American Journal of Medical Sciences*, vol. 2, no. 5, pp. 218–220, May 2010. [Online]. Available: <https://www.ncbi.nlm.nih.gov/pmc/articles/PMC3347647/>

- [20] K. E. Covinsky, R. M. Palmer, R. H. Fortinsky, S. R. Counsell, A. L. Stewart, D. Kresevic, C. J. Burant, and C. S. Landefeld, "Loss of independence in activities of daily living in older adults hospitalized with medical illnesses: increased vulnerability with age," *Journal of the American Geriatrics Society*, vol. 51, no. 4, pp. 451–458, Apr. 2003.
- [21] W. C. Shoemaker, H. Belzberg, C. C. Wo, D. P. Milzman, M. D. Pasquale, L. Baga, M. A. Fuss, G. J. Fulda, K. Yarbrough, J. P. Van DeWater, P. J. Ferraro, D. Thangathurai, P. Roffey, G. Velmahos, J. A. Murray, J. A. Asensio, K. ElTawil, W. R. Dougherty, M. J. Sullivan, R. S. Patil, J. Adibi, C. B. James, and D. Demetriades, "Multicenter study of noninvasive monitoring systems as alternatives to invasive monitoring of acutely ill emergency patients," *Chest*, vol. 114, no. 6, pp. 1643–1652, Dec. 1998.
- [22] J. C. Chaney and S. Derdak, "Minimally invasive hemodynamic monitoring for the intensivist: current and emerging technology," *Critical Care Medicine*, vol. 30, no. 10, pp. 2338–2345, Oct. 2002.
- [23] T. G. Papaioannou, A. D. Protopogerou, K. S. Stamatelopoulos, M. Vavuranakis, and C. Stefanadis, "Non-invasive methods and techniques for central blood pressure estimation: procedures, validation, reproducibility and limitations," *Current Pharmaceutical Design*, vol. 15, no. 3, pp. 245–253, 2009.
- [24] R. Kelly, C. Hayward, A. Avolio, and M. O'Rourke, "Noninvasive determination of age-related changes in the human arterial pulse," *Circulation*, vol. 80, no. 6, pp. 1652–1659, Dec. 1989.
- [25] G. M. Drzewiecki, J. Melbin, and A. Noordergraaf, "Arterial tonometry: review and analysis," *Journal of Biomechanics*, vol. 16, no. 2, pp. 141–152, 1983.
- [26] F. Verbeke, P. Segers, S. Heireman, R. Vanholder, P. Verdonck, and L. M. Van Bortel, "Non-invasive assessment of local pulse pressure: importance of brachial-to-radial pressure amplification," *Hypertension (Dallas, Tex.: 1979)*, vol. 46, no. 1, pp. 244–248, Jul. 2005.
- [27] D. S. Picone, M. G. Schultz, P. Otahal, S. Aakhus, A. M. Al-Jumaily, J. A. Black, W. J. Bos, J. B. Chambers, C.-H. Chen, H.-M. Cheng, A. Cremer, J. E. Davies, N. Dwyer, B. A. Gould, A. D. Hughes, P. S. Lacy, E. Laugesen, F. Liang, R. Melamed, S. Muecke, N. Ohte, S. Okada, S. Omboni, C. Ott, X. Peng, T. Pereira, G. Pucci, R. Rajani, P. Roberts-Thomson, N. B. Rossen, D. Sueta, M. D. Sinha, R. E. Schmieder, H. Smulyan, V. K. Srikanth, R. Stewart, G. A. Stouffer, K. Takazawa, J. Wang, B. E. Westerhof, F. Weber, T. Weber, B. Williams, H. Yamada, E. Yamamoto, and J. E. Sharman, "Accuracy of Cuff-Measured Blood Pressure: Systematic Reviews and Meta-Analyses," *Journal of the American College of Cardiology*, vol. 70, no. 5, pp. 572–586, Aug. 2017.
- [28] D. J. F. M. Thuijs, M. W. A. Bekker, D. P. Taggart, A. P. Kappetein, T. M. Kieser, D. Wendt, G. Di Giammarco, G. D. Trachiotis, J. D. Puskas, and S. J. Head,

## Bibliography

---

- “Improving coronary artery bypass grafting: a systematic review and meta-analysis on the impact of adopting transit-time flow measurement,” *European Journal of Cardio-Thoracic Surgery*, vol. 56, no. 4, pp. 654–663, Oct. 2019. [Online]. Available: <https://academic.oup.com/ejcts/article/56/4/654/5419275>
- [29] J. P. Mynard, A. Kondiboyina, R. Kowalski, M. M. Cheung, and J. J. Smolich, “Measurement, analysis and interpretation of pressure/flow waves in blood vessels,” *Frontiers in Physiology*, vol. 11, p. 1085, 2020.
- [30] N. Pelc, R. Herfkens, A. Shimakawa, and D. Enzmann, “Phase contrast cine magnetic resonance imaging,” *Magnetic resonance quarterly*, vol. 7, no. 4, pp. 229–254, Oct. 1991. [Online]. Available: <http://europepmc.org/abstract/MED/1790111>
- [31] N. Ohte, T. Saeki, H. Miyabe, S. Sakata, S. Mukai, J. Hayano, K. Niki, M. Sugawara, and G. Kimura, “Relationship between blood pressure obtained from the upper arm with a cuff-type sphygmomanometer and central blood pressure measured with a catheter-tipped micromanometer,” *Heart and Vessels*, vol. 22, no. 6, pp. 410–415, Nov. 2007.
- [32] A. L. Pauca, M. F. O’Rourke, and N. D. Kon, “Prospective evaluation of a method for estimating ascending aortic pressure from the radial artery pressure waveform,” *Hypertension (Dallas, Tex.: 1979)*, vol. 38, no. 4, pp. 932–937, Oct. 2001.
- [33] E. J. Kroeker and E. H. Wood, “Comparison of simultaneously recorded central and peripheral arterial pressure pulses during rest, exercise and tilted position in man,” *Circulation Research*, vol. 3, no. 6, pp. 623–632, Nov. 1955.
- [34] S. A. Hope, D. B. Tay, I. T. Meredith, and J. D. Cameron, “Use of arterial transfer functions for the derivation of aortic waveform characteristics,” *Journal of Hypertension*, vol. 21, no. 7, pp. 1299–1305, Jul. 2003.
- [35] W. J. Stok, B. E. Westerhof, and J. M. Karemaker, “Changes in finger-aorta pressure transfer function during and after exercise,” *Journal of Applied Physiology*, vol. 101, no. 4, pp. 1207–1214, Oct. 2006. [Online]. Available: <http://www.physiology.org/doi/10.1152/jappphysiol.00876.2005>
- [36] B. Fetics, E. Nevo, C.-H. Chen, and D. M. Kass, “Parametric model derivation of transfer function for noninvasive estimation of aortic pressure by radial tonometry,” *IEEE Transactions on Biomedical Engineering*, vol. 46, pp. 698–706, 1999.
- [37] M. Karamanoglu, M. F. O’Rourke, A. P. Avolio, and R. P. Kelly, “An analysis of the relationship between central aortic and peripheral upper limb pressure waves in man,” *European Heart Journal*, vol. 14, no. 2, pp. 160–167, Feb. 1993.
- [38] M. Sugimachi, T. Shishido, K. Miyatake, and K. Sunagawa, “A new model-based method of reconstructing central aortic pressure from peripheral arterial pressure,” *The Japanese Journal of Physiology*, vol. 51, no. 2, pp. 217–222, Apr. 2001.

- [39] A. C. Guyton and J. E. Hall, *Textbook of medical physiology*, 9th ed. Philadelphia : W.B. Saunders, 1996. [Online]. Available: <https://trove.nla.gov.au/work/28692053>
- [40] P. Hallock and I. C. Benson, "Studies on the elastic properties of human isolated aorta," *Journal of Clinical Investigation*, vol. 16, no. 4, pp. 595–602, Jul. 1937. [Online]. Available: <https://www.ncbi.nlm.nih.gov/pmc/articles/PMC424899/>
- [41] M. Prabhu, "Cardiac output measurement," *Anaesthesia & Intensive Care Medicine*, vol. 8, no. 2, pp. 63–66, 2007.
- [42] M. Engoren and D. Barbee, "Comparison of cardiac output determined by bioimpedance, thermodilution, and the fick method," *American Journal of Critical Care*, vol. 14, no. 1, pp. 40–45, 2005.
- [43] R. H. Thiele, K. Bartels, and T. J. Gan, "Cardiac output monitoring: a contemporary assessment and review," *Critical care medicine*, vol. 43, no. 1, pp. 177–185, 2015.
- [44] A. A. Udy, M. Altukroni, P. Jarett, J. A. Roberts, and J. Lipman, "A comparison of pulse contour wave analysis and ultrasonic cardiac output monitoring in the critically ill," *Anaesthesia and Intensive Care*, vol. 40, no. 4, pp. 631–637, Jul. 2012. [Online]. Available: <https://research.monash.edu/en/publications/a-comparison-of-pulse-contour-wave-analysis-and-ultrasonic-cardia>
- [45] J. Jansen, J. Schreuder, J. Mulier, N. Smith, J. Settels, and K. Wesseling, "A comparison of cardiac output derived from the arterial pressure wave against thermodilution in cardiac surgery patients," *British Journal of Anaesthesia*, vol. 87, no. 2, pp. 212–222, Aug. 2001. [Online]. Available: <https://linkinghub.elsevier.com/retrieve/pii/S0007091217376250>
- [46] M. T. Ganter, J. A. Alhashemi, A. M. Al-Shabasy, U. M. Schmid, P. Schott, S. A. Shalabi, A. M. Badri, S. Hartnack, and C. K. Hofer, "Continuous cardiac output measurement by un-calibrated pulse wave analysis and pulmonary artery catheter in patients with septic shock," *Journal of Clinical Monitoring and Computing*, vol. 30, no. 1, pp. 13–22, Feb. 2016.
- [47] P. Segers, E. R. Rietzschel, M. L. De Buyzere, S. J. Vermeersch, D. De Bacquer, L. M. Van Bortel, G. De Backer, T. C. Gillebert, and P. R. Verdonck, "Noninvasive (input) impedance, pulse wave velocity, and wave reflection in healthy middle-aged men and women," *Hypertension*, vol. 49, no. 6, pp. 1248–1255, Jun. 2007. [Online]. Available: <https://www.ahajournals.org/doi/10.1161/HYPERTENSIONAHA.106.085480>
- [48] S. S. Hickson, M. Butlin, M. Graves, V. Taviani, A. P. Avolio, C. M. McEniery, and I. B. Wilkinson, "The relationship of age with regional aortic stiffness and diameter," *JACC: Cardiovascular Imaging*, vol. 3, no. 12, pp. 1247–1255, 2010.



## Bibliography

---

- [49] Suga Hiroyuki and Sagawa Kiichi, "Instantaneous pressure-volume relationships and their ratio in the excised, supported canine left ventricle," *Circulation Research*, vol. 35, no. 1, pp. 117–126, Jul. 1974. [Online]. Available: <https://www.ahajournals.org/doi/abs/10.1161/01.res.35.1.117>
- [50] H. Suga, K. Sagawa, and A. A. Shoukas, "Load independence of the instantaneous pressure-volume ratio of the canine left ventricle and effects of epinephrine and heart rate on the ratio," *Circulation Research*, vol. 32, no. 3, pp. 314–322, Mar. 1973. [Online]. Available: <https://www.ahajournals.org/doi/10.1161/01.RES.32.3.314>
- [51] K. Sagawa, H. Suga, A. A. Shoukas, and K. M. Bakalar, "End-systolic pressure/volume ratio: a new index of ventricular contractility," *The American Journal of Cardiology*, vol. 40, no. 5, pp. 748–753, Nov. 1977.
- [52] B. A. Borlaug and D. A. Kass, "Ventricular-vascular interaction in heart failure," *Heart Failure Clinics*, vol. 4, no. 1, pp. 23–36, Jan. 2008.
- [53] P. D. Chantler and E. G. Lakatta, "Arterial-ventricular coupling with aging and disease," *Frontiers in Physiology*, vol. 3, p. 90, 2012.
- [54] C.-H. Chen, M. Nakayama, E. Nevo, B. J. Fetters, W. Maughan, and D. A. Kass, "Coupled systolic-ventricular and vascular stiffening with age," *Journal of the American College of Cardiology*, vol. 32, no. 5, pp. 1221–1227, Nov. 1998. [Online]. Available: <https://linkinghub.elsevier.com/retrieve/pii/S073510979800374X>
- [55] B. A. Borlaug, C. S. Lam, V. L. Roger, R. J. Rodeheffer, and M. M. Redfield, "Contractility and ventricular systolic stiffening in hypertensive heart disease," *Journal of the American College of Cardiology*, vol. 54, no. 5, pp. 410–418, Jul. 2009. [Online]. Available: <https://linkinghub.elsevier.com/retrieve/pii/S0735109709016477>
- [56] C. S. P. Lam, A. M. Shah, B. A. Borlaug, S. Cheng, A. Verma, J. Izzo, S. Oparil, G. P. Aurigemma, J. D. Thomas, B. Pitt, M. R. Zile, and S. D. Solomon, "Effect of antihypertensive therapy on ventricular-arterial mechanics, coupling, and efficiency," *European Heart Journal*, vol. 34, no. 9, pp. 676–683, Mar. 2013. [Online]. Available: <https://academic.oup.com/eurheartj/article-lookup/doi/10.1093/eurheartj/ehs299>
- [57] B. Ky, B. French, A. May Khan, T. Plappert, A. Wang, J. A. Chirinos, J. C. Fang, N. K. Sweitzer, B. A. Borlaug, D. A. Kass, M. St. John Sutton, and T. P. Cappola, "Ventricular-arterial coupling, remodeling, and prognosis in chronic heart failure," *Journal of the American College of Cardiology*, vol. 62, no. 13, pp. 1165–1172, Sep. 2013. [Online]. Available: <https://linkinghub.elsevier.com/retrieve/pii/S073510971302247X>
- [58] P. Reymond, F. Merenda, F. Perren, D. Rüfenacht, and N. Stergiopoulos, "Validation of a one-dimensional model of the systemic arterial tree," *American Journal of Physiology. Heart and Circulatory Physiology*, vol. 297, no. 1, pp. H208–222, Jul. 2009.

- [59] D. Burkhoff, I. Mirsky, and H. Suga, "Assessment of systolic and diastolic ventricular properties via pressure-volume analysis: a guide for clinical, translational, and basic researchers," *American Journal of Physiology. Heart and Circulatory Physiology*, vol. 289, no. 2, pp. H501–512, Aug. 2005.
- [60] P. Reant, L. Labrousse, S. Lafitte, P. Bordachar, X. Pillois, L. Tariosse, S. Bonoron-Adele, P. Padois, C. Deville, R. Roudaut, and P. Dos Santos, "Experimental validation of circumferential, longitudinal, and radial 2-dimensional strain during dobutamine stress echocardiography in ischemic conditions," *Journal of the American College of Cardiology*, vol. 51, no. 2, pp. 149–157, Jan. 2008.
- [61] M. Leitman, P. Lysyansky, S. Sidenko, V. Shir, E. Peleg, M. Binenbaum, E. Kaluski, R. Krakover, and Z. Vered, "Two-dimensional strain—a novel software for real-time quantitative echocardiographic assessment of myocardial function," *Journal of the American Society of Echocardiography: Official Publication of the American Society of Echocardiography*, vol. 17, no. 10, pp. 1021–1029, Oct. 2004.
- [62] S. Langeland, J. D'hooge, P. F. Wouters, H. A. Leather, P. Claus, B. Bijnens, and G. R. Sutherland, "Experimental validation of a new ultrasound method for the simultaneous assessment of radial and longitudinal myocardial deformation independent of insonation angle," *Circulation*, vol. 112, no. 14, pp. 2157–2162, Oct. 2005.
- [63] E. Donal, C. Bergerot, H. Thibault, L. Ernande, J. Loufoua, L. Augeul, M. Ovize, and G. Derumeaux, "Influence of afterload on left ventricular radial and longitudinal systolic functions: a two-dimensional strain imaging study," *European Journal of Echocardiography: The Journal of the Working Group on Echocardiography of the European Society of Cardiology*, vol. 10, no. 8, pp. 914–921, Dec. 2009.
- [64] C. H. Chen, B. Fetcs, E. Nevo, C. E. Rochitte, K. R. Chiou, P. A. Ding, M. Kawaguchi, and D. A. Kass, "Noninvasive single-beat determination of left ventricular end-systolic elastance in humans," *Journal of the American College of Cardiology*, vol. 38, no. 7, pp. 2028–2034, Dec. 2001.
- [65] T. Shishido, K. Hayashi, K. Shigemi, T. Sato, M. Sugimachi, and K. Sunagawa, "Single-beat estimation of end-systolic elastance using bilinearly approximated time-varying elastance curve." *Circulation*, vol. 102, no. 16, pp. 1983–1989, Oct. 2000. [Online]. Available: <http://europepmc.org/abstract/MED/11034949>
- [66] P. Reant, M. Dijos, E. Donal, A. Mignot, P. Ritter, P. Bordachar, P. Dos Santos, C. Leclercq, R. Roudaut, G. Habib, and S. Lafitte, "Systolic time intervals as simple echocardiographic parameters of left ventricular systolic performance: correlation with ejection fraction and longitudinal two-dimensional strain," *European Journal of Echocardiography*, vol. 11, no. 10, pp. 834–844, Dec. 2010. [Online]. Available: <https://academic.oup.com/ehjcmaging/article-lookup/doi/10.1093/ejehocard/jeq084>

## Bibliography

---

- [67] J. A. Chirinos, "Ventricular-arterial coupling: Invasive and non-invasive assessment," *Artery Research*, vol. 7, no. 1, Mar. 2013.
- [68] M. E. Safar and G. M. London, "Arterial and venous compliance in sustained essential hypertension," *Hypertension*, vol. 10, no. 2, pp. 133–139, Aug. 1987. [Online]. Available: <https://www.ahajournals.org/doi/10.1161/01.HYP.10.2.133>
- [69] D. Chemla, I. Antony, Y. Lecarpentier, and A. Nitenberg, "Contribution of systemic vascular resistance and total arterial compliance to effective arterial elastance in humans," *American Journal of Physiology-Heart and Circulatory Physiology*, vol. 285, no. 2, pp. H614–H620, Aug. 2003. [Online]. Available: <https://www.physiology.org/doi/10.1152/ajpheart.00823.2002>
- [70] B. A. Haluska, L. Jeffriess, M. Downey, S. G. Carlier, and T. H. Marwick, "Influence of cardiovascular risk factors on total arterial compliance," *Journal of the American Society of Echocardiography*, vol. 21, no. 2, pp. 123–128, Feb. 2008. [Online]. Available: <https://linkinghub.elsevier.com/retrieve/pii/S0894731707004713>
- [71] N. Stergiopoulos, J. J. Meister, and N. Westerhof, "Determinants of stroke volume and systolic and diastolic aortic pressure," *American Journal of Physiology-Heart and Circulatory Physiology*, vol. 270, no. 6, pp. H2050–H2059, Jun. 1996. [Online]. Available: <https://www.physiology.org/doi/10.1152/ajpheart.1996.270.6.H2050>
- [72] R. Heitmar, "Total arterial compliance: the future of cardiovascular risk assessment?" *Journal of Human Hypertension*, vol. 24, no. 4, pp. 227–229, Apr. 2010. [Online]. Available: <http://www.nature.com/articles/jhh2009106>
- [73] B. A. Haluska, L. Jeffries, S. Carlier, and T. H. Marwick, "Measurement of arterial distensibility and compliance to assess prognosis," *Atherosclerosis*, vol. 209, no. 2, pp. 474–480, Apr. 2010.
- [74] L. Van Bortel and J. Spek, "Influence of aging on arterial compliance," *Journal of Human Hypertension*, vol. 12, no. 9, pp. 583–586, Sep. 1998. [Online]. Available: <http://www.nature.com/articles/1000669>
- [75] A. Beltran, "Arterial compliance abnormalities in isolated systolic hypertension," *American Journal of Hypertension*, vol. 14, no. 10, pp. 1007–1011, Oct. 2001. [Online]. Available: [https://academic.oup.com/ajh/article-lookup/doi/10.1016/S0895-7061\(01\)02160-4](https://academic.oup.com/ajh/article-lookup/doi/10.1016/S0895-7061(01)02160-4)
- [76] L. Lind, "Arterial compliance and endothelium-dependent vasodilation are independently related to coronary risk in the elderly: the Prospective Investigation of the Vasculature in Uppsala Seniors (PIVUS) study," *Clinical Physiology and Functional Imaging*, vol. 28, no. 6, pp. 373–377, Nov. 2008. [Online]. Available: <http://doi.wiley.com/10.1111/j.1475-097X.2008.00816.x>

- [77] A. A. Shoukas and K. Sagawa, "Control of total systemic vascular capacity by the carotid sinus baroreceptor reflex," *Circulation Research*, vol. 33, no. 1, pp. 22–33, Jul. 1973. [Online]. Available: <https://www.ahajournals.org/doi/10.1161/01.RES.33.1.22>
- [78] P. Segers, P. Verdonck, Y. Deryck, S. Brimiouille, R. Naeije, S. Carlier, and N. Stergiopoulos, "Pulse pressure method and the area method for the estimation of total arterial compliance in dogs: sensitivity to wave reflection intensity," *Annals of Biomedical Engineering*, vol. 27, no. 4, pp. 480–485, Aug. 1999.
- [79] N. Stergiopoulos, P. Segers, and N. Westerhof, "Use of pulse pressure method for estimating total arterial compliance in vivo," *The American Journal of Physiology*, vol. 276, no. 2 Pt 2, pp. H424–428, Feb. 1999.
- [80] N. Stergiopoulos, J. J. Meister, and N. Westerhof, "Simple and accurate way for estimating total and segmental arterial compliance: the pulse pressure method," *Annals of Biomedical Engineering*, vol. 22, no. 4, pp. 392–397, Aug. 1994.
- [81] N. Stergiopoulos, J. Meister, and N. Westerhof, "Evaluation of methods for estimation of total arterial compliance," *American Journal of Physiology-Heart and Circulatory Physiology*, vol. 268, no. 4, pp. H1540–H1548, 1995.
- [82] I. S. Mackenzie, I. B. Wilkinson, and J. R. Cockcroft, "Assessment of arterial stiffness in clinical practice," *QJM: monthly journal of the Association of Physicians*, vol. 95, no. 2, pp. 67–74, Feb. 2002.
- [83] S. Sakuragi and W. P. Abhayaratna, "Arterial stiffness: methods of measurement, physiologic determinants and prediction of cardiovascular outcomes," *International Journal of Cardiology*, vol. 138, no. 2, pp. 112–118, Jan. 2010.
- [84] O. S. Randall, M. D. Esler, R. V. Calfee, G. F. Bulloch, A. S. Maisel, and B. Culp, "Arterial compliance in hypertension," *Australian and New Zealand Journal of Medicine*, vol. 6, pp. 49–59, Jun. 1976. [Online]. Available: <http://doi.wiley.com/10.1111/j.1445-5994.1976.tb03323.x>
- [85] W. W. Nichols, C. R. Conti, W. E. Walker, and W. R. Milnor, "Input impedance of the systemic circulation in man." *Circulation Research*, vol. 40, no. 5, pp. 451–458, May 1977. [Online]. Available: <https://www.ahajournals.org/doi/10.1161/01.RES.40.5.451>
- [86] C. J. Pepine, W. W. Nichols, and C. R. Conti, "Aortic input impedance in heart failure," *Circulation*, vol. 58, no. 3, pp. 460–465, Sep. 1978. [Online]. Available: <https://www.ahajournals.org/doi/10.1161/01.CIR.58.3.460>
- [87] J. P. Murgo, N. Westerhof, J. P. Giolma, and S. A. Altobelli, "Aortic input impedance in normal man: relationship to pressure wave forms," *Circulation*, vol. 62, no. 1, pp.

## Bibliography

---

- 105–116, Jul. 1980. [Online]. Available: <https://www.ahajournals.org/doi/10.1161/01.CIR.62.1.105>
- [88] W. Gundel, G. Cherry, B. Rajagopalan, L. B. Tan, G. Lee, and D. Schultz, “Aortic input impedance in man: acute response to vasodilator drugs,” *Circulation*, vol. 63, no. 6, pp. 1305–1314, Jun. 1981. [Online]. Available: <https://www.ahajournals.org/doi/10.1161/01.CIR.63.6.1305>
- [89] J. Merillon, G. Fontenier, J. Lerallut, M. Jaffrin, J. Chastre, P. Assayag, G. Motte, and R. Gourgon, “Aortic input impedance in heart failure: comparison with normal subjects and its changes during vasodilator therapy\*,” *European Heart Journal*, vol. 5, no. 6, pp. 447–455, Jun. 1984. [Online]. Available: <https://academic.oup.com/eurheartj/article-lookup/doi/10.1093/oxfordjournals.eurheartj.a061690>
- [90] W. W. Nichols, M. F. O’Rourke, A. P. Avolio, T. Yaginuma, J. P. Murgu, C. J. Pepine, and C. Conti, “Effects of age on ventricular-vascular coupling,” *The American Journal of Cardiology*, vol. 55, no. 9, pp. 1179–1184, Apr. 1985. [Online]. Available: <https://linkinghub.elsevier.com/retrieve/pii/0002914985906599>
- [91] C. Lucas, B. Wilcox, B. Ha, and G. Henry, “Comparison of time domain algorithms for estimating aortic characteristic impedance in humans,” *IEEE Transactions on Biomedical Engineering*, vol. 35, no. 1, pp. 62–68, Jan. 1988. [Online]. Available: <http://ieeexplore.ieee.org/document/1337/>
- [92] E. P. Kromer, D. Eisner, S. R. Holmer, A. Muntze, and G. A. J. Riegger, “Aortic input impedance and neurohormonal activation in patients with mild to moderate chronic congestive heart failure,” *Cardiovascular Research*, vol. 26, no. 3, pp. 265–272, Mar. 1992. [Online]. Available: <https://academic.oup.com/cardiovasres/article-lookup/doi/10.1093/cvr/26.3.265>
- [93] R. Kelly and D. Fitchett, “Noninvasive determination of aortic input impedance and external left ventricular power output: a validation and repeatability study of a new technique,” *Journal of the American College of Cardiology*, vol. 20, no. 4, pp. 952–963, Oct. 1992. [Online]. Available: <https://linkinghub.elsevier.com/retrieve/pii/073510979290198V>
- [94] C. T. Ting, K. P. Brin, S. J. Lin, S. P. Wang, M. S. Chang, B. N. Chiang, and F. C. Yin, “Arterial hemodynamics in human hypertension,” *Journal of Clinical Investigation*, vol. 78, no. 6, pp. 1462–1471, Dec. 1986. [Online]. Available: <http://www.jci.org/articles/view/112737>
- [95] G. F. Mitchell, J.-C. Tardif, J. M. O. Arnold, G. Marchiori, T. X. O’Brien, M. E. Dunlap, and M. A. Pfeffer, “Pulsatile hemodynamics in congestive heart failure,” *Hypertension*, vol. 38, no. 6, pp. 1433–1439, Dec. 2001. [Online]. Available: <https://www.ahajournals.org/doi/10.1161/hy1201.098298>

- [96] J.-P. L. Dujardin and D. N. Stone, "Characteristic impedance of the proximal aorta determined in the time and frequency domain: a comparison," *Medical & Biological Engineering & Computing*, vol. 19, no. 5, pp. 565–568, Sep. 1981. [Online]. Available: <http://link.springer.com/10.1007/BF02442770>
- [97] B. I. Levy, D. Babalis, P. Lacolley, P. Poitevin, and M. E. Safar, "Cardiac hypertrophy and characteristic impedance in spontaneously hypertensive rats," *Journal of Hypertension*, vol. 6, no. 4, pp. S110–111, Dec. 1988. [Online]. Available: <http://journals.lww.com/00004872-198812040-00031>
- [98] J. K.-J. Li, "Time domain resolution of forward and reflected waves in the aorta," *IEEE Transactions on Biomedical Engineering*, vol. BME-33, no. 8, pp. 783–785, Aug. 1986. [Online]. Available: <http://ieeexplore.ieee.org/document/4122389/>
- [99] N. Westerhof, N. Stergiopoulos, M. I. Noble, and B. E. Westerhof, *Snapshots of hemodynamics: an aid for clinical research and graduate education*. Springer, 2018.
- [100] P. B. Dobrin, "Mechanical properties of arteries," *Physiological Reviews*, vol. 58, no. 2, pp. 397–460, Apr. 1978.
- [101] S. Laurent, J. Cockcroft, L. Van Bortel, P. Boutouyrie, C. Giannattasio, D. Hayoz, B. Pannier, C. Vlachopoulos, I. Wilkinson, H. Struijker-Boudier, and on behalf of the European Network for Non-invasive Investigation of Large Arteries, "Expert consensus document on arterial stiffness: methodological issues and clinical applications," *European Heart Journal*, vol. 27, no. 21, pp. 2588–2605, Sep. 2006. [Online]. Available: <https://academic.oup.com/eurheartj/article-lookup/doi/10.1093/eurheartj/ehl254>
- [102] B. Pannier, A. P. Guérin, S. J. Marchais, M. E. Safar, and G. M. London, "Stiffness of capacitive and conduit arteries: prognostic significance for end-stage renal disease patients," *Hypertension*, vol. 45, no. 4, pp. 592–596, Apr. 2005. [Online]. Available: <https://www.ahajournals.org/doi/10.1161/01.HYP.0000159190.71253.c3>
- [103] G. F. Mitchell, S.-J. Hwang, R. S. Vasan, M. G. Larson, M. J. Pencina, N. M. Hamburg, J. A. Vita, D. Levy, and E. J. Benjamin, "Arterial stiffness and cardiovascular events: the Framingham heart study," *Circulation*, vol. 121, no. 4, pp. 505–511, Feb. 2010. [Online]. Available: <https://www.ahajournals.org/doi/10.1161/CIRCULATIONAHA.109.886655>
- [104] C. Vlachopoulos, K. Aznaouridis, D. Terentes-Printzios, N. Ioakeimidis, and C. Stefanadis, "Prediction of cardiovascular events and all-cause mortality with brachial-ankle elasticity index: a systematic review and meta-analysis," *Hypertension*, vol. 60, no. 2, pp. 556–562, Aug. 2012. [Online]. Available: <https://www.ahajournals.org/doi/10.1161/HYPERTENSIONAHA.112.194779>
- [105] S. C. Millasseau, A. D. Stewart, S. J. Patel, S. R. Redwood, and P. J. Chowienczyk, "Evaluation of carotid-femoral pulse wave velocity: influence of timing algorithm and

## Bibliography

---

- heart rate," *Hypertension*, vol. 45, no. 2, pp. 222–226, Feb. 2005. [Online]. Available: <https://www.ahajournals.org/doi/10.1161/01.HYP.0000154229.97341.d2>
- [106] P. Palatini, A. Benetos, G. Grassi, S. Julius, S. E. Kjeldsen, G. Mancia, K. Narkiewicz, G. Parati, A. C. Pessina, L. M. Ruilope, A. Zanchetti, and European Society of Hypertension, "Identification and management of the hypertensive patient with elevated heart rate: statement of a European Society of Hypertension Consensus Meeting," *Journal of Hypertension*, vol. 24, no. 4, pp. 603–610, Apr. 2006.
- [107] I. Tan, M. Butlin, B. Spronck, H. Xiao, and A. Avolio, "Effect of heart rate on arterial stiffness as assessed by pulse wave velocity," *Current Hypertension Reviews*, vol. 13, Jul. 2017. [Online]. Available: <http://www.eurekaselect.com/154381/article>
- [108] P. Albaladejo, X. Copie, P. Boutouyrie, B. Laloux, A. D. Déclère, H. Smulyan, and A. Bénétos, "Heart rate, arterial stiffness, and wave reflections in paced patients," *Hypertension*, vol. 38, no. 4, pp. 949–952, Oct. 2001. [Online]. Available: <https://www.ahajournals.org/doi/10.1161/hy1001.096210>
- [109] E. Haesler, X. Lyon, E. Pruvot, L. Kappenberger, and D. Hayoz, "Confounding effects of heart rate on pulse wave velocity in paced patients with a low degree of atherosclerosis," *Journal of Hypertension*, vol. 22, no. 7, pp. 1317–1322, Jul. 2004. [Online]. Available: <http://content.wkhealth.com/linkback/openurl?sid=WKPTLP:landingpage&an=00004872-200407000-00013>
- [110] P. Lantelme, C. Mestre, M. Lievre, A. Gressard, and H. Milon, "Heart rate: an important confounder of pulse wave velocity assessment," *Hypertension*, vol. 39, no. 6, pp. 1083–1087, Jun. 2002. [Online]. Available: <https://www.ahajournals.org/doi/10.1161/01.HYP.0000019132.41066.95>
- [111] B. Spronck, M. H. G. Heusinkveld, W. P. Donders, A. G. W. de Lepper, J. Op't Roodt, A. A. Kroon, T. Delhaas, and K. D. Reesink, "A constitutive modeling interpretation of the relationship among carotid artery stiffness, blood pressure, and age in hypertensive subjects," *American Journal of Physiology. Heart and Circulatory Physiology*, vol. 308, no. 6, pp. H568–582, Mar. 2015.
- [112] E. R. Nye, "The effect of blood pressure alteration on the pulse wave velocity," *British Heart Journal*, vol. 26, pp. 261–265, Mar. 1964.
- [113] M. Gao, H.-M. Cheng, S.-H. Sung, C.-H. Chen, N. B. Olivier, and R. Mukkamala, "Estimation of pulse transit time as a function of blood pressure using a nonlinear arterial tube-load model," *IEEE transactions on bio-medical engineering*, vol. 64, no. 7, pp. 1524–1534, Jul. 2017.
- [114] M. L. Muiesan, M. Salvetti, A. Paini, C. Monteduro, C. A. Rosei, C. Aggiusti, E. Belotti, F. Bertacchini, G. Galbassini, D. Stassaldi, M. Castellano, and E. A. Rosei, "Pulse wave

- velocity and cardiovascular risk stratification in a general population: the Vobarno study,” *Journal of Hypertension*, vol. 28, no. 9, pp. 1935–1943, Sep. 2010.
- [115] H. J. Joo, S.-A. Cho, J.-Y. Cho, J. H. Park, S. J. Hong, C. W. Yu, and D.-S. Lim, “The relationship between pulse wave velocity and coronary artery stenosis and percutaneous coronary intervention: a retrospective observational study,” *BMC Cardiovascular Disorders*, vol. 17, no. 1, Dec. 2017. [Online]. Available: <http://bmccardiovascdisord.biomedcentral.com/articles/10.1186/s12872-017-0476-7>
- [116] A. R. Khoshdel, S. L. Carney, B. R. Nair, and A. Gillies, “Better management of cardiovascular diseases by pulse wave velocity: combining clinical practice with clinical research using evidence-based medicine,” *Clinical Medicine and Research*, vol. 5, no. 1, pp. 45–52, Mar. 2007. [Online]. Available: <https://www.ncbi.nlm.nih.gov/pmc/articles/PMC1855337/>
- [117] Y. Shi, P. Lawford, and R. Hose, “Review of zero-D and 1-D models of blood flow in the cardiovascular system,” *BioMedical Engineering OnLine*, vol. 10, no. 1, p. 33, 2011. [Online]. Available: <http://biomedical-engineering-online.biomedcentral.com/articles/10.1186/1475-925X-10-33>
- [118] N. Westerhof, J.-W. Lankhaar, and B. E. Westerhof, “The arterial Windkessel,” *Medical & Biological Engineering & Computing*, vol. 47, no. 2, pp. 131–141, Feb. 2009. [Online]. Available: <http://link.springer.com/10.1007/s11517-008-0359-2>
- [119] J. R. Womersley, *An elastic tube theory of pulse transmission and oscillatory flow in mammalian arteries*. Wright-Patterson Air Force Base, Ohio,: Wright Air Development Center, Air Research and Development Command,, 1957.
- [120] C. Papapanayotou, Y. Cherruault, and B. De La Rochefoucauld, “A mathematical model of the circle of willis in the presence of an arteriovenous anomaly,” *Computers & Mathematics with Applications*, vol. 20, no. 4-6, pp. 199–206, 1990.
- [121] N. Stergiopoulos, D. F. Young, and T. R. Rogge, “Computer simulation of arterial flow with applications to arterial and aortic stenoses,” *Journal of Biomechanics*, vol. 25, no. 12, pp. 1477–1488, Dec. 1992.
- [122] M. S. Olufsen, C. S. Peskin, W. Y. Kim, E. M. Pedersen, A. Nadim, and J. Larsen, “Numerical simulation and experimental validation of blood flow in arteries with structured-tree outflow conditions,” *Annals of biomedical engineering*, vol. 28, no. 11, pp. 1281–1299, 2000.
- [123] J. P. Mynard and J. J. Smolich, “One-dimensional haemodynamic modeling and wave dynamics in the entire adult circulation,” *Annals of Biomedical Engineering*, vol. 43, no. 6, pp. 1443–1460, Jun. 2015. [Online]. Available: <http://link.springer.com/10.1007/s10439-015-1313-8>



## Bibliography

---

- [124] M. Willemet, S. Vennin, and J. Alastruey, “Computational assessment of hemodynamics-based diagnostic tools using a database of virtual subjects: application to three case studies,” *Journal of Biomechanics*, vol. 49, no. 16, pp. 3908–3914, Dec. 2016. [Online]. Available: <https://linkinghub.elsevier.com/retrieve/pii/S0021929016311551>
- [125] S. Vennin, Y. Li, M. Willemet, H. Fok, H. Gu, P. Charlton, J. Alastruey, and P. Chowienczyk, “Identifying hemodynamic determinants of pulse pressure: a combined numerical and physiological approach,” *Hypertension*, vol. 70, no. 6, pp. 1176–1182, Dec. 2017. [Online]. Available: <https://www.ahajournals.org/doi/10.1161/HYPERTENSIONAHA.117.09706>
- [126] N. Westerhof, F. Bosman, C. J. De Vries, and A. Noordergraaf, “Analog studies of the human systemic arterial tree,” *Journal of biomechanics*, vol. 2, no. 2, pp. 121–143, 1969.
- [127] P. Reymond, Y. Bohraus, F. Perren, F. Lazeyras, and N. Stergiopoulos, “Validation of a patient-specific one-dimensional model of the systemic arterial tree,” *American Journal of Physiology. Heart and Circulatory Physiology*, vol. 301, no. 3, pp. H1173–1182, Sep. 2011.
- [128] J. A. Sidey-Gibbons and C. J. Sidey-Gibbons, “Machine learning in medicine: a practical introduction,” *BMC medical research methodology*, vol. 19, no. 1, pp. 1–18, 2019.
- [129] J. D. Rodriguez, A. Perez, and J. A. Lozano, “Sensitivity analysis of k-fold cross validation in prediction error estimation,” *IEEE transactions on pattern analysis and machine intelligence*, vol. 32, no. 3, pp. 569–575, 2009.
- [130] R. D. Riley, J. Ensor, K. I. Snell, T. P. Debray, D. G. Altman, K. G. Moons, and G. S. Collins, “External validation of clinical prediction models using big datasets from e-health records or ipd meta-analysis: opportunities and challenges,” *bmj*, vol. 353, 2016.
- [131] J. M. Bland and D. G. Altman, “Statistical methods for assessing agreement between two methods of clinical measurement,” *Lancet (London, England)*, vol. 1, no. 8476, pp. 307–310, Feb. 1986.
- [132] A. Liaw and M. Wiener, “Classification and regression by randomForest,” *R News*, vol. 2, no. 3, pp. 18–22, 2002. [Online]. Available: <http://CRAN.R-project.org/doc/Rnews/>
- [133] A. J. Smola and B. Schölkopf, “A tutorial on support vector regression,” *Statistics and Computing*, vol. 14, no. 3, pp. 199–222, Aug. 2004. [Online]. Available: <http://link.springer.com/10.1023/B:STCO.0000035301.49549.88>
- [134] Robert Tibshirani, “Regression shrinkage and selection via the lasso,” *J. R. Stat. Soc. Ser.*, vol. B, pp. 267–288, 1996.
- [135] A. Natekin and A. Knoll, “Gradient boosting machine: a tutorial,” *Frontiers in Neurorobotics*, vol. 7, 2013. [Online]. Available: <http://journal.frontiersin.org/article/10.3389/fnbot.2013.00021/abstract>

- [136] T. Chen and C. Guestrin, "XGBoost: a scalable tree boosting system," in *Proceedings of the 22nd ACM SIGKDD International Conference on Knowledge Discovery and Data Mining - KDD '16*. San Francisco, California, USA: ACM Press, 2016, pp. 785–794. [Online]. Available: <http://dl.acm.org/citation.cfm?doid=2939672.2939785>
- [137] O. I. Abiodun, A. Jantan, A. E. Omolara, K. V. Dada, N. A. Mohamed, and H. Arshad, "State-of-the-art in artificial neural network applications: A survey," *Heliyon*, vol. 4, no. 11, p. e00938, 2018.
- [138] S.-C. Wang, "Artificial neural network," in *Interdisciplinary computing in java programming*. Springer, 2003, pp. 81–100.
- [139] D. E. Adkins, "Machine learning and electronic health records: a paradigm shift," *American Journal of Psychiatry*, vol. 174, no. 2, pp. 93–94, Feb. 2017. [Online]. Available: <http://ajp.psychiatryonline.org/doi/10.1176/appi.ajp.2016.16101169>
- [140] I. Goodfellow, Y. Bengio, and A. Courville, *Deep Learning*. MIT Press, 2016, <http://www.deeplearningbook.org>.
- [141] N. J. Dabanloo, F. Adaei, and A. M. Nasrabadi, "The performance of neural network in the estimation of cardiac output using arterial blood pressure waveforms." 2011, oCLC: 990720998. [Online]. Available: <http://ieeexplore.ieee.org/servlet/opac?punumber=6156579>
- [142] H. Xiao, A. Qasem, M. Butlin, and A. Avolio, "Estimation of aortic systolic blood pressure from radial systolic and diastolic blood pressures alone using artificial neural networks," *Journal of Hypertension*, vol. 35, no. 8, pp. 1577–1585, Aug. 2017.
- [143] J. M. J. Huttunen, L. Kärkkäinen, and H. Lindholm, "Pulse transit time estimation of aortic pulse wave velocity and blood pressure using machine learning and simulated training data," *PLOS Computational Biology*, vol. 15, no. 8, p. e1007259, Aug. 2019. [Online]. Available: <http://dx.plos.org/10.1371/journal.pcbi.1007259>
- [144] J. M. Huttunen, L. Kärkkäinen, M. Honkala, and H. Lindholm, "Deep learning for prediction of cardiac indices from photoplethysmographic waveform: a virtual database approach," *International Journal for Numerical Methods in Biomedical Engineering*, vol. 36, no. 3, Mar. 2020. [Online]. Available: <https://onlinelibrary.wiley.com/doi/abs/10.1002/cnm.3303>
- [145] S. V. Greve, M. K. Blicher, R. Kruger, T. Sehestedt, E. Gram-Kampmann, S. Rasmussen, J. K. Vishram, P. Boutouyrie, S. Laurent, and M. H. Olsen, "Estimated carotid–femoral pulse wave velocity has similar predictive value as measured carotid–femoral pulse wave velocity," *Journal of Hypertension*, vol. 34, no. 7, pp. 1279–1289, Jul. 2016. [Online]. Available: <https://journals.lww.com/00004872-201607000-00009>

## Bibliography

---

- [146] C. Vlachopoulos, D. Terentes-Printzios, S. Laurent, P. M. Nilsson, A. D. Protogerou, K. Aznaouridis, P. Xaplanteris, I. Koutagiar, H. Tomiyama, A. Yamashina, P. P. Sfikakis, and D. Tousoulis, "Association of estimated pulse wave velocity with survival: a secondary analysis of SPRINT," *JAMA Network Open*, vol. 2, no. 10, p. e1912831, Oct. 2019. [Online]. Available: <https://jamanetwork.com/journals/jamanetworkopen/fullarticle/2752573>
- [147] R. E. Climie, C. C. Mayer, R. M. Bruno, and B. Hametner, "Addressing the unmet needs of measuring vascular ageing in clinical practice—European COoperation in science and technology Action VascAgeNet," *Artery Research*, vol. 26, no. 2, p. 71, 2020. [Online]. Available: <https://www.atlantis-press.com/article/125938376>
- [148] V. Bikia, T. Fong, R. Climie, R.-M. Bruno, B. Hametner, C. Mayer, D. Terentes-Printzios, and P. Charlton, "Leveraging the potential of machine learning for assessing vascular ageing: state-of-the-art and future research," *European Heart Journal - Digital Health*, Accepted 2021.

## Chapter 2

---

# Non-invasive cardiac output and central systolic pressure from cuff pressure and pulse wave velocity

Vasiliki Bikia<sup>1</sup>, Stamatia Pagoulatou<sup>1</sup>, Bram Trachet<sup>1</sup>, Dimitrios Soulis<sup>2</sup>, Athanase D. Protogerou<sup>3</sup>, Theodore G. Papaioannou<sup>2</sup>, Nikolaos Stergiopoulos<sup>1</sup>

<sup>1</sup> *Institute of Bioengineering, École Polytechnique Fédérale de Lausanne, Switzerland*

<sup>2</sup> *Biomedical Engineering Unit, 1<sup>st</sup> Department of Cardiology, “Hippokration” Hospital, Medical School, National and Kapodistrian University of Athens, Greece*

<sup>3</sup> *Department of Pathophysiology, Medical School, National and Kapodistrian University of Athens, Greece*

Published in IEEE Journal of Biomedical and Health Informatics, 2020.

### Abstract

We introduce a novel approach to estimate cardiac output (CO) and central (aortic) systolic blood pressure (aSBP) from non-invasive measurements of peripheral cuff pressure and carotid-femoral pulse wave velocity (cfPWV). The adjustment of a previously validated one-dimensional arterial tree model is achieved via an optimization process. In the optimization loop, compliance and resistance of the generic arterial tree model, as well as aortic flow, are adjusted so that simulated brachial systolic and diastolic pressures and cfPWV converge towards the measured brachial systolic and diastolic pressures and cfPWV. The process is repeated until full convergence in terms of both brachial pressures and cfPWV is reached. To assess the accuracy of the proposed framework, we implemented the algorithm on in vivo anonymized data from 20 subjects and compared the method-derived estimates of CO and aSBP to patient-specific measurements obtained with Mobil-O-Graph apparatus (central

## **Chapter 2. Non-invasive cardiac output and central systolic pressure from cuff pressure and pulse wave velocity**

---

pressure) and two-dimensional transthoracic echocardiography (aortic blood flow). Both CO and aSBP estimates were found to be in good agreement with the reference values achieving an RMSE of 0.36 L/min and 2.46 mmHg, respectively. Our one-dimensional model can be successfully “tuned” to partially patient-specific standards by using non-invasive, easily obtained peripheral pressure data. The in vivo evaluation demonstrated that this method can potentially be used to obtain central aortic hemodynamic parameters in an accurate and non-invasive way.

## **2.1 Introduction**

Central hemodynamic quantities, such as cardiac output (CO) and central aortic pressure, have been generally shown to be more powerful predictors of clinical outcomes than corresponding measurements obtained in the peripheral arteries such as the radial, femoral or brachial arteries [1; 2]. Critically ill or intensive care unit patients often require continuous assessment of cardiac output for diagnostic purposes or for guiding therapeutic interventions [3; 4; 5], whereas several studies have shown the pathophysiological importance of central systolic blood pressure (aSBP) as the critical index for diagnosis and prevention of cardiovascular diseases [6; 7; 8]. But despite the diagnostic importance of central measurements, their clinical use is severely hampered by their invasive nature (in case of central blood pressure) or cost and need of special equipment and training (in case of aortic blood flow). Peripheral measurements such as systolic and diastolic brachial pressure, on the other hand, are non-invasive and can be monitored by any clinician on a regular basis [9]. This has given rise to substantial research efforts to develop non-invasive methods for estimating central cardiovascular hemodynamics from peripheral measurements [10; 11].

The state of the art of methods for obtaining central hemodynamic indices is based on generalized transfer functions (TF) [12; 13; 14], pulse wave analysis [15; 16; 17] or parameter estimation from pooled clinical data [18; 19]. None of these techniques accounts for the specific arterial tree properties of each subject [20; 21]. The use of mathematical models constitutes a valuable tool to investigate patient-specific aspects of aortic hemodynamics, which are difficult to assess in clinical practice. Patient-specific modelling is an emerging field which promises to have a significant impact on clinical practice [22]. Data assimilation has significantly promoted patient-specific modelling and has become an area of increasing interest [23].

Prompted by previous work in the field, the hypothesis formed in this study is that central hemodynamic parameters (i.e. CO and aSBP) can be accurately estimated by making better use of the patient-specific information that is embedded in easily obtained non-invasive cuff pressure and pulse wave velocity measurements. In contrast to current methods using population-based generalized TFs, this study relies on a generalized one-dimensional (1-D) model which is further partially personalized by using additional measurements of brachial systolic blood pressure (SBP) and diastolic blood pressure (DBP), and carotid-to-femoral pulse wave velocity (cfPWV). The method developed and presented in this study combines insights from both cardiovascular modelling and data assimilation methodology. This is done by feeding the 1-D model with the minimum number of inputs that allows for the calibrated prediction of the aforementioned central hemodynamic parameters. The proposed framework was evaluated with *in vivo* data from a population of 20 healthy adults [24]. Estimated values of CO and aSBP were compared to the corresponding CO and aSBP values measured by a non-invasive, validated, automated, oscillometric sphygmomanometer (Mobil-O-Graph) and

transthoracic two-dimensional (2-D) echocardiography – Doppler, respectively.

## **2.2 Methods & materials**

### **Brief description of the generic 1-D arterial tree model**

In this study, we adopted a validated 1-D model of the systemic arterial tree that has been previously described by Reymond et al. [25]. The arterial tree, as depicted in Figure 2.1, includes the main arteries of the systemic circulation, including a detailed network representation of the cerebral circulation and the coronary circulation. In brief, the governing equations of the model are obtained by integration of the longitudinal momentum and continuity of the Navier-Stokes equations over the arterial cross section. Flow and pressure waves throughout the vasculature are obtained by solving the governing equations with proper boundary conditions using an implicit finite-difference scheme. The arterial segments of the model are considered as long tapered tubes, and their compliance is defined by a nonlinear function of pressure and location as proposed by Langewouters [26]. The arterial wall behavior is considered to be nonlinear and viscoelastic according to Holenstein et al. [27]. Local arterial compliance is calculated after approximating pulse wave velocity (PWV) as an inverse power function of arterial lumen diameter, following the physiological values reported in the literature. Resistance of the peripheral vasculature is accounted for by coupling the distant vessels with three-element Windkessel models. At the proximal end, the arterial tree either receives a prescribed input aortic flow waveform or is coupled with a time-varying elastance model for the contractility of the left ventricle [28; 29]. Further details on the 1-D model can be found in the original publications [25; 22]. The model has been thoroughly validated and is able to predict pressure and flow waves in good quantitative and qualitative agreement with *in vivo* measurements, particularly with respect to shape details.

### **Rationale of the proposed method**

This work applied an optimization algorithm in order to partially adjust the generic 1-D arterial tree model to the specific patient under consideration. The rationale behind this methodology was that adjusting (some of the) model parameters may be sufficient to approximate the measured data [31]. Before the optimization, the aim was to identify the most sensitive parameters which mainly drive the variability of the model output.

In our analysis, peripheral SBP, DBP, and cfPWV were the model outputs. Our approach was based on the idea that, for any individual with a given set of peripheral SBP, DBP, and cfPWV values, there will be only one solution for the arterial tree model. Thus, if we simultaneously adjust the properties of the model and the input aortic blood flow to capture a given peripheral cuff pressure and cfPWV, then this allows for the calibrated derivation of CO and aSBP. In

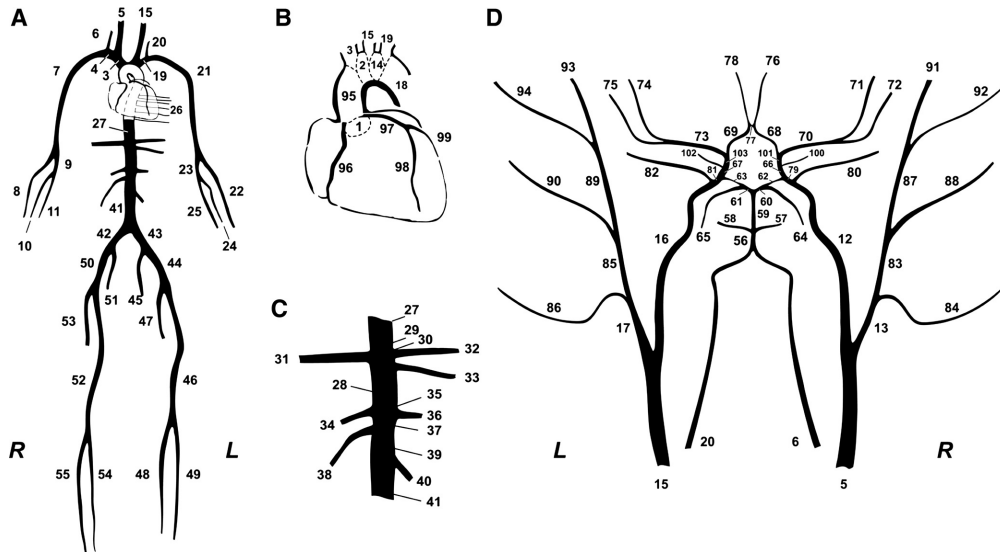


Figure 2.1 – Schematic representation of the 1-D model of the systemic circulation: (A) The main systemic arterial tree. (B) The aortic arch and the coronary network. (C) The principal abdominal aortic branches. (D) The detailed cerebral arterial tree, which is connected via the carotid arteries (segments 5 and 15) and the vertebrals (segments 6 and 20) to the main arterial tree (A). Adapted from [30].

order to identify and select those highly sensitive parameters, we performed a parameter identifiability analysis [32].

### Parameter identifiability analysis

The arterial tree model of this study is fully characterized by its geometry, the distensibility of all arterial segments, and the peripheral impedances (described by terminal compliances and resistances). Additionally, aortic flow is needed as proximal boundary condition. Table 2.1 summarizes the input and output parameters of the arterial tree model. For the following analysis, brachial pressure was selected as the peripheral pressure model output. Thus, the three model outputs became brachial SBP (brSBP), brachial DBP (brDBP), and cfPWV.

The sensitivity matrix  $V = \{v_{ij}\}$  was calculated for the entire set of parameters in the arterial tree model using the finite difference approximation [33]. Subsequently, the scaled sensitivity matrix was estimated to provide the dimension-free sensitivity information. The scaled sensitivity matrix  $S = \{s_{ij}\}$  was derived from the following formula:

$$s_{ij} = \frac{v_{ij}c}{SC_i} \quad (2.1)$$

Here, according to Brun et al. [32],  $\Delta\theta_j$  was set equal to the original set of parameters  $\theta$ , i.e.  $\theta_0$ ,



## Chapter 2. Non-invasive cardiac output and central systolic pressure from cuff pressure and pulse wave velocity

Table 2.1 – Input and output parameters of the 1-D arterial tree model.

	Corresponding variable	Value
<b>Input parameter</b>		
Blood density	$\rho$	1050 kg/m <sup>3</sup>
Blood viscosity	$\mu$	0.004 Pa.s
Geometry	arterial_diameter, arterial_length	(no_segments)x1 vector, (no_segments)x1 vector
Distensibility and terminal compliance	C	(no_segments)x1 vector
Total peripheral resistance	R	(no_terminal_segments)x1 vector
Aortic flow <sup>a</sup>	aortic_flow	(no_time_points)x1 vector
<b>Output</b>		
Pressure waves	pressures	(no_segments)x(no_time_points) vector
Flow waves	flows	(no_segments)x(no_time_points) vector
<sup>a</sup> The aortic flow is characterized by three parameters, namely the $Q_{max}$ , $T_{period}$ , $T_{systole}$ . no_segments: number of arterial segments, no_time_points: length of the time signal.		

whereas the optimal choice for  $SC_i$  was the mean value of the experimental observations for each model output (Table 2.2).

The scaled sensitivity matrix is presented in Figure 2.2. Each element  $s_{ij}$  corresponds to the sensitivity of the model output  $j = 1, 2, 3$ , i.e. brSBP, brDBP, and cfPWV, with respect to changes in the parameter  $i = 1, \dots, 7$ , i.e. arterial\_length, arterial\_diameter, C, R,  $T_{period}$ ,  $T_{systole}$ ,  $Q_{max}$ .

In order to acquire additional information on the sign and distribution of the values in each column  $j$ ,  $\delta_j^{msqr}$  [32] was computed and ranked in decreasing order. The decreasing order of  $\delta_j^{msqr}$  provided the parameters' importance ranking [32] (Table 2.3). It was observed that  $Q_{max}$ , C,  $T_{period}$ , and R were the most sensitive parameters. Since the sensitivities of the remaining parameters were not negligible, we chose to approximate them using previously published data (more details are provided in section 2.2.4. *Tuning of The Generic 1-D Arterial Tree Model* section). We assumed that the approximations do not impose a significant error in the results due to their small sensitivities. Based on the aforementioned considerations and the resulted importance ranking, we partitioned the set of parameters  $\theta$  into two components  $(\theta_K^T, \theta_{\bar{K}}^T)$  with  $K = 3$ , namely:

$$\theta_K^T = \{C, R, Q_{max}\}, \theta_{\bar{K}}^T = \{arterial\_length, arterial\_diameter, T_{period}, T_{systole}\}.$$

Only the component  $\theta_K^T$  was to be estimated from the measured data whereas the component  $\theta_{\bar{K}}^T$  (i.e. the remaining parameters) was fixed at a priori value; this is a common practice in identifiability analysis [32]. Specifically, the arterial\_length was adjusted based on height,

Table 2.2 – Description of the  $\Delta\theta_j$  and  $SC_i$  parameters.

Parameter	Unit	$\Delta\theta_j = \theta_0$
$Q_{max}$	mL/s	436.23
C	mL/mmHg	1.90
$T_{period}$	ms	790.00
R	mmHg.s/mL	1.00
arterial_length <sup>a</sup>	cm	180.00
arterial_diameter <sup>b</sup>	cm	2.94
$T_{systole}$	ms	270.00
State	Unit	$SC_i$
Brachial SBP	mmHg	117.55
Brachial DBP	mmHg	77.25
cfPWV	m/s	6.89
<sup>a</sup> Arterial length is defined with respect to height. The reference state of the arterial tree model corresponds to an individual with a height equal to 180 cm. <sup>b</sup> Arterial diameter is defined with respect to the diameter of the aorta. The alteration of the diameter for the different arteries is done uniformly.		

Table 2.3 – List of the input model parameters' importance ranking.

Parameter	$\delta_j^{msqr}$
$Q_{max}$	0.52
R	0.48
$T_{period}$	0.42
C	0.26
$T_{systole}$	0.11
arterial_diameter	0.1
arterial_length	0.08

arterial\_diameter was determined based on [34],  $T_{period}$  was directly assigned the patient's measured HR and  $T_{systole}$  was set to a HR-related value according to [35]. The hypothesis was that the subset of parameters, i.e. C, R,  $Q_{max}$ , can be uniquely estimated from the model outputs, i.e. brSBP, brDBP, and cfPWV.

In order to verify our hypothesis, we had to confirm that the set  $\theta_K^T$  was identifiable or, in other words, that  $\theta_K^T$  was sufficient to detect the variability in the model outputs (i.e. brSBP, brDBP, and cfPWV). If  $\theta_K^T$  is classified as identifiable, then we can deduce that brSBP, brDBP, and cfPWV can estimate  $\theta_K^T$  in a unique way.

The joint influence of the parameters  $\theta_K^T$  parameters on the model output was considered. To this respect, the collinearity of parametric sensitivity was used [32]. To calculate collinearity, we first normalized the scaled sensitivities  $\bar{S}$  and we defined the collinearity index  $\gamma_K$  as

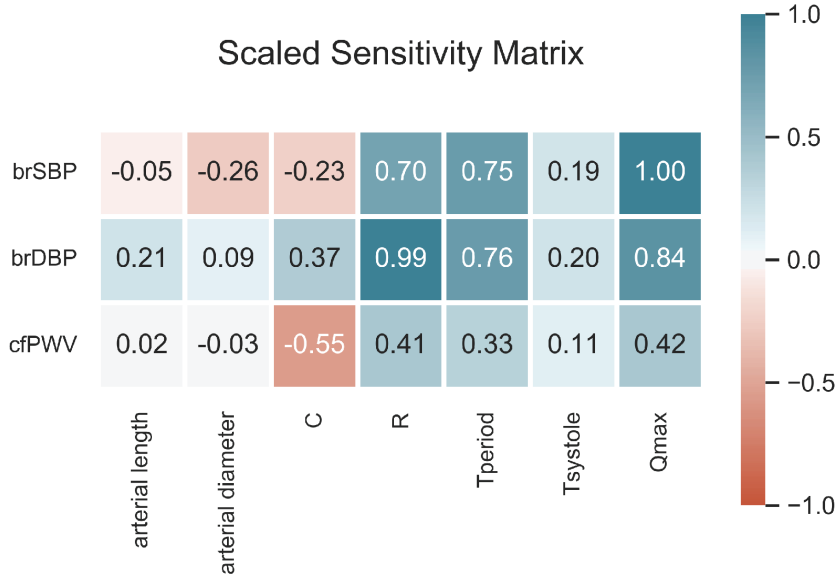


Figure 2.2 – Scaled sensitivity matrix for the entire set of input parameters of the 1-D arterial tree model. Adapted from [30].

follows:

$$\gamma_K = \frac{1}{\min_{\|b\|=1} \|\bar{S}_K \beta\|} = \frac{1}{\sqrt{\lambda_K}} \quad (2.2)$$

where  $\bar{S}_K$  is the submatrix of the normalized sensitivity matrix that consists of the columns that correspond to  $\theta_K^T$ , and  $\lambda_K$  is the smallest eigenvalue of  $\bar{S}_K^T \bar{S}_K$  [32], [36].

According to Brun et al. [32], a subset of parameters can be classified as identifiable if the collinearity index  $\gamma_K$  is smaller than 20. In our analysis,  $\gamma_K$  was found to be equal to 6.90 and thus, we deduced that there is a unique solution of model parameters for a given set of model outputs (i.e. brSBP, brDBP, and cfPWV).

### **Tuning of the generic 1-D arterial tree model**

After proving the validity of our primary hypothesis, the following step was to find the adjusted input model parameters that produce as output the given measured data (i.e. brachial SBP and DBP, and cfPWV). In this respect, the global compliance and global peripheral resistance of the entire arterial tree as well as the input aortic flow were adjusted. This was done by multiplying the compliance of each arterial segment by a common scaling factor. Similarly, a different scaling factor was used to adjust all peripheral resistances. Finally,  $Q_{max}$  was modified by multiplication with a third scaling factor. An optimization algorithm was employed to derive

the optimal compliance, resistance and aortic flow peak scaling factors. Once the “tuning” was completed, the 1-D model used the adjusted parameters and produced the flow and pressure waves for every segment of the arterial tree. From the solution, we were able to obtain the flow and pressure at the aorta, namely to compute the CO and aSBP.

In this approach, the distensibility and the terminal compliance (C) of each arterial segment were modified in a uniform way for young individuals. For older or hypertensive subjects, stiffening was considered as nonuniform and more pronounced in the proximal aortic path [37]. The importance of age-related nonuniform aortic stiffening for central hemodynamics and wave reflections has been demonstrated in previous studies [38]. In order to account for this, data for the age-related local nonuniform aortic stiffening were obtained from [39]. The nonuniform stiffening of the aorta was considered by changing the relative regional distensibility of the proximal aorta (segments 1-95-2-14-18-27 of the arterial tree in Figure 1.1) through multiplication with an age-related proximal factor (Figure 3). Therefore, two scaling factors were considered: a global scaling factor multiplied with all arterial compliances and a proximal scaling factor that was additionally multiplied only with the compliance of the proximal aorta. This was to satisfy the relative relation between the proximal distensibility and the peripheral distensibility. Figure 2.3 reports the scaling factors with respect to age. The goodness of fit was high with a coefficient of determination,  $R^2$ , equal to 0.99.

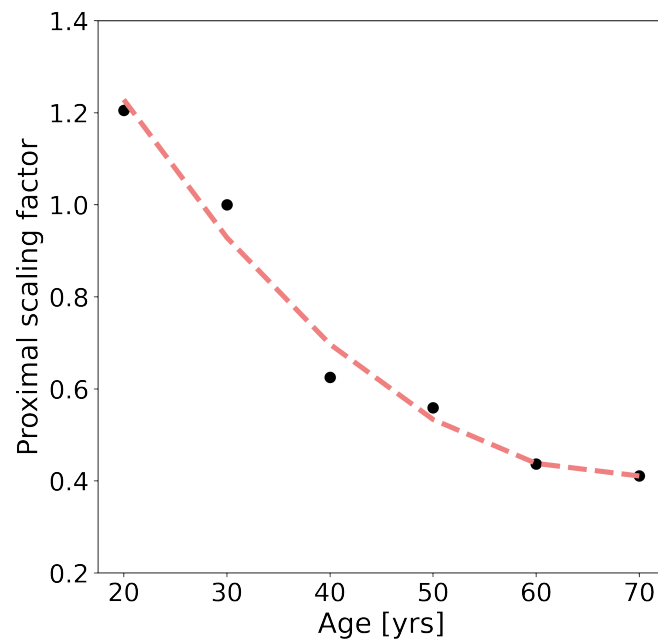


Figure 2.3 – Variation of the proximal scaling factor with respect to age for adjusting the relative distensibility of the proximal aorta. Adapted from [30].

Resistance (R) was altered in a uniform way for all terminal vessels in the model. Aortic flow was prescribed as an uncalibrated generic physiological wave, which was scaled with respect

## Chapter 2. Non-invasive cardiac output and central systolic pressure from cuff pressure and pulse wave velocity

---

to amplitude and time during the adjustment process. This concept was implemented in an iterative optimization process. The reason for employing an optimization process was to avoid searching the entire input model parameters space. Moreover, the geometry of the arterial vessels (i.e. *arterial\_length* and *arterial\_diameter*) was adjusted based on the age, gender, height, and body surface area (BSA) of each subject. For this purpose, data which associate aortic diameter size with age, gender and BSA were used from previous studies [34]. The length of the generic arterial tree segments was normalized and, subsequently, was multiplied by a scaling factor so as to be adjusted to the height of each subject.

### Optimization process

A schematic representation of the optimization algorithm is shown in Figure 2.4. In the first optimization iteration, the structure of the algorithm was as follows: an uncalibrated generic aortic flow curve was used as initial input to the model (Figure 2.5). For the generic uncalibrated aortic flow, an “average” physiologically shaped wave was selected. The scaling was performed based on the adjustment of three characteristic values, i.e. the velocity peak ( $Q_{max}$ ), time period ( $T_{period}$ ), and systolic duration ( $T_{systole}$ ) (Figure 2.5). The  $T_{period}$  of the uncalibrated aortic wave was adjusted with respect to the measured HR. Previously published data on the HR-related changes in systolic duration [35] were used to adapt the  $T_{systole}$  with respect to the given HR. Therefore, only  $Q_{max}$  remained to be optimized. A random  $Q_{max}$ , and therefore SV, was selected for the initial aortic flow input. The 1-D model subsequently computed all flows and pressures throughout the arterial tree, including the measured variables (brachial SBP and DBP, cfPWV) as well as the unknown quantities of interest (CO, aSBP). The model was expected to produce an inaccurate prediction of flows and pressures due to inaccurate model parameters and the inaccurate input aortic flow for the specific subject under investigation. Similarly, the calculated cfPWV was likely not the same as the measured cfPWV.

To address this issue, the non-invasive, patient-specific measurements were integrated into the model using a gradient-based optimization algorithm. The reference compliance, resistance and  $Q_{max}$  of the generic arterial tree were adjusted by multiplication with different scaling factors until brachial SBP, DBP, and cfPWV were correctly predicted for the uncalibrated input aortic flow (Figure 2.5). Scaling factors for the compliance were chosen so that a range of [0.10, 3.80] mL/mmHg was covered for total arterial compliance. These values correspond to an extensive range of arterial tree stiffness values [26; 40]. The reference total peripheral resistance in the model was 1 mmHg.s/mL. The scaling factor (which was multiplied with the reference resistance) varied within [0.40, 2.00] in order to cover normal values of total peripheral resistance (e.g. [0.40, 2.00] mmHg.s/mL) [41]. For scaling  $Q_{max}$ , the scaling factors were chosen so as the corresponding cardiac output is within [2.00, 8.00] L/min [42]. The limits were chosen so that the corresponding quantities as well as the pressure and flow values

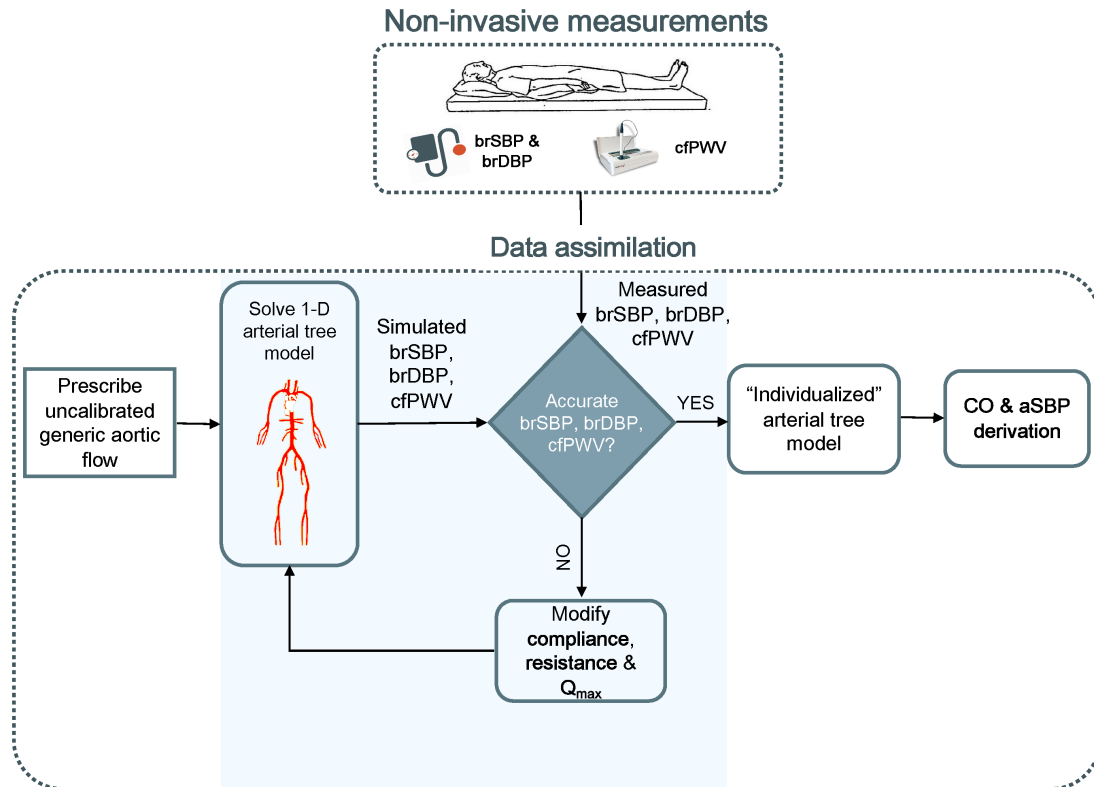


Figure 2.4 – Schematic representation of the optimization process for predicting non-invasive cardiac output and central systolic blood pressure. Adapted from [30].

generated by the arterial tree model comply with physiological hemodynamic conditions. It is to be emphasized that all parameter ranges were wider than what is to be physiologically expected, in order provide the optimization algorithm with sufficient solution space. The optimization loop ran and the process was repeated until convergence in terms of both brachial pressure and cfPWV was reached. The tolerated error for capturing brachial SBP and DBP was set to 0.01 %, whereas for cfPWV value it was 0.01 %. A maximum number of iterations ( $N_{MAX}^{iter} = 100$ ) was also defined for each optimization process. If the algorithm did not converge, the process was repeated starting from a different initial solution. In order to ensure that the algorithm was not stalled by a local minimum, several runs starting from a different random initial solution were performed.

### Model-derived pulse wave velocity

The PWV was derived using the tangential method [43]. The method uses the intersection point of two tangents on the arterial pressure wave as a characteristic marker. The first tangent is defined as the line that passes tangentially through the initial systolic upstroke, i.e. the maximum of the first derivative. The second tangent line is the horizontal line passing through

## Chapter 2. Non-invasive cardiac output and central systolic pressure from cuff pressure and pulse wave velocity

---

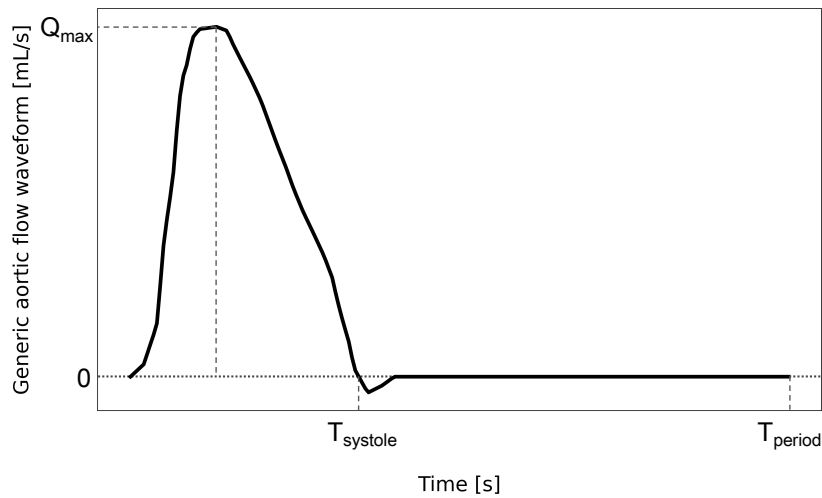


Figure 2.5 – Uncalibrated generic aortic flow waveform that is used as input to the 1-D arterial tree solver. Adapted from [30].

the minimum pressure point. Since our cohort study consists of cfPWV data, the method was applied to estimate the pulse transit time (PTT) between the carotid artery and the femoral artery. Total arterial length was determined by summation of the lengths of the arterial segments within the transmission path, i.e. the relevant carotid-femoral path (segments 5, 3, 2, 14, 18, 27, 28, 35, 37, 39, 41, 42, 44 of the generic arterial tree in Figure 2.1). Finally, the value of cfPWV was calculated by dividing the total length by the PTT.

### Measurement protocol

A preliminary assessment of the proposed methodology was carried out by testing the predictions of the method against *in vivo* data that were previously collected by Papaioannou et al. [24]. The study population included twenty-four subjects who were referred for non-invasive cardiovascular risk assessment. Subjects with risk factors or those receiving medication were also enrolled. Patients with aortic valve disease or arrhythmias were excluded. The measurement protocol was approved by the Scientific Board of Laikon General Hospital (Reference no: E53610/7/2013).

For each subject, brachial pressure waves were recorded at the brachial artery by oscillometric sphygmomanometry using the Mobil-O-Graph device (I.E.M. GmbH, Stolberg, Deutschland) [44; 45]. Central pressure waves were extracted by mathematical transformation of brachial pressure waves [46]. The cfPWV was computed using the SphygmoCor apparatus (AtCor Medical Pty Ltd, West Ryde, Australia). Pressure waves were recorded at the carotid and femoral artery by applanation tonometry (Millar SPT-301, Millar Instruments, TX, USA) as previously described [24]. SphygmoCor also provided recordings of the radial pressure waves [23] and was subsequently used for acquiring the aortic pressure waves [18] through the use of a generalized

transfer function. Despite the fact that both devices yield equally precise estimates, in the analysis we made use of the data measured with the Mobil-O-Graph in order to ensure that brachial and aortic pressure were recorded simultaneously. Especially, the brachial pressure data were used as input variables to the method and the corresponding central pressure data, measured using the same device, were used for the validation. Nevertheless, for the sake of completeness of this work, a second analysis using the SphygmoCor-derived pressure data was performed.

Two measurements of the aortic peak velocity profile at the ascending aorta were performed via transthoracic two-dimensional echocardiographic examination [24]. For this study's simulations, the average of the two measured signals was used. Aortic diameters were extracted from Doppler M-mode and CO was computed by applying the Witzig-Womersely theory [47] considering the profile of peak velocity. Cross-sectional area was assumed to be constant.

All the recorded waveforms were exported as raw data and subject to additional preprocessing. For further details on the measurements protocol, the reader is referred to the original publication [24].

### **Validation of the method-derived estimations**

Out of the 24 subjects, four were excluded from the study due to unreliable or insufficient data. The population samples included both women ( $n = 9$ ) and men ( $n = 11$ ) and covered an age range of  $38.1 \pm 12.6$  years. For each subject, the processed data from the recordings were used and the previously described methodology was adapted. The descriptive values of the hemodynamic parameters and clinical characteristics of the study population ( $n = 20$ ) are reported in Table 2.4.

We first implemented the method using as input the peripheral pressure data from the Mobil-O-Graph device. The model CO estimates were compared to the in vivo measurements via transthoracic echocardiography, whereas the predicted aSBPs were evaluated against the respective Mobil-O-Graph central pressure data. Then, the process was repeated using as input the peripheral pressure data from SphygmoCor. Similarly, COs were validated using as reference the transthoracic echocardiographic data and aSBP predictions were compared to the in vivo measurements from the respective SphygmoCor-derived central pressure data.

### **Sensitivity to measurement errors**

In order to assess the sensitivity of the method to errors in the measurements of the brachial pressure and the cfPWV, the analysis was repeated on the entire study population after (i) decreasing the brSBP with 10 % and (ii) increasing the brSBP with 10 %. In a similar approach, the effect of overestimating and underestimating the cfPWV value with 10 % was also examined.



### **Statistical analysis**

The agreement, bias, and precision between the method-derived predictions and the in vivo data were evaluated by using the Pearson's correlation coefficient ( $r$ ), intraclass correlation coefficient ( $ICC$ ), the Bland-Altman analysis and the root mean square error (RMSE). The statistical analysis was performed using the software package Prism (Prism 6, GraphPad Software Inc., San Diego, USA).

## **2.3 Results**

The comparisons between the model-derived estimations and the reference data are presented below.

### **Comparison between the model-derived CO estimates and the reference data**

Figure 2.6 shows the comparison between the model-CO estimates and the in vivo measurements via transthoracic echocardiography using the pressure data from the Mobil-O-Graph device. The corresponding Bland-Altman plot is depicted in Figure 2.6 (lower panel). The RMSE was found to be equal to 0.36 L/min. In 55 % of the cases, the difference between model-CO and reference CO was found to be below 0.30 L/min. Parameters of accuracy, correlation and agreement of CO estimation by the method in comparison to the reference method are summarized in Table 2.5. Figure 2.7 shows the model-predicted CO values compared to the in vivo echocardiographic CO values using the SphygmoCor pressure data. The Bland-Altman plot is given in Figure 2.7 (lower panel). The RMSE was 0.81 L/min and the Pearson's correlation coefficient was equal to 0.73 (Table 2.5). The difference between model-CO and reference CO was less than 0.3 L/min for the 25 % of the cases.

### **Comparison between the model-derived aSBP estimates and the reference data**

The scatterplot between the non-invasive aSBP predictions versus the in vivo measurements from the Mobil-O-Graph is presented in Figure 2.8 (top panel). The method yielded an accurate estimation of aSBP, with a RMSE of 2.46 mmHg, a Pearson's correlation coefficient of 0.98 and a high ICC of 0.98. The Bland-Altman analysis, as given in Figure 2.8 (lower panel), showed a good agreement between the model and the reference aSBP values. The difference between model-aSBP and reference aSBP was less than 1.50 mmHg for the 30 % of the cases, whereas in 60 % of them it ranged between 1.50 and 3.50 mmHg and only 10 % exceeded the 3.50 mmHg. Parameters of precision, correlation and agreement between the estimates and the real values are reported in Table 2.6. Figure 2.9 shows the aSBP predictions compared to the in vivo SphygmoCor aSBP values. The Bland-Altman plot is presented in Figure 2.9 (lower panel). The RMSE was equal to 3.42 mmHg and the Pearson's correlation coefficient was equal to 0.98

Table 2.4 – Descriptive hemodynamical parameters and clinical characteristics of the study population (n = 20).

Index	Women (n <sub>1</sub> = 9)				Men (n <sub>2</sub> = 11)			
	min	max	mean	SD	min	max	mean	SD
Age [years]	27	61	36.25	11.3	23	70	39.83	15.3
Height [cm]	152	178	165.67	8.43	170	192	179.91	6.93
Weight [kg]	49	80	61.89	12.17	71	128	92.27	17.7
Central SBP [mmHg]	93	117	103.11	8.24	99	136	117.45	10.71
Brachial SBP [mmHg]	98	121	110	8.05	107	145	123.73	10.77
Brachial DBP [mmHg]	60	81	70.67	6.24	74	98	82.64	7.61
Brachial pulse pressure [mmHg]	32	46	39.33	4.33	33	52	41.09	5.86
Mean arterial pressure [mmHg]	72.67	94	83.78	6.59	85	110.33	96.33	8.34
Mean aortic flow [L./min]	3	5.4	4.24	0.74	3	6.2	4.41	1.01
Heart rate [bpm]	51	84	70.11	10.4	51	89	71.45	10.88
Carotid-femoral PWV [m/s]	5.25	9.05	6.11	1.17	5.4	11.25	7.53	2.21
Smoking [%]	44.44				64.64			
Diabetes [%]	0				18.18			
Hypertension [%]	0				36.36			
Dyslipidemia [%]	0				36.36			
Renal disease [%]	0				9.09			
CVD [%]	0				36.36			
Stroke [%]	0				9.09			
History of CVD [%]	44.44				9.09			

## Chapter 2. Non-invasive cardiac output and central systolic pressure from cuff pressure and pulse wave velocity

---

Table 2.5 – Parameters of accuracy, correlation and agreement of CO estimation by the model in comparison to the reference method.

<b>Parameter</b>	<b>Value (using Mobil-O-Graph pressure data)</b>	<b>Value (using SphygmoCor pressure data)</b>
Mean difference [L/min]	0.04	0.04
Standard deviation of difference [L/min]	0.36	0.83
Limits of agreement [L/min]	(-0.66, 0.73)	(-1.54, 1.63)
Root mean square error [L/min]	0.36	0.81
Pearson's correlation coefficient	0.91	0.73
Intraclass correlation coefficient	0.91	0.69

Table 2.6 – Parameters of accuracy, correlation and agreement of aSBP estimation by the model in comparison to the reference method.

<b>Parameter</b>	<b>Value (using Mobil-O-Graph pressure data)</b>	<b>Value (using SphygmoCor pressure data)</b>
Mean difference [mmHg]	-0.27	0.82
Standard deviation of difference [mmHg]	2.51	3.41
Limits of agreement [mmHg]	(-5.07, 4.52)	(-5.69, 7.33)
Root mean square error [mmHg]	2.46	3.42
Pearson's correlation coefficient	0.98	0.98
Intraclass correlation coefficient	0.98	0.97

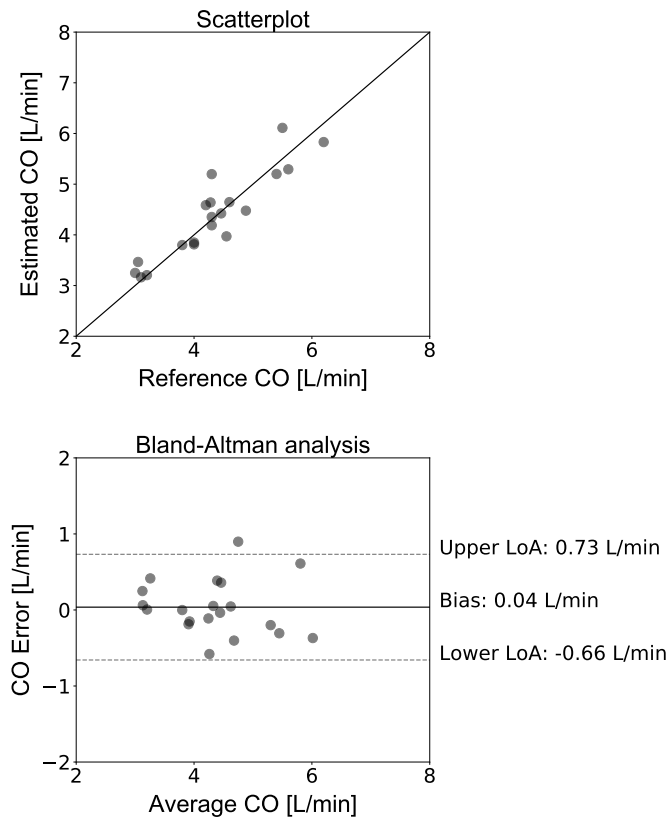


Figure 2.6 – Comparison between the estimated CO values and the reference in vivo data (using the Mobil-O-Graph pressure data). Top panel: Scatterplot between the values of CO derived from the method and the values of CO measured with 2-D transthoracic echocardiography (solid and dashed line represent equality and linear regression, respectively). Lower panel: Bland-Altman plot for CO prediction by the model versus 2-D transthoracic echocardiographic measurement. Limits of agreement are defined by the two horizontal dotted lines. Adapted from [30].

(Table 2.6). For 20% of the cases, the difference between model-aSBP and reference aSBP was less than 1.50 mmHg, for 40 % of them it ranged between 1.50 and 3.50mmHg and for the remaining 40 % it was found to be above 3.50 mmHg.

### Sensitivity of model predictions to input parameter measurement errors

Table 2.7 shows the sensitivity of the model predictions in terms of CO and aSBP when a  $\pm 10$  % error is introduced in the measurements of brachial SBP and cfPWV. In case of an overestimation of the brSBP, it was noted that CO and aSBP estimates were sensitive to the erroneously measured brachial SBP with relative (with respect to the actual value) errors of  $26.76 \pm 17.01$  % and  $8.98 \pm 5.45$  %, respectively. When an underestimation of the brSBP was assumed, the errors in CO and aSBP were calculated to be  $-20.67 \pm 18.11$  % and  $-11.88 \pm 4.28$  %.

## Chapter 2. Non-invasive cardiac output and central systolic pressure from cuff pressure and pulse wave velocity

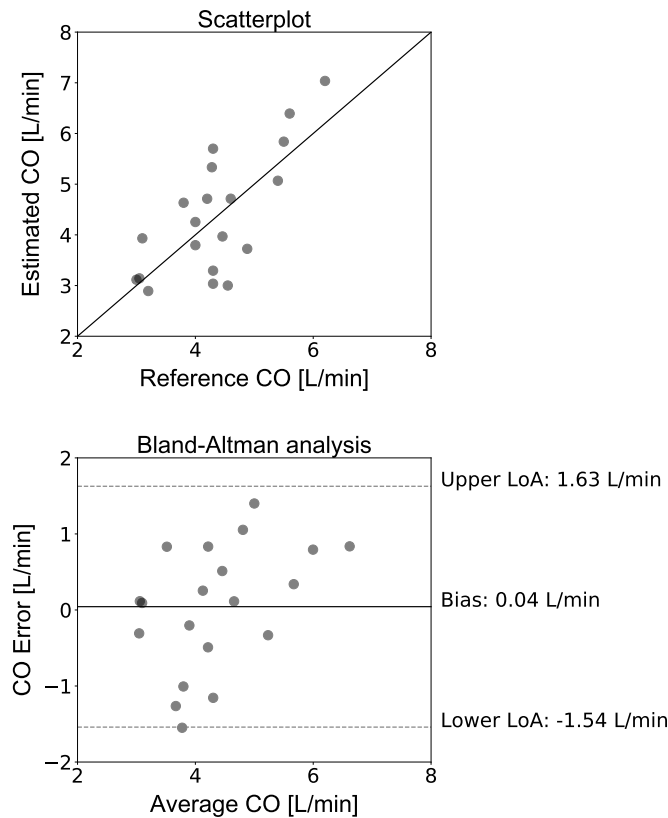


Figure 2.7 – Comparison between the estimated CO values and the reference in vivo data (using the SphygmoCor pressure data). Top panel: Scatterplot between the values of CO derived from the method and the values of CO measured with 2-D transthoracic echocardiography (solid and dashed line represent equality and linear regression, respectively). Lower panel: Bland-Altman plot for CO prediction by the model versus 2-D transthoracic echocardiographic measurement. Limits of agreement are defined by the two horizontal dotted lines. Adapted from [30].

%, respectively.

Likewise, a deliberate error of  $\pm 10\%$  was imposed to the cfPWV measurement. The algorithm was re-employed for the new input. The aSBP prediction seemed to be more robust to errors in cfPWV measurements than to errors in brSBP measurements (Table 2.7). A  $\pm 10\%$  error in the in vivo cfPWV rendered small errors in the aSBP estimations, equal to  $-4.34 \pm 4.41\%$  and  $-3.74 \pm 4.03\%$ , respectively. Relatively higher deviations of  $-12.73 \pm 6.23\%$  and  $11.84 \pm 9.56\%$  were reported for the CO estimates.

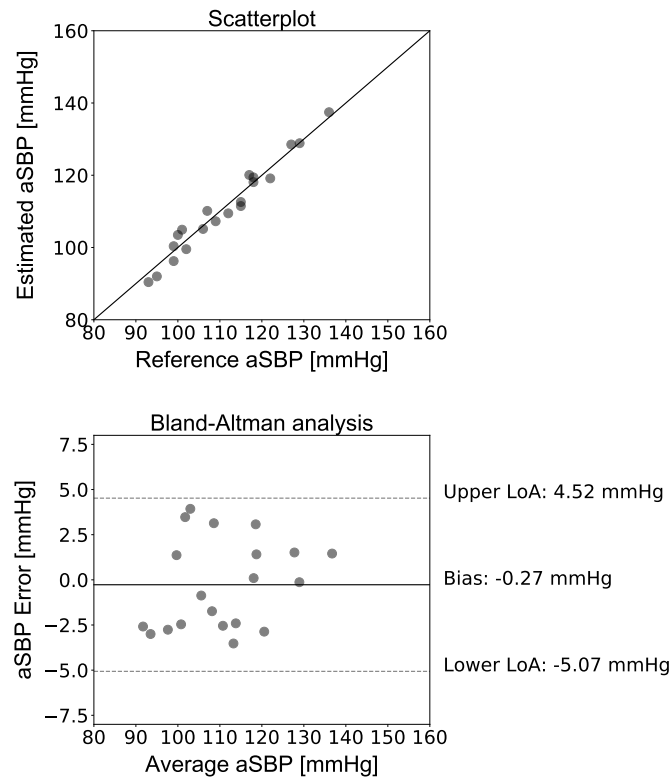


Figure 2.8 – Comparison between the estimated aSBP values and the reference in vivo data (using the Mobil-O-Graph pressure data). Top panel: Scatterplot between the values of aSBP derived from the model and the values of aSBP measured with Mobil-O-Graph (solid and dashed line represent equality and linear regression, respectively). Lower panel: Bland-Altman plot for aSBP prediction by the model versus in vivo measurement using the Mobil-O-Graph device. Limits of agreement are defined by the two horizontal dotted lines. Adapted from [30].

## 2.4 Discussion

In the present study, we implemented and assessed a novel method for predicting CO and aSBP based on non-invasive measurements of peripheral (brachial) pressure and pulse wave velocity. The method is based on the adjustment of a generic 1-D arterial model using the non-invasive recordings of the brachial cuff-based systolic and diastolic blood pressures and cfPWV, which are easily obtained in a clinical setting. The 1-D dimensional model of the arterial tree has been thoroughly validated in vivo and provides realistic flow and pressure waveforms [25; 22]. An optimization process was developed in order to fuse the computational model with the measurement data. We adjusted arterial model parameters such that model predictions fit the non-invasive recordings and thus render the generic model closer to a patient-specific model. This study demonstrated that creating a version of the generalized CV model closer to each patient's standards can potentially enhance the accuracy in the CO and aSBP prediction.

## Chapter 2. Non-invasive cardiac output and central systolic pressure from cuff pressure and pulse wave velocity

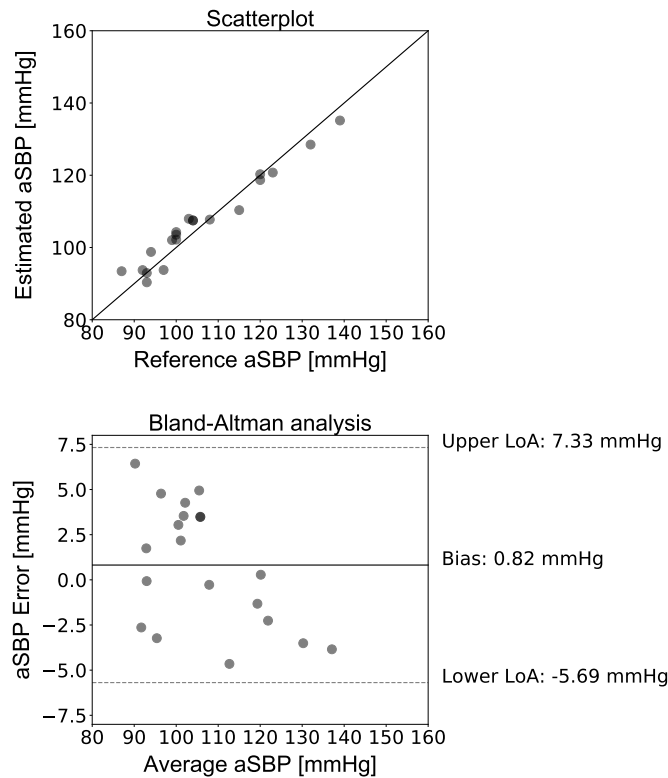


Figure 2.9 – Comparison between the estimated aSBP values and the reference in vivo data (using the SphygmoCor pressure data). Top panel: Scatterplot between the values of aSBP derived from the model and the values of aSBP measured with SphygmoCor (solid and dashed line represent equality and linear regression, respectively). Lower panel: Bland-Altman plot for aSBP prediction by the model versus in vivo measurement using the SphygmoCor device. Limits of agreement are defined by the two horizontal dotted lines. Adapted from [30].

Patient-specific models of the human vasculature are confronted with significant challenges that pertain to the unique characteristics of each individual. Geometry, in particular, cannot be completely defined for each arterial segment throughout the vasculature. In this study, the geometry of an individual was approximated by using data from a previously published study [34]. These data allowed for an estimation of the aortic size without the need for additional complicated or costly measurements. As anticipated, the aortic size approximation slightly deviated from the actual aortic dimension. However, having at our disposal the aortic diameter values (directly measured from echocardiography), we observed that the approximated diameter of the ascending aorta did not differ significantly from the true measured values (the difference was equal to  $0.25 \pm 0.44$  cm).

Peripheral non-invasive pressure measurements proved to be adequate to adjust the arterial tree model and were demonstrated to be informative to predict aortic hemodynamics. CO and aSBP estimates were found to be in good agreement with the reference methods. Figure 2.10 shows an aortic pressure waveform as resulted from the 1-D model. The model-derived

Table 2.7 – Estimates of relative errors in CO and aSBP after introducing: (i) a  $\pm 10\%$  error in the brachial SBP measurement and (ii) a  $\pm 10\%$  error in the cfPWV measurement.

Introduced error	CO estimate error [%]	aSBP estimate error [%]
	mean $\pm$ SD	mean $\pm$ SD
+10 % brSBP	26.76 $\pm$ 17.01	8.98 $\pm$ 5.45
-10 % brSBP	-20.67 $\pm$ 18.11	-11.88 $\pm$ 4.28
+10 % cfPWV	-12.73 $\pm$ 6.23	-4.34 $\pm$ 4.41
-10 % cfPWV	11.84 $\pm$ 9.56	-3.74 $\pm$ 4.03

aortic pressure wave bears all the characteristic details and shape of a physiological pressure signal. This observation further strengthens the physiological relevance of our results. To our knowledge, this novel work constitutes the first method that makes use of only three easily obtained inputs (e.g. non-invasive brSBP and brDBP, and PWV) to successfully adjust a 1-D generic arterial tree model and accurately predict hemodynamics at the aortic root (e.g. CO and aSBP). The fusion of clinically relevant non-invasive data with theory-based modelling avoids simplified assumptions that have been proposed by previous studies [18; 48]. Additionally, it should be noted that the clinical application of the proposed framework is highly facilitated by the fact that PWV can be routinely measured in clinical practice and has been identified as an independent predictor of cardiovascular disease [49; 50; 51], especially when it can be translated in conjunction with pressure measurements.

We performed an identifiability analysis as proposed by Brun et al. in order to identify the most sensitive parameters that drive the variability in the model output (i.e. brSBP, brDBP, and cfPWV). This analysis can be very informative to guide the strategy for inverse problem-solving methods. The sensitivity matrix demonstrated that  $Q_{max}$  was the most sensitive determinant of the model output, which may be explained from the fact that aortic flow serves as the proximal boundary condition. Total peripheral resistance,  $T_{period}$  and arterial compliance followed. The sensitivity to  $T_{period}$  was directly addressed by exploiting the HR information. The high sensitivities of compliance and resistance can most likely be attributed to our selection of the model outputs, namely bSBP and brDBP, and thus pulse pressure (PP) and mean arterial pressure (MAP). Arterial compliance is a major determinant of PP [52] and total peripheral resistance dictates MAP [53].

The mitigation of errors that are inevitably present in clinical measurements challenges the reliability of oscillometric devices. The majority of automatic cuff devices for measuring blood pressure are based on generalized models to estimate blood pressure from an oscillogram [54]. This can limit the accuracy of the device in a certain pressure range. A noteworthy approach has been proposed by Liu et al. [55]. They used a physiologic model in conjunction with model fitting [56]. The method has achieved to maintain blood pressure estimation accuracy whereas it was proven to be less sensitive to common physiologic deviations in the oscillogram. Here, artificial errors in brSBP and cfPWV measurements were manually introduced in a discrete way



## Chapter 2. Non-invasive cardiac output and central systolic pressure from cuff pressure and pulse wave velocity

---

in order to study the effect of each error on the predictions. However, it should be emphasized that measurements errors in brSBP and cfPWV may also happen concurrently and be highly interdependent.

The sensitivity analysis in measurements' errors in brSBP and cfPWV demonstrated evidence that the CO and aSBP predictions are expected to be more sensitive to errors in brSBP than to errors in cfPWV. The aSBP prediction seems to be determined mainly from the brSBP information, while brSBP is rather sensitive to the resistance (sensitivity matrix, Figure 2.2) that dictates the mean blood pressure. The strong sensitivity of aSBP estimation to brSBP errors is to be expected, since the input brSBP and the estimated aSBP are strongly related to mean blood pressure, which is practically the same in both central and peripheral arterial sites.

CfPWV, on the other hand, is related to arterial compliance, which is a weaker determinant of stroke volume and CO, compared to arterial resistance and by extension to mean pressure, as also described in earlier work by Stergiopoulos et al. [57]. In our analysis, this is clearly demonstrated in the scaled sensitivity matrix (Figure 2.2); the sensitivity between cfPWV and  $Q_{max}$ , and thus CO, is approximately 2.5 times smaller (equal to 0.42) compared to the sensitivity between brSBP and  $Q_{max}$  (equal to 1.00).

In order to evaluate the method's predictions, data from Mobil-O-Graph device were used. However, SphygmoCor data were also available and, therefore, we additionally compared our method's estimates using the data from the SphygmoCor device. Overall, a better performance was observed when pressure data from Mobil-O-Graph were used. It is possible that the discrepancies in CO and aSBP estimations between the two office devices may be attributed to differences between the two measurement techniques. First, differences exist in the technique of signal acquisition as well as the arterial site of recording; Mobil-O-Graph uses oscillometry at the brachial artery level and SphygmoCor uses applanation tonometry at the radial or carotid artery. Furthermore, differences exist in the computational method of central blood pressure derivation; Mobil-O-Graph applies the ArcSolver as previously described in [58; 59] and [60], whereas SphygmoCor applies a generalized transfer function [18]. The central aortic pressure derived from Mobil-O-Graph is simultaneously recorded with the brachial pressure. In contrast, SphygmoCor uses a generalized transfer function to transform the radial pressure wave into aortic pressure wave [48]. Since brachial pressure is the one that drives the optimization process, Mobil-O-Graph's simultaneous brachial and central pressures acquisition may potentially lead to a more accurate aortic-peripheral PP amplification and thus more accurate prediction. Additionally, SphygmoCor's generalized transfer function is likely to deviate from our partially individualized method at a greater extent than Mobil-O-Graph's "per patient" scheme. Finally, differences in measurement accuracy between the two apparatuses may be also due to different calibration methods [60].

Part of the state of the art has focused on the improvement of the already available generalized

TFs. Swamy et al. have presented a work on an adaptive generalized TF using information on the wave propagation delay time between aortic and peripheral pressure waves [61]. However, this information was obtained using prior knowledge of the aortic flow. Some of the previous authors have proposed an improved adaptive generalized TF using arterial wave transmission and reflection coefficient information [62]. Their results have showed significant accuracy improvement in aSBP estimations (RMSE equal to 3.43 mmHg), especially in patients with low PP amplification.

Hahn et al. have introduced a novel approach on the central aortic pressure wave from measured peripheral pressure wave by employing an individualized transmission line (TL) model [63]. The method was evaluated on swine data and achieved a high correlation of 0.92 between the predicted aSBP and the reference aSBP. Nevertheless, the use of a TL model may be regarded as a simplification due to the actual curvature of the arterial line and the multiple reflection sites that may not be accurately described by a lumped terminal impedance. Moreover, the methods presented above employ a single pressure waveform and thus, the individualization is considered to be more simplified compared to a technique that fuses multiple non-invasive measurements.

Approaches comparable to ours have been developed to address the challenges of patient-specific hemodynamic monitoring. Tosello et al. [64] have proposed a new technique for determining central blood pressure using a multiscale mathematical model which is adjusted based on age, height, weight, brachial pressure, left ventricular end-systolic and end-diastolic volumes and aortic PWV. The estimation derived from their method presented low performance (significant overestimation of 7.8 mmHg for aSBP prediction) when compared against data from the SphygmoCor device. In their work, a large number of input variables are needed, including also central qualities (e.g. end-systolic and end-diastolic volumes). Here, however, aSBP can be predicted with a higher accuracy and by using fewer input parameters for the partial individualization of the model. Therefore, this simplifies the measurement process and potentially decreases the total cost of monitoring. Recently, Guala et al. published a validation of the same multiscale model using invasive catheter data [65]. Their model provided an underestimation of both central systolic and diastolic pressure values; the difference between the invasive aortic pressure and the model-derived estimates was  $4.30 \pm 16.70$  mmHg for central systolic pressure and  $3.80 \pm 10.40$  mmHg for central diastolic pressure. Validation using invasive data should be conducted for our proposed methodology, so as to be able to perform a fair comparison between the performance of the two models.

Additionally, important cardiovascular risk predictors have recently been estimated from the fusion of multiple non-invasive measurements (i.e. pulse pressure waveforms at the arm and the ankle) [66]. The method provides predictions of central SBP and PP, PP amplification, and PTT. The RMSE for aSBP was reported to be rather low (1.99 mmHg). An advantage of the technique is that it also yields the entire central pressure waveform. Nevertheless, the use of a

## **Chapter 2. Non-invasive cardiac output and central systolic pressure from cuff pressure and pulse wave velocity**

---

lumped-parameter model to describe the arterial tree may not be sufficient for considering the intermediate reflections between the central and the distal arterial sites. Hence, this may be considered as a simplification when compared to a complete model of the systemic circulation.

A particularly interesting study was performed by Swamy et al. [67], in which CO is estimated using peripheral pressure waves from multiple arterial sites. In the proposed methodology, the aortic pressure wave is computed by applying a multichannel blind system identification algorithm [68]. The concept is based on the assumption that an arterial path between two arterial sites can be described by a transfer function of a finite impulse response (FIR) filter. The filter parameters were defined through a deconvolution algorithm. Subsequently, CO was estimated via fitting a Windkessel model to the computed aortic pressure wave. The lumped parameters of the Windkessel model (compliance and resistance) were calculated by extracting the time constant from the aortic pressure wave. Although this method illustrated an effective way of identifying CO (with a normalized RMSE of 12.9 %), it constitutes a relatively simplified approach which is based on a mathematical transfer function with less physiological information on the patient-based cardiovascular system in comparison to a complete model of systemic circulation.

Fazeli and Hahn have also proposed an improved Windkessel approach for individualized CO and total peripheral resistance (TPR) estimation [69]. Their approach is based on “tuning” a Windkessel model using measurements of systolic, diastolic, and mean arterial blood pressure. The method outperformed the standard Windkessel method (prediction improved by 16 %) providing also an optimal patient- and time-specific time constant that is needed to estimate CO and TPR. A limitation of the study pertains to the simple linear model that was used to associate pressure and arterial compliance. This may be far from the actual highly nonlinear relationship between the two [70] and may affect the validity of the method when applied on a wider range of pulse pressure values.

### **Limitations**

A number of limitations need to be considered. The gold-standard technique for central aortic pressure is an invasive, catheter-based measurement. In this study, evaluation was conducted using central aortic pressure waves obtained from the Mobil-O-Graph device. Although the Mobil-O-Graph has been successfully validated in the past [44], significant errors may be present in the Mobil-O-graph estimations. Therefore, the validation presented here is only of relative and limited value. It cannot be used to demonstrate any potential advantage in comparison to the existing generalized mathematical models. Similarly, the reference method used for aortic flow was transcutaneous echocardiography, which can only allow us to conclude that the prediction of this method is a fair estimate of the true value. Future studies using gold-standard invasive measurement techniques are required for full validation

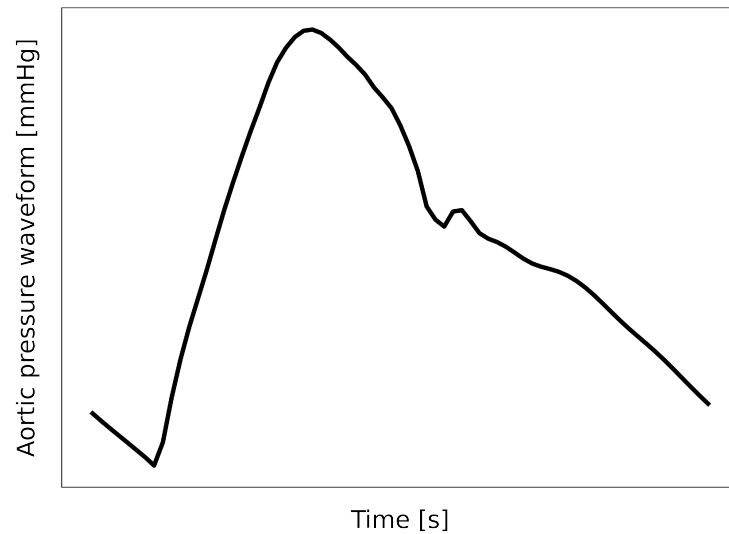


Figure 2.10 – Arbitrary aortic pressure waveform that was yielded from the 1-D arterial tree solver. Adapted from [30].

of the proposed method. From an ethical perspective, it was not possible to perform invasive measurements in the context of a validation study.

Another limitation lies in the small sample size of older subjects who exhibit high PWV values. Also, the subject cohort is quite uniform in terms of PP (e.g. standard deviation of PP equal to 4 mmHg). This does not allow us to assess how well the method adapts to large variations in PP. To further enhance the robustness of the proposed method, validation on a larger population (including a larger number of patients older than 50 years and a wider range of PP levels) should be performed.

Furthermore, the integration of previously published data in the adjustment of arterial diameter leads to an “average” version of the 1-D cardiovascular model in terms of geometric configuration. Even if we tune the model with the patient-specific measurements that we have at our disposal, the patient-specific character of the method cannot be entirely justified. However, a fully personalized model would not be possible, since this would require us to obtain numerous non-invasive and invasive measurements for every individual. Since CO is known to be particularly dependent on arterial geometry measurements [71], individualized CO prediction still remains a challenge.

In addition, the use of previously published data on HR-related systolic duration leads to an approximation of the aortic flow wave. However, the difference between the approximated  $T_{systole}$  and the actual  $T_{systole}$  (derived from the reference ultrasound aortic flows) was found to be  $-10.05 \pm 6.72$  ms and thus not very considerable. Furthermore, the sensitivity analysis demonstrated that the model outputs were less sensitive to changes in  $T_{systole}$  (Figure 2.2).

## Chapter 2. Non-invasive cardiac output and central systolic pressure from cuff pressure and pulse wave velocity

---

When the actual systolic duration was used as an input to the model, the CO and aSBP predictions were improved by 0.84 % and 0.63 %, respectively. As anticipated, the more information is embedded into the system, the more accurate our predictions become. However, our assumptions do not seem to significantly underestimate the prediction capacity of our method in the study population. Moreover, we should comment that the aortic flow wave that we imposed as a proximal boundary condition had a constant shape (only  $Q_{max}$ ,  $T_{period}$ , and  $T_{systole}$  were modified), while the systolic duration was defined as a relative approximation with respect to HR. These points also contribute to characterizing the model as partially patient-specific.

This study demonstrates the method's capacity to predict absolute CO for each subject. However, clinical research is particularly interested in monitoring CO changes within the same patient [72]; especially for patients in the intensive care unit [73]. Thus, another limitation pertains to the lack of available data to validate changes in the estimated CO within an individual. Our future work envisages the evaluation of our method on inter-patient changes in CO.

Another potential limitation may be the inconvenience in acquiring cfPWV. The cfPWV measurement requires sequential recording of the carotid and femoral pressure pulse via applanation tonometry [74; 75]. The measurement process also takes some time to obtain the two signals sequentially, whereas it is intrusive in that it requires palpation of the femoral pressure pulse near the groin [76]. Alternatively, the volume-clamp technique [77] proposes the use of the finger pressure waveform for estimating aSBP and CO. Nevertheless, this technique excludes the arterial stiffness information embedded in cfPWV which potentially enhances the physiological relevance of CO calculation.

Nobody can exclude that certain combinations of cardiac and arterial parameters may yield similar pressure and PWV values. We tested our method on a synthetic case of reduced contractility in the presence of increased total peripheral resistance and assessed its performance. Particularly, the cardiac contractility was reduced by decreasing the end-systolic elastance ( $E_{es}$ ) by 20 % while total peripheral resistance was increased by 40 % in order to maintain pressure at normal levels. This yielded brachial SBP and DBP, and cfPWV, which were isolated and used as input to the inverse method. After the optimization process, the estimated CO and aSBP for the case of reduced contractility were close to their real values (-0.21 % error in aSBP prediction and 3.30 % in CO prediction). Nevertheless, it is possible that there are extreme cases for which our algorithm may fall short in making an accurate prediction. Therefore, further investigation on the method's performance in such cases should be performed in order to evaluate the potential errors in a larger scale.

Finally, this method has been designed and applied on a healthy population. Hence, its applicability might be limited in the case of pathological conditions, such as aneurysm or aortic valve disease, where the relationship between input and output values is significantly modified and often poorly specified. Investigation of the method's performance on such populations could also be of particular interest.

### **Conclusion**

In conclusion, it was demonstrated that a generic 1-D model of the systemic circulation can be effectively adjusted to partially patient-specific standards using non-invasive measurements of brachial pressure and PWV. The *in vivo* evaluation suggests that this novel method predicts CO and aSBP with good accuracy and specificity. Further clinical validation against gold-standard measurements remains to be performed in order to verify that the proposed technique may be employed for non-invasive CO and aSBP monitoring in the clinical setting.

## **Chapter 2. Non-invasive cardiac output and central systolic pressure from cuff pressure and pulse wave velocity**

---

## Bibliography

- [1] T. K. Waddell, A. M. Dart, T. L. Medley, J. D. Cameron, and B. A. Kingwell, "Carotid pressure is a better predictor of coronary artery disease severity than brachial pressure," *Hypertension (Dallas, Tex.: 1979)*, vol. 38, no. 4, pp. 927–931, Oct. 2001.
- [2] M. E. Safar, J. Blacher, B. Pannier, A. P. Guerin, S. J. Marchais, P.-M. Guyonvarc'h, and G. M. London, "Central pulse pressure and mortality in end-stage renal disease," *Hypertension (Dallas, Tex.: 1979)*, vol. 39, no. 3, pp. 735–738, Mar. 2002.
- [3] H. Berkenstadt, N. Margalit, M. Hadani, Z. Friedman, E. Segal, Y. Villa, and A. Perel, "Stroke volume variation as a predictor of fluid responsiveness in patients undergoing brain surgery," *Anesthesia & Analgesia*, vol. 92, no. 4, pp. 984–989, Apr. 2001. [Online]. Available: <https://insights.ovid.com/crossref?an=00000539-200104000-00034>
- [4] M. McKendry, H. McGloin, D. Saberi, L. Caudwell, A. R. Brady, and M. Singer, "Randomised controlled trial assessing the impact of a nurse delivered, flow monitored protocol for optimisation of circulatory status after cardiac surgery," *BMJ*, vol. 329, no. 7460, p. 258, Jul. 2004. [Online]. Available: <http://www.bmj.com/lookup/doi/10.1136/bmj.38156.767118.7C>
- [5] N. Lees, M. Hamilton, and A. Rhodes, "Clinical review: goal-directed therapy in high risk surgical patients," *Critical Care*, vol. 13, no. 5, p. 231, 2009. [Online]. Available: <https://www.ncbi.nlm.nih.gov/pmc/articles/PMC2784362/>
- [6] A. Avolio, "Central aortic blood pressure and cardiovascular risk: a paradigm shift?" *Hypertension (Dallas, Tex.: 1979)*, vol. 51, no. 6, pp. 1470–1471, Jun. 2008.
- [7] L. Yang, B. Qin, X. Zhang, Y. Chen, and J. Hou, "Association of central blood pressure and cardiovascular diseases in diabetic patients with hypertension," *Medicine*, vol. 96, no. 42, Oct. 2017. [Online]. Available: <https://www.ncbi.nlm.nih.gov/pmc/articles/PMC5662393/>
- [8] A. Song-Tao, Q. Yan-Yan, and W. Li-Xia, "The severity of coronary artery disease evaluated by central systolic pressure and fractional diastolic pressure," *North American Journal of Medical Sciences*, vol. 2, no. 5, pp. 218–220, May 2010. [Online]. Available: <https://www.ncbi.nlm.nih.gov/pmc/articles/PMC3347647/>



## Bibliography

---

- [9] P. L. Marino, *The ICU book*, 2nd ed. Baltimore: Lippincott Williams & Wilkins, 1998, oCLC: 833333761.
- [10] X. Xiao, E. T. Ozawa, Y. Huang, and R. D. Kamm, "Model-based assessment of cardiovascular health from noninvasive measurements," *Annals of Biomedical Engineering*, vol. 30, no. 5, pp. 612–623, May 2002. [Online]. Available: <http://link.springer.com/10.1114/1.1484217>
- [11] S. Söderström, G. Nyberg, M. F. O'Rourke, J. Sellgren, and J. Pontén, "Can a clinically useful aortic pressure wave be derived from a radial pressure wave?" *British Journal of Anaesthesia*, vol. 88, no. 4, pp. 481–488, Apr. 2002. [Online]. Available: <http://www.sciencedirect.com/science/article/pii/S0007091217364723>
- [12] S. A. Hope, D. B. Tay, I. T. Meredith, and J. D. Cameron, "Use of arterial transfer functions for the derivation of aortic waveform characteristics," *Journal of Hypertension*, vol. 21, no. 7, pp. 1299–1305, Jul. 2003.
- [13] W. J. Stok, B. E. Westerhof, and J. M. Karemaker, "Changes in finger-aorta pressure transfer function during and after exercise," *Journal of Applied Physiology*, vol. 101, no. 4, pp. 1207–1214, Oct. 2006. [Online]. Available: <http://www.physiology.org/doi/10.1152/jappphysiol.00876.2005>
- [14] B. Fetics, E. Nevo, C.-H. Chen, and D. M. Kass, "Parametric model derivation of transfer function for noninvasive estimation of aortic pressure by radial tonometry," *IEEE Transactions on Biomedical Engineering*, vol. 46, pp. 698–706, 1999.
- [15] A. A. Udy, M. Altukroni, P. Jarett, J. A. Roberts, and J. Lipman, "A comparison of pulse contour wave analysis and ultrasonic cardiac output monitoring in the critically ill," *Anaesthesia and Intensive Care*, vol. 40, no. 4, pp. 631–637, Jul. 2012. [Online]. Available: <https://research.monash.edu/en/publications/a-comparison-of-pulse-contour-wave-analysis-and-ultrasonic-cardia>
- [16] J. Jansen, J. Schreuder, J. Mulier, N. Smith, J. Settels, and K. Wesseling, "A comparison of cardiac output derived from the arterial pressure wave against thermodilution in cardiac surgery patients," *British Journal of Anaesthesia*, vol. 87, no. 2, pp. 212–222, Aug. 2001. [Online]. Available: <https://linkinghub.elsevier.com/retrieve/pii/S0007091217376250>
- [17] M. T. Ganter, J. A. Alhashemi, A. M. Al-Shabasy, U. M. Schmid, P. Schott, S. A. Shalabi, A. M. Badri, S. Hartnack, and C. K. Hofer, "Continuous cardiac output measurement by un-calibrated pulse wave analysis and pulmonary artery catheter in patients with septic shock," *Journal of Clinical Monitoring and Computing*, vol. 30, no. 1, pp. 13–22, Feb. 2016.
- [18] M. Karamanoglu, M. F. O'Rourke, A. P. Avolio, and R. P. Kelly, "An analysis of the relationship between central aortic and peripheral upper limb pressure waves in man," *European Heart Journal*, vol. 14, no. 2, pp. 160–167, Feb. 1993.

- [19] M. Sugimachi, T. Shishido, K. Miyatake, and K. Sunagawa, "A new model-based method of reconstructing central aortic pressure from peripheral arterial pressure," *The Japanese Journal of Physiology*, vol. 51, no. 2, pp. 217–222, Apr. 2001.
- [20] P. Hallock and I. C. Benson, "Studies on the elastic properties of human isolated aorta," *Journal of Clinical Investigation*, vol. 16, no. 4, pp. 595–602, Jul. 1937. [Online]. Available: <https://www.ncbi.nlm.nih.gov/pmc/articles/PMC424899/>
- [21] A. C. Guyton and J. E. Hall, *Textbook of medical physiology*, 9th ed. Philadelphia : W.B. Saunders, 1996. [Online]. Available: <https://trove.nla.gov.au/work/28692053>
- [22] P. Reymond, Y. Bohraus, F. Perren, F. Lazeyras, and N. Stergiopoulos, "Validation of a patient-specific one-dimensional model of the systemic arterial tree," *American Journal of Physiology. Heart and Circulatory Physiology*, vol. 301, no. 3, pp. H1173–1182, Sep. 2011.
- [23] J.-X. Wang, X. Hu, and S. C. Shadden, "Data-augmented modeling of intracranial pressure," *arXiv:1807.10345 [physics]*, Jul. 2018, arXiv: 1807.10345. [Online]. Available: <http://arxiv.org/abs/1807.10345>
- [24] T. G. Papaioannou, D. Soulis, O. Vardoulis, A. Protogerou, P. P. Sfikakis, N. Stergiopoulos, and C. Stefanadis, "First in vivo application and evaluation of a novel method for non-invasive estimation of cardiac output," *Medical Engineering & Physics*, vol. 36, no. 10, pp. 1352–1357, Oct. 2014.
- [25] P. Reymond, F. Merenda, F. Perren, D. Rüfenacht, and N. Stergiopoulos, "Validation of a one-dimensional model of the systemic arterial tree," *American Journal of Physiology. Heart and Circulatory Physiology*, vol. 297, no. 1, pp. H208–222, Jul. 2009.
- [26] G. Langewouters, *Visco-elasticity of the human aorta in vitro in relation to pressure and age (Ph.D. thesis)*. Amsterdam: Free University of Amsterdam: Krips Repro, 1982. [Online]. Available: <https://books.google.gr/books?id=qvSrHAAACAAJ>
- [27] R. Holenstein, P. Niederer, and M. Anliker, "A viscoelastic model for use in predicting arterial pulse waves," *Journal of Biomechanical Engineering*, vol. 102, no. 4, pp. 318–325, Nov. 1980.
- [28] K. Sagawa, H. Suga, A. A. Shoukas, and K. M. Bakalar, "End-systolic pressure/volume ratio: a new index of ventricular contractility," *The American Journal of Cardiology*, vol. 40, no. 5, pp. 748–753, Nov. 1977.
- [29] Suga Hiroyuki and Sagawa Kiichi, "Instantaneous pressure-volume relationships and their ratio in the excised, supported canine left ventricle," *Circulation Research*, vol. 35, no. 1, pp. 117–126, Jul. 1974. [Online]. Available: <https://www.ahajournals.org/doi/abs/10.1161/01.res.35.1.117>

## Bibliography

---

- [30] V. Bikia, S. Pagoulatou, B. Trachet, D. Soulis, A. D. Protogerou, T. G. Papaioannou, and N. Stergiopoulos, “Noninvasive cardiac output and central systolic pressure from cuff-pressure and pulse wave velocity,” *IEEE Journal of Biomedical and Health Informatics*, vol. 24, no. 7, pp. 1968–1981, 2019.
- [31] D. G. Watts and D. M. Bates, *Nonlinear regression analysis and its applications*, ser. Wiley Series in Probability and Statistics. John Wiley & Sons, Inc, 1988.
- [32] R. Brun, P. Reichert, and H. R. Künsch, “Practical identifiability analysis of large environmental simulation models,” *Water Resources Research*, vol. 37, no. 4, pp. 1015–1030, 2001. [Online]. Available: <https://agupubs.onlinelibrary.wiley.com/doi/abs/10.1029/2000WR900350>
- [33] T. Turányi, “Sensitivity analysis of complex kinetic systems: tools and applications,” *Journal of Mathematical Chemistry*, vol. 5, no. 3, pp. 203–248, Sep. 1990. [Online]. Available: <https://doi.org/10.1007/BF01166355>
- [34] A. Wolak, H. Gransar, L. E. J. Thomson, J. D. Friedman, R. Hachamovitch, A. Gutstein, L. J. Shaw, D. Polk, N. D. Wong, R. Saouaf, S. W. Hayes, A. Rozanski, P. J. Slomka, G. Germano, and D. S. Berman, “Aortic size assessment by noncontrast cardiac computed tomography: normal limits by age, gender, and body surface area,” *JACC. Cardiovascular imaging*, vol. 1, no. 2, pp. 200–209, Mar. 2008.
- [35] H. M. Mertens, H. Mannebach, G. Trieb, and U. Gleichmann, “Influence of heart rate on systolic time intervals: effects of atrial pacing versus dynamic exercise,” *Clinical Cardiology*, vol. 4, no. 1, pp. 22–27, Jan. 1981. [Online]. Available: <https://onlinelibrary.wiley.com/doi/10.1002/clc.4960040106>
- [36] R. Goldstein, “Conditioning diagnostics: collinearity and weak data in regression,” *Technometrics*, vol. 35, no. 1, pp. 85–86, 1993, publisher: Taylor & Francis \_eprint: <https://www.tandfonline.com/doi/pdf/10.1080/00401706.1993.10484997>. [Online]. Available: <https://www.tandfonline.com/doi/abs/10.1080/00401706.1993.10484997>
- [37] B. M. Kaess, J. Rong, M. G. Larson, N. M. Hamburg, J. A. Vita, D. Levy, E. J. Benjamin, R. S. Vasan, and G. F. Mitchell, “Aortic stiffness, blood pressure progression, and incident hypertension,” *JAMA : the journal of the American Medical Association*, vol. 308, no. 9, pp. 875–881, Sep. 2012. [Online]. Available: <https://www.ncbi.nlm.nih.gov/pmc/articles/PMC3594687/>
- [38] P. Reymond, N. Westerhof, and N. Stergiopoulos, “Systolic hypertension mechanisms: effect of global and local proximal aorta stiffening on pulse pressure,” *Annals of Biomedical Engineering*, vol. 40, no. 3, pp. 742–749, Mar. 2012.
- [39] E. Kimoto, T. Shoji, K. Shinohara, M. Inaba, Y. Okuno, T. Miki, H. Koyama, M. Emoto, and Y. Nishizawa, “Preferential stiffening of central over peripheral arteries in type

- 2 diabetes,” *Diabetes*, vol. 52, no. 2, pp. 448–452, Feb. 2003. [Online]. Available: <http://diabetes.diabetesjournals.org/cgi/doi/10.2337/diabetes.52.2.448>
- [40] P. Segers et al., “Three- and four-element Windkessel models: assessment of their fitting performance in a large cohort of healthy middle-aged individuals,” *Proceedings of the Institution of Mechanical Engineers, Part H: Journal of Engineering in Medicine*, 2008. [Online]. Available: <https://www.ncbi.nlm.nih.gov/pubmed/18595354>
- [41] Z. Lu and R. Mukkamala, “Continuous cardiac output monitoring in humans by invasive and noninvasive peripheral blood pressure waveform analysis,” *Journal of Applied Physiology*, vol. 101, no. 2, pp. 598–608, Aug. 2006. [Online]. Available: <https://www.physiology.org/doi/10.1152/jappphysiol.01488.2005>
- [42] R. B. P. de Wilde, J. J. Schreuder, P. C. M. van den Berg, and J. R. C. Jansen, “An evaluation of cardiac output by five arterial pulse contour techniques during cardiac surgery,” *Anaesthesia*, vol. 62, no. 8, pp. 760–768, Aug. 2007. [Online]. Available: <http://doi.wiley.com/10.1111/j.1365-2044.2007.05135.x>
- [43] O. Vardoulis, T. G. Papaioannou, and N. Stergiopoulos, “Validation of a novel and existing algorithms for the estimation of pulse transit time: advancing the accuracy in pulse wave velocity measurement,” *American Journal of Physiology-Heart and Circulatory Physiology*, vol. 304, no. 11, pp. H1558–H1567, Jun. 2013. [Online]. Available: <http://www.physiology.org/doi/10.1152/ajpheart.00963.2012>
- [44] P. M. L. Franssen and B. P. M. Imholz, “Evaluation of the Mobil-O-Graph new generation ABPM device using the ESH criteria,” *Blood Pressure Monitoring*, vol. 15, no. 4, pp. 229–231, Aug. 2010.
- [45] W. Wei, M. Tölle, W. Zidek, and M. van der Giet, “Validation of the mobil-O-Graph: 24 h-blood pressure measurement device,” *Blood Pressure Monitoring*, vol. 15, no. 4, pp. 225–228, Aug. 2010.
- [46] S. Wassertheurer, C. Mayer, and F. Breitenecker, “Modeling arterial and left ventricular coupling for non-invasive measurements,” *Simulation Modelling Practice and Theory*, vol. 16, no. 8, pp. 988–997, Sep. 2008. [Online]. Available: <http://linkinghub.elsevier.com/retrieve/pii/S1569190X08000865>
- [47] J. R. Womersley, *An elastic tube theory of pulse transmission and oscillatory flow in mammalian arteries*. Wright-Patterson Air Force Base, Ohio.: Wright Air Development Center, Air Research and Development Command, 1957.
- [48] C. H. Chen, E. Nevo, B. Fetcs, P. H. Pak, F. C. Yin, W. L. Maughan, and D. A. Kass, “Estimation of central aortic pressure waveform by mathematical transformation of radial tonometry pressure: validation of generalized transfer function,” *Circulation*, vol. 95, no. 7, pp. 1827–1836, Apr. 1997.

## Bibliography

---

- [49] H. J. Joo, S.-A. Cho, J.-Y. Cho, J. H. Park, S. J. Hong, C. W. Yu, and D.-S. Lim, "The relationship between pulse wave velocity and coronary artery stenosis and percutaneous coronary intervention: a retrospective observational study," *BMC Cardiovascular Disorders*, vol. 17, no. 1, Dec. 2017. [Online]. Available: <http://bmccardiovascdisord.biomedcentral.com/articles/10.1186/s12872-017-0476-7>
- [50] M. L. Muiesan, M. Salvetti, A. Paini, C. Monteduro, C. A. Rosei, C. Aggiusti, E. Belotti, F. Bertacchini, G. Galbassini, D. Stassaldi, M. Castellano, and E. A. Rosei, "Pulse wave velocity and cardiovascular risk stratification in a general population: the Vobarno study," *Journal of Hypertension*, vol. 28, no. 9, pp. 1935–1943, Sep. 2010.
- [51] A. R. Khoshdel, S. L. Carney, B. R. Nair, and A. Gillies, "Better management of cardiovascular diseases by pulse wave velocity: combining clinical practice with clinical research using evidence-based medicine," *Clinical Medicine and Research*, vol. 5, no. 1, pp. 45–52, Mar. 2007.
- [52] N. Stergiopoulos and N. Westerhof, "Determinants of pulse pressure," *Hypertension*, vol. 32, no. 3, pp. 556–559, Sep. 1998. [Online]. Available: <https://www.ahajournals.org/doi/10.1161/01.HYP.32.3.556>
- [53] B. A. Greene, "Cardiac output and total peripheral resistance in anesthesiology: clinical applications," *Journal of the American Medical Association*, vol. 166, no. 9, pp. 1003–1010, Mar. 1958. [Online]. Available: <https://jamanetwork.com/journals/jama/fullarticle/323440>
- [54] C. R. Jones, K. Taylor, P. Chowienczyk, L. Poston, and A. H. Shennan, "A validation of the Mobil O Graph (version 12) ambulatory blood pressure monitor," *Blood Pressure Monitoring*, vol. 5, no. 4, pp. 233–238, Aug. 2000.
- [55] J. Liu, H.-M. Cheng, C.-H. Chen, S.-H. Sung, J.-O. Hahn, and R. Mukkamala, "Patient-specific oscillometric blood pressure measurement: validation for accuracy and repeatability," *IEEE journal of translational engineering in health and medicine*, vol. 5, p. 1900110, 2017.
- [56] J. Liu, H.-M. Cheng, C.-H. Chen, S.-H. Sung, M. Moslehpour, J.-O. Hahn, and R. Mukkamala, "Patient-specific oscillometric blood pressure measurement," *IEEE Transactions on Biomedical Engineering*, vol. 63, no. 6, pp. 1220–1228, Jun. 2016.
- [57] N. Stergiopoulos, J. J. Meister, and N. Westerhof, "Determinants of stroke volume and systolic and diastolic aortic pressure," *American Journal of Physiology-Heart and Circulatory Physiology*, vol. 270, no. 6, pp. H2050–H2059, Jun. 1996. [Online]. Available: <https://www.physiology.org/doi/10.1152/ajpheart.1996.270.6.H2050>
- [58] W. Weiss, C. Gohlisch, C. Harsch-Gladisch, M. Tölle, W. Zidek, and M. van der Giet, "Oscillometric estimation of central blood pressure: validation of the Mobil-O-Graph in

- comparison with the SphygmoCor device,” *Blood Pressure Monitoring*, vol. 17, no. 3, pp. 128–131, Jun. 2012.
- [59] T. Weber, S. Wassertheurer, M. Rammer, E. Maurer, B. Hametner, C. C. Mayer, J. Kropf, and B. Eber, “Validation of a brachial cuff-based method for estimating central systolic blood pressure,” *Hypertension (Dallas, Tex.: 1979)*, vol. 58, no. 5, pp. 825–832, Nov. 2011.
- [60] T. G. Papaioannou, T. D. Karageorgopoulou, T. N. Sergentanis, A. D. Protogerou, T. Psaltopoulou, J. E. Sharman, T. Weber, J. Blacher, S. S. Daskalopoulou, S. Wassertheurer, A. W. Khir, C. Vlachopoulos, N. Stergiopoulos, C. Stefanadis, W. W. Nichols, and D. Tousoulis, “Accuracy of commercial devices and methods for noninvasive estimation of aortic systolic blood pressure: a systematic review and meta-analysis of invasive validation studies,” *Journal of Hypertension*, vol. 34, no. 7, pp. 1237–1248, 2016.
- [61] G. Swamy, D. Xu, N. B. Olivier, and R. Mukkamala, “An adaptive transfer function for deriving the aortic pressure waveform from a peripheral artery pressure waveform,” *American Journal of Physiology-Heart and Circulatory Physiology*, vol. 297, no. 5, pp. H1956–H1963, Nov. 2009. [Online]. Available: <https://www.physiology.org/doi/10.1152/ajpheart.00155.2009>
- [62] M. Gao, W. C. Rose, B. Fetics, D. A. Kass, C.-H. Chen, and R. Mukkamala, “A simple adaptive transfer function for deriving the central blood pressure waveform from a radial blood pressure waveform,” *Scientific Reports*, vol. 6, Sep. 2016. [Online]. Available: <https://www.ncbi.nlm.nih.gov/pmc/articles/PMC5021949/>
- [63] J. Hahn, A. T. Reisner, F. A. Jaffer, and H. H. Asada, “Subject-specific estimation of central aortic blood pressure using an individualized transfer function: a preliminary feasibility study,” *IEEE Transactions on Information Technology in Biomedicine*, vol. 16, no. 2, pp. 212–220, Mar. 2012.
- [64] F. Tosello, A. Guala, D. Leone, C. Camporeale, G. Bruno, L. Ridolfi, F. Veglio, and A. Milan, “Central pressure appraisal: clinical validation of a subject-specific mathematical model,” *PLOS ONE*, vol. 11, no. 3, p. e0151523, Mar. 2016. [Online]. Available: <https://journals.plos.org/plosone/article?id=10.1371/journal.pone.0151523>
- [65] A. Guala, F. Tosello, D. Leone, L. Sabia, F. D’Ascenzo, C. Moretti, M. Bollati, F. Veglio, L. Ridolfi, and A. Milan, “Multiscale mathematical modeling vs. the generalized transfer function approach for aortic pressure estimation: a comparison with invasive data,” *Hypertension Research: Official Journal of the Japanese Society of Hypertension*, vol. 42, no. 5, pp. 690–698, May 2019.
- [66] Z. Ghasemi, J. C. Lee, C.-S. Kim, H.-M. Cheng, S.-H. Sung, C.-H. Chen, R. Mukkamala, and J.-O. Hahn, “Estimation of cardiovascular risk predictors from non-invasively measured diametric pulse volume waveforms via multiple measurement information

## Bibliography

---

- fusion,” *Scientific Reports*, vol. 8, no. 1, Dec. 2018. [Online]. Available: <http://www.nature.com/articles/s41598-018-28604-6>
- [67] G. Swamy and R. Mukkamala, “Estimation of the aortic pressure waveform and beat-to-beat relative cardiac output changes from multiple peripheral artery pressure waveforms,” *IEEE transactions on bio-medical engineering*, vol. 55, no. 5, pp. 1521–1529, May 2008.
- [68] D. B. McCombie, A. T. Reisner, and H. H. Asada, “Laguerre-model blind system identification: cardiovascular dynamics estimated from multiple peripheral circulatory signals,” *IEEE Transactions on Biomedical Engineering*, vol. 52, no. 11, pp. 1889–1901, Nov. 2005.
- [69] N. Fazeli and J.-O. Hahn, “Estimation of cardiac output and peripheral resistance using square-wave-approximated aortic flow signal,” *Frontiers in Physiology*, vol. 3, Jul. 2012. [Online]. Available: <https://www.ncbi.nlm.nih.gov/pmc/articles/PMC3429069/>
- [70] S. J. Marchais, A. P. Guerin, B. Pannier, G. Delavaud, and G. M. London, “Arterial compliance and blood pressure,” *Drugs*, vol. 46 Suppl 2, pp. 82–87, 1993.
- [71] A. Sahlén, N. Hamid, M. R. Amanullah, J. M. Fam, K. K. Yeo, Y. H. Lau, C. S. P. Lam, and Z. P. Ding, “Impact of aortic root size on left ventricular afterload and stroke volume,” *European Journal of Applied Physiology*, vol. 116, no. 7, pp. 1355–1365, Jul. 2016. [Online]. Available: <http://link.springer.com/10.1007/s00421-016-3392-0>
- [72] Y. Mehta, “Newer methods of cardiac output monitoring,” *World Journal of Cardiology*, vol. 6, no. 9, p. 1022, 2014. [Online]. Available: <http://www.wjgnet.com/1949-8462/full/v6/i9/1022.htm>
- [73] J. Huygh, Y. Peeters, J. Bernards, and M. L. N. G. Malbrain, “Hemodynamic monitoring in the critically ill: an overview of current cardiac output monitoring methods,” *F1000Research*, vol. 5, p. 2855, Dec. 2016. [Online]. Available: <https://f1000research.com/articles/5-2855/v1>
- [74] A. Adji, M. F. O’Rourke, and M. Namasivayam, “Arterial stiffness, its assessment, prognostic value, and implications for treatment,” *American Journal of Hypertension*, vol. 24, no. 1, pp. 5–17, Jan. 2011.
- [75] C. M. McEniery, n. Yasmin, I. R. Hall, A. Qasem, I. B. Wilkinson, J. R. Cockcroft, and ACCT Investigators, “Normal vascular aging: differential effects on wave reflection and aortic pulse wave velocity: the Anglo-Cardiff Collaborative Trial (ACCT),” *Journal of the American College of Cardiology*, vol. 46, no. 9, pp. 1753–1760, Nov. 2005.
- [76] M. R. Nelson, J. Stepanek, M. Cevette, M. Covalciuc, R. T. Hurst, and A. J. Tajik, “Noninvasive measurement of central vascular pressures with arterial tonometry: clinical revival of the pulse pressure waveform?” *Mayo Clinic Proceedings*, vol. 85, no. 5, pp.

460–472, May 2010. [Online]. Available: <https://www.ncbi.nlm.nih.gov/pmc/articles/PMC2861976/>

- [77] J. Y. Wagner, J. Grond, J. Fortin, I. Negulescu, M. Schöfthaler, and B. Saugel, “Continuous noninvasive cardiac output determination using the CNAP system: evaluation of a cardiac output algorithm for the analysis of volume clamp method-derived pulse contour,” *Journal of Clinical Monitoring and Computing*, vol. 30, no. 4, pp. 487–493, Aug. 2016. [Online]. Available: <https://doi.org/10.1007/s10877-015-9744-1>



## **Bibliography**

---

## Chapter 3

---

# Validation of a non-invasive inverse problem-solving method for stroke volume: do physics-based models add to the traditional statistical approaches?

Vasiliki Bikia<sup>1</sup>, Carmel M McEniery<sup>2</sup>, Emma Marie Roussel<sup>1</sup>, Georgios Rovas<sup>1</sup>, Stamatia Pagoulatou<sup>1</sup>, Ian B Wilkinson<sup>2</sup>, Nikolaos Stergiopoulos<sup>1</sup>

<sup>1</sup> *Institute of Bioengineering, École Polytechnique Fédérale de Lausanne, Switzerland*

<sup>2</sup> *Division of Experimental Medicine and Immunotherapeutics, University of Cambridge, UK*

Under review.

### Abstract

Monitoring biomarkers of vascular and cardiac function is crucial for cardiovascular disease identification, treatment, and assessment of therapeutic response. Stroke volume (SV) is a major biomarker of cardiac function, reflecting ventricular-vascular coupling. Despite this, hemodynamic monitoring and management seldomly includes assessments of SV and remains predominantly guided by brachial cuff blood pressure (BP). Recently, we proposed a mathematical inverse-problem solving method for acquiring non-invasive estimates of mean aortic flow and SV using age, weight, height, and measurements of brachial BP and carotid-femoral pulse wave velocity (cfPWV). This approach relies on the adjustment of a validated one-dimensional model of the systemic circulation and applies an optimization process for deriving a quasi-personalized profile of an individual's arterial hemodynamics. Following the promising results of our initial validation, our first aim was to validate our method against measurements of SV derived from magnetic resonance imaging (MRI) in healthy individuals covering a wide range of ages (n=144; age range 18 to 85 years). Our second aim was to investigate whether the performance of the inverse problem-solving method for estimating

### **Chapter 3. Validation of a non-invasive inverse problem-solving method for stroke volume: do physics-based models add to the traditional statistical approaches?**

---

SV is superior to traditional statistical approaches using multilinear regression models. Our findings demonstrate that the inverse method yielded higher agreement between estimated and reference data ( $r = 0.83$ ,  $P$ -value  $< 0.001$ ) in comparison to the agreement achieved using a traditional regression model ( $r = 0.74$ ,  $P$ -value  $< 0.001$ ) across a wide range of age decades. Contrary to multilinear regression approaches which depend on the collected data for building the regression equations, the inverse method is not specific to a particular dataset, but relies on the information provided by patient-specific measurements. This latter aspect enhances the applicability and generalization ability of the inverse method in the clinical setting and highlights the importance of physics-based mathematical modelling in improving predictive tools for hemodynamic monitoring.

### 3.1 Introduction

Over the last decades, hemodynamic monitoring has risen to the forefront of efficient and sustainable healthcare. Monitoring of biomarkers for vascular and cardiac function is a crucial factor in cardiovascular disease identification, treatment, and assessment of therapeutic response [1]. Stroke volume (SV) is a major biomarker of cardiovascular function, reflecting the interdependent performance of the heart and major blood vessels. Despite this, hemodynamic management of patients via SV remains limited and guided predominantly by simple brachial cuff blood pressure (BP) observations alone [2]. Such approaches compromise the utility and effectiveness of hemodynamically-guided interventions [3; 4].

Clinically, the most reliable and accurate technique for cardiac output (CO) estimation is thermodilution, with SV derived by dividing CO by heart rate (HR). Although thermodilution is clinically feasible, it is highly invasive and associated with increased risk, and therefore is not suitable for routine investigation. To overcome these limitations, several less invasive methods for assessing CO and SV have been developed. Such methods include either minimally invasive techniques such as pulse contour analysis or oesophageal doppler, which are still relatively invasive and thus are excluded from the routine clinical examination, or non-invasive techniques such as inert gas rebreathing, doppler ultrasound or magnetic resonance imaging (MRI). The latter, while completely non-invasive and reasonably accurate, is expensive and requires costly equipment and expert technical staff [5]. Moreover, none of these methods are practical for routine, continuous bedside monitoring of SV.

Recently, we proposed a mathematical inverse-problem solving method for acquiring non-invasive estimates of mean aortic flow using age, weight, height, and measurements of brachial BP and cfPWV [6]. CfPWV can be routinely measured in clinical practice, has a satisfactory repeatability, and has been identified as an independent predictor of clinical outcomes [101], making it a valuable adjunct to BP measurements in routine assessments of risk. Therefore, the required (input) measurements for our proposed method are simple and readily available from the clinic. Moreover, our approach relies on the adjustment of a validated one-dimensional (1-D) model of the systemic circulation [7] and applies an optimization process for deriving a quasi-personalized profile of an individual's arterial hemodynamics. As such, we believe it provides a more sophisticated method for SV estimation compared with traditional statistical modelling approaches. An initial clinical validation of the method was conducted in 20 healthy individuals against aortic flow data measured using ultrasound [8], with the results indicating that the estimates of mean aortic flow were in good agreement with the reference ultrasound-derived flow values.

Following the promising results of our initial validation, we wished to validate our method using a more precise MRI-derived measure of SV in a larger group of individuals covering a wide age range. A second aim was to investigate whether the performance of our inverse

### **Chapter 3. Validation of a non-invasive inverse problem-solving method for stroke volume: do physics-based models add to the traditional statistical approaches?**

---

problem-solving method is superior to traditional statistical approaches using multilinear regression models.

## **3.2 Methods & materials**

### **Study population**

The dataset used for the current study was obtained from a previous investigation of MRI-derived regional aortic stiffness and diameter, as part of the Anglo-Cardiff Collaborative Trial (ACCT) [9]. Subjects were recruited from the Cambridge arm of ACCT and were free of clinical cardiovascular disease and medication. Approval was obtained from the local research ethics committee, and written informed consent was obtained from all participants.

### **Protocol**

All participants fasted for 4 h before any measurements were undertaken. Brachial cuff blood pressure and cfPWV were measured after 10 min of supine rest. After a further 20 min of rest, participants entered the MRI scanner. Cine phase contrast magnetic resonance imaging (PC-MRI) sequences were then performed perpendicular to the aorta at the level of the ascending aorta, located 1 cm distal to the aortic valve.

### **Aortic flow measurements**

Images were acquired using a 1.5-T MRI system (Signa HDx, GE Healthcare, Waukesha, Wisconsin). An 8-channel abdominal/pelvic coil was placed over the subject lying supine and a cuff placed around the left arm for brachial BP measurement. Three plane localizer images were obtained to identify the ascending and descending aorta through to the bifurcation. A multi-slice, electrocardiographically triggered, black blood fast spin echo sequence was acquired in an oblique sagittal orientation to demonstrate the full length of the aorta. An electrocardiographically gated, segmented k-space, cine phase contrast sequence (PC-MRI) was used with the following parameters: 30° flip angle, 5-mm slice thickness, 280x280-mm field of view, 6.7 repetition time, 256x256 matrix, 2 excitations, and 150 cm/s through-plane velocity encoding, with 1 view per segment. The duration of each sequence was approximately 5 min, with a total acquisition time of approximately 30 min. One hundred temporal phases were retrospectively reconstructed with a true temporal resolution of  $2.0 \pm 6.7$  ms due to the interleaved positive and negative velocity encoding.

PC-MRI images allowed for deriving the aortic flow waveforms. Data analysis was performed offline using CV Flow software (Medis, Leiden, the Netherlands). Aortic contours were automatically detected in each slice location to obtain aortic flow-time curves and aortic areas

through the cardiac cycle. In addition, up-sampling to 1 kHz was performed by interpolation with custom software (version 2.6, Python Software Foundation, Wolfeboro Falls, New Hampshire). In turn, the aortic flow waves permitted the accurate computation of the SV values. The MRI-derived SV values ( $SV_{MRI}$ ) were used as the reference data, against which the model-derived SV estimations ( $SV_{inverse}$ ) were compared. It should be noted that PC-MRI constitutes a very well validated technique and, most importantly, is considered as the non-invasive gold standard for SV derivation [10].

### Arm cuff pressure and pulse wave velocity

Brachial SBP ( $brSBP_{oscillometric}$ ) and DBP ( $brDBP_{oscillometric}$ ) were measured in duplicate in the nondominant arm, according to the British Hypertension Society Guidelines using a validated oscillometric device (HEM-711A-E, Omron Corp., Matsusaka, Japan). CfPWV ( $cfPWV_{SphygmoCor}$ ) was measured using the SphygmoCor (AtCor Medical) device by sequentially recording electrocardiographic-gated carotid and femoral artery waveforms as previously described [11].

### Inverse problem-solving method

#### 1-D arterial tree model

In this study, we adopted a validated 1-D model of the systemic arterial tree that has been previously described by Reymond et al. [7]. The arterial tree includes the main arteries of the systemic circulation, including a network representation of the coronary circulation. In brief, the governing equations of the model are obtained by integration of the longitudinal momentum and continuity of the Navier-Stokes equations over the arterial cross section. Flow and pressure waves throughout the vasculature are obtained by solving the governing equations with proper boundary conditions using an implicit finite-difference scheme. The arterial segments of the model are considered as long tapered tubes, and their compliance is defined by a nonlinear function of pressure and location as proposed by Langewouters [12]. The arterial wall behaviour is considered to be nonlinear and viscoelastic according to [13]. Local arterial compliance (C) is calculated after approximating pulse wave velocity (PWV) as an inverse power function of arterial lumen diameter, following the physiological values reported in the literature. Resistance of the peripheral vasculature (R) and terminal compliances (C) are accounted for by coupling the distant vessels with three-element Windkessel models. At the proximal end, the arterial tree either receives a prescribed input aortic flow waveform or is coupled with a time-varying elastance model for the contractility of the left ventricle [14; 15]. In this study, we used a generic waveform with fixed shape as input to the arterial tree model. The aortic flow wave is characterized by three parameters, namely the heart cycle period ( $T_{period}$ ), the systolic duration ( $T_{systole}$ ), and the aortic flow peak ( $Q_{max}$ ). In order to decrease

### **Chapter 3. Validation of a non-invasive inverse problem-solving method for stroke volume: do physics-based models add to the traditional statistical approaches?**

---

the computational cost of our method, we removed the brain circulation of the original 1-D model. Three-element Windkessel models were used as terminal boundary conditions at the left and right common carotid and vertebral arteries. Pressure and flow from the original configuration were used to derive the parameters of the three-element Windkessel models via fitting. The purpose of removing the cerebral circulation was to decrease the computational time of the simulation. The model has been thoroughly validated [7; 16] and is able to predict pressure and flow waves in good agreement with in vivo measurements. These waves can be used for pulse wave analysis techniques to derive several parameters of interest.

#### **Simulated pulse wave velocity**

CfPWV was derived using the foot-to-foot tangent method [43]. The method uses the intersection point of two tangents on the arterial pressure wave as a characteristic marker. The first tangent is defined as the line that passes tangentially through the initial systolic upstroke, i.e. the maximum of the first derivative. The second tangent line is the horizontal line passing through the minimum pressure point. By applying the method, the pulse transit time ( $PTT_{simulated}$ ) between the carotid artery and the femoral artery was estimated. Total arterial length was determined by summation of the lengths of the arterial segments within the transmission path, i.e. the relevant carotid-femoral path. Finally, simulated cfPWV ( $cfPWV_{simulated}$ ) was calculated by dividing the total length by the  $PTT_{simulated}$ .

#### **Optimization of the 1-D model**

In the current study, we have applied an optimization algorithm in order to partially adjust the generic 1-D arterial tree model to the specific participant under consideration (Figure 3.1). The rationale behind this approach was that adjusting some of the model parameters may be sufficient to approximate the measured data, namely  $brSBP_{oscillometric}$ ,  $brDBP_{oscillometric}$ ,  $cfPWV_{SphygmoCor}$  [17].

The arterial tree model of this study is fully characterized by its geometry, the distensibility of all arterial segments and the peripheral impedances (described by terminal compliances and resistances). Additionally, aortic flow is needed as a proximal boundary condition. Identifiability analysis [18] demonstrated that, for any individual with a given set of peripheral SBP, DBP, cfPWV, HR, and SV values, there will be only one solution for the arterial tree model [6]. Therefore, if the generic arterial tree model modifies its parameters in order to approximate the measured brSBP, brDBP and cfPWV, the model will approximate the hemodynamic profile of the participant under consideration and will yield a partially personalized model. This personalized model will allow for the derivation of SV.

### Inverse method for derivation of SV

In applying our optimization algorithm, for an individual, the following information is required: gender, age, height, weight, brSBP, brDBP, HR, and cfPWV. In the first step, the method uses the demographic data (i.e. gender, age, height, weight) for adjusting the geometry of the arterial tree model. Arterial length is adjusted in accordance to height. The reference state of the arterial tree model corresponds to an individual with a height equal to 180 cm. Uniform adjustment of the arterial lengths is done via multiplication with a common scaling factor. Arterial diameter is uniformly adjusted based on previously published data that associate aortic diameter with age, gender, and BSA [19]. This completes the anatomical adjustment of the arterial tree model.

The inverse method additionally accounts for the non-uniform aortic stiffening which occurs with aging [20]. For older individuals, stiffening is considered as non-uniform and more pronounced in the proximal aorta. This gradient in distensibility is adjusted by changing the relative regional distensibility of the proximal aorta through multiplication with an age-related proximal factor based on published literature [21].

Subsequently, the  $T_{period}$  is computed from the HR, whereas previously published data on the HR-related changes in systolic duration ( $T_{systole}$ ) [22] are used to adapt the  $T_{systole}$  with respect to the measured HR. As a result, the only remaining flow-related parameter to be optimized for the aortic flow input is  $Q_{max}$ .

Following these model adaptations, the optimization algorithm is employed for adjusting the  $Q_{max}$ , C, R. An arbitrary parameter set of C, R,  $Q_{max}$  is used in the first optimization iteration of the algorithm. Under all conditions, the 1-D model computes the simulated flows and pressure waves throughout the arterial tree, including the variables that correspond to the measured data ( $brSBP_{oscillometric}$ ,  $brDBP_{oscillometric}$ ,  $cfPWV_{SphygmoCor}$ ) as well as the the quantity of interest, namely the SV. The standard (non-optimised) model is expected to estimate inaccurate flows and pressures (and thus  $brSBP_{simulated}$  and  $brDBP_{simulated}$ ) due to the inaccurate input model parameters and the inaccurate input aortic flow for the specific individual under investigation. Similarly, the  $cfPWV_{simulated}$  is not the same as the measured  $cfPWV_{SphygmoCor}$ . To address this issue, the non-invasive, participant-specific measurements are integrated into the model using a gradient descent optimization algorithm. The reference C, R, and  $Q_{max}$  of the generic arterial tree are adjusted by multiplication with different scaling factors until the model-simulated  $brSBP_{simulated}$ ,  $brDBP_{simulated}$  and  $cfPWV_{simulated}$  are identical with the measured  $brSBP_{oscillometric}$ ,  $brDBP_{oscillometric}$ , and  $cfPWV_{SphygmoCor}$ . Once convergence is achieved, the simulated SV is considered as the final estimation for the specific participant. A more analytical description of the “tuning” process can be found in the original publication [6]. The methodology described above was repeated for the entire study population (n = 144). The estimated  $SV_{inverse}$  were compared to the  $SV_{MRI}$ . Accuracy was also assessed independently for the different age groups, i.e. 20-29, 30-39, 40-49, 50-59, 60-69,



**Chapter 3. Validation of a non-invasive inverse problem-solving method for stroke volume: do physics-based models add to the traditional statistical approaches?**

and  $age \geq 70$  years.

Finally, we evaluated the errors resulting from the use of an approximated aortic flow waveform. We compared the  $T_{systole}$ ,  $Q_{max}$ , as well as the time of  $Q_{max}$  ( $t_{Q_{max}}$ ) derived from the approximated flow waveform to the actual values extracted from the reference MRI aortic flow waveform. Consequently, we performed one-way ANOVA for the three estimated characteristics across the different age groups to investigate whether an age-dependent effect was observed.

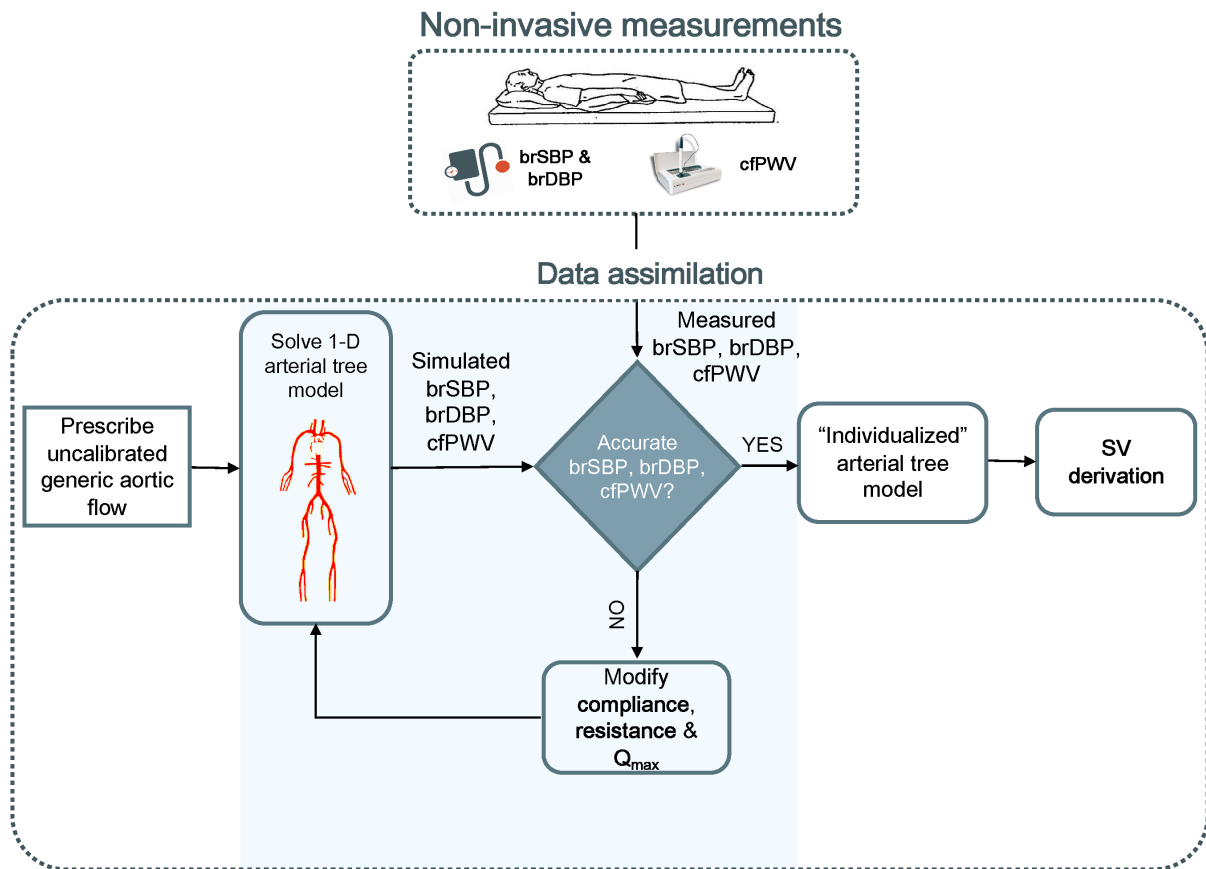


Figure 3.1 – Schematic representation of the optimization process for predicting non-invasive stroke volume. Adapted from [6]

**Multilinear regression analysis**

In addition to the modelling analyses described above, we tested the performance of multilinear regression analysis using  $SV_{MRI}$  as the dependent variable. Overall, this approach allowed us to compare our inverse method with the more traditional multilinear regression method for estimating SV. For the multilinear regression method, the same parameters used as inputs to the inverse method were used as independent variables, namely age, gender, weight,

height, HR, brSBP, brDBP and cfPWV. We followed two different approaches for testing the performance of multilinear regression to: (i) a train/test split cross validation (CV) (1CV), and (ii) a 10-fold CV (10CV). For the 1CV approach, 100 out of the 144 participants were kept for defining the regression coefficients. Subsequently, the resulting regression equation was tested on the remaining 44 participants. This resulted in one multilinear regression model. The 10CV approach required that the group of 144 participants was randomly split into 10 equal subsets. One subset was allocated as the testing group to validate the regression equation, while the other 9 subsets were used for defining the regression coefficients. This procedure was repeated 10 times so that all participants were used for testing. The performance metrics were derived by the average performance of all 10 models. The reason for adopting two CV approaches was to facilitate a more complete comparison between the two methods of estimating SV, i.e. inverse method and multilinear regression. We performed ordinary least squares (OLS) estimation of the regression coefficients using the statsmodels library [23] for only 1CV setting. Hypothesis testing for each regression coefficient was realized using the  $t$ -statistic.

### Statistical analysis

The statistical analysis was performed in Python (Python Software Foundation, Python Language Reference, version 3.6.8, Available at <http://www.python.org>). All values are presented as means $\pm$ SD. The agreement, bias and precision between the model estimations (estimated data) and the reference data obtained from the MRI images were evaluated using the Pearson's correlation coefficient ( $r$ ), the mean absolute error (MAE), the normalized root mean square error (nRMSE) and Bland-Altman analyses [24]. The computed nRMSE was based on the difference between the minimum and maximum values of the dependent variable ( $y$ ) and was computed as  $RMSE/(y_{max} - y_{min})$ . Linear least-squares regression was performed for the estimated and reference data. The slope and the intercept of the regression line were reported. Two-sided  $P$ -value for hypothesis tests was calculated using Wald Tests with  $t$ -distribution of the test statistic. The null hypothesis was that the slope is zero. One-way analysis of variance (ANOVA) for unbalanced data (each group had different sample sizes) was performed on the estimations for the six age groups. A  $P$ -value below 0.05 was considered statistically significant.

## 3.3 Results

Table 3.1 shows the subject characteristics of the study population ( $n = 144$ ), including the  $SV_{MRI}$  reference data. The comparisons between the model-derived estimations for SV using (i) the inverse method ( $SV_{inverse}$ ) and (ii) multilinear regression ( $SV_{regression}$ ), and the reference  $SV_{MRI}$  data are presented below for each of the targeted outputs.

**Chapter 3. Validation of a non-invasive inverse problem-solving method for stroke volume: do physics-based models add to the traditional statistical approaches?**

Table 3.1 – Subject characteristics and hemodynamic parameters according to the age group.

Parameter	All (n = 144)	20-29 yrs (n <sub>1</sub> = 27)	30-39 yrs (n <sub>2</sub> = 23)	40-49 yrs (n <sub>3</sub> = 24)	50-59 yrs (n <sub>4</sub> = 24)	60-69 yrs (n <sub>5</sub> = 23)	≥ 70 yrs (n <sub>6</sub> = 23)
Age [years]	49±17	24±3	34±3	44±2	57±3	63±2	74±3
Gender [M/F]	62/82	11/16	12/11	9/15	10/14	9/14	11/12
Height [cm]	169±10	172±9	171±9	169±10	168±9	169±10	165±10
Weight [kg]	70±12	67±11	73±11	73±15	68±10	73±13	68±10
Brachial SBP [mmHg]	122±16	112±13	116±9	120±14	117±12	128±16	138±16
Brachial DBP [mmHg]	71±8	63±4	68±5	72±9	71±8	75±6	75±8
Brachial PP [mmHg]	51±12	48±12	48±9	48±8	46±8	53±13	63±13
Mean arterial pressure [mmHg]	88±10	79±6	84±6	88±10	86±8	93±9	96±10
Carotid-femoral PWV [m/s]	7±2	6±1	6±1	7±1	7±1	8±1	10±2
Heart rate [bpm]	66±12	68±12	61±9	66±12	65±11	66±10	69±14
Stroke volume [mL]	84±21	92±26	97±17	90±19	80±16	79±15	68±11

### Estimation of SV using the inverse method

The comparison between  $SV_{inverse}$  and  $SV_{MRI}$  is presented in 3.2. The slope and the intercept of the regression line were 1.1 ( $P$ -value < 0.001) and -8.8 mL, respectively. The nRMSE was found to be equal to 13.8 %. Bland-Altman analysis yielded a low bias of 1.5 mL and LoA equal to (-29.7, 32.7) mL. The estimation error was out of the LoA only for the 7 % of the study population. Variability of the mean difference between estimated and measured SV values was 15.9 mL. Although several overestimations were observed for high values of SV, the majority of the estimated data were tightly distributed around the line of equality ( $x = y$ ). The mean absolute error (MAE) in SV estimation was computed for the different age groups of the study population (Figure 3.3). The overall variability of the MAE was  $\pm 2.2$  mL ( $P$ -value < 0.0001), while higher MAE values (> 12 mL) were reported for participants aged between 30-49 years. Estimations of SV had the lowest errors for participants aged between 60-69 years. Overall, the MAE values differed significantly between age groups of the study population ( $P$ -value < 0.001).

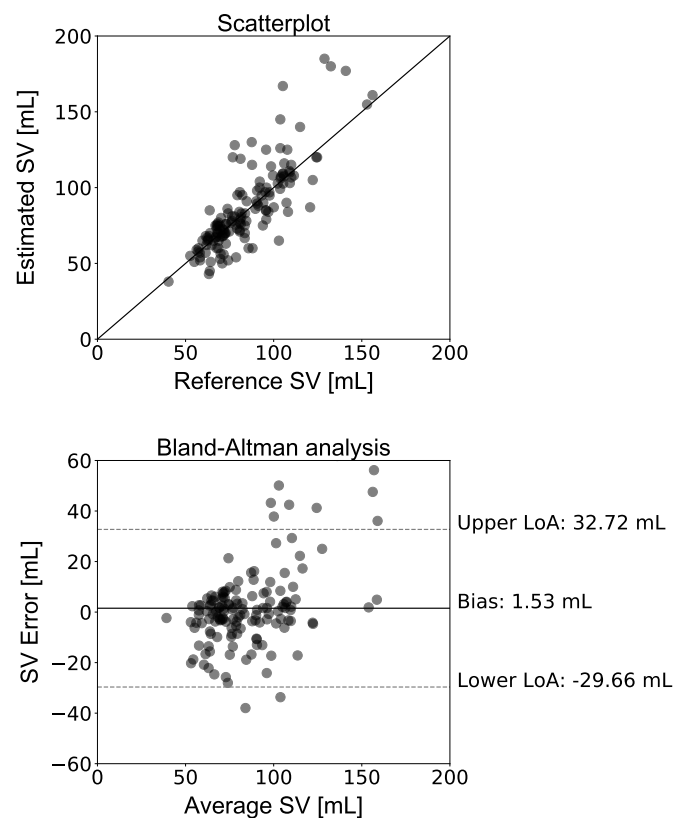


Figure 3.2 – Comparison between the estimated SV values and the reference in vivo data. Scatterplot and Bland–Altman plot between the estimated SV (using the inverse method) and the reference SV (using the PC-MRI method). The solid line of the scatterplots represents equality. In Bland–Altman plots, limits of agreement (LoA) are defined by the two horizontal dashed lines.

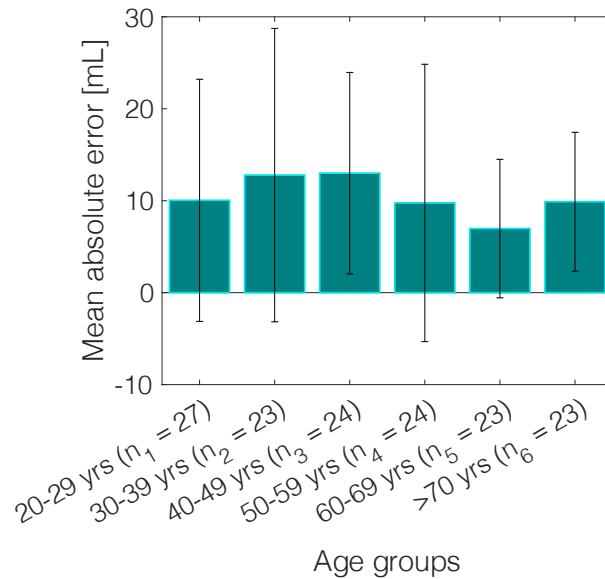


Figure 3.3 – Variation of the mean absolute error in the stroke volume estimation across the age groups.

### Approximated aortic flow characteristics

Table 3.2 reports the measured (MRI) and estimated aortic flow characteristics for all participants and the different age groups. The estimated  $T_{systole}$  was slightly lower than the measured values for all age groups. The correlation between the estimated and measured data was  $r = 0.6$  and the mean absolute percentage error was 10 %. The estimation of  $Q_{max}$  was satisfactory with  $r = 0.7$ , and a small overestimation of the measured values. Finally, assuming a fixed aortic flow wave shape led to a less precise approximation of  $t_{Q_{max}}$  with a correlation coefficient of  $r = 0.41$ .

### Estimation of SV using multilinear regression analysis

Hypothesis testing indicated that all of the specified coefficients, except for those corresponding to gender ( $P$ -value = 0.52) and brDBP ( $P$ -value = 0.28), were significantly different from zero. Therefore, the multilinear regression analysis was repeated, excluding gender and brDBP from the model.

The regression equation for the 1CV scheme was as follows:

$$SV = -0.34 \times (age) + 0.38 \times (weight) + 40.14 \times (height) + 0.47 \times (brSBP) - 0.45 \times (HR) - 4.23 \times (cfPWV). \quad (3.1)$$

Table 3.2 – Real and estimated aortic flow characteristics according to age group.

Parameter	Mean ±SD														P-value
	All (n = 144)		20-29 yrs (n <sub>1</sub> = 27)		30-39 yrs (n <sub>2</sub> = 23)		40-49 yrs (n <sub>3</sub> = 24)		50-59 yrs (n <sub>4</sub> = 24)		60-69 yrs (n <sub>5</sub> = 23)		≥ 70 (n <sub>6</sub> = 23)		
	Real	Est	Real	Est	Real	Est	Real	Est	Real	Est	Real	Est	Real	Est	
T <sub>systole</sub> [ms]	323 ±58	296 ±13	313 ±46	294 ±13	332 ±57	302 ±10	323 ±40	296 ±13	333 ±97	297 ±13	322 ±33	297 ±12	316 ±55	292 ±16	0.2
Q <sub>max</sub> [mL/s]	400 ±96	464 ±129	448 ±129	582 ±129	441 ±78	538 ±120	417 ±85	448 ±98	368 ±72	435 ±99	386 ±76	413 ±93	330 ±65	348 ±72	<.0001
t <sub>Qmax</sub> [ms]	89 ±23	122 ±21	83 ±19	119 ±22	99 ±23	131 ±19	88 ±19	121 ±21	90 ±26	123 ±21	90 ±23	121 ±22	83 ±27	117 ±23	0.3

### Chapter 3. Validation of a non-invasive inverse problem-solving method for stroke volume: do physics-based models add to the traditional statistical approaches?

---

For the 10CV scheme, the comparison between the regression-estimated SV ( $SV_{regression}$ ) and the reference  $SV_{MRI}$  is presented in Figure 3.4. The slope and intercept of the regression line were 0.57 ( $P$ -value  $< 0.0001$ ) and 36.32 mL, respectively. The LoA were equal to  $\pm 27$  mL and the bias was zero. Results of the new hypothesis testing for the OLS regression coefficients reported a  $P$ -value below 0.01 for all independent variables. Correlation and agreement between  $SV_{regression}$  values (using both testing schemes) and the reference  $SV_{MRI}$  values are presented in 3.3. Multilinear regression models yielded a lower correlation ( $r = 0.74$ ) compared with the inverse method ( $r = 0.83$ ), whereas the LoA were narrower in the case of multilinear regression analysis.

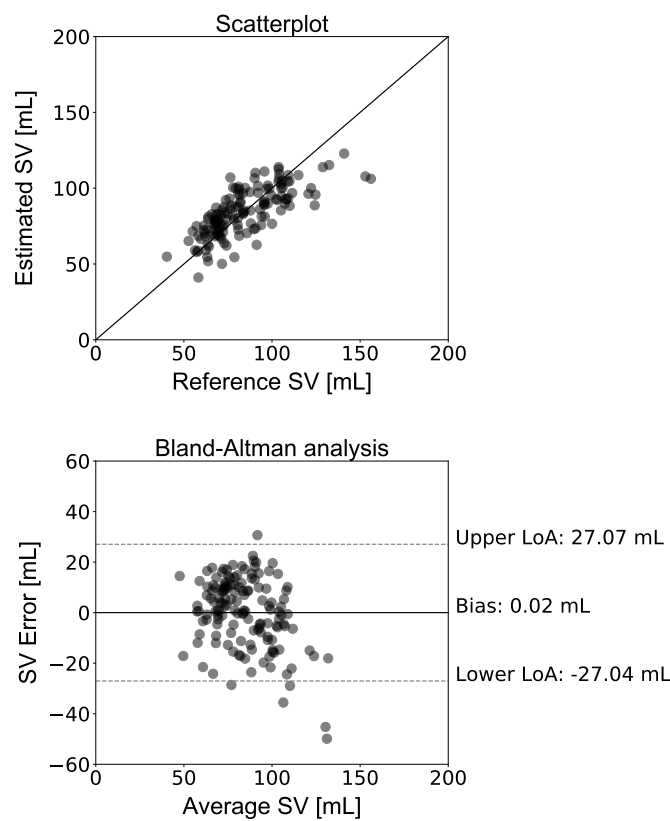


Figure 3.4 – Comparison between the estimated SV values and the reference in vivo data. Scatterplot and Bland–Altman plot between the predicted SV (using the multilinear regression method) and the reference SV (using the PC-MRI method). The solid line of the scatterplots represents equality. In Bland–Altman plots, limits of agreement (LoA) are defined by the two horizontal dashed lines.

### 3.4 Discussion

In the present study, we validated a previously developed inverse problem-solving method for the estimation of a major hemodynamic parameter, the SV. The original method, based on

Table 3.3 – Overall comparison between the SV estimates and the reference MRI SV.

	<b>mean±SD [mL]</b>	<b><i>r</i></b>	<b>MAE [mL]</b>	<b>Bias (LoA) [mL]</b>
Measured (n=144)	84.4±20.4	-	-	-
Measured (n=44) *	82.6±19	-	-	-
<b>Inverse (n=144)</b>	<b>86±27.8</b>	<b>0.83</b>	<b>10.4</b>	<b>1.5 (-29.7, 32.7)</b>
Inverse (n=44) *	84.5±26.1	0.85	10.1	1.9 (-25.4, 29.2)
<b>MLR10CV (n=144)</b>	<b>84.5±15.8</b>	<b>0.74</b>	<b>11</b>	<b>0.02 (-27, 27.1)</b>
MLR1CV (n=44) *	84.6±14.5	0.79	10.8	2 (-20.7, 24.8)
1CV corresponds to train/test split equal to 100/44.				
10CV corresponds to 10-fold CV.				
*Values correspond only to the test set (44 subjects).				

non-invasive measurements of brachial BP and cfPWV [6] underwent a preliminary validation in a small ( $n = 20$ ) cohort of human subjects. Here, we have implemented and tested our method on a further 144 healthy individuals and compared the  $SV_{inverse}$  (estimated data derived from the inverse method) to  $SV_{MRI}$  (measured data derived from the non-invasive gold standard of MRI). Additionally, we have compared the performance of the inverse method against the predictive capacity of a traditional linear regression approach which uses the same set of inputs as those used in the inverse method. The two key findings of this study are that the inverse problem-solving method yields accurate estimates of SV across a wide range of ages and SV values, in a simple and cost-efficient manner in comparison to PC-MRI; and that a traditional statistical approach such as multilinear regression analysis is inferior to the more sophisticated inverse problem-solving technique, for a given set of clinical data.

The SV, together with BP, are fundamental and independent indicators of cardiovascular function and are essential for the understanding of cardiovascular physiology and pathology [25]. However, in clinical practice, BP and BP-derived surrogates of SV are often used either interchangeably with, or as replacements for, direct measurements of flow. This simplification potentially compromises our understanding of cardiovascular physiology and limits the clinical utility of hemodynamic analyses [3; 26]. While notable research efforts have been made for estimating SV using BP recordings [27; 28; 29; 30], none of these techniques accounts for the specific arterial tree properties unique to each individual.

Current doppler ultrasound technologies in the clinical setting include echocardiography, transoesophageal doppler, and transcutaneous doppler. However, these techniques are associated with several limitations concerning applicability, cost and accuracy. For instance, transoesophageal doppler is largely limited to perioperative monitoring as the ultrasound transducer is inserted into the oesophagus and requires sedation. On the other hand, MRI allows for improved spatial resolution, larger imaging windows, and higher tissue contrast



### **Chapter 3. Validation of a non-invasive inverse problem-solving method for stroke volume: do physics-based models add to the traditional statistical approaches?**

---

than ultrasound-based techniques. Specifically, PC-MRI allows for accurate determination of the presence, magnitude, and direction of flow, as well as for the estimation of flow velocity, volume flow rate, and displaced volumes. In spite of these advantages, MRI remains inconvenient and expensive for routine examinations and requires long imaging times. As a result, monitoring SV effectively in a reliable, simple and cost-efficient way remains an unmet need.

Mathematical modelling of the human cardiovascular system offers valuable tools to investigate patient-specific aspects of arterial hemodynamics, which are difficult to assess in clinical practice. Data assimilation aims to address relevant challenges and can significantly promote patient-specific modelling [31]. Rather than relying on simplified equations, we have followed a data assimilation approach, which is based on the adjustment of a generic 1-D arterial model using the non-invasive data of the peripheral cuff-based SBP, DBP and cfPWV, which are easily obtained in a clinical setting. Successful tuning permits the creation of a personalized cardiovascular model which, consequently, provides access to key hemodynamic information including SV. The tuning is conducted via an optimization process which allows for the fusion between the computational model and the measured data. This study, along with the initial validation [6], demonstrated that creating a partially personalized model can improve the prediction of SV.

Acquisition of cfPWV requires sequential recording of the carotid and femoral pressure pulse via applanation tonometry [32]. CfPWV has a satisfactory reproducibility, while being an independent index of cardiovascular risk and/or mortality [33]. In our study, the role of cfPWV, as an index of arterial stiffness, was to facilitate the adjustment of the generic arterial tree model. Given that arterial distensibility, the inverse of arterial stiffness, constitutes a major parameter of the vasculature, combining the information provided by arterial stiffness and BP allowed us to determine aortic hemodynamics and thus SV.

The data from the Anglo-Cardiff Collaborative Trial allowed us to have an approximately equally split dataset for seven age groups, i.e. 20-29, 30-39, 40-49, 50-59, 60-69, and  $\geq 70$  years, which enabled an accurate comparison of the age-based results. Predictions of SV were precise across the different age groups, with a low variability of the MAE ( $\pm 2.2$  mL). Lower errors were reported for the 6<sup>th</sup> decade of life. It was observed that the highest absolute errors corresponded to high values of SV, while predictions were more accurate for SV values below 130 mL. Overall, there was good agreement and high precision between the  $SV_{inverse}$  and the  $SV_{MRI}$  data across different age decades and SV values, which indicates a robust performance of the inverse method.

We also investigated the validity of the assumption of a fixed aortic flow shape by comparing the estimated values of  $T_{period}$ ,  $T_{systole}$ ,  $Q_{max}$ , and  $t_{Qmax}$  with their actual values. The inverse method relies on a previously published formula [22] which provides a HR-related approximation of  $T_{systole}$ . Overall, it was observed that the estimated  $T_{systole}$  values did not vary significantly between age groups, while the variability within the same age group was also

rather small. Our results also indicated that the formula slightly underestimated the  $T_{systole}$  values. It is likely that this underestimation led to the overestimation of  $Q_{max}$ . Given that the method yielded accurate estimates of SV, for achieving the same SV, an underestimated  $T_{systole}$  would naturally lead to an overestimated  $Q_{max}$ . Finally, assuming a fixed shape for aortic flow wave resulted in deviations in the value of  $t_{Q_{max}}$  (mean absolute percentage error was equal to 47 %). Despite the reported deviations in the timing features of the aortic flow wave, the estimated  $Q_{max}$  was in satisfactory agreement with the reference  $Q_{max}$ . Given that our method aims to minimize the required inputs for estimating SV, the use of a fixed shape wave is a well-advised approximation. Nonetheless, future work will aim to personalize the aortic flow wave shape with respect to subject characteristics, such as age and gender.

Multilinear regression analysis was performed using two cross-validation approaches, namely 1CV and 10CV. Hypothesis testing was conducted, where the  $P$ -value for each independent variable tested the null hypothesis that the variable has no correlation with the dependent variable. Coefficients of gender and brDBP were not statistically significantly different to zero, indicating that there was insufficient evidence in our sample to conclude that a non-zero correlation exists. All other regression coefficients were reported to be statistically significantly different from zero.

We compared the inverse method with the conventional multilinear regression analysis. Comparison indicated a higher correlation for the former. The LoA were broader for the inverse method, which also reported a higher bias. This outcome was expected, if we consider that the regression equation was constructed using a subset of the study population. The MAE was lower for the inverse method. A notable advantage of the inverse method relies on its generalization ability. Statistical learning models (such as linear regression) are often prone to generalization issues. These models are dependent on the specific training data used for developing the regression equation, and while they are able to provide accurate estimates for a hold-out (not considered in the process of developing the regression model) test subset of the same dataset, they are not likely to perform adequately for other independent datasets [34]. This lack of accuracy might be attributed to differences in the measurement protocol (e.g. physician preferences, local care standards), medication selection or other clinical decisions which influence the model development [34]. Specifically, regression analysis requires prior knowledge of large sets of collected data in order to estimate the coefficients of the regression equation. On the other hand, the inverse method is able to offer improved performance without dependency on pre-defined, dataset-derived regression coefficients.

#### **Limitations**

The limitations of the inverse method have been acknowledged in the original publication [6]. Another limitation pertains to the synchronization of the clinical measurements. In particular, contrary to the simulated data produced by the 1-D arterial tree model, which corresponds to

### **Chapter 3. Validation of a non-invasive inverse problem-solving method for stroke volume: do physics-based models add to the traditional statistical approaches?**

---

completely simultaneous pressure and flow waves, the in vivo measurements were performed with a time difference. Nevertheless, the intervals between the measurements were rather short and therefore, we may deduce that there was not a high variation in the measured data. Finally, we used aortic flow data derived from PC-MRI as a reference method with which to compare our estimated SV values. Although PC-MRI is considered a well-validated method for aortic flow measurements, the gold standard technique is thermodilution. Next validation steps will include testing our method against thermodilution-derived SV data.

#### **Conclusion**

We have demonstrated that SV can be estimated accurately using a previously developed inverse problem-solving method. The method relies on the use of non-invasive, easily-obtained clinical measurements of brachial cuff BP and cfPWV. Values of SV estimated using our inverse method compared favorably with the reference SV data derived from PC-MRI. In addition, agreement between predictions and reference values was higher with the inverse method than traditional linear regression. These results, along with the inherent generalization limitations of regression equations, highlight the importance of physics-based mathematical modelling in improving predictive tools for hemodynamic monitoring.

## Bibliography

- [1] J.-L. Vincent, P. Pelosi, R. Pearse, D. Payen, A. Perel, A. Hoeft, S. Romagnoli, V. M. Ranieri, C. Ichai, P. Forget, G. Della Rocca, and A. Rhodes, "Perioperative cardiovascular monitoring of high-risk patients: a consensus of 12," *Critical Care (London, England)*, vol. 19, p. 224, 5 2015, pMID: 25953531 PMID: PMC4424585.
- [2] R. A. Phillips, B. E. Smith, and V. M. Madigan, "Stroke volume monitoring: Novel continuous wave doppler parameters, algorithms and advanced noninvasive haemodynamic concepts," *Current Anesthesiology Reports*, vol. 7, no. 4, pp. 387–398, 12 2017.
- [3] S. W. Thiel, M. H. Kollef, and W. Isakow, "Non-invasive stroke volume measurement and passive leg raising predict volume responsiveness in medical icu patients: an observational cohort study," *Critical Care (London, England)*, vol. 13, no. 4, p. R111, 2009, pMID: 19586543 PMID: PMC2750155.
- [4] L. Meng and P. Heerdt, "Perioperative goal-directed haemodynamic therapy based on flow parameters: a concept in evolution," *British Journal of Anaesthesia*, vol. 117, pp. iii3–iii17, 12 2016.
- [5] T. R. Porter, S. K. Shillcutt, M. S. Adams, G. Desjardins, K. E. Glas, J. J. Olson, and R. W. Troughton, "Guidelines for the use of echocardiography as a monitor for therapeutic intervention in adults: A report from the american society of echocardiography," *Journal of the American Society of Echocardiography*, vol. 28, no. 1, pp. 40–56, 1 2015.
- [6] V. Bikia, S. Pagoulatou, B. Trachet, D. Soulis, A. D. Protogerou, T. G. Papaioannou, and N. Stergiopulos, "Noninvasive cardiac output and central systolic pressure from cuff-pressure and pulse wave velocity," *IEEE Journal of Biomedical and Health Informatics*, vol. 24, no. 7, pp. 1968–1981, 7 2020.
- [7] P. Reymond, F. Merenda, F. Perren, D. Rüfenacht, and N. Stergiopulos, "Validation of a one-dimensional model of the systemic arterial tree," *American Journal of Physiology - Heart and Circulatory Physiology*, vol. 297, no. 1, pp. H208–H222, 7 2009, pMID: 19429832.
- [8] T. G. Papaioannou, D. Soulis, O. Vardoulis, A. Protogerou, P. P. Sfikakis, N. Stergiopulos, and C. Stefanadis, "First in vivo application and evaluation of a novel method for non-

## Bibliography

---

- invasive estimation of cardiac output,” *Medical Engineering Physics*, vol. 36, no. 10, pp. 1352–1357, 10 2014, pMID: 25108554.
- [9] C. M. McEniery, n. Yasmin, I. R. Hall, A. Qasem, I. B. Wilkinson, J. R. Cockcroft, and A. Investigators, “Normal vascular aging: differential effects on wave reflection and aortic pulse wave velocity: the anglo-cardiff collaborative trial (acct),” *Journal of the American College of Cardiology*, vol. 46, no. 9, pp. 1753–1760, 11 2005, pMID: 16256881.
- [10] J. Lotz, C. Meier, A. Leppert, and M. Galanski, “Cardiovascular flow measurement with phase-contrast mr imaging: Basic facts and implementation,” *RadioGraphics*, vol. 22, no. 3, pp. 651–671, 5 2002.
- [11] I. B. Wilkinson, S. A. Fuchs, I. M. Jansen, J. C. Spratt, G. D. Murray, J. R. Cockcroft, and D. J. Webb, “Reproducibility of pulse wave velocity and augmentation index measured by pulse wave analysis:,” *Journal of Hypertension*, vol. 16, no. Supplement, pp. 2079–2084, 12 1998.
- [12] G. Langewouters, *Visco-elasticity of the human aorta in vitro in relation to pressure and age (Ph.D. thesis)*. Amsterdam: Free University of Amsterdam: Krips Repro, 1982. [Online]. Available: <https://books.google.gr/books?id=qvSrHAAACAAJ>
- [13] R. Holenstein, P. Niederer, and M. Anliker, “A viscoelastic model for use in predicting arterial pulse waves,” *Journal of Biomechanical Engineering*, vol. 102, no. 4, pp. 318–325, 11 1980, pMID: 6965195.
- [14] K. Sagawa, H. Suga, A. A. Shoukas, and K. M. Bakalar, “End-systolic pressure/volume ratio: a new index of ventricular contractility,” *The American Journal of Cardiology*, vol. 40, no. 5, pp. 748–753, 11 1977, pMID: 920611.
- [15] S. Hiroyuki and S. Kiichi, “Instantaneous pressure-volume relationships and their ratio in the excised, supported canine left ventricle,” *Circulation Research*, vol. 35, no. 1, pp. 117–126, 7 1974.
- [16] P. Reymond, Y. Bohraus, F. Perren, F. Lazeyras, and N. Stergiopulos, “Validation of a patient-specific one-dimensional model of the systemic arterial tree,” *American Journal of Physiology. Heart and Circulatory Physiology*, vol. 301, no. 3, pp. H1173–1182, 9 2011, pMID: 21622820.
- [17] D. G. Watts and D. M. Bates, *Nonlinear regression analysis and its applications*, ser. Wiley Series in Probability and Statistics. John Wiley Sons, Inc, 1988.
- [18] R. Brun, P. Reichert, and H. R. Künsch, “Practical identifiability analysis of large environmental simulation models,” *Water Resources Research*, vol. 37, no. 4, pp. 1015–1030, 2001.

- [19] A. Wolak, H. Gransar, L. E. J. Thomson, J. D. Friedman, R. Hachamovitch, A. Gutstein, L. J. Shaw, D. Polk, N. D. Wong, R. Saouaf, S. W. Hayes, A. Rozanski, P. J. Slomka, G. Germano, and D. S. Berman, "Aortic size assessment by noncontrast cardiac computed tomography: normal limits by age, gender, and body surface area," *JACC. Cardiovascular imaging*, vol. 1, no. 2, pp. 200–209, 3 2008, PMID: 19356429.
- [20] B. M. Kaess, J. Rong, M. G. Larson, N. M. Hamburg, J. A. Vita, D. Levy, E. J. Benjamin, R. S. Vasan, and G. F. Mitchell, "Aortic stiffness, blood pressure progression, and incident hypertension," *JAMA : the journal of the American Medical Association*, vol. 308, no. 9, pp. 875–881, 9 2012, PMID: 22948697 PMID: PMC3594687.
- [21] E. Kimoto, T. Shoji, K. Shinohara, M. Inaba, Y. Okuno, T. Miki, H. Koyama, M. Emoto, and Y. Nishizawa, "Preferential stiffening of central over peripheral arteries in type 2 diabetes," *Diabetes*, vol. 52, no. 2, pp. 448–452, 2 2003.
- [22] A. M. Weissler, W. S. Harris, and C. D. Schoenfeld, "Systolic time intervals in heart failure in man," *Circulation*, vol. 37, no. 2, pp. 149–159, 2 1968.
- [23] S. Seabold and J. Perktold, "statsmodels: econometric and statistical modeling with python," 9th Python in Science Conference, 2010.
- [24] J. M. Bland and D. G. Altman, "Statistical methods for assessing agreement between two methods of clinical measurement," *Lancet (London, England)*, vol. 1, no. 8476, pp. 307–310, 2 1986, PMID: 2868172.
- [25] W. W. Nichols, M. F. O'Rourke, and C. Vlachopoulos, *McDonald's blood flow In arteries*, 6th ed. London: Arnold, 2011.
- [26] P. Asfar, F. Meziani, J.-F. Hamel, F. Grelon, B. Megarbane, N. Anguel, J.-P. Mira, P.-F. Dequin, S. Gergaud, N. Weiss, F. Legay, Y. Le Tulzo, M. Conrad, R. Robert, F. Gonzalez, C. Guitton, F. Tamion, J.-M. Tonnelier, P. Guezennec, T. Van Der Linden, A. Vieillard-Baron, E. Marriotte, G. Pradel, O. Lesieur, J.-D. Ricard, F. Hervé, D. du Cheyron, C. Guerin, A. Mercat, J.-L. Teboul, and P. Radermacher, "High versus low blood-pressure target in patients with septic shock," *New England Journal of Medicine*, vol. 370, no. 17, pp. 1583–1593, 4 2014.
- [27] G. Swamy and R. Mukkamala, "Estimation of the aortic pressure waveform and beat-to-beat relative cardiac output changes from multiple peripheral artery pressure waveforms," *IEEE transactions on bio-medical engineering*, vol. 55, no. 5, pp. 1521–1529, 5 2008, PMID: 18440898.
- [28] N. Fazeli and J.-O. Hahn, "Estimation of cardiac output and peripheral resistance using square-wave-approximated aortic flow signal," *Frontiers in Physiology*, vol. 3, 7 2012, PMID: 22934049 PMID: PMC3429069. [Online]. Available: <https://www.ncbi.nlm.nih.gov/pmc/articles/PMC3429069/>

## Bibliography

---

- [29] J. Jansen, J. Schreuder, J. Mulier, N. Smith, J. Settels, and K. Wesseling, "A comparison of cardiac output derived from the arterial pressure wave against thermodilution in cardiac surgery patients," *British Journal of Anaesthesia*, vol. 87, no. 2, pp. 212–222, 8 2001.
- [30] M. T. Ganter, J. A. Alhashemi, A. M. Al-Shabasy, U. M. Schmid, P. Schott, S. A. Shalabi, A. M. Badri, S. Hartnack, and C. K. Hofer, "Continuous cardiac output measurement by un-calibrated pulse wave analysis and pulmonary artery catheter in patients with septic shock," *Journal of Clinical Monitoring and Computing*, vol. 30, no. 1, pp. 13–22, 2 2016, PMID: 25721853.
- [31] J.-X. Wang, X. Hu, and S. C. Shadden, "Data-augmented modeling of intracranial pressure," *arXiv:1807.10345 [physics]*, 7 2018, arXiv: 1807.10345. [Online]. Available: <http://arxiv.org/abs/1807.10345>
- [32] A. Adji, M. F. O'Rourke, and M. Namasivayam, "Arterial stiffness, its assessment, prognostic value, and implications for treatment," *American Journal of Hypertension*, vol. 24, no. 1, pp. 5–17, 1 2011, PMID: 20940710.
- [33] S. Laurent, J. Cockcroft, L. Van Bortel, P. Boutouyrie, C. Giannattasio, D. Hayoz, B. Pannier, C. Vlachopoulos, I. Wilkinson, H. Struijker-Boudier, and on behalf of the European Network for Non-invasive Investigation of Large Arteries, "Expert consensus document on arterial stiffness: methodological issues and clinical applications," *European Heart Journal*, vol. 27, no. 21, pp. 2588–2605, 9 2006.
- [34] K. Shameer, K. W. Johnson, B. S. Glicksberg, J. T. Dudley, and P. P. Sengupta, "Machine learning in cardiovascular medicine: are we there yet?" *Heart*, vol. 104, no. 14, pp. 1156–1164, 7 2018.

## Chapter 4

---

# Non-invasive estimation of aortic hemodynamics and cardiac contractility using machine learning

Vasiliki Bikia<sup>1</sup>, Theodore G. Papaioannou<sup>2</sup>, Stamatia Pagoulatou<sup>1</sup>, Georgios Rovas<sup>1</sup>, Evangelos Oikonomou<sup>2</sup>, Gerasimos Siasos<sup>2</sup>, Dimitris Tousoulis<sup>2</sup>, Nikolaos Stergiopoulos<sup>1</sup>

<sup>1</sup> *Institute of Bioengineering, École Polytechnique Fédérale de Lausanne, Switzerland*

<sup>2</sup> *Biomedical Engineering Unit, 1<sup>st</sup> Department of Cardiology, “Hippokration” Hospital, Medical School, National and Kapodistrian University of Athens, Greece*

Published in Nature Scientific Reports, 2020.

### Abstract

Cardiac and aortic characteristics are crucial for cardiovascular disease detection. However, non-invasive estimation of aortic hemodynamics and cardiac contractility is still challenging. This paper investigated the potential of estimating aortic systolic pressure (aSBP), cardiac output (CO), and end-systolic elastance ( $E_{es}$ ) from cuff pressure and pulse wave velocity (PWV) using regression analysis. The importance of incorporating ejection fraction (EF) as additional input for estimating  $E_{es}$  was also assessed. The models, including Random Forest, Support Vector Regressor, Ridge, Gradient Boosting, were trained/validated using synthetic data ( $n = 4,018$ ) from an in silico model. When cuff pressure and PWV were used as inputs, the normalized-RMSEs/correlations for aSBP, CO, and  $E_{es}$  (best-performing models) were  $3.36 \pm 0.74$  %/0.99,  $7.60 \pm 0.68$  %/0.96, and  $16.96 \pm 0.64$  %/0.37, respectively. Using EF as additional input for estimating  $E_{es}$  significantly improved the predictions ( $7.00 \pm 0.78$  %/0.92). Results showed that the use of non-invasive pressure measurements allows estimating aSBP and CO with acceptable accuracy. In contrast,  $E_{es}$  cannot be predicted from pressure signals



#### **Chapter 4. Non-invasive estimation of aortic hemodynamics and cardiac contractility using machine learning**

---

alone. The addition of the EF information greatly improves the estimated  $E_{es}$ . The accuracy of the model-derived aSBP compared to in vivo measured aSBP ( $n = 783$ ) was very satisfactory ( $5.26 \pm 2.30\% / 0.97$ ). Future in vivo evaluation of CO and  $E_{es}$  estimations remains to be conducted. This novel methodology has the potential to improve the non-invasive monitoring of aortic hemodynamics and cardiac contractility.

## 4.1 Introduction

Clinical parameters directly measured in the heart or at the root of the aorta are crucial for detection, diagnosis, prognosis, treatment, and management of cardiovascular diseases [1; 2; 3; 4]. Aortic hemodynamics, such as aortic systolic blood pressure (aSBP) and cardiac output (CO), are direct and more informative parameters for assessing cardiovascular health than corresponding measurements obtained at the peripheral arteries [1; 5; 6]. However, the gold standard techniques for measuring aSBP and CO are catheter-based and expensive [7; 8]. Furthermore, there is a need for non-invasive estimation of cardiac contractility. End-systolic elastance ( $E_{es}$ ), i.e. the slope of the end-systolic pressure–volume relation (ESPVR), is a pivotal determinant of left ventricular (LV) systolic performance and a powerful index of the arterio-ventricular interaction [4; 9; 10]. Despite its clinical importance, the clinical use of this measure is limited by the need for invasive acquisition of multiple LV pressure–volume loops under varying loading conditions [11].

Peripheral blood pressure (BP) measurements acquired by cuff sphygmomanometry have a fundamental role in the everyday clinical setting [12]. Recognizing the important differences between peripheral and central aortic pressures, significant efforts were oriented towards the non-invasive estimation of aortic hemodynamics, in particular aSBP, based on peripheral pressure measurements [13]. Among commonly used approaches for obtaining aSBP are generalized transfer functions (GTFs) [14; 15; 16], moving average models [17; 18] and pulse wave analysis-based methods [8; 19; 20]. Nevertheless, the totality of them relies on the acquisition of the entire peripheral pressure waveform which can be tedious and susceptible to errors [21].

Prediction of CO constitutes a more challenging task due to its dependency on the patient-specific arterial dimensions [22]. Non-invasive CO monitoring has been addressed using single-beat pulse contour analysis [23; 24; 25] which, however, allows for the derivation of only an uncalibrated estimation instead of the absolute CO value. Finally, notable studies have been developed and validated against invasive techniques for estimating  $E_{es}$  for a single cardiac cycle [26; 27]. The first fully non-invasive method was introduced by Chen et al. [26]. They proposed a simple equation to derive  $E_{es}$  from pressure arm cuff, echo-Doppler cardiography, and electrocardiograms.

Despite the good precision of previous techniques, there has been no holistic and complete study to investigate the possibility of estimating aortic hemodynamics and cardiac contractility using readily available non-invasive measurements on the same population. This is mainly attributed to two inherent limitations, i.e. the lack of invasive data in a large scale and the ethical limitation to perform invasive measurements on a healthy population, if no diagnostic reason has been provided.

Cardiovascular models hold a valuable position for addressing the challenge of limited access

## Chapter 4. Non-invasive estimation of aortic hemodynamics and cardiac contractility using machine learning

---

on in vivo data [28]. They constitute a faithful representation of the real cardiovascular system and allow the study of pathophysiological mechanisms and diseases [29; 30]. Furthermore, they can provide a complete set of parameters to describe the system, while the simulated signals are noise-free.

The present study aimed to evaluate whether aortic hemodynamics (i.e. aSBP and CO) and cardiac contractility (i.e.  $E_{es}$ ) can be accurately predicted by the use of brachial systolic blood pressure (brSBP) and diastolic blood pressure (brDBP), heart rate (HR), carotid-femoral pulse wave velocity (cfPWV), and, if necessary, ejection fraction (EF). These quantities were chosen as they are readily available in clinical practice and have been shown to provide information on the cardiovascular state [2; 3; 4; 31]. To overcome the aforementioned limitations, we performed our experiments using synthetic data ( $n = 4,018$ ), which were generated using a previously validated one-dimensional (1-D) mathematical model of the cardiovascular system [32]. Regression analysis was performed to establish the relationship between the non-invasive measurements [brSBP, brDBP, HR, cfPWV, (and EF)] and the invasive quantities of interest (aSBP, CO, and  $E_{es}$ ). The regression pipeline of the present study is presented in Figure 4.1. A ten-fold cross validation (CV) scheme was employed for the training/testing of the proposed approach. We evaluated four models including Random Forest [33], Support Vector Regressor (SVR) [34], Ridge [35], and Gradient Boosting [36]. In addition, averaging of the multiple predictions was performed. Two approaches were investigated: (i) prediction of aSBP, CO, and  $E_{es}$  using brSBP, brDBP, HR, and cfPWV as inputs, and (ii) prediction of  $E_{es}$  using brSBP, brDBP, HR, cfPWV, and EF. The accuracy of our prediction was evaluated by comparing the model-derived values with the reference simulated data. The accuracy of the aSBP model was subsequently validated using a large clinical dataset including in vivo hemodynamic measurements ( $n = 783$ ). Lack of CO and  $E_{es}$  in vivo data impeded the clinical evaluation of the corresponding models.

### 4.2 Methods & materials

A regression pipeline was applied for estimating aortic hemodynamics and LV contractility index. The schematic representation of the methodology is presented in Figure 4.1. The input data comprised brSBP, brDBP, HR, cfPWV, and EF for every subject. These data were fed to the regression models to estimate aSBP, CO, and  $E_{es}$ . First, brSBP, brDBP, HR, and cfPWV were used as input predictors for all three outputs, i.e. aSBP, CO, and  $E_{es}$ . A second regression analysis was performed using EF as an additional input feature only for the estimation of  $E_{es}$ . The outputs of each testing set were blinded and kept as the ground truth against which our predictions were later compared.

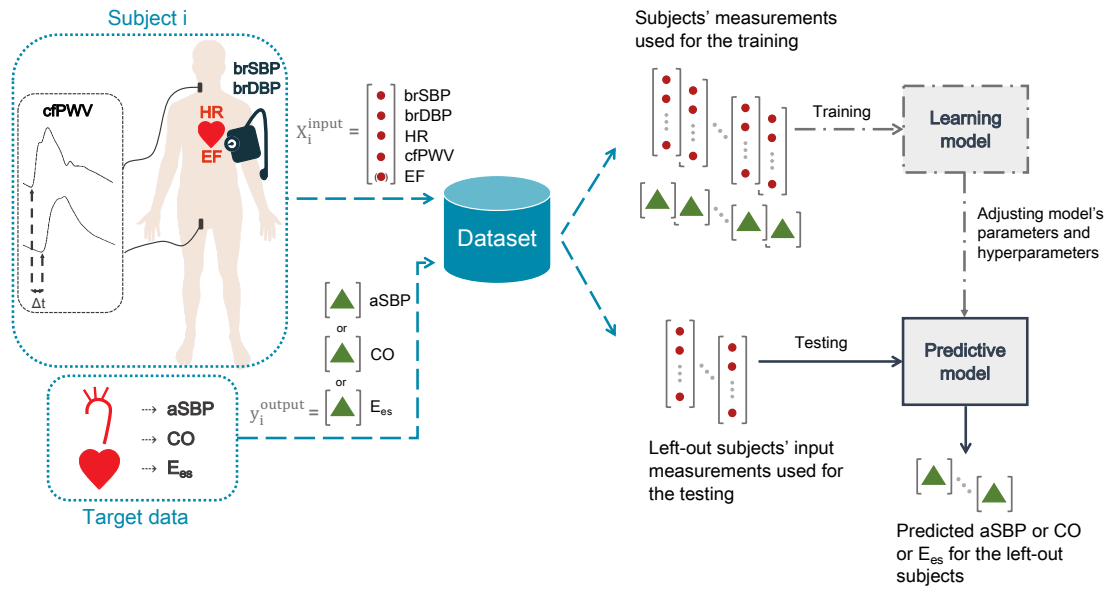


Figure 4.1 – Schematic illustration of the regression pipeline. Brachial systolic blood pressure (brSBP), brachial diastolic blood pressure (brDBP), heart rate (HR), carotid-femoral pulse wave velocity (cfPWV), and ejection fraction (EF) were used as features for predicting aortic systolic blood pressure (aSBP), cardiac output (CO), and end-systolic elastance ( $E_{es}$ ). Regression models were trained to map the input data to the respective target data of interest. The methodology presented here was followed for each regression process (in terms of set of inputs, model, and output). Adapted from [37].

### Brief description of the in silico model of cardiovascular dynamics

In the present study, we used a 1-D in silico model of the cardiovascular system, that has been previously described and validated against in vivo data [32]. The arterial tree includes the main arteries of the systemic circulation, as well as the cerebral circulation and the coronary circulation. In summary, the governing equations of the model are derived by integrating the longitudinal momentum and continuity equations over the arterial cross section. Pressure and flow are acquired across the arterial tree by solving the governing equations employing an implicit finite-difference scheme. Local arterial compliance is calculated, provided that pulse wave velocity (PWV) is approximated as an inverse power function of the arterial lumen diameter. Three-element Windkessel models [38] are coupled to the distal vessels to account for the peripheral resistance. The contractility of the left ventricle is modeled using a time-varying elastance model [4; 9]. This elastance model considers a linear ESPVR characterized by its slope, the  $E_{es}$ , and its intercept, the dead volume,  $V_d$ , as well as a linear end-diastolic pressure–volume relation characterized by its slope, the end-diastolic elastance ( $E_{ed}$ ).

### Synthetic population generation

A dataset of 4,018 synthetic hemodynamic cases was created. The 1-D cardiovascular model ran using different combinations of arbitrary input parameters. The distributions of the input parameters were based on physiologically relevant data from the literature. The cardiovascular parameters were chosen to represent healthy individuals. Due to the limited amount of probabilistic information, the sampling was selected to be random Gaussian. The values of  $E_{es}$  and  $E_{ed}$  ranged within [1.03, 3.5] mmHg/mL and [0.05, 0.2] mmHg/mL, respectively [39; 40; 41]. HR varied between 60 and 100 bpm. The LV filling pressure lied between 7 and 23 mmHg according to [42]. The  $V_d$  and the time of maximal elastance ( $t_{max}$ ) were kept unchanged. Their selected values were equal to the mean values of  $V_d = 15$  mL and  $t_{max} = 340.00$  ms as reported by previously published works [32; 43]. Arterial geometry was modified to simulate different body types by adapting the length and the diameter of the arterial vessels. The heights covered a range of [150, 200] cm while the limits for aortic diameter were set to [1.9, 4] cm [44; 45]. Total peripheral resistance varied within 0.5–2 mmHg.s/mL [46]. Total arterial compliance was chosen within the range of [0.1, 3.8] mL/mmHg in order to account for a wide range of different values of arterial tree stiffness [47; 48]. It should be noted that evidence of nonuniform aortic stiffening was integrated for the elderly and hypertensive virtual subjects, following the methodology described by Bikia et al. [49].

### Virtual dataset

The parameters of interest were estimated from the 1-D model-derived pressure and flow waves (simulation's outputs). Synthetic brSBP, brDBP as well as HR data were obtained from the pressure wave at the left brachial artery. Similarly, aSBP was derived from the pressure waveform at the aortic root. CfPWV was derived using the tangential method [50]. The method computed the intersection (foot) of two tangents, i.e. the line passing tangentially through the systolic upstroke and the horizontal line passing through the point of minimum pressure. Subsequently, the pulse transit time was estimated between the foot of the wave at the two sites, namely, between the carotid artery and the femoral artery. The length between the two arterial sites was calculated by summing the lengths of the arterial segments within the transmission path. Finally, the cfPWV was estimated by dividing the arterial length of the path by the pulse transit time. Given that the ESPVR was known, the EF was derived by dividing the blood volume that is ejected within each heartbeat, i.e. the stroke volume (SV), by the end-diastolic volume (EDV). The value of the  $E_{es}$  was defined as the slope of the ESPVR. Then, all simulated information was discarded, except for the “measured” brSBP, brDBP, HR, cfPWV, and EF (inputs) and the aSBP, CO, and  $E_{es}$  data (outputs). The total dataset (organized in pairs of inputs and outputs) was kept for the training/testing process.

### **Blending the dataset with random noise**

The synthetic data were corrupted with random noise in order to represent a more realistic data collection. The introduced noise was equivalent to a random relative error within the range of  $[-6, 6]$  % with respect to the actual value. This magnitude of error was selected based on published data from previous studies [51].

### **Clinical dataset**

For the clinical validation of the aSBP estimations, we used clinical data from 783 subjects who underwent non-invasive cardiovascular assessment for research purposes, at the First University Department of Cardiology (Hippokraton General Hospital, Athens, Greece). Anonymized data were analyzed in compliance with the Declaration of Helsinki of the World Medical Association and the National Regulations for clinical research.

The cfPWV was measured in every subject as previously described [52; 53; 52]. In brief, cfPWV measurement was performed using the SphygmoCor apparatus (AtCor Medical Pty Ltd, West Ryde, Australia). First, short-term continuous arterial pressure waveforms were recorded by use of a hand-held tonometer (Millar, Houston, USA), simultaneously with ECG acquisition (for the synchronization of the continuous pressure waves recorded at the carotid and the femoral artery). Then, the recorded pressure waveforms were processed by proprietary software that automatically computes pulse transit time from the carotid to the femoral artery using the tangential method [50]. Finally, cfPWV was calculated by the ratio of the distance between the two recording sites (calculated as the length from the suprasternal notch to femoral artery minus the length from the carotid artery to the suprasternal notch) to the pulse transit time. CfPWV measurements were performed with the subject at the supine position after 5 min resting period.

Non-invasive estimation of the aortic pressure waveforms was performed by the SphygmoCor System (AtCor Medical Pty Ltd), as previously described [54; 55]. Radial pressure waves were first recorded by applanation tonometry and central pressure waves were derived by use of validated transfer functions [56]. Multiple recordings were performed in every subject to accomplish optimal quality control criteria (quality index:  $> 85\%$ ). Calibration of the recorded pulse waves was performed using the brachial systolic and diastolic BPs, which were measured by cuff sphygmomanometry. The accuracy of this apparatus has been previously evaluated by comparing the estimated aortic BPs with intra-aortic catheter-based BP measurements [54]. Furthermore, the reproducibility of this technique has been also found to be acceptable under several different conditions and populations [57].

## Chapter 4. Non-invasive estimation of aortic hemodynamics and cardiac contractility using machine learning

---

Table 4.1 – List of the hyperparameters which were chosen to be optimized and their corresponding values.

Model	Hyperparameters to be optimized	Values
Random Forest	max_depth	{5, 10, 20}
	n_estimators	{500, 700, 1000}
Support Vector Regressor	C	{1, 10, 100}
	gamma	{0.001, 0.01, 0.1, 1}
Ridge	alpha	{1, 10, 100, 200}
Gradient Boosting	learning_rate	{0.01, 0.05, 1}
	n_estimators	{100, 500, 1000, 1750}

### Regression analysis

Four regression models were trained/tested to estimate the corresponding target outputs. The models that were employed were Random Forest [33], SVR [34], Ridge [35], and Gradient Boosting [36]. By definition, a regression model comprises the following components: (i) the unknown hyperparameters,  $\beta$ , (ii) the independent variables,  $X_i$ , and (iii) the dependent variable,  $Y_i$ . In this analysis, the objective was to investigate whether the regression model can estimate aSBP, CO, and  $E_{es}$  from single-beat input predictors [brSBP, brDBP, HR, cfPWV, (EF)]. The training/testing scheme was based on a ten-fold CV scheme [58] (Figure 4.2). Following a ten-fold CV, all cases were divided into ten equal sets in a random manner. In each fold, one set was left out being the testing group, and the rest of sets were used as the training group to tune the parameters of the models. Hyperparameter tuning was performed internally in each fold using GridSearch with a ten-fold CV in order to optimize the  $\beta$  parameters of each fold's model (Figure 4.2). The hyperparameters that were chosen to be optimized are reported in the Table 4.1. The hyperparameters' values that are not reported in Table 13 were set to their default value.

We investigated two approaches: (i) one to predict aSBP, CO, and  $E_{es}$  using brSBP, brDBP, HR, and cfPWV, and (ii) a second one to predict solely  $E_{es}$  using brSBP, brDBP, HR, cfPWV, and EF. Consequently, we evaluated the accuracy of each regression model for every target variable on a subject level. Additionally, averaging of the multiple predictions was tested as an ensemble learning approach. The training/testing pipeline was implemented using the Scikit-learn library [59] in a Python programming environment. The Pandas and Numpy packages were also used [60; 61].

### In silico validation of the model-derived predictions

We first assessed the performance of each regression model for every target variable on a subject level for the virtual population. Ten-fold CV as described above was used to evaluate the accuracy of the trained models. Moreover, we calculated the percentages of the cases

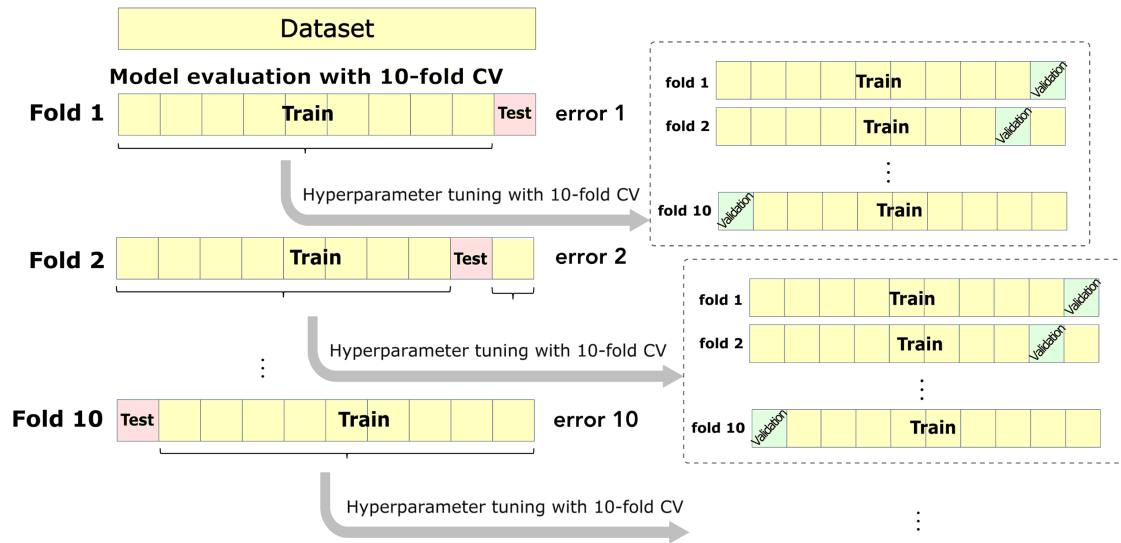


Figure 4.2 – Experimental design for the evaluation of the regression models. The model evaluation was done using ten-fold cross validation (CV) (external CV). In every external fold, we performed hyperparameter tuning with ten-fold CV (internal CV). Adapted from [37].

whose aSBP errors met the international standards ( $< 5 \pm 8$  mmHg) of the European Society of Hypertension International Protocol [62]. The error threshold for CO was set to 0.3 and 0.5 L/min based on the objective criteria suggested by Critchley and Critchley [63]. Finally, given that the only clinically acceptable technique for measuring  $E_{es}$  is the invasive end-systolic pressure–volume relationship, there are not meta-analyses using  $E_{es}$  data. In this respect, for the  $E_{es}$  values within the range of [1, 4.5] mmHg/mL, thresholds of 0.05 and 0.20 mmHg/mL should be adequate to provide an accurate estimation of  $E_{es}$ .

### Sensitivity analysis for the training size

In order to assess the effect of the number of training samples on our models' accuracy, sensitivity analysis was performed. The regression analysis was repeated after decreasing the training size from 95 to 15 % of the total number of cases. For each training size, the predictions were evaluated in terms of RMSE between the estimated and reference data. Hyperparameter tuning was implemented for each different training set under consideration.

### In vivo validation of the model-derived aSBP predictions

Moreover, in vivo validation was performed only for the best performing aSBP estimator, i.e. SVR. The validation was realized in two steps. First, we trained/tested an SVR model using only in vivo data following the experimental design described in Figure 4.2. Consequently, an SVR model was trained with the totality of the in silico data ( $n = 4,018$ ) and, then, was tested on



## Chapter 4. Non-invasive estimation of aortic hemodynamics and cardiac contractility using machine learning

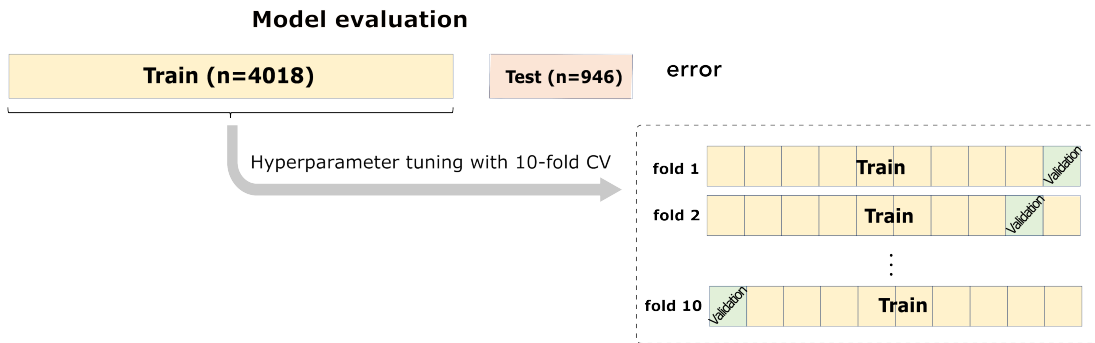


Figure 4.3 – Experimental design for the evaluation of the synthetically trained model against the in vivo data. Adapted from [37].

the in vivo data ( $n = 783$ ), as depicted in Figure 4.3. During training, hyperparameter tuning was performed using GridSearch with ten-fold CV.

### Feature importance evaluation

We assessed the importance of each input feature using the scores returned by the Random forest model. The average importance of each feature was then calculated by averaging the scores from every fold  $k$  ( $k = 1, 2, \dots, 10$ ).

### Statistical analysis

The algorithms and the statistical analysis were implemented in Python (Python Software Foundation, Python Language Reference, version 3.6.8, Available at <http://www.python.org>). We performed OLS estimation of the regression coefficients using each of the target parameters, i.e. aSBP, CO, and  $E_{es}$ , as dependent variable and brSBP, brDBP, cfPWV, HR, and EF (only for  $E_{es}$ ) as independent variables (using Statsmodels library [64]). Hypothesis testing for each regression coefficient was realized using the  $t$ -statistic. The agreement, bias and precision between the method-derived predictions and the real values were evaluated by using the Pearson's correlation coefficient ( $r$ ), the coefficient of determination ( $R^2$ ), the root mean square error (RMSE), and the normalized root mean square error (nRMSE). The computed nRMSE was based on the difference between the minimum and maximum values of the dependent variable. Bias and limits of agreement as described by [65] were reported. The level of statistical significance was set at  $P$ -value  $< 0.05$ .

Table 4.2 – Distributions of the parameters of the in silico population (n = 4,018).

Parameter	Value (n = 4,018)			
	min	max	mean	SD
End-systolic elastance [mmHg/mL]	1.03	3.50	2.29	0.40
End-diastolic elastance [mmHg/mL]	0.05	0.20	0.12	0.09
Filling pressure [mmHg]	7.00	23.00	15.12	2.10
Total arterial compliance [mL/mmHg]	0.10	3.80	1.86	0.90
Total peripheral resistance [mmHg.s/mL]	0.50	1.30	0.80	0.19
Heart rate [bpm]	61.11	10.00	82.57	8.15
Aortic diameter [cm]	2.00	4.00	3.00	1.00
Height [cm]	150.00	200.00	175.00	25.00
Brachial systolic blood pressure [mmHg]	81.80	199.20	133.71	25.07
Brachial diastolic blood pressure [mmHg]	39.73	125.69	76.06	21.86
Aortic systolic blood pressure [mmHg]	76.05	188.31	121.71	24.96
Carotid-to-femoral pulse wave velocity [m/s]	5.53	14.27	8.89	1.63
Cardiac output [L/min]	3.26	10.56	5.94	1.22
Ejection fraction [%]	29.74	69.31	50.83	6.81

### 4.3 Results

Table 4.2 aggregates the cardiovascular parameters of the in silico study population. The comparisons between the model-derived predictions and the reference data are presented below for each of the targeted outputs.

#### Prediction of aSBP, CO, and $E_{es}$ from brSBP, brDBP, HR, and cfPW

For the four models, the comparison between the predicted aSBP and the actual aSBP is presented in Table 4.3. The average difference (in absolute value) between the model-aSBP and the reference aSBP was less than 5 mmHg in 87 % of the total cases for Random Forest, 89 % for SVR, 75 % for Ridge, and 88 % for Gradient Boosting, respectively. Accuracy, correlation and agreement of model-CO estimates in comparison to the reference data are summarized in Table 4.4. The difference between model-CO and reference CO was less than 0.3/0.5 L/min in 62/84 % of the population for Random Forest, 65/86 % for SVR, 50/74 % for Ridge, and 63/85 % for Gradient Boosting. Finally, the  $E_{es}$  predictions are compared to the reference data in Table 4.5. High errors were reported for all of the regression models, whereas correlation between the estimated and the reference data was significantly poor.

#### Prediction of $E_{es}$ from brSBP, brDBP, HR, cfPWV, and EF

The statistics of the second regression analysis for  $E_{es}$ , i.e. after additional knowledge of EF, are presented in Table 4.6. Differences between the predicted  $E_{es}$  and the actual  $E_{es}$  were

**Chapter 4. Non-invasive estimation of aortic hemodynamics and cardiac contractility using machine learning**

Table 4.3 – Regression statistics between the model predicted aSBP and the reference aSBP. The input features include brSBP, brDBP, HR, and cfPWV.

Model	Slope	Intercept [mmHg]	$r$	$R^2$	$P$ -value	nRMSE [%]	MAE [mmHg]
RF	1.01	-1.13	0.99	0.98	<0.001	3.57±0.79	2.61±0.87
SVR	1.01	-1.00	0.99	0.98	<0.001	3.36±0.74	2.43±0.77
Ridge	0.99	1.64	0.98	0.96	<0.001	4.96±2.04	3.73±1.71
GB	1.01	-0.87	0.99	0.98	<0.001	3.55±0.88	2.58±0.90
Ensemble Averaging (all)	1.01	-0.85	0.99	0.98	<0.001	3.53±1.00	2.59±1.01
Ensemble Averaging (RF, SVR, GB)	1.01	-1.13	0.99	0.98	<0.001	3.40±0.79	2.47±0.84

Table 4.4 – Regression statistics between the model predicted CO and the reference CO. The input features include brSBP, brDBP, HR, and cfPWV.

Model	Slope	Intercept [L/min]	$r$	$R^2$	$P$ -value	nRMSE [%]	MAE [L/min]
RF	0.99	0.03	0.95	0.90	<0.001	7.94±0.95	0.29±0.08
SVR	1.01	-0.06	0.96	0.92	<0.001	7.60±0.68	0.27±0.06
Ridge	0.99	0.05	0.93	0.86	<0.001	10.15±1.00	0.36±0.05
GR	1.00	0.01	0.95	0.90	<0.001	7.80±0.86	0.28±0.07
Ensemble Averaging (all)	1.02	-0.11	0.96	0.92	<0.001	7.59±0.72	0.27±0.06
Ensemble Averaging (RF, SVR, GB)	1.01	-0.05	0.96	0.92	<0.001	7.48±0.73	0.27±0.06

Table 4.5 – Regression statistics between the model predicted  $E_{es}$  and the reference  $E_{es}$ . The input features include brSBP, brDBP, HR, and cfPWV.

Model	Slope	Intercept [mmHg/mL]	$r$	$R^2$	$P$ -value	nRMSE [%]	MAE [mmHg/mL]
RF	0.93	0.17	0.36	0.13	<0.001	17.02±0.63	0.30±0.02
SVR	0.87	0.30	0.35	0.12	<0.001	17.11±0.67	0.30±0.02
Ridge	1.00	-0.00	0.37	0.14	<0.001	16.96±0.64	0.30±0.02
GB	0.99	0.02	0.33	0.10	<0.001	17.23±0.72	0.31±0.02
Ensemble Averaging (all)	1.01	-0.02	0.37	0.14	<0.001	16.98±0.65	0.30±0.02
Ensemble Averaging (RF, SVR, GB)	0.99	0.02	0.36	0.13	<0.001	17.02±0.66	0.30±0.02

Table 4.6 – Regression statistics between the model predicted  $E_{es}$  and the reference  $E_{es}$ . The input features include brSBP, brDBP, HR, cfPWV, and EF.

Model	Slope	Intercept [mmHg/mL]	$r$	$R^2$	$P$ -value	nRMSE [%]	MAE [mmHg/mL]
RF	1.02	-0.04	0.91	0.83	<0.001	7.57±0.92	0.13±0.02
SVR	1.00	0.00	0.92	0.85	<0.001	7.00±0.78	0.12±0.01
Ridge	0.97	0.06	0.87	0.76	<0.001	9.04±1.36	0.16±0.03
GB	1.00	-0.01	0.91	0.83	<0.001	7.43±0.81	0.13±0.01
Ensemble Averaging (all)	1.03	-0.08	0.92	0.85	<0.001	7.20±0.76	0.13±0.01
Ensemble Averaging (RF, SVR, GB)	1.02	-0.05	0.92	0.85	<0.001	7.04±0.70	0.12±0.01

found to be less than 0.05/0.20 mmHg/mL in the 47/78 %, 51/81 %, 39/70 %, and 47/78 % of the entire population, for Random Forest, SVR, Ridge, and Gradient Boosting, respectively. The scatterplots and Bland–Altman graphs for the best performing models are provided in Figures 4.4, 4.5, and 4.6. The plotted data are corrupted with random noise (see Blending the dataset with random noise in Methods). Table 4.7 presents the frequency of selection for each hyperparameter value over the ten-fold CV for the best performing model. For the aSBP and  $E_{es}$  estimators, we observed an apparent consistency for the values of the C and gamma hyperparameters. Specifically, C and gamma were set at 100 and 0.001 for aSBP, and 10 and 0.001 for  $E_{es}$ , respectively, in the totality of the 10 folds. Such a consistency is not evident for the CO estimator where C was set at 100 for the 60 % of the times. Nevertheless, gamma was again consistently selected to be 0.001.

### Sensitivity analysis for the training size

The training size, that is, the number of data instances used for training, plays a major role on the accuracy of the predictions. To investigate the sensitivity to the number of training data, the training size was modified from 95 to 15 % of the total number of cases (Figures 4.7, 4.8, and 4.9). For all models except for Ridge, the RMSEs were increased gradually with decreasing training size. For the Random Forest, SVR, and Gradient Boosting, the RMSEs of the aSBP predictions were less than 4.20 mmHg. Using Ridge, the RMSE varied at a lesser extent, while it was consistently higher compared to the rest of the models. For the CO predictions, all RMSE values were less than 0.50 L/min. In particular, RMSE for SVR did not exceed 0.38 L/min, even when only the 15 % of the entire population was used for the training. Finally, all RMSEs of  $E_{es}$  estimations were equal or below 0.20 mmHg/mL.

## Chapter 4. Non-invasive estimation of aortic hemodynamics and cardiac contractility using machine learning

Table 4.7 – Statistical results in percentage of times that the hyperparameter value was selected during the hyperparameter tuning with ten-fold cross validation process. Values selected consistently are presented in bold.

Model	Hyper-parameter	Values	aSBP	CO	$E_{es}$
			Times selected [%]	Times selected [%]	Times selected [%]
SVR	C	1	0 %	0 %	0 %
		10	0 %	40 %	<b>100 %</b>
		100	<b>100 %</b>	<b>60 %</b>	0 %
	gamma	0.001	<b>100 %</b>	<b>100 %</b>	<b>100 %</b>
		0.01	0 %	0 %	0 %
		0.1	0 %	0 %	0 %
		1	0 %	0 %	0 %

Table 4.8 – Average feature importances for the prediction of aSBP, CO, and  $E_{es}$ .

Feature	aSBP	Feature	CO	Feature	$E_{es}$
brSBP	0.98	brSBP	0.54	EF	0.65
brDBP	0.02	cfPWV	0.33	brDBP	0.16
HR	0.004	brDBP	0.08	HR	0.11
cfPWV	0.003	HR	0.04	cfPWV	0.05
				brSBP	0.02

### Feature importance evaluation

Figure 4.10 presents the correlation matrix reporting the inter-feature correlations, and the correlations between the inputs and the target outputs. Table 4.8 presents the average importances of the input features, sorted in a descending order for predicting aSBP, CO, and  $E_{es}$ , respectively. For estimating aSBP, brSBP was found to be a critical contributor; the importance level (0.98) indicated that brSBP should be sufficient for estimating aSBP. The features of brSBP and cfPWV were the dominant contributors in the estimation of CO. Finally, EF was found to play the most significant role in the  $E_{es}$  prediction, followed by brDBP and HR. To further verify the sensitivity of the model's performance to the input features, we present the RMSE variation for different subsets of input features (only for the best performing models) (Table 4.9). For aSBP, it was shown again that the brSBP is the most pivotal predictor of aSBP; when brSBP was removed from the input features, the RMSE increased significantly. On the contrary, a precise prediction of CO requires the use of at least one of the brachial BP values; exclusion of the latter resulted to a deterioration of the model's performance. Finally,  $E_{es}$  appears to be mainly sensitive to EF which significantly contributes to the accuracy of the  $E_{es}$  estimation. Results of the hypothesis testing for the ordinary least squares (OLS) regression coefficients are summarized in Table 4.10. All of the specified coefficients were statistically significantly different from zero.

Table 4.9 – Model performance for the best performing configurations (SVR) using different subsets of the input features.

Input subsets	RMSE ( $r$ )		
	aSBP (SVR)	CO (SVR)	$E_{es}$ (SVR)
brSBP, brDBP, HR, cfPWV, EF	-	-	0.15 mmHg/mL (0.92)
brSBP, brDBP, HR, EF	-	-	0.17 mmHg/mL (0.91)
brSBP, brDBP, cfPWV, EF	-	-	0.17 mmHg/mL (0.91)
brSBP, HR, cfPWV, EF	-	-	0.22 mmHg/mL (0.83)
brDBP, HR, cfPWV, EF	-	-	0.17 mmHg/mL (0.91)
brSBP, brDBP, HR, cfPWV	3.13 mmHg (0.99)	0.34 L/min (0.96)	0.37 mmHg/mL (0.37)
brSBP, brDBP, HR	3.31 mmHg (0.99)	0.38 L/min (0.95)	0.38 mmHg/mL (0.33)
brSBP, brDBP, cfPWV	3.09 mmHg (0.99)	0.42 L/min (0.93)	0.38 mmHg/mL (0.35)
brSBP, HR, cfPWV	3.88 mmHg (0.99)	0.59 L/min (0.85)	0.38 mmHg/mL (0.35)
brDBP, HR, cfPWV	7.68 mmHg (0.94)	0.59 L/min (0.86)	0.38 mmHg/mL (0.32)

Table 4.10 –  $t$ -statistics for the OLS regression coefficients.

Input Feature	aSBP		CO		$E_{es}$	
	$t$ -value	$P$ -value	$t$ -value	$P$ -value	$t$ -value	$P$ -value
Intercept	-31.296	<0.001	-22.304	<0.001	-60.951	<0.001
brSBP	148.210	<0.001	82.000	<0.001	-12.704	<0.001
brDBP	11.241	<0.001	-51.739	<0.001	32.673	<0.001
cfPWV	-9.087	<0.001	-18.746	<0.001	3.685	<0.001
HR	16.776	<0.001	47.129	<0.001	21.960	<0.001
EF					118.028	<0.001

## Chapter 4. Non-invasive estimation of aortic hemodynamics and cardiac contractility using machine learning

Table 4.11 – Distributions of the parameters of the in vivo population (n = 783).

Parameter	Value (n = 783)			
	min	max	mean	SD
Age [years]	28.00	88.00	60.83	11.47
Height [cm]	143.00	195.00	171.60	7.94
Weight [kg]	40.00	145.00	82.29	14.10
Heart rate [bpm]	41.00	107.00	64.06	10.65
Brachial systolic blood pressure [mmHg]	90.00	180.00	126.37	15.70
Brachial diastolic blood pressure [mmHg]	40.00	120.00	77.89	11.21
Central systolic blood pressure [mmHg]	82.00	172.00	117.95	15.18
Carotid-femoral pulse wave velocity [m/s]	4.70	19.60	8.92	2.25
Hypertension	64 %			
Dyslipidemia	64 %			
Smoking *	23 %			
Renal transplant LD	1 %			
Renal transplant DD	0.3 %			
Breast cancer	2 %			
Coronary artery disease	81 %			
* 65 % of the remaining population declared to be smokers in the past.				

### In vivo evaluation of the aSBP estimations

After the in silico validation, the performance of the aSBP estimator was evaluated anew using clinical data. The population included both women (n = 136) and men (n = 647). The descriptive and clinical characteristics of the clinical population are presented in Table 4.11. First, we assessed the capacity of an SVR model, which was trained using only in silico data, to make an accurate prediction for the human population. Then, we compared the latter's performance with an SVR model which was trained using in vivo data. The regression statistics between the model predictions and the reference data are summarized in Table 4.12. For the in vivo data, the hypothesis testing's results for the OLS regression coefficients are presented in Table 4.13. Figure 4.11 provides the correlation matrix for the in vivo dataset.

## 4.4 Discussion

The present study demonstrated that accurate estimations of central hemodynamics (namely aSBP and CO) and LV  $E_{es}$  from readily available non-invasive clinical measurements can be obtained by using machine learning models. Our basic hypothesis was whether brSBP, brDBP (cuff BP), HR, and cfPWV provide sufficient information to predict aSBP, CO, and  $E_{es}$ . However, for the determination of  $E_{es}$ , data from peripheral pressure fall short to provide a precise estimate. Our results indicated that additional information, such as the EF, which is directly measured in the heart (rather than the periphery) may improve the non-invasive

Table 4.12 – Regression statistics between the model predicted aSBP and the reference aSBP. The input features include brSBP, brDBP, HR, and cfPWV. The testing set consists of in vivo data only.

SVR (tested using in vivo data)	Slope	Intercept [mmHg]	$r$	$R^2$	$P$ -value	nRMSE [%]	Bias (LoA) [mmHg]
Model trained using in silico data	0.99	2.94	0.94	0.88	<0.001	5.93	-1.67 (8.62,-11.95)
Model trained using in vivo data	1.00	0.31	0.97	0.94	<0.001	5.26±2.3	0.43 (8.73,-7.88)

Table 4.13 –  $t$ -statistics for the OLS regression coefficients.

Input Feature	aSBP	
	$t$ -value	$P$ -value
Intercept	6.504	<0.001
brSBP	91.182	<0.001
brDBP	12.094	<0.001
cfPWV	3.296	<0.001
HR	-18.110	<0.001

$E_{es}$  predictions. To our best knowledge, this is the first work to evaluate the use of machine learning models in predicting cardiac contractility.

The best performing prediction model for all three target outputs was SVR which outperformed the other models accomplishing the highest accuracy. The  $E_{es}$  estimation was effectively achieved only with the inclusion of EF in the set of input features. In order to evaluate the robustness of our regression models, sensitivity to the training size was investigated. The RMSE was gradually increased with decreasing the number or training samples for Random Forest, SVR, and Gradient boosting. Variations were less distinct for Ridge. Despite the increase in RMSE with changes in the training size, the errors lied within acceptable limits [62; 66; 67; 68; 69] for Random Forest, SVR, and Gradient Boosting.

Moreover, we tested the performance of an ensemble predictor which used averaging of the single models' predictions. The ensemble prediction model did not outperform the best performing single prediction model (SVR). However, such an approach may benefit the estimations' accuracy by reducing the variance of the predictor and thus may improve the model's generalization ability [70]. To avoid overwhelm the reader with an exhaustive report of several other approaches, we did not explore other ensemble learning techniques. Such an extensive exploration of different ensemble techniques would be out of the scope of this study.



## Chapter 4. Non-invasive estimation of aortic hemodynamics and cardiac contractility using machine learning

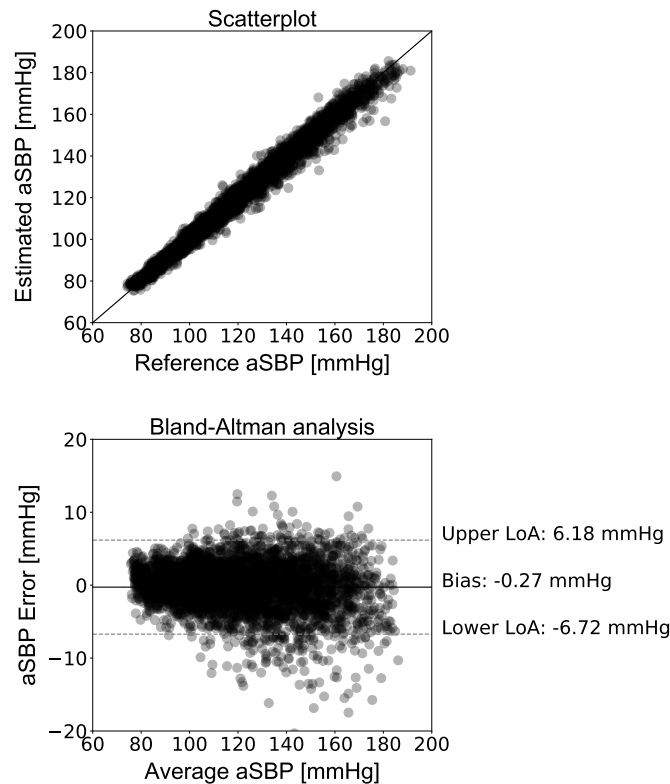


Figure 4.4 – Comparison between the estimated and the reference aSBP data. Scatterplot and Bland–Altman plot between the predicted aSBP (using the SVR model) and the reference aSBP (using the in silico data). The solid line of the scatterplots represents equality. In Bland–Altman plot, limits of agreement (LoA), within which 95 % of errors are expected to lie, are defined by the two horizontal dashed lines. Adapted from [37].

Following the in silico validation, in vivo validation was performed only for the aSBP. The aSBP predictions were found to be precise in the both investigated scenarios, i.e. SVR trained with in silico data, and SVR trained with in vivo data. The accuracy was slightly higher in the second scenario despite the smaller size of the training dataset. This is expected if we consider that the in vivo data may contain more physiologically relevant content and thus be more informative compared to the in silico data in the training of the model. Interestingly, the hyperparameter tuning led to the same selection for the hyperparameters  $C = 100$  (selected 100 % of the times) and  $\gamma = 0.001$  (selected 100 % of the times) when the SVR model was validated using the in vivo population. These findings may verify that the in silico predictive models can be rather informative for the design of clinical studies.

The principal reason that brSBP, brDBP, HR, and cFPWV were selected as the model inputs was the simplicity of their measurement in a clinical setting. Brachial cuff pressure constitutes a readily available and cost-efficient measurement in traditional medicine. At the same time, the use of pressure-based cFPWV is steadily increasing, as a result of numerous studies

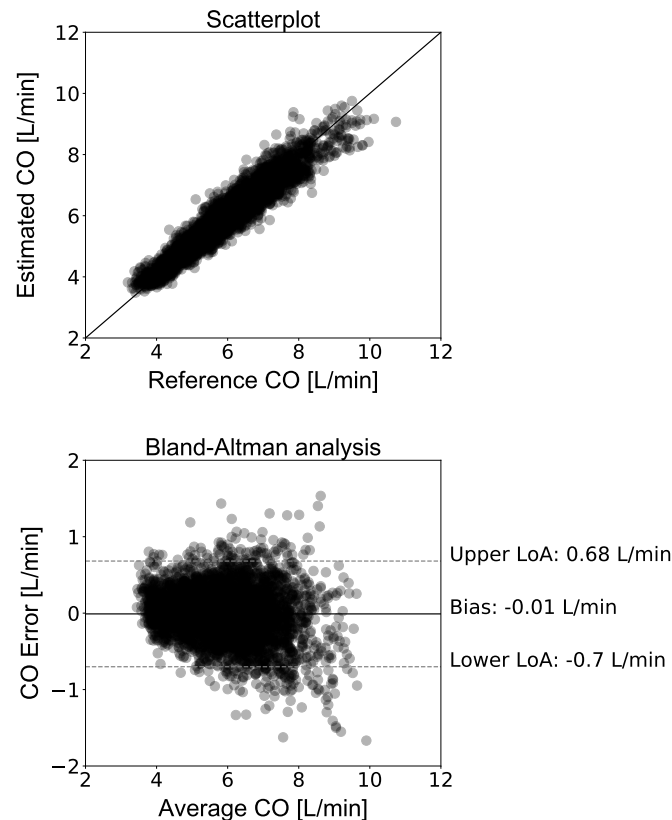


Figure 4.5 – Comparison between the estimated and the reference CO data. Scatterplot and Bland–Altman plot between the predicted CO (using the SVR model) and the reference CO (using the in silico data). The solid line of the scatterplots represents equality. In Bland–Altman plot, limits of agreement (LoA), within which 95 % of errors are expected to lie, are defined by the two horizontal dashed lines. Adapted from [37].

demonstrating its importance as an independent predictor of cardiovascular disease [71; 72; 73]. The convenience and the cost-efficiency of the aforementioned measurements render them suitable for easy, non-invasive, regular medical check-ups.

Based on the feature importances' assessment, the aSBP prediction was found to be determined mainly from the brSBP. The strong dependency between aSBP and brSBP errors is to be expected, given that the two values are strongly related to mean BP, which is practically the same in both the aorta and the brachial artery. Moreover, brSBP seemed to be a significant predictor of CO. Resistance, and thus mean BP, is a strong determinant of CO. Given that brSBP is related to mean BP, this means that brSBP is indirectly related to CO. In addition, cfPWV is a measure of arterial compliance, which is also determinant of stroke volume and thus CO. Finally, EF and  $E_{es}$  have been reported to be positively correlated [74] and this further explains the high importance level of EF for predicting  $E_{es}$ . The results using different subsets of the input features further verified each feature's contribution to the predictions of the target

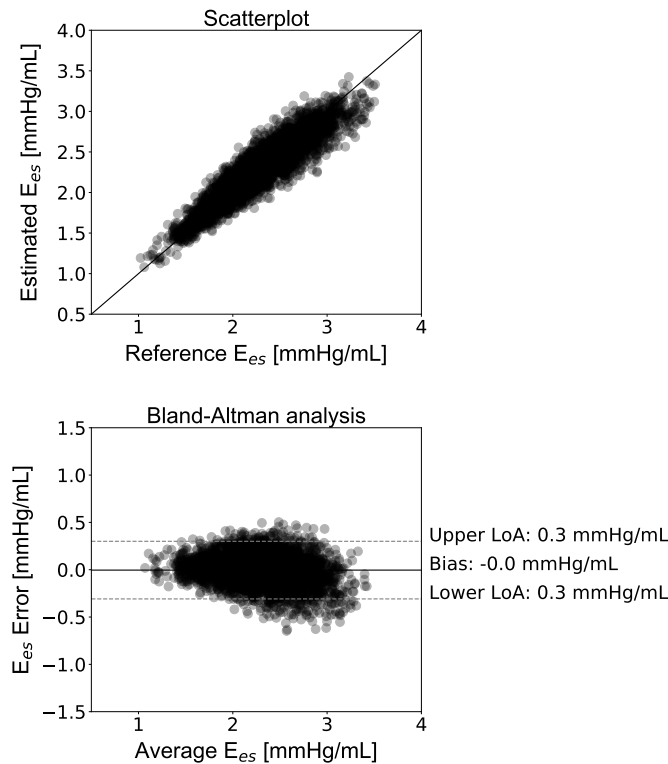


Figure 4.6 – Comparison between the estimated and the reference  $E_{es}$  data. Scatterplot and Bland–Altman plot between the predicted  $E_{es}$  (using the SVR model) and the reference  $E_{es}$  (using the in silico data) with the ejection fraction as regression input. The solid line of the scatterplots represents equality. In Bland–Altman plot, limits of agreement (LoA), within which 95 % of errors are expected to lie, are defined by the two horizontal dashed lines. Adapted from [37].

output variables.

Prior work proposed by Xiao et al. [75] used an artificial neural network (ANN) to predict aSBP from invasive radial SBP and DBP, and HR. The differences between the predicted aSBP and the measured aSBP were found to be low and equal to  $-0.30 \pm 5.90$  mmHg. Despite providing accurate results, invasive radial BP is not commonly measured on a regular basis, and thus its modelling imposes a substantial limitation on the clinical application of their proposed model. When an ANN with the same configuration, as the one reported in the study of Xiao et al., was employed to estimate aSBP in our study, the results indicated a similarly good prediction performance. In particular, the employment of the ANN using only the in silico data ( $n = 4,018$ ) achieved an  $RMSE = 3.79 \pm 1.88$  mmHg and  $r = 0.99$  ( $P$ -value  $< 0.001$ ). Training/testing the ANN with only the in vivo data ( $n = 783$ ) achieved an  $RMSE = 3.38 \pm 1.09$  and  $r = 0.97$  ( $P$ -value  $< 0.001$ ). In the case of the in vivo data, we observed that the accuracy is slightly improved by the use of ANN compared to the best performing configuration (SVR achieved an  $RMSE = 3.53 \pm 1.27$  mmHg,  $r = 0.97$ ,  $P$ -value  $< 0.001$ ).

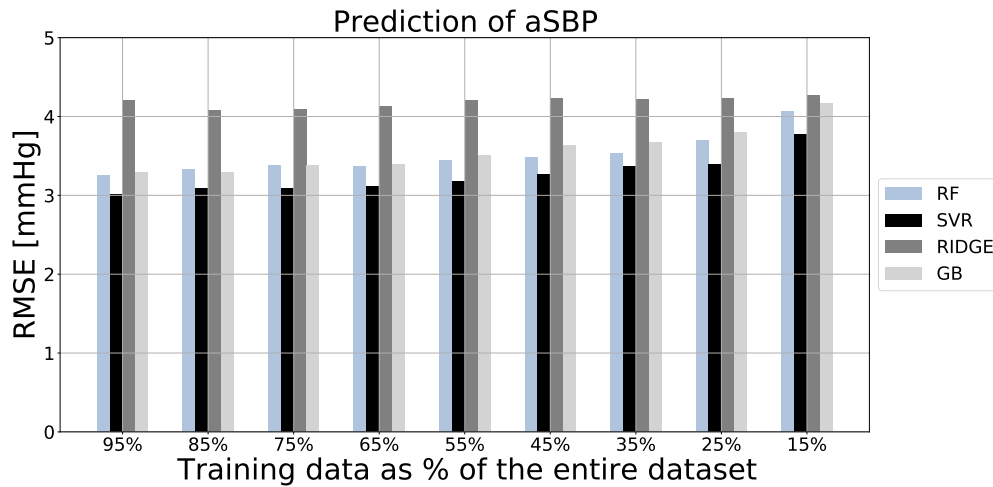


Figure 4.7 – Sensitivity of RMSE to changes in the training size for the aortic systolic blood pressure (aSBP) estimator. RMSE root mean square error; RF random forest; SVR support vector regressor; GB gradient boosting. Adapted from [37].

In general, the majority of previous aSBP estimators relies on features extraction from the pressure waveforms [75; 76]. In our approach, apart from peripheral SBP and DBP, and HR, we incorporated the cfPWV measurement. The idea was that cfPWV being an index of aortic stiffening would improve the performance of the model and strengthen the clinical relevance of our results. However, feature importances indicated that brSBP may be sufficient for estimating aSBP. Using only brSBP, brDBP, and HR as inputs would not alter significantly the accuracy of the estimation of aSBP (using the in silico data); namely, the RMSE would slightly increase from 3.13 to 3.31 mmHg for the best performing model. In the case that only brSBP and brDBP were used as input features, the accuracy would deteriorate with a RMSE of 3.46 mmHg which could still be acceptable. The use of only brSBP as an input, however, would essentially increase the error at 5.33 mmHg. For the clinical dataset, the same errors were equal to 3.52 mmHg (brSBP, brDBP, HR as inputs) and 4.11 mmHg (brSBP, brDBP as inputs). Finally, using only the brSBP predictor would lead to an RMSE = 4.20 mmHg.

In addition to prediction models for aSBP, estimation of CO from arterial BP characteristics has been a fertile area of research. Dabanloo et al. [25] has evaluated the performance of neural networks in predicting CO from invasive arterial pressure waves. Upon comparison between the predicted CO and thermodilution-derived CO, their best performing model provided a mean absolute error equal to 0.54 L/min and a correlation coefficient of 0.89. Nevertheless, their model made use of the entire pressure waveform, from which input features were extracted, whereas it provided only an uncalibrated estimation of CO rather than its absolute value.

The results presented in this study are also compliant with the findings of Bikia et al. [49], who suggested that brachial BP and cfPWV can be used to predict central SBP and CO (RMSE equal

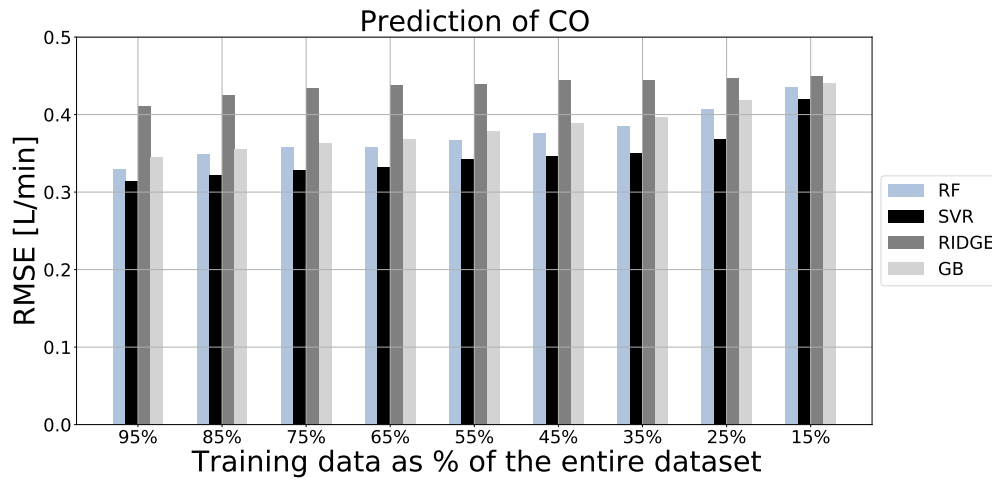


Figure 4.8 – Sensitivity of RMSE to changes in the training size for the cardiac output (CO) estimator. RMSE root mean square error; RF random forest; SVR support vector regressor; GB gradient boosting. Adapted from [37].

to 2.46 mmHg and 0.36 L/min, respectively). Following an inverse problem-solving approach, a generalized model of the cardiovascular system was adjusted to quasi-patient-specific standards using measurements of brSBP, brDBP, HR, and cfPWV. Additional geometrical information on the aortic diameter size of each subject was also integrated. The aortic diameter was approximated using previously published age- and BSA-related data [44]. A similar approximation of the aortic geometry could be embedded in the present study and improve the accuracy of the results. Therefore, employment of machine learning on clinical data could be further reinforced with the inclusion of additional input features such as age, height, and weight. However, given that the errors are already rather low, it is not anticipated that such an improvement would be of particular clinical significance.

Additionally, this study aimed to effectively predict  $E_{es}$  while utilizing a small number of required inputs. Chen et al. [26] proposed a method to estimate  $E_{es}$  from cuff pressure, stroke volume, and EF. Their method provided accurate predictions of  $E_{es}$  with differences equal to  $0.43 \pm 0.50$  mmHg/mL. In contrast to Chen’s approach, we excluded stroke volume from our input vector and, on the other hand, we introduced cfPWV which constitutes an index of aortic stiffness and thus a powerful index of arterio-ventricular coupling [77]. In an attempt to remove EF from the set of inputs,  $E_{es}$  was found to be poorly predicted. This underachieving performance may be rather expected given that a specific combination of brachial SBP and DBP, and cfPWV might not be unique for only a particular  $E_{es}$  value. Importantly, our study emphasized on the significance of EF in accurately predicting  $E_{es}$ .

The use of EF is further encouraged from the fact that EF constitutes a non-invasive parameter which can be derived via several cardiac imaging modalities. The Simpson’s method [78] has been the most commonly used technique; however, it might underestimate EF when

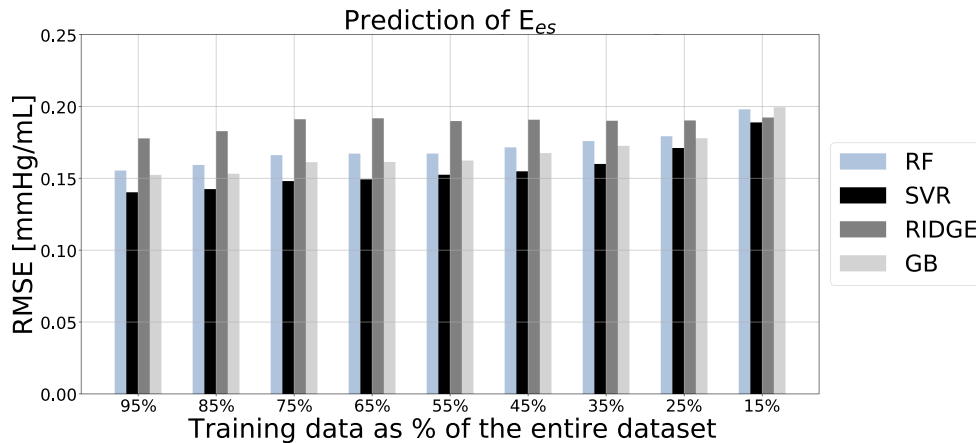


Figure 4.9 – Sensitivity of RMSE to changes in the training size for the end-systolic elastance ( $E_{es}$ ) estimator. RMSE root mean square error; RF random forest; SVR support vector regressor; GB gradient boosting. Adapted from [37].

compared to the magnetic resonance imaging (MRI), which has been shown to be the gold standard non-invasive technique for assessing LV function and thus EF [79]. Of course, the latter are not considered as convenient and cost-efficient as a cuff- or tonometry-based pressure measurement. It is likely that the EF-related information may be derived from another measured parameter which is directly or indirectly related to the cardiac contractility, e.g. electrical signals of cardiac events [80]. Further investigation towards this direction will be conducted in future work.

It should be noted that the aim of the current study is not to propose necessarily a tool that could provide simultaneous predictions of aSBP, CO, and  $E_{es}$ . The models developed in this study could be considered as independent predictors for each of the target parameters in different clinical occasions. In particular, aSBP and CO are major hemodynamical indices that are often useful to the clinician and their non-invasive estimation is highly desirable in a routine clinical examination. On the other hand,  $E_{es}$  is less often required. Currently,  $E_{es}$  is measured invasively with the acquisition of the LV pressure–volume loops. The invasive nature of this technique severely limits the use of  $E_{es}$  in clinical practice.

The booming of data has led to efforts of transferring one type of information to another using machine learning models. Specifically, in relation to patho-physiology, the advancement on measuring and imaging techniques has encouraged the employment of machine learning for estimating clinical pathophysiological indices and validating their results. This promising area of research could not exclude applications on cardiovascular health [25; 75; 81; 82]. High correlation between peripheral pressure and central aortic pressure indicates the potential to estimate the latter from the former. However, the correlations for a complete set of cardiovascular variables have not been thoroughly investigated. In this work, we performed a first study to elucidate which input parameters (non-invasive measurements) are considered

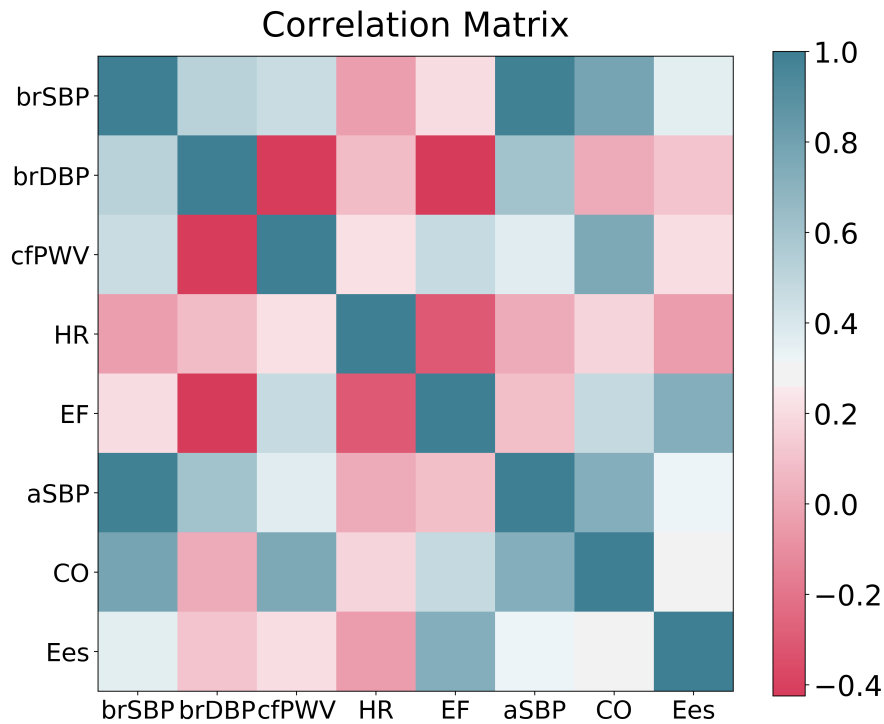


Figure 4.10 – Correlation matrix for the in silico dataset. Adapted from [37].

necessary when machine learning is employed for predicting aortic hemodynamics and contractility index (invasive measurements). A major advantage of the present study pertains to the well-balanced dataset that was used for the training/testing scheme. The use of synthetic data allowed for covering a wide range of hemodynamical characteristics, whereas it provided us with access to cardiovascular quantities which are difficult to obtain non-invasively in the real clinical setting, i.e. aortic BP or  $E_{es}$ .

Cardiovascular models have attracted great interest due to the increasing impact of cardiovascular disease. They have provided a valuable alternative for the assessment of pressure and flow in the entire arterial network providing additional pathophysiological insights, which are difficult to acquire in vivo. Numerous previous studies have used in silico data for the estimation of aortic BP, cardiac output, aortic PWV and many more [83; 84; 85; 82; 86]. Importantly, in silico studies allow for the preliminary evaluation of predictive models across a wide range of cardiovascular parameters [28] in a quick and cost-efficient way, while their results can be rather informative of the design of clinical studies [87; 88].

### Limitations

Several limitations need to be acknowledged. The data used for the training/testing scheme were derived from a simulator instead of a real human population. While synthetic data can

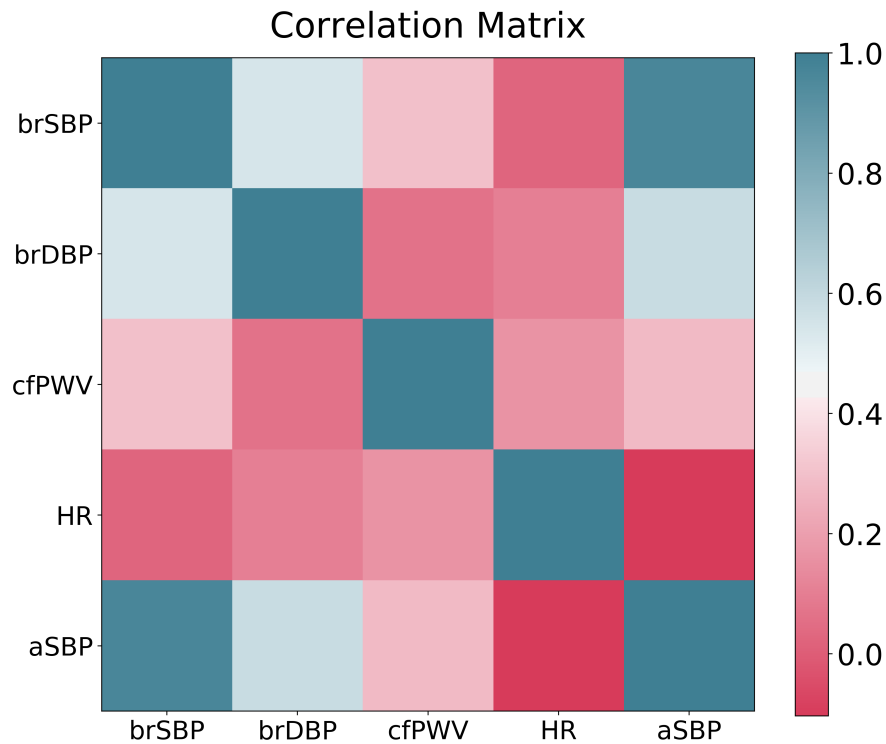


Figure 4.11 – Correlation matrix for the in vivo dataset. Adapted from [37].

mimic numerous properties of the real clinical data, they do not copy the original content in an identical way. Nevertheless, the goal here was to define the minimum necessary input information that is required to estimate aortic hemodynamics and  $E_{es}$ . Thus, despite that the use of synthetic data might not lead to exactly the same results with the results coming from clinical data, it should not undermine the reliability of the study's findings. The latter has been verified by the in vivo validation of our aSBP estimations. Clinical validation was not possible for the CO and  $E_{es}$  estimators, due to the lack of the respective data. At the initial stage of our research, we found it reasonable to start with an in silico validation of our predictive models, instead of collecting measurements of CO and  $E_{es}$  in a large cohort. In addition, the cost and the complexity of the respective measurements would make it difficult to incorporate them in the current study. Future work should include the use of real-world data for all parameters that will finally verify the application of the proposed method in the clinical setting. Finally, the proposed models have been designed and tested on data coming from a generalized model of the cardiovascular system which was developed according to published data [32]. Hence, the precision of the predictions might be compromised in the case of pathological conditions, such as atherosclerosis, aneurysm or aortic valve disease. It is of great importance that in vivo validation of the models should be conducted using pathological clinical data as well.



## **Conclusion**

In summary, this study showed that the use of non-invasive arm cuff pressure and PWV alone potentially allows for the estimation of aSBP and CO with acceptable accuracy. This might not be the case for  $E_{es}$  prediction. Nevertheless, the estimated  $E_{es}$  can be greatly improved when EF is used as an additional input in the prediction model. Following validation on in vivo invasive data, this approach may provide a promising potential in the prediction of aortic hemodynamics and LV contractility using unintrusive, readily available standard clinical measurements.

## Bibliography

- [1] T. K. Waddell, A. M. Dart, T. L. Medley, J. D. Cameron, and B. A. Kingwell, "Carotid pressure is a better predictor of coronary artery disease severity than brachial pressure," *Hypertension*, vol. 38, no. 4, pp. 927–931, 2001.
- [2] M. E. Safar, J. Blacher, B. Pannier, A. P. Guerin, S. J. Marchais, P.-M. Guyonvarc'h, and G. M. London, "Central pulse pressure and mortality in end-stage renal disease," *Hypertension*, vol. 39, no. 3, pp. 735–738, 2002.
- [3] H. Berkenstadt, N. Margalit, M. Hadani, Z. Friedman, E. Segal, Y. Villa, and A. Perel, "Stroke volume variation as a predictor of fluid responsiveness in patients undergoing brain surgery," *Anesthesia & Analgesia*, vol. 92, no. 4, pp. 984–989, 2001.
- [4] K. Sagawa, H. Suga, A. A. Shoukas, and K. M. Bakalar, "End-systolic pressure/volume ratio: a new index of ventricular contractility," *The American journal of cardiology*, vol. 40, no. 5, pp. 748–753, 1977.
- [5] A. Song-Tao, Q. Yan-Yan, and W. Li-Xia, "The severity of coronary artery disease evaluated by central systolic pressure and fractional diastolic pressure," *North American journal of medical sciences*, vol. 2, no. 5, p. 218, 2010.
- [6] N. Lees, M. Hamilton, and A. Rhodes, "Clinical review: goal-directed therapy in high risk surgical patients," *Critical Care*, vol. 13, no. 5, pp. 1–8, 2009.
- [7] R. A. Nishimura and B. A. Carabello, "Hemodynamics in the cardiac catheterization laboratory of the 21st century," *Circulation*, vol. 125, no. 17, pp. 2138–2150, 5 2012.
- [8] M. T. Ganter, J. A. Alhashemi, A. M. Al-Shabasy, U. M. Schmid, P. Schott, S. A. Shalabi, A. M. Badri, S. Hartnack, and C. K. Hofer, "Continuous cardiac output measurement by un-calibrated pulse wave analysis and pulmonary artery catheter in patients with septic shock," *Journal of clinical monitoring and computing*, vol. 30, no. 1, pp. 13–22, 2016.
- [9] H. Suga and K. Sagawa, "Instantaneous pressure-volume relationships and their ratio in the excised, supported canine left ventricle," *Circulation research*, vol. 35, no. 1, pp. 117–126, 1974.

## Bibliography

---

- [10] H. Suga, K. Sagawa, and A. A. Shoukas, "Load independence of the instantaneous pressure-volume ratio of the canine left ventricle and effects of epinephrine and heart rate on the ratio," *Circulation research*, vol. 32, no. 3, pp. 314–322, 1973.
- [11] K. Sagawa, "The end-systolic pressure-volume relation of the ventricle: definition, modifications and clinical use." *Circulation*, vol. 63, no. 6, pp. 1223–1227, 6 1981.
- [12] B. Williams, G. Mancia, W. Spiering, E. Agabiti Rosei, M. Azizi, M. Burnier, D. L. Clement, A. Coca, G. de Simone, A. Dominiczak, T. Kahan, F. Mahfoud, J. Redon, L. Ruilope, A. Zanchetti, M. Kerins, S. E. Kjeldsen, R. Kreutz, S. Laurent, G. Y. H. Lip, R. McManus, K. Narkiewicz, F. Ruschitzka, R. E. Schmieder, E. Shlyakhto, C. Tsioufis, V. Aboyans, I. Desormais, and ESC Scientific Document Group, "2018 ESC/ESH Guidelines for the management of arterial hypertension," *European Heart Journal*, vol. 39, no. 33, pp. 3021–3104, Sep. 2018.
- [13] T. G. Papaioannou, A. D. Protogerou, K. S. Stamatelopoulos, M. Vavuranakis, and C. Stefanadis, "Non-invasive methods and techniques for central blood pressure estimation: procedures, validation, reproducibility and limitations," *Current pharmaceutical design*, vol. 15, no. 3, pp. 245–253, 2009.
- [14] S. A. Hope, D. B. Tay, I. T. Meredith, and J. D. Cameron, "Use of arterial transfer functions for the derivation of aortic waveform characteristics," *Journal of Hypertension*, vol. 21, no. 7, pp. 1299–1305, Jul. 2003.
- [15] W. J. Stok, B. E. Westerhof, and J. M. Karemaker, "Changes in finger-aorta pressure transfer function during and after exercise," *Journal of Applied Physiology*, vol. 101, no. 4, pp. 1207–1214, Oct. 2006. [Online]. Available: <http://www.physiology.org/doi/10.1152/jappphysiol.00876.2005>
- [16] B. Fetics, E. Nevo, C.-H. Chen, and D. M. Kass, "Parametric model derivation of transfer function for noninvasive estimation of aortic pressure by radial tonometry," *IEEE Transactions on Biomedical Engineering*, vol. 46, pp. 698–706, 1999.
- [17] B. Williams, P. S. Lacy, P. Yan, C.-N. Hwee, C. Liang, and C.-M. Ting, "Development and validation of a novel method to derive central aortic systolic pressure from the radial pressure waveform using an N-point moving average method," *Journal of the American College of Cardiology*, vol. 57, no. 8, pp. 951–961, Feb. 2011. [Online]. Available: <http://www.sciencedirect.com/science/article/pii/S0735109710048035>
- [18] Y.-T. Shih, H.-M. Cheng, S.-H. Sung, W.-C. Hu, and C.-H. Chen, "Application of the N-point moving average method for brachial pressure waveform-derived estimation of central aortic systolic pressure," *Hypertension*, vol. 63, no. 4, pp. 865–870, Apr. 2014. [Online]. Available: <https://www.ahajournals.org/doi/10.1161/HYPERTENSIONAHA.113.02229>

- [19] A. A. Udy, M. Altukroni, P. Jarett, J. A. Roberts, and J. Lipman, "A comparison of pulse contour wave analysis and ultrasonic cardiac output monitoring in the critically ill," *Anaesthesia and Intensive Care*, vol. 40, no. 4, pp. 631–637, Jul. 2012. [Online]. Available: <https://research.monash.edu/en/publications/a-comparison-of-pulse-contour-wave-analysis-and-ultrasonic-cardia>
- [20] J. Jansen, J. Schreuder, J. Mulier, N. Smith, J. Settels, and K. Wesseling, "A comparison of cardiac output derived from the arterial pressure wave against thermodilution in cardiac surgery patients," *British Journal of Anaesthesia*, vol. 87, no. 2, pp. 212–222, Aug. 2001. [Online]. Available: <https://linkinghub.elsevier.com/retrieve/pii/S0007091217376250>
- [21] N. Langwieser, L. Pechtl, A. S. Meidert, A. Hapfelmeier, C. Bradaric, T. Ibrahim, K.-L. Laugwitz, R. M. Schmid, J. Y. Wagner, and B. Saugel, "Radial artery applanation tonometry for continuous noninvasive arterial blood pressure monitoring in the cardiac intensive care unit," *Clinical Research in Cardiology*, vol. 104, no. 6, pp. 518–524, Jun. 2015. [Online]. Available: <http://link.springer.com/10.1007/s00392-015-0816-5>
- [22] J. Christie, L. M. Sheldahl, F. E. Tristani, K. B. Sagar, M. J. Ptacin, and S. Wann, "Determination of stroke volume and cardiac output during exercise: comparison of two-dimensional and Doppler echocardiography, Fick oximetry, and thermodilution." *Circulation*, vol. 76, no. 3, pp. 539–547, Sep. 1987. [Online]. Available: <https://www.ahajournals.org/doi/10.1161/01.CIR.76.3.539>
- [23] G. Swamy and R. Mukkamala, "Estimation of the aortic pressure waveform and beat-to-beat relative cardiac output changes from multiple peripheral artery pressure waveforms," *IEEE transactions on bio-medical engineering*, vol. 55, no. 5, pp. 1521–1529, May 2008.
- [24] N. Fazeli and J.-O. Hahn, "Estimation of cardiac output and peripheral resistance using square-wave-approximated aortic flow signal," *Frontiers in Physiology*, vol. 3, Jul. 2012. [Online]. Available: <https://www.ncbi.nlm.nih.gov/pmc/articles/PMC3429069/>
- [25] N. J. Dabanloo, F. Aadaei, and A. M. Nasrabadi, "The performance of neural network in the estimation of cardiac output using arterial blood pressure waveforms." 2011, oCLC: 990720998. [Online]. Available: <http://ieeexplore.ieee.org/servlet/opac?punumber=6156579>
- [26] C. H. Chen, B. Fetics, E. Nevo, C. E. Rochitte, K. R. Chiou, P. A. Ding, M. Kawaguchi, and D. A. Kass, "Noninvasive single-beat determination of left ventricular end-systolic elastance in humans," *Journal of the American College of Cardiology*, vol. 38, no. 7, pp. 2028–2034, Dec. 2001.
- [27] T. Shishido, K. Hayashi, K. Shigemi, T. Sato, M. Sugimachi, and K. Sunagawa, "Single-beat estimation of end-systolic elastance using bilinearly approximated time-varying

## Bibliography

---

- elastance curve." *Circulation*, vol. 102, no. 16, pp. 1983–1989, Oct. 2000. [Online]. Available: <http://europepmc.org/abstract/MED/11034949>
- [28] Y. Shi, P. Lawford, and R. Hose, "Review of 0-d and 1-d models of blood flow in the cardiovascular system," *BioMedical Engineering OnLine*, vol. 10, no. 1, p. 33, 2011. [Online]. Available: <http://biomedical-engineering-online.biomedcentral.com/articles/10.1186/1475-925X-10-33>
- [29] P. Reymond, N. Westerhof, and N. Stergiopoulos, "Systolic hypertension mechanisms: effect of global and local proximal aorta stiffening on pulse pressure," *Annals of Biomedical Engineering*, vol. 40, no. 3, pp. 742–749, Mar. 2012.
- [30] M. H. G. Heusinkveld, T. Delhaas, J. Lumens, W. Huberts, B. Spronck, A. D. Hughes, and K. D. Reesink, "Augmentation index is not a proxy for wave reflection magnitude: mechanistic analysis using a computational model," *Journal of Applied Physiology*, vol. 127, no. 2, pp. 491–500, Aug. 2019. [Online]. Available: <https://www.physiology.org/doi/10.1152/jappphysiol.00769.2018>
- [31] A. Avolio, "Central aortic blood pressure and cardiovascular risk: a paradigm shift?" *Hypertension (Dallas, Tex.: 1979)*, vol. 51, no. 6, pp. 1470–1471, Jun. 2008.
- [32] P. Reymond, F. Merenda, F. Perren, D. Rüfenacht, and N. Stergiopoulos, "Validation of a one-dimensional model of the systemic arterial tree," *American Journal of Physiology. Heart and Circulatory Physiology*, vol. 297, no. 1, pp. H208–222, Jul. 2009.
- [33] A. Liaw and M. Wiener, "Classification and regression by randomForest," *R News*, vol. 2, no. 3, pp. 18–22, 2002. [Online]. Available: <http://CRAN.R-project.org/doc/Rnews/>
- [34] A. J. Smola and B. Schölkopf, "A tutorial on support vector regression," *Statistics and Computing*, vol. 14, no. 3, pp. 199–222, Aug. 2004. [Online]. Available: <http://link.springer.com/10.1023/B:STCO.0000035301.49549.88>
- [35] Robert Tibshirani, "Regression shrinkage and selection via the lasso," *J. R. Stat. Soc. Ser.*, vol. B, pp. 267–288, 1996.
- [36] A. Natekin and A. Knoll, "Gradient boosting machine: a tutorial," *Frontiers in Neurorobotics*, vol. 7, 2013. [Online]. Available: <http://journal.frontiersin.org/article/10.3389/fnbot.2013.00021/abstract>
- [37] V. Bikia, T. G. Papaioannou, S. Pagoulatou, G. Rovas, E. Oikonomou, G. Siasos, D. Tousoulis, and N. Stergiopoulos, "Noninvasive estimation of aortic hemodynamics and cardiac contractility using machine learning," *Scientific Reports*, vol. 10, no. 1, pp. 1–17, 2020.
- [38] N. Westerhof, J.-W. Lankhaar, and B. E. Westerhof, "The arterial windkessel," *Medical & Biological Engineering & Computing*, vol. 47, no. 2, pp. 131–141, Feb. 2009. [Online]. Available: <http://link.springer.com/10.1007/s11517-008-0359-2>

- [39] C.-H. Chen, M. Nakayama, E. Nevo, B. J. Fetters, W. Maughan, and D. A. Kass, "Coupled systolic-ventricular and vascular stiffening with age," *Journal of the American College of Cardiology*, vol. 32, no. 5, pp. 1221–1227, Nov. 1998. [Online]. Available: <https://linkinghub.elsevier.com/retrieve/pii/S073510979800374X>
- [40] P. H. Pak, W. L. Maughan, K. L. Baughman, R. S. Kieval, and D. A. Kass, "Mechanism of acute mechanical benefit from vdd pacing in hypertrophied heart: similarity of responses in hypertrophic cardiomyopathy and hypertensive heart disease," *Circulation*, vol. 98, no. 3, pp. 242–248, Jul. 1998. [Online]. Available: <https://www.ahajournals.org/doi/10.1161/01.CIR.98.3.242>
- [41] M. D. Feldman, P. H. Pak, C. C. Wu, H. L. Haber, C. M. Heesch, J. D. Bergin, E. R. Powers, T. D. Cowart, W. Johnson, A. M. Feldman, and D. A. Kass, "Acute cardiovascular effects of OPC-18790 in patients with congestive heart failure: time- and dose-dependence analysis based on pressure-volume relations," *Circulation*, vol. 93, no. 3, pp. 474–483, Feb. 1996. [Online]. Available: <https://www.ahajournals.org/doi/10.1161/01.CIR.93.3.474>
- [42] H. Senzaki, C.-H. Chen, and D. A. Kass, "Single-beat estimation of end-systolic pressure-volume relation in humans: a new method with the potential for noninvasive application," *Circulation*, vol. 94, no. 10, pp. 2497–2506, Nov. 1996. [Online]. Available: <https://www.ahajournals.org/doi/10.1161/01.CIR.94.10.2497>
- [43] M. R. Starling, R. A. Walsh, L. J. Dell'Italia, G. B. Mancini, J. C. Lasher, and J. L. Lancaster, "The relationship of various measures of end-systole to left ventricular maximum time-varying elastance in man." *Circulation*, vol. 76, no. 1, pp. 32–43, Jul. 1987. [Online]. Available: <https://www.ahajournals.org/doi/10.1161/01.CIR.76.1.32>
- [44] A. Wolak, H. Gransar, L. E. J. Thomson, J. D. Friedman, R. Hachamovitch, A. Gutstein, L. J. Shaw, D. Polk, N. D. Wong, R. Saouaf, S. W. Hayes, A. Rozanski, P. J. Slomka, G. Germano, and D. S. Berman, "Aortic size assessment by noncontrast cardiac computed tomography: normal limits by age, gender, and body surface area," *JACC. Cardiovascular imaging*, vol. 1, no. 2, pp. 200–209, Mar. 2008.
- [45] R. B. Devereux, G. de Simone, D. K. Arnett, L. G. Best, E. Boerwinkle, B. V. Howard, D. Kitzman, E. T. Lee, T. H. Mosley, A. Weder, and M. J. Roman, "Normal limits in relation to age, body size and gender of two-dimensional echocardiographic aortic root dimensions in persons  $\geq 15$  years of age," *The American Journal of Cardiology*, vol. 110, no. 8, pp. 1189–1194, Oct. 2012. [Online]. Available: <https://linkinghub.elsevier.com/retrieve/pii/S0002914912015342>
- [46] Z. Lu and R. Mukkamala, "Continuous cardiac output monitoring in humans by invasive and noninvasive peripheral blood pressure waveform analysis," *Journal of Applied Physiology*, vol. 101, no. 2, pp. 598–608, Aug. 2006. [Online]. Available: <https://www.physiology.org/doi/10.1152/jappphysiol.01488.2005>

## Bibliography

---

- [47] G. Langewouters, *Visco-elasticity of the human aorta in vitro in relation to pressure and age (Ph.D. thesis)*. Amsterdam: Free University of Amsterdam: Krips Repro, 1982. [Online]. Available: <https://books.google.gr/books?id=qvSrHAAACAAJ>
- [48] P. Segers et al., “Three- and four-element Windkessel models: assessment of their fitting performance in a large cohort of healthy middle-aged individuals,” *Proceedings of the Institution of Mechanical Engineers, Part H: Journal of Engineering in Medicine*, 2008. [Online]. Available: <https://www.ncbi.nlm.nih.gov/pubmed/18595354>
- [49] V. Bikia, S. Pagoulatou, B. Trachet, D. Soulis, A. D. Protogerou, T. G. Papaioannou, and N. Stergiopoulos, “Noninvasive cardiac output and central systolic pressure from cuff-pressure and pulse wave velocity,” *IEEE Journal of Biomedical and Health Informatics*, vol. 24, no. 7, pp. 1968–1981, Jul. 2020. [Online]. Available: <https://ieeexplore.ieee.org/document/8918060/>
- [50] O. Vardoulis, T. G. Papaioannou, and N. Stergiopoulos, “Validation of a novel and existing algorithms for the estimation of pulse transit time: advancing the accuracy in pulse wave velocity measurement,” *American Journal of Physiology-Heart and Circulatory Physiology*, vol. 304, no. 11, pp. H1558–H1567, Jun. 2013. [Online]. Available: <http://www.physiology.org/doi/10.1152/ajpheart.00963.2012>
- [51] J. Liu, H.-M. Cheng, C.-H. Chen, S.-H. Sung, J.-O. Hahn, and R. Mukkamala, “Patient-specific oscillometric blood pressure measurement: validation for accuracy and repeatability,” *IEEE journal of translational engineering in health and medicine*, vol. 5, p. 1900110, 2017.
- [52] T. G. Papaioannou, E. Oikonomou, G. Lazaros, E. Christoforatu, G. Vogiatzi, S. Tsalamandris, C. Chasikidis, A. Kalambogias, T. Mavratzas, E. Stofa, V.-C. Mystakidi, G. Latsios, S. Deftereos, and D. Tousoulis, “Arterial stiffness and subclinical aortic damage of reclassified subjects as stage 1 hypertension according to the new 2017 ACC/AHA blood pressure guidelines,” *VASA. Zeitschrift fur Gefasskrankheiten*, vol. 48, no. 3, pp. 236–243, May 2019.
- [53] D. Tousoulis, P. Fountoulakis, E. Oikonomou, C. Antoniadis, G. Siasos, S. Tsalamandris, G. Georgiopoulos, Z. Pallantza, E. Pavlou, A. Milliou, M. N. Assimakopoulos, N. Barm-paresos, I. Giannarakis, P. Siamata, and J. C. Kaski, “Acute exposure to diesel affects inflammation and vascular function,” *European Journal of Preventive Cardiology*, p. 2047487319898020, Jan. 2020.
- [54] T. G. Papaioannou, T. D. Karageorgopoulou, T. N. Sergeantanis, A. D. Protogerou, T. Psaltopoulou, J. E. Sharman, T. Weber, J. Blacher, S. S. Daskalopoulou, S. Wassertheurer, A. W. Khir, C. Vlachopoulos, N. Stergiopoulos, C. Stefanadis, W. W. Nichols, and D. Tousoulis, “Accuracy of commercial devices and methods for noninvasive estimation of aortic systolic blood pressure: a systematic review and meta-analysis of invasive validation studies,” *Journal of Hypertension*, vol. 34, no. 7, pp. 1237–1248, 2016.

- [55] N. Ioakeimidis, E. Emmanouil, D. Terentes-Printzios, I. Dima, K. Aznaouridis, D. Tousoulis, and C. Vlachopoulos, "Acute effect of heat-not-burn versus standard cigarette smoking on arterial stiffness and wave reflections in young smokers," *European Journal of Preventive Cardiology*, p. 2047487320918365, Apr. 2020.
- [56] M. Karamanoglu, M. F. O'Rourke, A. P. Avolio, and R. P. Kelly, "An analysis of the relationship between central aortic and peripheral upper limb pressure waves in man," *European Heart Journal*, vol. 14, no. 2, pp. 160–167, Feb. 1993.
- [57] A. Siebenhofer, C. Kemp, A. Sutton, and B. Williams, "The reproducibility of central aortic blood pressure measurements in healthy subjects using applanation tonometry and sphygmocardiography," *Journal of human hypertension*, vol. 13, no. 9, pp. 625–629, 1999.
- [58] T.-T. Wong, "Performance evaluation of classification algorithms by k-fold and leave-one-out cross validation," *Pattern Recognition*, vol. 48, no. 9, pp. 2839–2846, Sep. 2015. [Online]. Available: <https://linkinghub.elsevier.com/retrieve/pii/S0031320315000989>
- [59] F. Pedregosa, G. Varoquaux, A. Gramfort, V. Michel, B. Thirion, O. Grisel, M. Blondel, P. Prettenhofer, R. Weiss, V. Dubourg, J. Vanderplas, A. Passos, D. Cournapeau, M. Brucher, M. Perrot, and E. Duchesnay, "Scikit-learn: machine learning in Python," vol. 12, pp. 2825–2830, 2011.
- [60] W. McKinney, "Data structures for statistical computing in Python," in *Proceedings of the 9th Python in Science Conference*, 2010, pp. 51–56, doi: 10.25080/Majora-92bf1922-00a.
- [61] T. E. Oliphant, "A guide to NumPy." Trelgol Publishing USA, 2006, vol. 1.
- [62] E. O'Brien, N. Atkins, G. Stergiou, N. Karpettas, G. Parati, R. Asmar, Y. Imai, J. Wang, T. Mengden, A. Shennan *et al.*, "European society of hypertension international protocol revision 2010 for the validation of blood pressure measuring devices in adults," *Blood pressure monitoring*, vol. 15, no. 1, pp. 23–38, 2010.
- [63] L. A. H. Critchley and J. A. J. H. Critchley, "A meta-analysis of studies using bias and precision statistics to compare cardiac output measurement techniques," *Journal of Clinical Monitoring and Computing*, vol. 15, no. 2, pp. 85–91, 1999. [Online]. Available: <http://link.springer.com/10.1023/A:1009982611386>
- [64] S. Seabold and J. Perktold, "statsmodels: econometric and statistical modeling with Python," 2010.
- [65] J. M. Bland and D. G. Altman, "Statistical methods for assessing agreement between two methods of clinical measurement," *Lancet (London, England)*, vol. 1, no. 8476, pp. 307–310, Feb. 1986.



## Bibliography

---

- [66] L. A. H. Critchley, L. Huang, and J. Zhang, "Continuous cardiac output monitoring: what do validation studies tell us?" *Current Anesthesiology Reports*, vol. 4, no. 3, pp. 242–250, Sep. 2014. [Online]. Available: <http://link.springer.com/10.1007/s40140-014-0062-9>
- [67] T. Nishikawa and S. Dohi, "Errors in the measurement of cardiac output by thermodilution," *Canadian Journal of Anaesthesia*, vol. 40, no. 2, pp. 142–153, Feb. 1993. [Online]. Available: <http://link.springer.com/10.1007/BF03011312>
- [68] A. Nitenberg, I. Antony, and A. Loiseau, "Left ventricular contractile performance, ventriculoarterial coupling, and left ventricular efficiency in hypertensive patients with left ventricular hypertrophy," *American Journal of Hypertension*, vol. 11, no. 10, pp. 1188–1198, Oct. 1998. [Online]. Available: [https://academic.oup.com/ajh/article-lookup/doi/10.1016/S0895-7061\(98\)00131-9](https://academic.oup.com/ajh/article-lookup/doi/10.1016/S0895-7061(98)00131-9)
- [69] Z. Popović, M. Mirić, S. Gradinac, A. N. Nešković, M. Bojić, and A. D. Popović, "Partial left ventriculectomy improves left ventricular end systolic elastance in patients with idiopathic dilated cardiomyopathy," *Heart*, vol. 83, no. 3, pp. 316–319, Mar. 2000. [Online]. Available: <http://heart.bmj.com/cgi/doi/10.1136/heart.83.3.316>
- [70] T. G. Dietterich, "Ensemble methods in machine learning," in *Multiple Classifier Systems*, G. Goos, J. Hartmanis, and J. van Leeuwen, Eds. Berlin, Heidelberg: Springer Berlin Heidelberg, 2000, vol. 1857, pp. 1–15, series Title: Lecture Notes in Computer Science. [Online]. Available: [http://link.springer.com/10.1007/3-540-45014-9\\_1](http://link.springer.com/10.1007/3-540-45014-9_1)
- [71] H. J. Joo, S.-A. Cho, J.-Y. Cho, J. H. Park, S. J. Hong, C. W. Yu, and D.-S. Lim, "The relationship between pulse wave velocity and coronary artery stenosis and percutaneous coronary intervention: a retrospective observational study," *BMC Cardiovascular Disorders*, vol. 17, no. 1, Dec. 2017. [Online]. Available: <http://bmccardiovascdisord.biomedcentral.com/articles/10.1186/s12872-017-0476-7>
- [72] M. L. Muiesan, M. Salvetti, A. Paini, C. Monteduro, C. A. Rosei, C. Aggiusti, E. Belotti, F. Bertacchini, G. Galbassini, D. Stassaldi, M. Castellano, and E. A. Rosei, "Pulse wave velocity and cardiovascular risk stratification in a general population: the Vobarno study," *Journal of Hypertension*, vol. 28, no. 9, pp. 1935–1943, Sep. 2010.
- [73] A. R. Khoshdel, S. L. Carney, B. R. Nair, and A. Gillies, "Better management of cardiovascular diseases by pulse wave velocity: combining clinical practice with clinical research using evidence-based medicine," *Clinical Medicine and Research*, vol. 5, no. 1, pp. 45–52, Mar. 2007. [Online]. Available: <https://www.ncbi.nlm.nih.gov/pmc/articles/PMC1855337/>
- [74] M. I. Monge García, Z. Jian, J. J. Settels, C. Hunley, M. Cecconi, F. Hatib, and M. R. Pinsky, "Determinants of left ventricular ejection fraction and a novel method to improve its assessment of myocardial contractility," *Annals*

- of Intensive Care*, vol. 9, no. 1, p. 48, Dec. 2019. [Online]. Available: <https://annalsofintensivecare.springeropen.com/articles/10.1186/s13613-019-0526-7>
- [75] H. Xiao, A. Qasem, M. Butlin, and A. Avolio, “Estimation of aortic systolic blood pressure from radial systolic and diastolic blood pressures alone using artificial neural networks,” *Journal of Hypertension*, vol. 35, no. 8, pp. 1577–1585, Aug. 2017.
- [76] Z. Ghasemi, J. C. Lee, C.-S. Kim, H.-M. Cheng, S.-H. Sung, C.-H. Chen, R. Mukkamala, and J.-O. Hahn, “Estimation of cardiovascular risk predictors from non-invasively measured diametric pulse volume waveforms via multiple measurement information fusion,” *Scientific Reports*, vol. 8, no. 1, Dec. 2018. [Online]. Available: <http://www.nature.com/articles/s41598-018-28604-6>
- [77] F. Antonini-Canterin, S. Carerj, V. Di Bello, G. Di Salvo, S. La Carrubba, O. Vriza, D. Pavan, A. Balbarini, G. L. Nicolosi, and On behalf of the Research Group of the Italian Society of Cardiovascular Echography (SIEC), “Arterial stiffness and ventricular stiffness: a couple of diseases or a coupling disease? A review from the cardiologist’s point of view,” *European Journal of Echocardiography*, vol. 10, no. 1, pp. 36–43, Jan. 2009. [Online]. Available: <https://academic.oup.com/ehjcard/article-lookup/doi/10.1093/ejehocard/jen236>
- [78] J. E. Otterstad, “Measuring left ventricular volume and ejection fraction with the biplane Simpson’s method,” *Heart*, vol. 88, no. 6, pp. 559–560, Dec. 2002. [Online]. Available: <http://heart.bmj.com/cgi/doi/10.1136/heart.88.6.559>
- [79] R. Simpson, D. Bromage, L. Dancy, A. McDiarmid, M. Monaghan, T. McDonagh, and D. Sado, “Comparing echocardiography and cardiac magnetic resonance measures of ejection fraction: implications for HFMR research,” in *British Cardiovascular Imaging Meeting 2018*. BMJ Publishing Group Ltd and British Cardiovascular Society, May 2018, pp. A3.1–A3. [Online]. Available: <http://heart.bmj.com/lookup/doi/10.1136/heartjnl-2018-BCVI.6>
- [80] P. Reant, M. Dijos, E. Donal, A. Mignot, P. Ritter, P. Bordachar, P. Dos Santos, C. Leclercq, R. Roudaut, G. Habib, and S. Lafitte, “Systolic time intervals as simple echocardiographic parameters of left ventricular systolic performance: correlation with ejection fraction and longitudinal two-dimensional strain,” *European Journal of Echocardiography*, vol. 11, no. 10, pp. 834–844, Dec. 2010. [Online]. Available: <https://academic.oup.com/ehjcard/article-lookup/doi/10.1093/ejehocard/jeq084>
- [81] J. P. Howard, C. M. Cook, T. P. van de Hoef, M. Meuwissen, G. A. de Waard, M. A. van Lavieren, M. Echavarría-Pinto, I. Danad, J. J. Piek, M. Götzberg, R. K. Al-Lamee, S. Sen, S. S. Nijjer, H. Seligman, N. van Royen, P. Knaapen, J. Escaned, D. P. Francis, R. Petraco, and J. E. Davies, “Artificial intelligence for aortic pressure waveform analysis during coronary angiography,” *JACC: Cardiovascular*

## Bibliography

---

- Interventions*, vol. 12, no. 20, pp. 2093–2101, Oct. 2019. [Online]. Available: <https://linkinghub.elsevier.com/retrieve/pii/S1936879819314219>
- [82] J. M. J. Huttunen, L. Kärkkäinen, and H. Lindholm, “Pulse transit time estimation of aortic pulse wave velocity and blood pressure using machine learning and simulated training data,” *PLOS Computational Biology*, vol. 15, no. 8, p. e1007259, Aug. 2019. [Online]. Available: <http://dx.plos.org/10.1371/journal.pcbi.1007259>
- [83] N. Stergiopoulos, B. E. Westerhof, and N. Westerhof, “Physical basis of pressure transfer from periphery to aorta: a model-based study,” *American Journal of Physiology-Heart and Circulatory Physiology*, vol. 274, no. 4, pp. H1386–H1392, Apr. 1998. [Online]. Available: <https://www.physiology.org/doi/10.1152/ajpheart.1998.274.4.H1386>
- [84] B. Trachet, P. Reymond, J. Kips, A. Swillens, M. De Buyzere, B. Suys, N. Stergiopoulos, and P. Segers, “Numerical validation of a new method to assess aortic pulse wave velocity from a single recording of a brachial artery waveform with an occluding cuff,” *Annals of Biomedical Engineering*, vol. 38, no. 3, pp. 876–888, Mar. 2010. [Online]. Available: <http://link.springer.com/10.1007/s10439-010-9945-1>
- [85] T. G. Papaioannou, O. Vardoulis, and N. Stergiopoulos, “The “systolic volume balance” method for the noninvasive estimation of cardiac output based on pressure wave analysis,” *American Journal of Physiology-Heart and Circulatory Physiology*, vol. 302, no. 10, pp. H2064–H2073, May 2012. [Online]. Available: <https://www.physiology.org/doi/10.1152/ajpheart.00052.2012>
- [86] J. M. Huttunen, L. Kärkkäinen, M. Honkala, and H. Lindholm, “Deep learning for prediction of cardiac indices from photoplethysmographic waveform: a virtual database approach,” *International Journal for Numerical Methods in Biomedical Engineering*, vol. 36, no. 3, Mar. 2020. [Online]. Available: <https://onlinelibrary.wiley.com/doi/abs/10.1002/cnm.3303>
- [87] M. Willemet, S. Vennin, and J. Alastruey, “Computational assessment of hemodynamics-based diagnostic tools using a database of virtual subjects: application to three case studies,” *Journal of Biomechanics*, vol. 49, no. 16, pp. 3908–3914, Dec. 2016. [Online]. Available: <https://linkinghub.elsevier.com/retrieve/pii/S0021929016311551>
- [88] S. Vennin, Y. Li, M. Willemet, H. Fok, H. Gu, P. Charlton, J. Alastruey, and P. Chowienczyk, “Identifying hemodynamic determinants of pulse pressure: a combined numerical and physiological approach,” *Hypertension*, vol. 70, no. 6, pp. 1176–1182, Dec. 2017. [Online]. Available: <https://www.ahajournals.org/doi/10.1161/HYPERTENSIONAHA.117.09706>

## Chapter 5

---

# Artificial intelligence-based estimation of end-systolic elastance from arm pressure and systolic timing intervals

Vasiliki Bikia<sup>1</sup>, Dionysios Adamopoulos<sup>2</sup>, Georgios Rovas<sup>1</sup>, Stamatia Pagoulatou<sup>1</sup>, Nikolaos Stergiopoulos<sup>1</sup>

<sup>1</sup> *Institute of Bioengineering, École Polytechnique Fédérale de Lausanne, Switzerland*

<sup>2</sup> *Cardiology Department, Geneva University Hospitals, Geneva, Switzerland*

Published in *Frontiers in Artificial Intelligence*, 2021.

### Abstract

Left ventricular end-systolic elastance ( $E_{es}$ ) is a major determinant of cardiac systolic function and ventricular-arterial interaction. Previous methods for the  $E_{es}$  estimation require the use of the echocardiographic ejection fraction (EF). However, given that EF expresses the stroke volume as a fraction of end-diastolic volume (EDV), accurate interpretation of EF is attainable only with the additional measurement of EDV. Hence, there is still a need for a simple, reliable, non-invasive method to estimate  $E_{es}$ . This study proposes a novel artificial intelligence-based approach to estimate  $E_{es}$  using the information embedded in clinically relevant systolic time intervals, namely the pre-ejection period (PEP) and ejection time (ET). We developed a training/testing scheme using virtual subjects ( $n = 4,645$ ) from a previously validated *in silico* model. Extreme Gradient Boosting regressor was employed to model  $E_{es}$  using as inputs arm cuff pressure, PEP, and ET. Results showed that  $E_{es}$  can be predicted with high accuracy achieving a normalized RMSE equal to 9.15 % ( $r = 0.92$ ) for a wide range of  $E_{es}$  values from 1.2 to 4.5 mmHg/mL. The proposed model was found to be less sensitive to measurement errors ( $\pm 10$  % to 30 % of the actual value) in blood pressure, presenting

## **Chapter 5. Artificial intelligence-based estimation of end-systolic elastance from arm pressure and systolic timing intervals**

---

low test errors for the different levels of noise (RMSE did not exceed 0.32 mmHg/mL). In contrast, high sensitivity was reported for measurement errors in the systolic timing features. It was demonstrated that  $E_{es}$  can be reliably estimated from the traditional arm pressure and echocardiographic PEP and ET. This approach constitutes a step towards the development of an easy and clinically applicable method for assessing left ventricular systolic function.

## 5.1 Introduction

The concept of end-systolic elastance ( $E_{es}$ ), first introduced by [1], has become widely accepted. The  $E_{es}$ , i.e. the slope of the end-systolic pressure-volume relationship (ESPVR), constitutes a pivotal determinant of left ventricular (LV) systolic performance and is now considered an established index of contractility [2; 1; 3]. Assessment of  $E_{es}$  is of high importance in physiological studies and clinical practice. The effective matching between  $E_{es}$  and vascular load leads to optimal mechanical function. Age-related arterial stiffening [4] and hypertension [5] are related to the stiffening of the left ventricle, which is accompanied by an increased value of  $E_{es}$ . It has also been shown that antihypertensive treatment reduces  $E_{es}$  and enhances arterial-ventricular coupling [6]. Furthermore, the intercept of the ESPVR has been linked with prognosis in chronic heart failure [7]. Derivation of  $E_{es}$  requires the measurement of multiple invasive pressure-volume (P-V) loops under various loading conditions which limits its use in the routine clinical setting. In an attempt to address this limitation, research has been directed towards the development of methods for deriving  $E_{es}$  from easily obtained non-invasive single-beat measurements [8; 9; 10].

In our previous work [11], we demonstrated that  $E_{es}$  could be accurately determined using brachial systolic (brSBP) and diastolic blood pressure (brDBP), heart rate (HR), and ejection fraction (EF). The importance of EF on obtaining an accurate  $E_{es}$  estimation has been also indicated by other published methods [8; 9]. Nevertheless, accurate interpretation of EF renders essential the additional knowledge of physical determinants of myocardial contraction, namely the preload and afterload [12; 13]. The question that arises is whether  $E_{es}$  could be derived in a faster and more optimized way while reducing the complexity of the required measurements. Our primary hypothesis is that EF information could be replaced by other cardiac functional parameters, e.g. electrical or acoustic signals of cardiac events, that are related to the LV contractility in a direct or indirect manner.

Previous studies have highlighted the relevance of the timing of cardiac events in assessing the contractile state of the heart [14; 15; 16]. Pre-ejection period (PEP), i.e. the period between the onset of ventricular contraction and the aortic valve opening, serves as a major index of excitation-contraction coupling and may potentially be used to evaluate contractility [17; 18]. Concurrently, LV ejection time (ET), delimited by the opening and closing of the aortic valve, provides incremental prognostic information on cardiac performance [16; 19].

The objective of this study was to propose a novel method for the estimation of  $E_{es}$  using brSBP, brDBP, HR (via sphygmomanometry), and contractility-related timing parameters (via ECG and echocardiography), i.e. PEP and ET. The analysis relied on the use of machine learning regression analysis. To appraise our concept, we developed and evaluated this method using synthetic data generated from a previously validated *in silico* model [20]. An *in silico* model constitutes a computer program that allows for simulating human physiology,

cardiovascular mechanisms, and/or progression of disease. The utility of such models in medicine has essentially facilitated the visualization and prediction of physiological responses under different cardiovascular conditions. In the present study, the *in silico* model provides additional hemodynamic insights, which would be difficult to acquire *in vivo*, and is used for the preliminary assessment and design of the proposed methodology.

## 5.2 Methods & materials

### Data analysis

#### Study population

The population used in the present *in silico* study reflected a wide range of hemodynamical properties and states. Different hemodynamic cases ( $n = 4,645$ ) were simulated by modifying key cardiac and systemic parameters of a previously validated *in silico* model. The /one mathematical cardiovascular model, which was adopted in the current study, has been well described in [20]. The arterial tree model incorporates all the major arteries of the systemic circulation, as well as a detailed network representation of the cerebral circulation and the coronary circulation. The governing equations of the model are acquired by integrating the longitudinal momentum and continuity of the Navier-Stokes equations over the arterial cross-sectional area. By solving the governing equations with proper boundary conditions, flow and pressure are obtained in all arterial locations. The arterial segments of the model are considered as long tapered tubes, and their compliance is calculated by a nonlinear function of pressure and location as described by Langewouters [21]. Distal vessels are terminated with three-element Windkessel models [22] and intimal shear is modeled using the Witzig-Womersley theory [23]. At the proximal end, the arterial tree is coupled with a varying elastance model of the left ventricle [1; 3]. This time-varying elastance model (VEM) describes the relationship between the LV pressure,  $P_{LV}$ , and volume,  $V_{LV}$ , namely:

$$E(t) = \frac{P_{LV}(t)}{V_{LV}(t) - V_d} \quad (5.1)$$

where  $V_d$  indicates the dead volume of the left ventricle. Further details on the 1-D model can be found in the original publications [20; 24].

Concerning data generation,  $E_{es}$  varied in the range of 1–4.5 mmHg/mL so that the dataset includes cases with normal as well as dilated and hypertrophied hearts [25; 4; 26]. The filling pressure lied in the range of 7–23 mmHg according to [25; 4; 26]. The dead volume ( $V_d$ ) and the time of maximal elastance ( $t_{es}$ ) were modified according to [27; 20]. The HR values were within the range of 60 and 100 bpm. Total peripheral resistance and arterial compliance were altered to simulate a wide variety of arterial tree configurations [21; 28; 29]. In addition to the

modification of cardiac and systemic parameters, arterial geometry was changed with respect to arterial length and diameter for each segment to approximate different body types [44; 30]. The variation of the geometry was done in a uniform way for all arterial segments based on the variation of the aortic diameter. No topological variations (e.g. in the circle of Willis, number of branches from aortic arch, etc.) were considered. Nonuniform aortic stiffening was considered for the elderly and hypertensive virtual subjects following the approach described in Bikia et al. [11].

Given that the literature data are only provided in terms of mean and standard deviation or/and minimum and maximum values, we chose to perform random Gaussian sampling for varying the model's parameters. We filtered the generated data to ensure that they correspond to physiological human conditions. Particularly, the physiological validity of each subject was assessed by comparing the simulated brachial and aortic systolic blood pressure (SBP), DBP, MAP, and pulse pressure (PP) to the reference values reported in the previous studies by McEniery et al. [31] (normotensive cases) and [32] (hypertensive cases). A subject was discarded from the dataset if any of the blood pressure values was not satisfying the minimum and maximum thresholds indicated as  $\text{mean} \pm 2.807\text{SD}$  (99.5 % confidence intervals). Such an approach for generating synthetic data has been applied by a previous similar study [33].

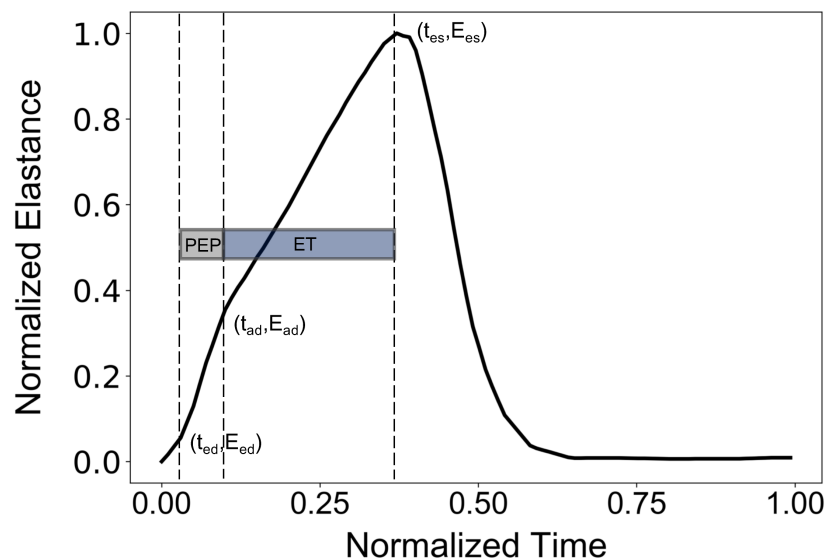


Figure 5.1 – Representative elastance curve  $E(t)$  with the indicated  $t_{ed}$  (early time point of isovolumic contraction),  $t_{ad}$  (ending time point of isovolumic contraction), and  $t_{es}$  (end-systolic time point). Adapted from [34].



## Chapter 5. Artificial intelligence-based estimation of end-systolic elastance from arm pressure and systolic timing intervals

---

Table 5.1 – List of the hyperparameters which were chosen to be optimized and their corresponding values.

Hyperparameter	Values
learning_rate	{0.005, 0.01, 0.05, 0.1, 0.15}
max_depth	{3, 5, 10}
n_estimators	{500, 750, 1,000, 1,250, 1,500, 1,750}

Table 5.2 – List of the selected hyperparameters for all the predictive models.

Model	Selected hyperparameters		
	learning_rate	max_depth	n_estimators
XGB <sub>Es</sub> M1	0.05	3	1,750
XGB <sub>Es</sub> M2	0.01	3	1,500
XGB <sub>Es</sub> M3	0.1	3	1,250
XGB <sub>Vd</sub> M1	0.01	3	500
XGB <sub>Vd</sub> M2	0.01	3	500
XGB <sub>Vd</sub> M3	0.1	3	1,750

### Features extraction

The relevant features were extracted from the flow and pressure waves produced by the in silico model. Synthetic brSBP, brDBP, brPP as well as HR data were calculated from the pressure wave at the left brachial artery.

Normally, PEP and ET could be extracted from the synchronous recordings of the aortic blood flow and the ECG signal. Here, the values of PEP and ET were derived following Shishido et al. [8], as illustrated in Figure 5.1. The reason that we employed this approach to calculate PEP and ET was the absence of a model of cardiac electrical activity that would indicate the starting position of Q-wave. PEP was calculated as the duration of the isovolumic contraction. The early isovolumic point ( $t_{ed}$ ) was defined as the time point when the time derivative of LV pressure is above 30 % of  $dP/dt_{max}$ . The end of the isovolumic contraction ( $t_{ad}$ ) was calculated from the first inflection point of the elastance curve at the upstroke area. End-systole ( $t_{es}$ ) was measured as the time point when  $dP/dt$  reaches 20 % of  $dP/dt_{min}$ . PEP and ET were obtained as  $t_{ad}-t_{ed}$  and  $t_{es}-t_{ad}$ , respectively.

### Regression analysis

The dataset was organized in pairs of inputs and outputs in order to be used for the training/testing process. The input features included the “measured” brSBP, brDBP, HR, PEP, and ET, as well as the  $t_{ed}$ ,  $t_{ad}$ , and  $t_{es}$ . The inclusion of the latter timing points was done to improve the descriptive cardiovascular profile of each subject and further enhance the regressor’s performance. Furthermore, a predictive model was developed including stroke volume

(SV) and ejection fraction (EF) as additional input features. Hence, three predictive models were developed and evaluated based on the different inputs' sets: i) one using brSBP, brDBP, HR, PEP, ET,  $t_{ed}$ ,  $t_{ad}$ , and  $t_{es}$  (M1), ii) a second one with only brSBP, brDBP, HR, PEP, and ET (M2), and finally, iii) a third model including all features from model M1 as well as SV and EF (M3). We additionally investigated the predictive capacity of our framework to estimate  $V_d$ . Nevertheless, the estimation of  $V_d$  was not considered as the main focus of the present study.

We used Extreme Gradient Boosting (XGB) [35] for the regression analysis. The 70 % of the dataset (3,251 subjects) was used for the training of the XGB model. The remaining 30 % (1,394 subjects) was kept for the testing. The regressor  $f(\cdot)$  was described as  $Y_{Ees} \approx f_{Ees}(X; \beta)$ , where  $\beta$  represents the unknown model parameters,  $X$ , the independent variables, and  $Y_{Ees}$ , the dependent variable. The unknown parameters of the model were optimized via an inner cross validation loop, i.e. hyperparameter tuning. Hyperparameter tuning was performed using GridSearch with ten-fold cross validation. The hyperparameters that were chosen to be optimized are reported in Table 5.1. The hyperparameters' values that are not reported in Table 5.1 were set to their default value. The selected hyperparameters' values for the six predictive models are also reported in Table 5.2. Consequently, the prediction accuracy for each regression model was evaluated on a subject level.

We assessed the importance of each input feature using two concepts, i.e. the feature importance scores returned by the XGB model, and the permutation feature importances. A major difference between the two concepts is that the feature importances from XGB are calculated based on the learning process through the training data, while the permutation feature importances are yielded from the estimations on a test set.

More specifically, the feature importance by XGB provides a score that indicates how useful and valuable each feature was in the construction of the boosted decision trees within the model. The hierarchical structure of a decision tree leads us to the final prediction by traversing through the nodes of the tree. Each node consists of a feature which is further split into more nodes as the tree develops vertically. The more times a feature is used to make key decisions with decision trees, the higher its relative importance. Formally, the feature importance score is calculated for a single decision tree by the amount that each feature split point improves the performance measure, weighted by the number of observations the node is responsible for. The feature importance scores are then averaged across all of the trees within the model. This importance is calculated explicitly for each feature and allows features to be ranked and compared to each other.

We additionally provide the permutation feature importances which are helpful to interpret the changes in model's performance when the information of a feature is discarded. The concept of permutation feature importances relies on measuring the importance of a feature by calculating the increase in the model's prediction error after permuting the feature. Permutation of a feature is achieved by shuffling the values of the feature on the test set. A

## **Chapter 5. Artificial intelligence-based estimation of end-systolic elastance from arm pressure and systolic timing intervals**

---

feature is considered as significant if shuffling its values increases the (trained) model error, demonstrating that the model relied on the feature for the prediction. A feature is unimportant if shuffling its values does not change the model error, showing that the model ignored the feature for the prediction. The concept of permutation feature importance was first introduced by Breiman [36]. Essentially, permutation feature importances express the increase in model error when the feature's information is destroyed. For calculating the permutation importances, we randomly shuffled the values of each feature and we computed the RMSE after the permutation. This was repeated 20 times and the mean and standard deviation of the increase in RMSE were reported.

Moreover, the accuracy of a machine learning regressor is largely dependent on the size of the initial training datasets. Thus, the investigation of how large a training dataset needs to be in order to build a reliable predictive model is imperative. To obtain this information the learning curve was computed. Learning curves allow for visualizing the effect of the number of data instances on the performance. The learning curve was fitted using the observed accuracy (in terms of RMSE) according to a given training sample size. The training size was modified from 1 to 98 % of the total number of subjects (50 samples of training size). The learning curve is presented in Figure 5.2. We observed that as the number of training data increases, the RMSE of testing decreases and starts saturating while approaching the 4,000 data instances. Given that it is not clear whether a steady state is utterly achieved (a state where no substantial improvement occurs by increasing the number of training data), we decided to include all the training dataset for performing the regression analysis. Hence, the model with the selected hyperparameters was fit to the entire training set ( $n = 3,251$ ), and the performance metrics reported in the Results' section correspond to the testing set ( $n = 1,394$ ). The training/testing pipeline was implemented using the Scikit-learn library [37] in a Python programming environment. The Pandas and NumPy packages were also used [38; 39].

### **Sensitivity to noise**

We assessed the sensitivity of our model to errors in the measurement of PEP and ET. In addition, sensitivity analysis was performed for errors in the blood pressure measurements (i.e. amplitude of brachial pressure waveform). The data were artificially corrupted using three levels of errors, i.e.  $\pm 10\%$ ,  $\pm 20\%$ , and  $\pm 30\%$  with respect to their actual value. Errors in measurements were simulated with a random distribution, i.e. for a noise level equal to  $\pm 20\%$ , the error of each measurement was randomly drawn from the range of  $[-20, 20]\%$ . The effect of erroneous inputs was evaluated and the model's performance was reported for the six experiments [3 noise levels x 2 sets of inputs (systolic timing intervals and blood pressure values)]. The experiments were performed using the hyperparameters which were selected from the M1 model (Table 5.2) which did not account for the noise.

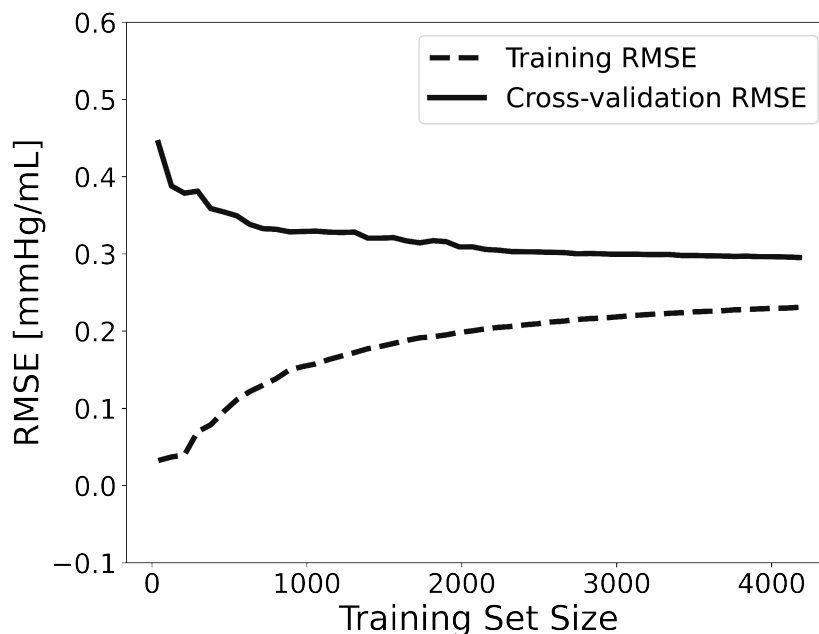


Figure 5.2 – Learning curve visualizing the effect of the number of data instances on the model’s performance. Adapted from [34].

### Statistical analysis

The statistical analysis was performed in Python (Python Software Foundation, Python Language Reference, version 3.6.8, Available at <http://www.python.org>). All values are presented as mean  $\pm$  SD. The agreement, bias, and precision between the model predictions and the real values were evaluated by using the Pearson’s correlation coefficient ( $r$ ), the mean absolute error (MAE), the normalized root mean square error (nRMSE), and the Bland-Altman analysis [40]. The computed nRMSE was based on the difference between the minimum and maximum values of the dependent variable ( $y$ ) and was computed as  $\text{RMSE}/(y_{\max} - y_{\min})$ . Linear least-squares regression was performed for the estimated and reference data. The slope and the intercept of the regression line were reported. Two-sided  $P$ -value for a hypothesis test whose null hypothesis is that the slope is zero, using Wald test with  $t$ -distribution of the test statistic, was calculated. A  $P$ -value below 0.05 was considered as statistically significant.

## 5.3 Results

Table 5.3 summarizes the cardiac and vascular characteristics of the 4,645 subjects included in this study.

## Chapter 5. Artificial intelligence-based estimation of end-systolic elastance from arm pressure and systolic timing intervals

---

Table 5.3 – Summary of the cardiovascular characteristics of the virtual study cohort (n = 4,645).

<b>Variable</b>	<b>mean±SD n = 4,645</b>
End-systolic elastance [mmHg/mL]	3.06±0.74
End-diastolic elastance [mmHg/mL]	0.13±0.04
Filling pressure [mmHg]	15.32±3.47
Heart rate [bpm]	79.61±8.27
Dead volume [mL]	22.68±14.07
Ejection fraction [%]	53.74±9.33
$t_{es}$ [ms]	355.09±26.24
$t_{ad}$ [ms]	65.75±18.46
$t_{ed}$ [ms]	13.25±1.02
Pre-ejection time [ms]	52.5±18.19
Ejection time [ms]	289.35±26.85
Stroke volume [mL]	78.7±21.62
Aortic systolic blood pressure [mmHg]	132.32±24.67
Aortic diastolic blood pressure [mmHg]	100.73±16.97
Aortic PP [mmHg]	31.59±13.47
Mean arterial pressure [mmHg]	115.4±19.92
Brachial systolic blood pressure [mmHg]	141.41±25.89
Brachial diastolic blood pressure [mmHg]	97.77±16.59
Brachial PP [mmHg]	43.64±16.61
PP amplification	1.41±0.10
Total peripheral resistance [mmHg.s/mL]	1.13±0.23
Total arterial compliance [mL/mmHg]	1.97±0.69
Aortic diameter [mm]	28.57±1.95
Height [cm]	175.00±25.00
PP amplification = Brachial PP/Aortic PP.	

Table 5.4 – Regression statistics between the model-predicted  $E_{es}$  and the reference  $E_{es}$ .

Model	Slope	Intercept [mmHg/mL]	$r$	$P$ -value	nRMSE [%]	MAE [mmHg/mL]
XGB $_{E_{es}}$ M1	0.83	0.53	0.92	<0.0001	8.54 %	0.22
XGB $_{E_{es}}$ M2	0.52	1.45	0.74	<0.0001	15.26 %	0.41
XGB $_{E_{es}}$ M3	0.88	0.38	0.95	<0.0001	7.32 %	0.19
Model	Slope	Intercept [mL]	$r$	$P$ -value	nRMSE [%]	MAE [mL]
XGB $_{V_d}$ M1	0.00	22.55	<0.1	0.79	25.79	11.92
XGB $_{V_d}$ M2	0.00	22.58	<0.1	0.79	25.79	11.91
XGB $_{V_d}$ M3	0.86	3.28	0.93	<0.0001	9.12	3.62

### Comparison between the estimated $E_{es}$ and the reference $E_{es}$

Table 5.4 displays the statistical comparisons between the non-invasive  $E_{es}$  estimates and the reference  $E_{es}$ . The Bland-Altman plot shows that the estimated  $E_{es}$  had low bias. The limits of agreement between the estimated and reference  $E_{es}$  (within which 95 % of errors are expected to lie) were found to be (-0.57, 0.60) mmHg/mL. The scatterplot and the Bland-Altman plots of the estimated  $E_{es}$  against the real  $E_{es}$  are presented in Figures 5.3, 5.4, and 5.5. Finally, standard error of estimate (SEE) was reported to be 0.15 mmHg/mL. The absolute difference between the non-invasive  $E_{es}$  estimates and the real  $E_{es}$  values was reported to be lower than 0.5 mmHg/mL in 91 % of the total cases for XGB. At large, the regressor performed adequately towards the accurate prediction of  $E_{es}$ .

The results for the  $V_d$  estimation are also reported in Table 5.4. For the XGB $_{V_d}$  M1 and XGB $_{V_d}$  M2 models, no agreement was achieved between the predictions and the reference data ( $r < 0.1$ ). Inclusion of the SV and EF led to improved accuracy, achieving a nRMSE equal to 9.12 % and a correlation of 0.93. Figure 5.6 illustrates the scatterplot and the Bland-Altman plot for the predicted and real  $V_d$  values only for the best-performing model (XGB $_{V_d}$  M3).

Table 5.5 presents the average permutation importances of the input features, sorted in descending order for predicting  $E_{es}$ . Following the concept of permutation,  $t_{ed}$ ,  $t_{es}$  and PEP yielded the highest increase in the prediction error on test data (increase in RMSE was equal or more than 0.46 mmHg/mL). The XGB-based feature importances are also given in Table 5.5. PEP had a critical contribution (0.440) followed by  $t_{ad}$  and  $t_{es}$  with 0.186 and 0.107, respectively.

### Sensitivity to noise

When the systolic time intervals, i.e. PEP and ET, were randomly overestimated or underestimated, the performance of the model gradually deteriorated. Corruption of the data with random noise gave a rise to the error between the predictions and reference values. The

Table 5.5 – Feature importances for the prediction of  $E_{es}$ .

<b>Feature</b>	<b>Permutation importance [mmHg/mL] mean±SD</b>	<b>Importance score by XGB</b>
$t_{ed}$	0.460±0.005	0.099
$t_{es}$	0.400±0.006	0.107
PEP	0.139±0.003	0.440
brDBP	0.032±0.001	0.073
ET	0.025±0.001	0.015
brSBP	0.022±0.001	0.030
HR	0.006±0.001	0.050
$t_{ad}$	0.001±0.000	0.186

performance of the model for the different levels of noise is presented in Table 5.6. Standard deviation of the RMSE values at the noise levels was  $\pm 0.11$  mmHg/mL. At the level of maximal noise ( $\pm 30\%$ ), RMSE reached the value of 0.55 mmHg/mL, while the Pearson's correlation coefficient substantially decreased at 0.68. The estimated  $E_{es}$  values were considerably influenced by noise corruption.

Errors in brachial blood pressure measurements impacted to a lesser extent the estimation of  $E_{es}$ . With increasing the magnitude of the introduced noise, we did not notice a pronounced variation in the RMSE after the noise level of 20 %, namely RMSEs varied by  $\pm 0.01$  mmHg/mL. When the noise level was  $\pm 30\%$ , RMSE found to be equal to 0.32 ( $r = 0.91$ ) for the XGB model. Overall, cardiac elastance values were minimally affected.

## 5.4 Discussion

In the present study, we found that  $E_{es}$  could be estimated non-invasively from arm cuff pressure and systolic time intervals following a machine learning approach. We developed and tested our method using synthetic data from a previously validated *in silico* model of cardiovascular dynamics. The study population corresponded to an extensive range of cardiac and arterial systemic conditions. The regression results showed that cuff pressure in conjunction with systolic time intervals (STIs) achieved a low test error and can capture the LV  $E_{es}$  value with sufficient accuracy. The present work is in line with previous efforts towards the non-invasive estimation of  $E_{es}$  using easily obtained single-beat non-invasive measurements.

In our previous study [41], we demonstrated that the non-invasive estimation of  $E_{es}$  can be achieved when arm cuff pressure, carotid-femoral pulse wave velocity (cfPWV), and EF are used as inputs to a regressor. Conventionally, EF is often used to assess LV systolic function and can be measured using different cardiac imaging techniques, including magnetic resonance imaging (MRI), the Simpson's method, speckle tracking strains, etc. However, these imaging

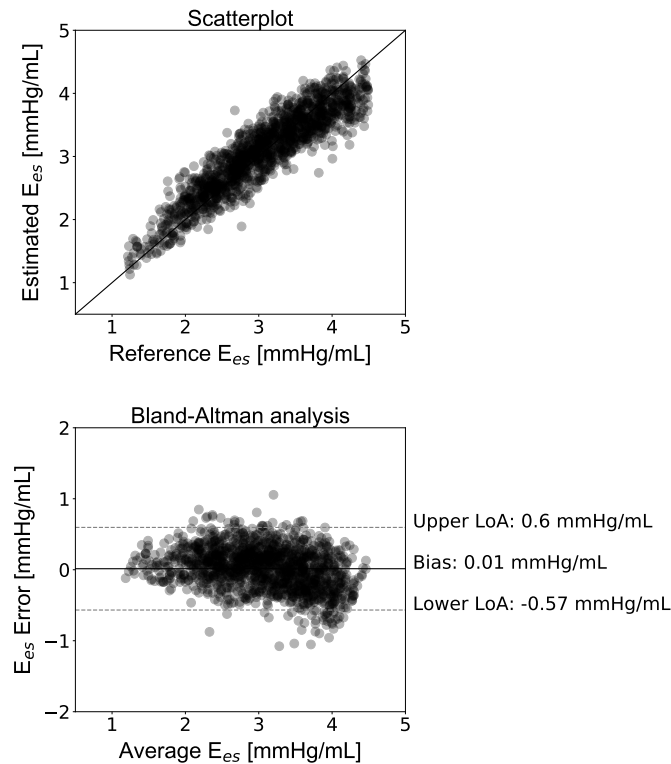


Figure 5.3 – Comparison between the estimated  $E_{es}$  values and the reference  $E_{es}$  for the  $XGB_{E_{es}}$  M1 model. Scatterplot and Bland–Altman plot between the values of  $E_{es}$  derived from the model and the real  $E_{es}$ . The solid line of the scatterplot represents equality. In Bland–Altman plot, limits of agreement (LoA), within which 95 % of errors are expected to lie, are defined by the two horizontal dashed lines. Adapted from [34].

modalities are tedious and require a highly trained technician. To facilitate the assessment of cardiac performance, several studies have focused on the use of STIs which can be conveniently obtained via Pulse Doppler echocardiography [14; 15; 42]. Motivated by this concept, we chose to reformulate the regression pipeline for the estimation of  $E_{es}$  and replace EF with simple systolic timing parameters. A strong argument reinforcing our methodology arrives from the fact that interpretation of EF is limited when preload and afterload are not known [12].

The XGB model achieved high accuracy in the estimated  $E_{es}$  with  $r = 0.92$ . In 91 % of the total cases, the average difference between the non-invasive  $E_{es}$  and the reference  $E_{es}$  was reported to be lower than 0.50 mmHg/mL. Given that, for a normal heart,  $E_{es}$  lies within the ranges of [1.5–3.5] mmHg/mL, while for dilated hearts and hypertrophied hearts is near 1 mmHg/mL and 4 mmHg/mL, respectively [4; 9], such an error should allow for reasonably accurate assessment of systolic function in normal and pathological hearts.

Furthermore, based on the learning curve (Figure 5.2), the training error was reported to be



## Chapter 5. Artificial intelligence-based estimation of end-systolic elastance from arm pressure and systolic timing intervals

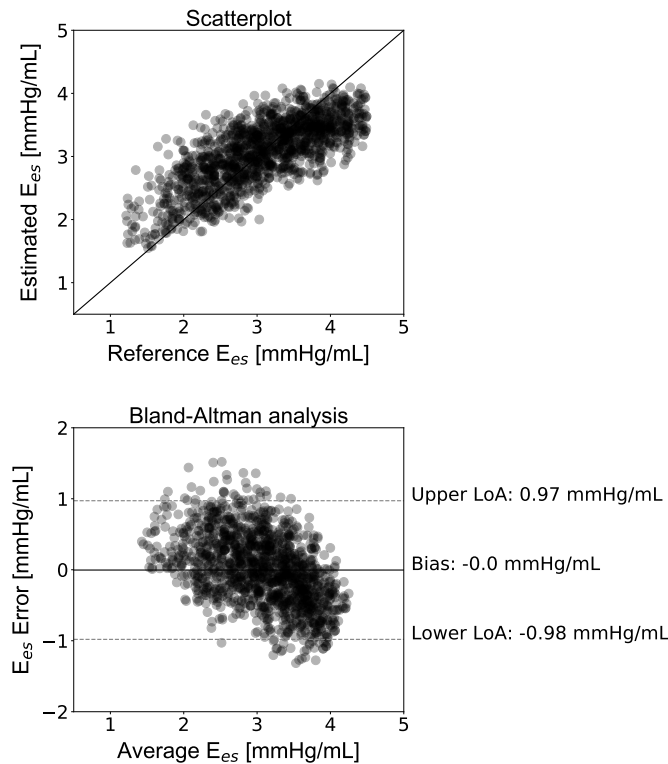


Figure 5.4 – Comparison between the estimated and the reference  $E_{es}$  data for the  $XGB_{E_{es}}$  M2 model. Scatterplot and Bland–Altman plot between the values of  $E_{es}$  derived from the model and the real  $E_{es}$ . The solid line of the scatterplot represents equality. In Bland–Altman plot, limits of agreement (LoA), within which 95 % of errors are expected to lie, are defined by the two horizontal dashed lines. Adapted from [34].

low, and, hence, the training data are fitted well by the estimated model (low bias). The small gap between the two curves indicated a low variance. The learning curve well predicted a low RMSE close to 0.29 mmHg/mL for the training data size equal to or larger than 4,000. Based on this learning curve, we can deduce that our particular predictive model needs a training dataset of 4,000 to reach an error of 0.29 mmHg/mL. These findings could be utilized as a starting reference point for future studies that develop similar estimators.

The individual time points, i.e.  $t_{ed}$  (early time point of isovolumic contraction),  $t_{ad}$  (ending time point of isovolumic contraction), and  $t_{es}$  (end-systolic time point), were incorporated in the input to enhance the performance of the model. In the spirit of completeness, we further investigated the change in the accuracy of the predictive model when the latter time points were not considered as input features. In that case, the XGB model predicted  $E_{es}$  achieving an RMSE equal to 0.50 mmHg/mL and a correlation coefficient of 0.74. The feature importances were re-ranked as follows: PEP: 0.555, brDBP: 0.154, brSBP: 0.103, HR: 0.101, and ET: 0.087. Given the deterioration in the accuracy, we chose to keep the aforementioned time points (given that they are available when PEP and ET are measured) in the input vector in order to

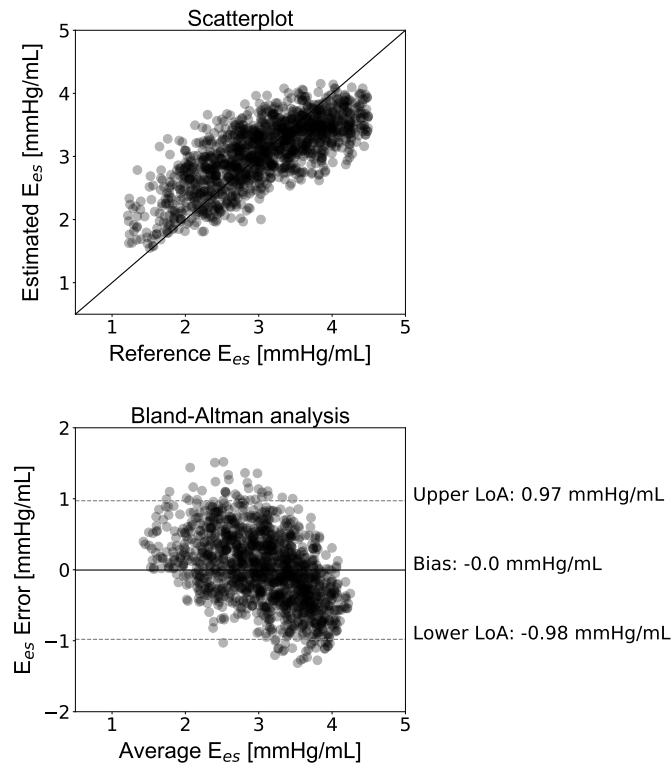


Figure 5.5 – Comparison between the estimated and the reference  $E_{es}$  data for the  $XGB_{E_{es}}$  M3 model. Scatterplot and Bland–Altman plot between the values of  $E_{es}$  derived from the model and the real  $E_{es}$ . The solid line of the scatterplot represents equality. In Bland–Altman plot, limits of agreement (LoA), within which 95 % of errors are expected to lie, are defined by the two horizontal dashed lines. Adapted from [34].

maximize our model’s performance.

In order to further evaluate the robustness of our models, we quantified the effect that measurement errors might have on the  $E_{es}$  estimates. Especially, we performed the regression analysis while introducing artificial noise to the STIs and the brachial pressure recordings. An erroneous measurement of the STIs appeared to have a greater impact on the  $E_{es}$  estimation compared to an error in the brachial blood pressure features. Overall, the sensitivity analysis on errors in the input features demonstrated that estimated  $E_{es}$  values were considerably affected by random errors in the systolic timing features (namely,  $t_{ed}$ ,  $t_{ad}$ ,  $t_{es}$ , PEP, and ET). In contrast, the overall regression performance was altered only slightly when random noise corrupted brSBP and brDBP without significantly affecting the accuracy of the estimated  $E_{es}$  values. This can be further explained if we consider the permutation feature importances for our model; the timing intervals and, in particular,  $t_{ed}$  and  $t_{es}$  held the first places in the ranking (RMSE would increase at least by 1.4 mmHg/mL after permutating one of those two features).

## Chapter 5. Artificial intelligence-based estimation of end-systolic elastance from arm pressure and systolic timing intervals

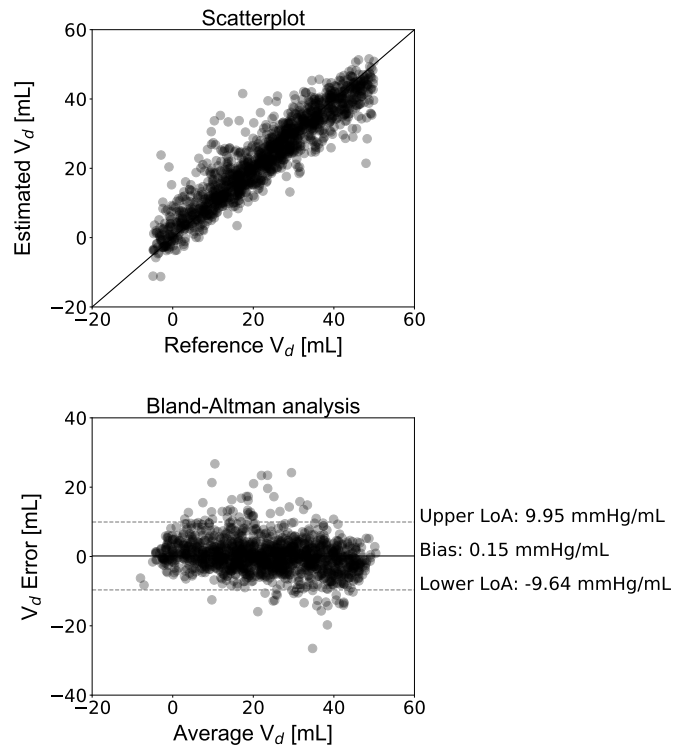


Figure 5.6 – Comparison between the estimated and the reference  $V_d$  data for the XGB $V_d$  M3 model. Scatterplot and Bland–Altman plot between the values of  $V_d$  derived from the model and the real  $V_d$ . The solid line of the scatterplot represents equality. In Bland–Altman plot, limits of agreement (LoA), within which 95 % of errors are expected to lie, are defined by the two horizontal dashed lines. Adapted from [34].

Based on the permutation feature importances, the time points  $t_{ed}$  and  $t_{es}$  were the most significant contributors to the precise estimation of  $E_{es}$ . If permutation of a feature leads to a predictive model with insufficient prediction capacity (high errors), then the information provided by this feature is significant and the corresponding feature is considered as important. The threshold for an error to indicate poor prediction is dependent on the problem under consideration. In the present study, the error threshold for a precise estimation was set to be lower than 0.50 mmHg/mL, and, therefore, all the features with permutation importances leading to errors higher than the threshold were considered as largely important. The discrepancies in the features' ranking between the two approaches for calculating the importance level can be explained by the fact that the one is based on the training process, while the other one relies on the predictions on the testing dataset. Moreover, the feature importance method by XGB favors features that have high cardinality. In our dataset, all PEP values were unique for all the 4,645 data instances, and this might encourage the algorithm to consider it as the most important feature. It is recommended that interpretation of the importances is done in a combinatorial manner, so that a more complete overview is provided using different insights and aspects. Yet, PEP had a critical contribution using both concepts. The high correlation

Table 5.6 – Regression statistics between the model-predicted  $E_{es}$  and the reference  $E_{es}$  when artificial noise is considered.

Model	Slope	Intercept [mmHg/mL]	$r$	$P$ -value	nRMSE [%]	MAE [mmHg/mL]
XGB $E_{es}$ M1 (noise-free)	0.82	0.57	0.92	<0.0001	9.15	0.24
XGB $E_{es}$ M1 ( $\pm 10\%$ noise in STIs)	0.72	0.87	0.84	<0.0001	12.51	0.33
XGB $E_{es}$ M1 ( $\pm 20\%$ noise in STIs)	0.59	1.26	0.74	<0.0001	15.26	0.40
XGB $E_{es}$ M1 ( $\pm 30\%$ noise in STIs)	0.54	1.40	0.68	<0.0001	16.78	0.44
XGB $E_{es}$ M1 ( $\pm 10\%$ noise in BP)	0.83	0.53	0.92	<0.0001	9.15	0.24
XGB $E_{es}$ M1 ( $\pm 20\%$ noise in BP)	0.81	0.58	0.91	<0.0001	9.46	0.24
XGB $E_{es}$ M1 ( $\pm 30\%$ noise in BP)	0.81	0.57	0.91	<0.0001	9.76	0.25

between PEP and LV function has been also demonstrated by previous studies [42]. Finally, the important contribution of brDBP (4<sup>th</sup> higher increase in error) can be explained by the fact that brDBP is strongly related to the mean arterial blood pressure, which indicates the pressure against which the heart pumps.

### Clinical application of the proposed method

Systolic time intervals can be easily and precisely measured in the clinical practice and may be used for detecting alterations in LV systolic function [16]. The correlation between these STIs measurements and conventional LV function parameters has been emphasized in numerous previous studies [42] paving the way to further explore the potential in using more complicated nonlinear machine learning approaches.

From a wider perspective, the incorporation of STIs values as features to approximate  $E_{es}$  has been a promising research direction. Several researchers have demonstrated the ability in acquiring these STIs measurements from more simplified modalities including electrocardiography (ECG), phonocardiography (PCG), or seismocardiography (SCG) [43; 44]. Such methods provided unobtrusive detection of cardiac time intervals and offer the potential to be integrated into wearable devices. Interestingly, PEP and ET could be very easily obtained using ECG and a precise electronic stethoscope. More specifically, the initiation of the PEP interval is placed at the initial point of the Q-wave (point 1, Figure 5.7). In addition, an electronic stethoscope able to capture the time intervals in the scale of milliseconds would allow us to determine the moment of the aortic valve closure (point 2, Figure 5). Now, if we set a new time

## Chapter 5. Artificial intelligence-based estimation of end-systolic elastance from arm pressure and systolic timing intervals

Proposed Framework on the Estimation of  $E_{es}$  through Exploitation of Simpler Measuring Modalities

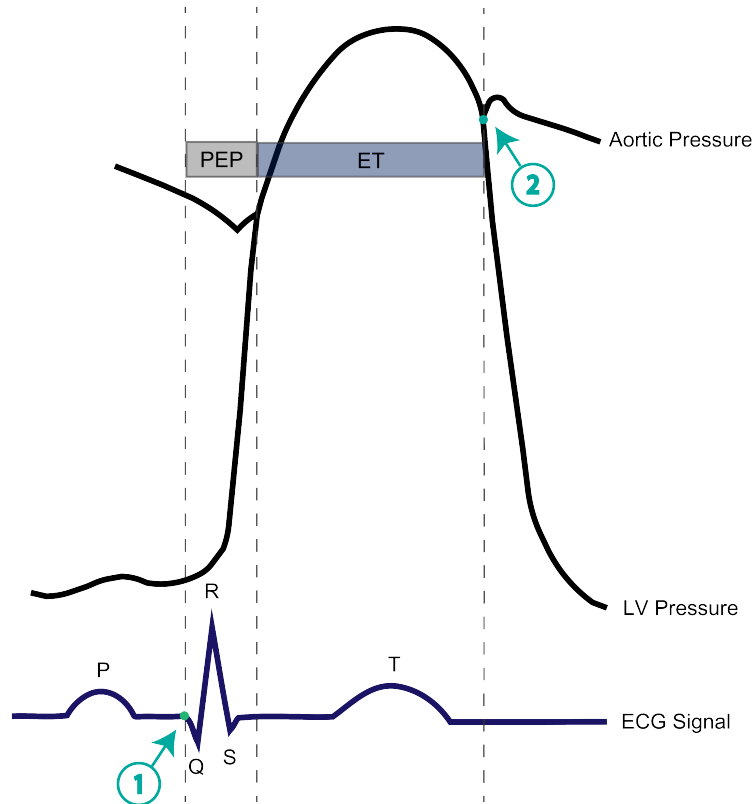


Figure 5.7 – Representation of the aortic pressure, the left ventricular pressure, the ECG including the timing components of pre-ejection period (PEP), ejection time (ET), and the newly introduced Q-aoClos interval. The Q-aoClos interval is the time period from the initial trace of Q-wave (point 1) (as measured via ECG) until the closure of the aortic valve (point 2) (as recorded via a phonographic device). Adapted from [34].

interval which is the sum of PEP and ET (Q-aoClos interval, Figure 5.7), we can measure the exact duration of the latter using ECG and stethoscope alone. The ECG signal could indicate the initiation of Q-wave, while phonocardiography would allow us to detect the closure of the aortic valve. To test this hypothesis, we performed the regression analysis using as inputs only the arm cuff pressure, the Q-aoClos interval, namely, the summation of PEP and ET, the time point at the beginning of Q-wave (time 1), and the time point at the closure of the aortic valve (point 2). Our results indicated that  $E_{es}$  could be effectively estimated achieving an nRMSE and Pearson's correlation coefficient equal to 10.37 % and 0.89, respectively, whereas limits of agreement were  $\pm 0.67$  mmHg/mL and bias was zero. In that case, the selected hyperparameters were learning\_rate = 0.05, max\_depth = 3, n\_estimators = 1,250. This finding creates a rather promising proof-of-evidence towards the non-invasive estimation of  $E_{es}$  reducing the complexity and the cost of the technique for acquiring the necessary measurements. The

proposed methodological concept could be easily integrated in a medical device such as a smart stethoscope.

### Prior work on the $E_{es}$ estimation

Several methods have been proposed for the  $E_{es}$  estimation using non-invasive single-beat measurements. First, Chen et al. [9] proposed a simple equation for estimating  $E_{es}$  from arm cuff pressure, SV, and EF. Their proposed method incorporates an estimated normalized ventricular elastance at arterial end-diastole which was derived from regression on previously recorded studies. The authors achieved accurate estimations with differences between estimated and real values equal to  $0.43 \pm 0.50$  mmHg/mL and a high correlation of 0.91. Here, we decided, however, to simplify our method by replacing the measurements of the stroke volume and ejection fraction with the more accurately obtained pre-ejection period and ejection time intervals. In addition, the calculation of EF as assessed by echocardiography can be rather sensitive to errors and derived approximately. Removal of EF from our calculation may reduce the error imposed by such an approximation.

Moreover, Shishido et al. [8] suggested the estimation of  $E_{es}$  from pressure values, systolic time intervals, and stroke volume. Their analysis relies on the approximation of the time-varying elastance curve by two linear functions corresponding to the isovolumic contraction phase and the ejection phase. The slope ratio of these functions is calculated and used for estimating  $E_{es}$  by the employment of a simple equation. Their model provided reliable predictions of  $E_{es}$  in anesthetized dogs with  $r = 0.93$  and  $SEE = 2.10$  mmHg/mL. In accordance with our findings, this methodology evidences the utility of systolic time intervals on the estimation of  $E_{es}$ . A limitation of their study pertains to the fact that the authors developed their model using the same population which was used for the model's testing rather than an independent group.

Recently, Pagoulatou et al. [10] proposed and validated a novel method for non-invasively estimating  $E_{es}$  based on sphygmomanometric pressure measurements and standard echocardiographic examination, comprising the measurement of aortic flow and ejection fraction. Their method is based on the adjustment of the aforementioned model of the cardiovascular system to patient-specific standards and subsequently allows for the derivation of  $E_{es}$  and  $V_d$  via an inverse model-fitting approach. Invasive validation of their technique on 19 patients yielded accurate estimates of  $E_{es}$  [ $r = 0.89$ ,  $nRMSE = 9\%$ ,  $bias = -0.13$  mmHg/mL with limits of agreement (-0.9, 0.6) mmHg/mL], while it was demonstrated that the method is robust to measurement noise.

### Limitations

This study has potential limitations that need to be acknowledged. The major limitation of the present study is the use of synthetic data and not real in vivo recordings. Nevertheless,

## Chapter 5. Artificial intelligence-based estimation of end-systolic elastance from arm pressure and systolic timing intervals

---

synthetic data can sufficiently simulate the content of the real clinical measurements, while they allow for controlling the distribution of rare but relevant conditions or events. In addition, the *in silico* model that was used for the data generation has been thoroughly validated against *in vivo* data and provides realistic representations of the physiological signals. Another limitation pertains to the fact that PEP and ET used for the training/testing scheme were extracted from the elastance curve, albeit this framework has been designed to use only echocardiographic measures. This approach was selected due to the lack of ECG information, given that cardiac electrical events are not yet included in our *in silico* model. Sensitivity analysis was performed in order to examine the model's performance with respect to over- and underestimation of these two features. Furthermore, our proposed method does not provide the entire ESPVR, given that the inputs do not provide adequate information to predict  $V_d$ . However, we observed that when the SV and EF were included in the input vector, our method is able to estimate  $V_d$  with an nRMSE = 9.12 % and  $r = 0.93$ . Finally, the current dataset was created using the mathematical model of a healthy individual free of pathology. Hence, implementation of the method is limited in cases of aortic valve stenosis, regurgitation, or other valve pathologies, where the relationship between the peripheral pressure and the STIs is modified. Further investigation towards this direction will be performed in our future studies.

### Conclusion

At large, this study provided evidence that accurate estimates of  $E_{es}$  could be yielded from pressure data and contractility-related timing parameters using a data-driven approach. Based on our findings, we conclude that data-driven approaches might be valuable for estimating  $E_{es}$ . The STIs appeared to be a promising source of information for assessing  $E_{es}$  and their usefulness should be emphasized. At large, our results were found to be in good agreement with the actual  $E_{es}$  values over an extensive range of LV contractility values and loading conditions. The proposed methodological concept could be easily transferred to the bedside and potentially facilitate the clinical use of  $E_{es}$  for monitoring the contractile state of the heart in the real-life setting.

## Bibliography

- [1] Suga Hiroyuki and Sagawa Kiichi, "Instantaneous pressure-volume relationships and their ratio in the excised, supported canine left ventricle," *Circulation Research*, vol. 35, no. 1, pp. 117–126, Jul. 1974. [Online]. Available: <https://www.ahajournals.org/doi/abs/10.1161/01.res.35.1.117>
- [2] H. Suga, K. Sagawa, and A. A. Shoukas, "Load independence of the instantaneous pressure-volume ratio of the canine left ventricle and effects of epinephrine and heart rate on the ratio," *Circulation Research*, vol. 32, no. 3, pp. 314–322, Mar. 1973. [Online]. Available: <https://www.ahajournals.org/doi/10.1161/01.RES.32.3.314>
- [3] K. Sagawa, H. Suga, A. A. Shoukas, and K. M. Bakalar, "End-systolic pressure/volume ratio: a new index of ventricular contractility," *The American Journal of Cardiology*, vol. 40, no. 5, pp. 748–753, Nov. 1977.
- [4] C.-H. Chen, M. Nakayama, E. Nevo, B. J. Fetts, W. Maughan, and D. A. Kass, "Coupled systolic-ventricular and vascular stiffening with age," *Journal of the American College of Cardiology*, vol. 32, no. 5, pp. 1221–1227, Nov. 1998. [Online]. Available: <https://linkinghub.elsevier.com/retrieve/pii/S073510979800374X>
- [5] B. A. Borlaug, C. S. Lam, V. L. Roger, R. J. Rodeheffer, and M. M. Redfield, "Contractility and ventricular systolic stiffening in hypertensive heart disease," *Journal of the American College of Cardiology*, vol. 54, no. 5, pp. 410–418, Jul. 2009. [Online]. Available: <https://linkinghub.elsevier.com/retrieve/pii/S0735109709016477>
- [6] C. S. P. Lam, A. M. Shah, B. A. Borlaug, S. Cheng, A. Verma, J. Izzo, S. Oparil, G. P. Aurigemma, J. D. Thomas, B. Pitt, M. R. Zile, and S. D. Solomon, "Effect of antihypertensive therapy on ventricular-arterial mechanics, coupling, and efficiency," *European Heart Journal*, vol. 34, no. 9, pp. 676–683, Mar. 2013. [Online]. Available: <https://academic.oup.com/eurheartj/article-lookup/doi/10.1093/eurheartj/ehs299>
- [7] B. Ky, B. French, A. May Khan, T. Plappert, A. Wang, J. A. Chirinos, J. C. Fang, N. K. Sweitzer, B. A. Borlaug, D. A. Kass, M. St. John Sutton, and T. P. Cappola, "Ventricular-arterial coupling, remodeling, and prognosis in chronic heart failure," *Journal of the American*



## Bibliography

---

- College of Cardiology*, vol. 62, no. 13, pp. 1165–1172, Sep. 2013. [Online]. Available: <https://linkinghub.elsevier.com/retrieve/pii/S073510971302247X>
- [8] T. Shishido, K. Hayashi, K. Shigemi, T. Sato, M. Sugimachi, and K. Sunagawa, “Single-beat estimation of end-systolic elastance using bilinearly approximated time-varying elastance curve.” *Circulation*, vol. 102, no. 16, pp. 1983–1989, Oct. 2000. [Online]. Available: <http://europepmc.org/abstract/MED/11034949>
- [9] C. H. Chen, B. Fetts, E. Nevo, C. E. Rochitte, K. R. Chiou, P. A. Ding, M. Kawaguchi, and D. A. Kass, “Noninvasive single-beat determination of left ventricular end-systolic elastance in humans,” *Journal of the American College of Cardiology*, vol. 38, no. 7, pp. 2028–2034, Dec. 2001.
- [10] S. Pagoulatou, K.-P. Rommel, K.-P. Kresoja, M. von Roeder, P. Lurz, H. Thiele, V. Bikia, G. Rovas, D. Adamopoulos, and N. Stergiopoulos, “In vivo application and validation of a novel non-invasive method to estimate the end-systolic elastance,” *American Journal of Physiology-Heart and Circulatory Physiology*, p. ajpheart.00703.2020, Feb. 2021. [Online]. Available: <https://journals.physiology.org/doi/10.1152/ajpheart.00703.2020>
- [11] V. Bikia, T. G. Papaioannou, S. Pagoulatou, G. Rovas, E. Oikonomou, G. Siasos, D. Tousoulis, and N. Stergiopoulos, “Noninvasive estimation of aortic hemodynamics and cardiac contractility using machine learning,” *Scientific Reports*, vol. 10, no. 1, p. 15015, Dec. 2020. [Online]. Available: <http://www.nature.com/articles/s41598-020-72147-8>
- [12] H. Krayenbühl, W. Bussmann, M. Turina, and E. Lüthy, “Is the ejection fraction an index of myocardial contractility?” *Cardiology*, vol. 53, no. 1, pp. 1–10, 1968. [Online]. Available: <https://www.karger.com/Article/FullText/166167>
- [13] M. A. Konstam and F. M. Abboud, “Ejection fraction: misunderstood and overrated (changing the paradigm in categorizing heart failure),” *Circulation*, vol. 135, no. 8, pp. 717–719, Feb. 2017.
- [14] A. M. Weissler, W. S. Harris, and C. D. Schoenfeld, “Systolic time intervals in heart failure in man,” *Circulation*, vol. 37, no. 2, pp. 149–159, Feb. 1968. [Online]. Available: <https://www.ahajournals.org/doi/10.1161/01.CIR.37.2.149>
- [15] A. M. Weissler, W. W. O’Neill, Y. H. Sohn, R. S. Stack, P. C. Chew, and A. H. Reed, “Prognostic significance of systolic time intervals after recovery from myocardial infarction,” *The American Journal of Cardiology*, vol. 48, no. 6, pp. 995–1002, Dec. 1981. [Online]. Available: <https://linkinghub.elsevier.com/retrieve/pii/0002914981903118>
- [16] H. Boudoulas, “Systolic time intervals,” *European Heart Journal*, vol. 11, no. suppl I, pp. 93–104, Jan. 1990. [Online]. Available: [https://academic.oup.com/eurheartj/article-lookup/doi/10.1093/eurheartj/11.suppl\\_I.93](https://academic.oup.com/eurheartj/article-lookup/doi/10.1093/eurheartj/11.suppl_I.93)

- [17] T. Gillebert, N. Deveire, M. Debuyzere, and J. Sutter, "Time intervals and global cardiac function. Use and limitations," *European Heart Journal*, vol. 25, no. 24, pp. 2185–2186, Dec. 2004. [Online]. Available: <https://academic.oup.com/eurheartj/article-lookup/doi/10.1016/j.ehj.2004.10.017>
- [18] J. Krohova, B. Czipelova, Z. Turianikova, Z. Lazarova, I. Tonhajzerova, and M. Javorka, "Preejection period as a sympathetic activity index: a role of confounding factors," *Physiological Research*, pp. S265–S275, Aug. 2017. [Online]. Available: [http://www.biomed.cas.cz/physiolres/pdf/2017/66\\_S265.pdf](http://www.biomed.cas.cz/physiolres/pdf/2017/66_S265.pdf)
- [19] T. Biering-Sørensen, G. Querejeta Roca, S. M. Hegde, A. M. Shah, B. Claggett, T. H. Mosley, K. R. Butler, and S. D. Solomon, "Left ventricular ejection time is an independent predictor of incident heart failure in a community-based cohort: systolic ejection time predicts heart failure," *European Journal of Heart Failure*, vol. 20, no. 7, pp. 1106–1114, Jul. 2018. [Online]. Available: <http://doi.wiley.com/10.1002/ejhf.928>
- [20] P. Reymond, F. Merenda, F. Perren, D. Rüfenacht, and N. Stergiopoulos, "Validation of a one-dimensional model of the systemic arterial tree," *American Journal of Physiology. Heart and Circulatory Physiology*, vol. 297, no. 1, pp. H208–222, Jul. 2009.
- [21] G. Langewouters, *Visco-elasticity of the human aorta in vitro in relation to pressure and age (Ph.D. thesis)*. Amsterdam: Free University of Amsterdam: Krips Repro, 1982. [Online]. Available: <https://books.google.gr/books?id=qvSrHAAACAAJ>
- [22] N. Westerhof, J.-W. Lankhaar, and B. E. Westerhof, "The arterial Windkessel," *Medical & Biological Engineering & Computing*, vol. 47, no. 2, pp. 131–141, Feb. 2009. [Online]. Available: <http://link.springer.com/10.1007/s11517-008-0359-2>
- [23] J. R. Womersley, *An elastic tube theory of pulse transmission and oscillatory flow in mammalian arteries*. Wright-Patterson Air Force Base, Ohio: Wright Air Development Center, Air Research and Development Command, 1957.
- [24] P. Reymond, Y. Bohraus, F. Perren, F. Lazeyras, and N. Stergiopoulos, "Validation of a patient-specific one-dimensional model of the systemic arterial tree," *American Journal of Physiology. Heart and Circulatory Physiology*, vol. 301, no. 3, pp. H1173–1182, Sep. 2011.
- [25] M. D. Feldman, P. H. Pak, C. C. Wu, H. L. Haber, C. M. Heesch, J. D. Bergin, E. R. Powers, T. D. Cowart, W. Johnson, A. M. Feldman, and D. A. Kass, "Acute cardiovascular effects of OPC-18790 in patients with congestive heart failure: time- and dose-dependence analysis based on pressure-volume relations," *Circulation*, vol. 93, no. 3, pp. 474–483, Feb. 1996. [Online]. Available: <https://www.ahajournals.org/doi/10.1161/01.CIR.93.3.474>
- [26] P. H. Pak, W. L. Maughan, K. L. Baughman, R. S. Kieval, and D. A. Kass, "Mechanism of acute mechanical benefit from vdd pacing in hypertrophied heart:

## Bibliography

---

- similarity of responses in hypertrophic cardiomyopathy and hypertensive heart disease,” *Circulation*, vol. 98, no. 3, pp. 242–248, Jul. 1998. [Online]. Available: <https://www.ahajournals.org/doi/10.1161/01.CIR.98.3.242>
- [27] M. R. Starling, R. A. Walsh, L. J. Dell’Italia, G. B. Mancini, J. C. Lasher, and J. L. Lancaster, “The relationship of various measures of end-systole to left ventricular maximum time-varying elastance in man.” *Circulation*, vol. 76, no. 1, pp. 32–43, Jul. 1987. [Online]. Available: <https://www.ahajournals.org/doi/10.1161/01.CIR.76.1.32>
- [28] Z. Lu and R. Mukkamala, “Continuous cardiac output monitoring in humans by invasive and noninvasive peripheral blood pressure waveform analysis,” *Journal of Applied Physiology*, vol. 101, no. 2, pp. 598–608, Aug. 2006. [Online]. Available: <https://www.physiology.org/doi/10.1152/jappphysiol.01488.2005>
- [29] P. Segers et al., “Three- and four-element Windkessel models: assessment of their fitting performance in a large cohort of healthy middle-aged individuals,” *Proceedings of the Institution of Mechanical Engineers, Part H: Journal of Engineering in Medicine*, 2008. [Online]. Available: <https://www.ncbi.nlm.nih.gov/pubmed/18595354>
- [30] R. B. Devereux, G. de Simone, D. K. Arnett, L. G. Best, E. Boerwinkle, B. V. Howard, D. Kitzman, E. T. Lee, T. H. Mosley, A. Weder, and M. J. Roman, “Normal limits in relation to age, body size and gender of two-dimensional echocardiographic aortic root dimensions in persons  $\geq 15$  years of age,” *The American Journal of Cardiology*, vol. 110, no. 8, pp. 1189–1194, Oct. 2012. [Online]. Available: <https://linkinghub.elsevier.com/retrieve/pii/S0002914912015342>
- [31] C. M. McEniery, n. Yasmin, I. R. Hall, A. Qasem, I. B. Wilkinson, J. R. Cockcroft, and ACCT Investigators, “Normal vascular aging: differential effects on wave reflection and aortic pulse wave velocity: the Anglo-Cardiff Collaborative Trial (ACCT),” *Journal of the American College of Cardiology*, vol. 46, no. 9, pp. 1753–1760, Nov. 2005.
- [32] B. Bordin Pelazza and S. R. F. Filho, “Comparison between central and brachial blood pressure in hypertensive elderly women and men,” *International Journal of Hypertension*, vol. 2017, p. 6265823, Sep. 2017, publisher: Hindawi. [Online]. Available: <https://doi.org/10.1155/2017/6265823>
- [33] P. H. Charlton, J. Mariscal Harana, S. Vennin, Y. Li, P. Chowienczyk, and J. Alastruey, “Modeling arterial pulse waves in healthy aging: a database for in silico evaluation of hemodynamics and pulse wave indexes,” *American Journal of Physiology-Heart and Circulatory Physiology*, vol. 317, no. 5, pp. H1062–H1085, Nov. 2019. [Online]. Available: <https://www.physiology.org/doi/10.1152/ajpheart.00218.2019>
- [34] V. Bikia, D. Adamopoulos, S. Pagoulatou, G. Rovas, and N. Stergiopoulos, “Ai-based estimation of end-systolic elastance from arm-pressure and systolic time intervals,” *Frontiers in Artificial Intelligence*, vol. 4, p. 16, 2021.

- [35] T. Chen and C. Guestrin, "XGBoost: a scalable tree boosting system," in *Proceedings of the 22nd ACM SIGKDD International Conference on Knowledge Discovery and Data Mining - KDD '16*. San Francisco, California, USA: ACM Press, 2016, pp. 785–794. [Online]. Available: <http://dl.acm.org/citation.cfm?doid=2939672.2939785>
- [36] L. Breiman, "Random forests," *Machine Learning*, vol. 45, no. 1, pp. 5–32, 2001. [Online]. Available: <http://link.springer.com/10.1023/A:1010933404324>
- [37] F. Pedregosa, G. Varoquaux, A. Gramfort, V. Michel, B. Thirion, O. Grisel, M. Blondel, P. Prettenhofer, R. Weiss, V. Dubourg, J. Vanderplas, A. Passos, D. Cournapeau, M. Brucher, M. Perrot, and E. Duchesnay, "Scikit-learn: machine learning in Python," vol. 12, pp. 2825–2830, 2011.
- [38] T. E. Oliphant, "A guide to NumPy." Trelgol Publishing USA, 2006, vol. 1.
- [39] W. McKinney, "Data structures for statistical computing in Python," in *Proceedings of the 9th Python in Science Conference*, 2010, pp. 51–56, doi: 10.25080/Majora-92bf1922-00a.
- [40] J. M. Bland and D. G. Altman, "Statistical methods for assessing agreement between two methods of clinical measurement," *Lancet (London, England)*, vol. 1, no. 8476, pp. 307–310, Feb. 1986.
- [41] V. Bikia, S. Pagoulatou, B. Trachet, D. Soulis, A. D. Protogerou, T. G. Papaioannou, and N. Stergiopoulos, "Noninvasive cardiac output and central systolic pressure from cuff-pressure and pulse wave velocity," *IEEE Journal of Biomedical and Health Informatics*, vol. 24, no. 7, pp. 1968–1981, Jul. 2020. [Online]. Available: <https://ieeexplore.ieee.org/document/8918060/>
- [42] P. Reant, M. Dijos, E. Donal, A. Mignot, P. Ritter, P. Bordachar, P. Dos Santos, C. Leclercq, R. Roudaut, G. Habib, and S. Lafitte, "Systolic time intervals as simple echocardiographic parameters of left ventricular systolic performance: correlation with ejection fraction and longitudinal two-dimensional strain," *European Journal of Echocardiography*, vol. 11, no. 10, pp. 834–844, Dec. 2010. [Online]. Available: <https://academic.oup.com/ehjcard/article-lookup/doi/10.1093/ehjcard/jeq084>
- [43] P. Dehkordi, F. Khosrow-Khavar, M. Di Rienzo, O. T. Inan, S. E. Schmidt, A. P. Blaber, K. Sørensen, J. J. Struijk, V. Zakeri, P. Lombardi, M. M. H. Shandhi, M. Borairi, J. M. Zanetti, and K. Tavakolian, "Comparison of different methods for estimating cardiac timings: a comprehensive multimodal echocardiography investigation," *Frontiers in Physiology*, vol. 10, p. 1057, Aug. 2019. [Online]. Available: <https://www.frontiersin.org/article/10.3389/fphys.2019.01057/full>
- [44] H. U. Chung, A. Y. Rwei, A. Hourlier-Fargette, S. Xu, K. Lee, E. C. Dunne, Z. Xie, C. Liu, A. Carlini, D. H. Kim, D. Ryu, E. Kulikova, J. Cao, I. C. Odland, K. B. Fields, B. Hopkins,

## Bibliography

---

A. Banks, C. Ogle, D. Grande, J. B. Park, J. Kim, M. Irie, H. Jang, J. Lee, Y. Park, J. Kim, H. H. Jo, H. Hahm, R. Avila, Y. Xu, M. Namkoong, J. W. Kwak, E. Suen, M. A. Paulus, R. J. Kim, B. V. Parsons, K. A. Human, S. S. Kim, M. Patel, W. Reuther, H. S. Kim, S. H. Lee, J. D. Leedle, Y. Yun, S. Rigali, T. Son, I. Jung, H. Arafa, V. R. Soundararajan, A. Ollech, A. Shukla, A. Bradley, M. Schau, C. M. Rand, L. E. Marsillio, Z. L. Harris, Y. Huang, A. Hamvas, A. S. Paller, D. E. Weese-Mayer, J. Y. Lee, and J. A. Rogers, "Skin-interfaced biosensors for advanced wireless physiological monitoring in neonatal and pediatric intensive-care units," *Nature Medicine*, vol. 26, no. 3, pp. 418–429, Mar. 2020. [Online]. Available: <http://www.nature.com/articles/s41591-020-0792-9>

## Chapter 6

---

# Estimation of cardiac contractility from brachial pressure waveform via deep learning

Vasiliki Bikia<sup>1</sup>, Marija Lazaroska<sup>1</sup>, Deborah Scherrer<sup>1</sup>, Méline Zhao<sup>1</sup>, Georgios Rovas<sup>1</sup>,  
Stamatia Pagoulatou<sup>1</sup>, Nikolaos Stergiopoulos<sup>1</sup>

<sup>1</sup> *Institute of Bioengineering, École Polytechnique Fédérale de Lausanne, Switzerland*

Published in *Frontiers in Bioengineering and Biotechnology*, 2021.

### Abstract

Determination of left ventricular (LV) end-systolic elastance ( $E_{es}$ ) is of utmost importance for assessing the cardiac systolic function and hemodynamical state in humans. Yet, the clinical use of  $E_{es}$  is not established due to the invasive nature and high costs of the existing measuring techniques. The objective of this study is to introduce a method to assess cardiac contractility, using as a sole measurement an arterial blood pressure (BP) waveform. Particularly, we aim to provide evidence on the potential in using the morphology of the brachial BP waveform and its time derivative for predicting LV  $E_{es}$  via convolution neural networks (CNNs). The requirement of a broad training dataset is addressed by the use of an *in silico* dataset ( $n = 3,748$ ) which is generated by a validated one-dimensional mathematical model of the cardiovascular system. We evaluated two CNN configurations: (i) a one-channel CNN (CNN<sub>1</sub>) with only the raw brachial BP signal as an input, and (ii) a two-channel CNN (CNN<sub>2</sub>) using as inputs both the brachial BP wave and its time derivative. Accurate predictions were yielded using both CNN configurations. For CNN<sub>1</sub>, Pearson's correlation coefficient ( $r$ ) and RMSE were equal to 0.86 and 0.27 mmHg/mL, respectively. The performance was found to be greatly improved for CNN<sub>2</sub> ( $r = 0.97$  and RMSE = 0.13 mmHg/mL). Moreover, all absolute errors from CNN<sub>2</sub> were

## Chapter 6. Estimation of cardiac contractility from brachial pressure waveform via deep learning

---

found to be less than 0.5 mmHg/mL. Importantly, the brachial BP wave appeared to be a promising source of information for estimating  $E_{es}$ . Predictions were found to be in good agreement with the reference  $E_{es}$  values over an extensive range of LV contractility values and loading conditions. Therefore, the proposed methodology could be easily transferred to the bedside and potentially facilitate the clinical use of  $E_{es}$  for monitoring the contractile state of the heart in the real-life setting.

## 6.1 Introduction

Left ventricular (LV) contractility is a major determinant of the cardiac systolic function, ventricular-arterial interaction [1; 2] as well as hemodynamical state [3]. Currently, the gold standard method for evaluating LV systolic function is the invasive measurement of LV pressure-volume loops under varying load conditions, whereby the end-systolic pressure-volume relation (ESPVR) is derived [1; 4; 2]. The ESPVR, described by its slope, i.e. the end-systolic elastance ( $E_{es}$ ), and its intercept, i.e. the dead volume ( $V_d$ ), has been proved to be less load sensitive than other indices of ventricular contractility [5]. For an increased value of  $E_{es}$ , the left ventricle is able to eject a higher blood volume against the same afterload, which is indicative of increased contractility [4]. Evaluation of  $E_{es}$  is of utmost significance in clinical practice. The age-induced vascular stiffening [6] and hypertension [7] are strongly associated to the stiffening of the left ventricle, which is followed by an increase in  $E_{es}$ . Furthermore, continuous and reliable monitoring of  $E_{es}$  is critical in patients with heart failure or septic cardiomyopathy [3]. Yet, the bedside use of  $E_{es}$  is not established due to the invasive nature and high costs of the existing measuring techniques [8]. Such limitations create an inescapable need for a new method that will permit the  $E_{es}$  derivation in a fast, easy, non-invasive manner using easily obtained measurements (such as applanation tonometry).

Arterial pulse waves contain a wealth of information for assessing the cardiovascular health in humans. Importantly, the morphology of the arterial pulse is affected by the mechanical and structural properties of the heart and the arterial network [9]. Clinical studies have investigated the arterial hemodynamics in normal and diseased human hearts under varying loading conditions and inotropic states, showing that the shape of the arterial BP waveform is highly sensitive to changes in LV  $E_{es}$  [10]. Interestingly, Ostadal et al. have presented data verifying that continuous monitoring of  $dP/dt_{max}$  (where BP time-signal is measured via arterial line) enables the assessment of the LV function in patients with acute heart failure [11]. In particular, the  $dP/dt_{max}$  can be calculated from a BP waveform, obtained either minimally invasively from a peripheral arterial line [12; 13; 14] or non-invasively using, for instance, a tonometry-based device [15]. Nonetheless, there is no current study to investigate the importance of exploiting the entire BP waveform (time sequence and its time derivative) for further facilitating the non-invasive monitoring of LV contractility.

Recent advancements in the field of artificial intelligence have introduced novel methods towards the predictive modelling for clinical use, creating a promising opportunity for further methodological advancements [16]. Yet, only few studies have leveraged machine learning and deep learning techniques for cardiac monitoring [17; 18; 19]. Motivated by the evidence provided by the current state of knowledge, the present study aims to explore the opportunity in using the entire brachial BP wave for predicting LV  $E_{es}$  via convolution neural networks (CNNs). The requirement of a broad training dataset is addressed by the use of an *in silico* cohort, which was generated by a validated one-dimensional (1-D) cardiovascular simulator



[20]. In silico models permit studying and understanding of various pathophysiological conditions, whereas they provide additional hemodynamic insights, which would be difficult to obtain in vivo. Concurrently, accurate measurement of  $E_{es}$  is challenging in a human cohort and thus a preliminary in silico verification of the proposed concept would benefit the future in vivo validation. Our aim was to propose an original conceptual methodology for continuous monitoring of the cardiac performance and to evaluate its feasibility in silico. The result of the in silico experiments can be considered as preliminary implications for the accuracy of the predictions under ideal conditions.

## 6.2 Methods & materials

### Brief description of the cardiovascular simulator

We adopted a 1-D mathematical model of the cardiovascular (Figure 6.1) which has been previously described in [20]. The arterial tree network includes all major vessels of the systemic circulation, as well as the cerebral circulation and the coronary circulation. The governing equations of the model are derived by integrating the longitudinal momentum and continuity of the Navier-Stokes equations over the arterial cross-section. The model solves the governing equations with proper boundary conditions and provides flow and pressure at every arterial location of the network. Every arterial segment is modelled as a long, tapered tube, and its compliance is defined as a non-linear function of pressure and location [21]. Terminal vessels are coupled with three-element Windkessel models [22] and intimal shear is modeled following the Witzig-Womersley theory [23]. At the proximal end (at the root of the aorta), the arterial tree is coupled with a time-varying elastance model (VEM) of the left ventricle [1; 4]. Specifically, VEM simulates the relationship between the LV pressure ( $P_{LV}$ ) and LV volume ( $V_{LV}$ ), namely:

$$E(t) = \frac{P_{LV}}{V_{LV} - V_d} \quad (6.1)$$

where  $V_d$  is the LV dead volume. Table 6.1 summarizes all the inputs and outputs of the 1-D cardiovascular model. A detailed description of the 1-D simulator can be found in the original publications [20; 24]).

### Description of the in silico dataset

For generating various hemodynamic cases, the 1-D cardiovascular simulator ran using different combinations of arbitrary input model parameters. The distributions of the input model parameters were based on literature data, by identifying the normal values and ranges of the parameters. Given that the literature data are only provided in terms of mean and standard deviation or/and minimum and maximum values, the exact distribution of each parameter was

Table 6.1 – List of the inputs and outputs of the 1-D cardiovascular model.

	<b>Variable notation</b>	<b>Value</b>
<b>Inputs</b>		
End-systolic elastance [mmHg/mL]	<i>Ees</i>	2.6
End-diastolic elastance [mmHg/mL]	<i>Eed</i>	0.08
Filling pressure [mmHg]	<i>Pfill</i>	14
Time of maximal elastance [ms]	<i>tes</i>	340
Heart rate [bpm]	<i>HR</i>	75
Dead volume [mL]	<i>Vd</i>	15
Venous resistance [mmHg.s/mL]	<i>Rven</i>	0.003
Arterial distensibility [ $10^{-3}$ /mmHg]	<i>C</i>	(no_segments)x1 vector
Terminal compliances [mL/mmHg]	<i>Ct</i>	(no_terminal_segments)x1 vector
Peripheral resistances [mmHg.s/mL]	<i>Rt</i>	(no_terminal_segments)x1 vector
Arterial inlet diameter [cm]	<i>din</i>	(no_segments)x1 vector
Arterial outlet diameter [cm]	<i>dout</i>	(no_segments)x1 vector
Arterial length [cm]	<i>len</i>	(no_segments)x1 vector
Blood density [ $\text{kg/m}^3$ ]	$\rho$	1050
Blood viscosity [Pa.s]	$\mu$	0.004
<b>Outputs</b>		
Pressure waves [mmHg]	<i>pressures</i>	(no_segments)x(no_time_points) vector
Flow waves [mL/s]	<i>flows</i>	(no_segments)x(no_time_points) vector

## Chapter 6. Estimation of cardiac contractility from brachial pressure waveform via deep learning

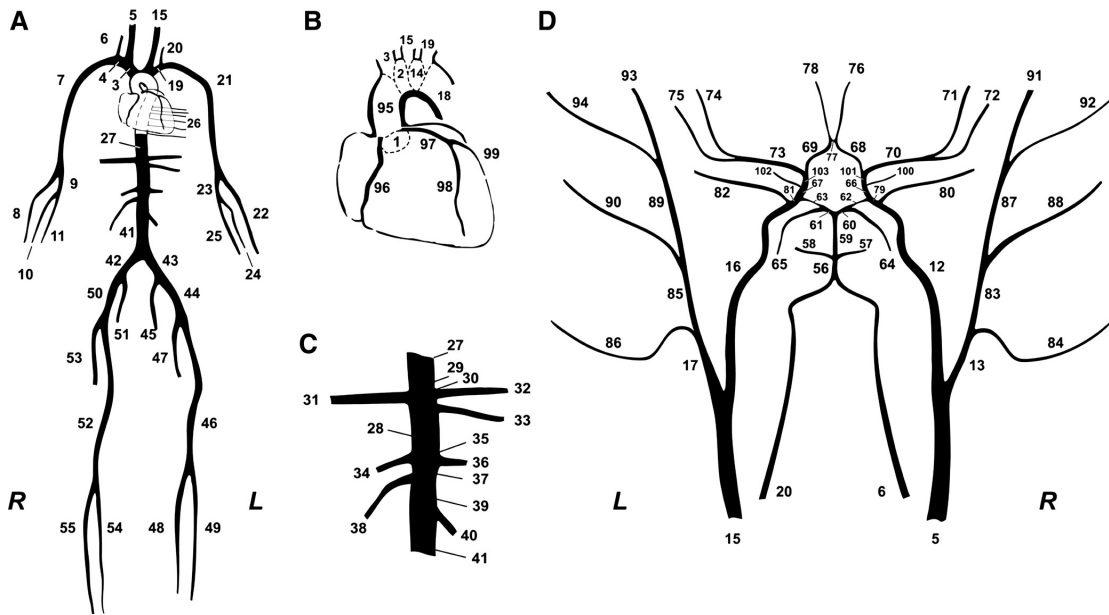


Figure 6.1 – Schematic representation of the model of systemic circulation developed by [20]. (A) Main systemic arterial tree. (B) Detail of the aortic arch and the coronary network. (C) Detail of the principal abdominal aorta branches. (D) Blown-up schematic of the detailed cerebral arterial tree, which is connected via the carotids (segments 5 and 15) and the vertebrals (segments 6 and 20) to the main arterial tree shown in (A). Adapted from [20].

unknown. In addition, varying the parameters while accounting for dependencies between parameters was not feasible due to the lack of sufficient data to inform inter-dependencies. Therefore, the sampling was selected to be random Gaussian.

The selected distributions of the input model parameters are summarized in Table 6.2. The parameters of arterial distensibility and terminal compliance were altered simultaneously, while nonuniform aortic stiffening was considered for the elderly and hypertensive virtual subjects, following the methodology described in our previous work [25; 26]. Peripheral resistances were modified uniformly in order to achieve the specific value of total peripheral resistance in the selected range.

Furthermore, the geometry of the arterial network (namely length, inlet diameter, and outlet diameter of the arterial segments) was modified to simulate different body types by adapting the length and the diameter of all arterial vessels. The reference state of the arterial tree model corresponds to an individual with a height equal to 180 cm. Different heights were simulated via multiplication of the reference arterial lengths with a scaling factor (uniform adaptation). As per the arterial diameters, previous studies have associated the variation of the aortic diameter with respect to age, gender, weight, and height [27]. However, there exist no sufficient available data to demonstrate the diameter variation of multiple arterial segments

Table 6.2 – Selected distributions of the model’s input parameters based on the literature

Parameter	mean±SD	Reference
End-systolic elastance [mmHg/mL]	2.3±1	[6]
End-diastolic elastance [mmHg/mL]	0.2±0.11	[6]
Filling pressure [mmHg]	15±5.4	[29]
Time of maximal elastance [ms]	327±39	[30]
Heart rate [bpm]	63.7±9.5	[31]
Aortic distensibility [ $10^{-3}$ /mmHg]	5.86±3.23	[32]
Total peripheral resistance [mmHg.s/mL]	1.28±0.31	[31]
Aortic diameter [cm]	33.2±4.1	[27]
Height [cm]	169.2±8.9	[31]

with respect to an individual’s demographic profile. As a result, we modified all arterial segments following a uniform distribution based on the variation of the aortic diameter.

In order to eliminate the likelihood of creating unrealistic hemodynamical profiles, we examined the physiological validity of every case and discarded any implausible generated virtual subject. The physiological validity of each subject was evaluated by comparing the simulated brachial and aortic BP values [i.e. SBP, DBP, MAP, and pulse pressure (PP)] to the reference values reported in the literature [28]. A subject was discarded from the data if any of the BP values did not lie within the range of mean  $\pm$  2.807SD (assuming 99.5 % confidence intervals). For deriving the dataset, we ran the model 10,000 times to generate 10,000 cases. Out of the 10,000 cases, 3,748 samples were accepted after applying the above filtering criteria.

### Data pre-processing

The brachial BP waveform was derived from the left simulated brachial artery. The train/validation/test split was set to be 60 % (2290 cases)/20 % (764 cases)/20 % (764 cases). By computing the MSE with decreasing training size, we noticed that similar results can also be achieved with fewer samples (e.g. 1603) and, therefore, we may deduce that a training size of 2290 is sufficient.

The BP waveforms were up-sampled so that each wave consists of 200 samples. This selection allowed us to ensure a sampling frequency higher than the 100-Hz threshold suggested for the pulse wave velocity techniques [33] (which require substantially high signal resolution). This value was considered as a fair trade-off between computational time and high signal fidelity.

Subsequently, the data were normalized using the `MinMaxScaler()` function from Sklearn library. The Min-max normalization method is a standard normalization approach which guarantees that all features will be on the same scale, e.g. between zero and one. Other methods, such as the z-score or feature clipping, are preferable when there are several outliers in

## Chapter 6. Estimation of cardiac contractility from brachial pressure waveform via deep learning

---

the data. Nonetheless, given that the filtering of the in silico population essentially disregards the outliers, the Min-max method may be sufficient for our learning algorithm.

### Convolution neural networks

We evaluated two model configurations with respect to the inputs:

1. One-channel CNN (CNN<sub>1</sub>): Using as a sole input the entire BP waveform.
2. Two-channels CNN (CNN<sub>2</sub>): Using as inputs the entire BP waveform and its time derivative.

The time derivative of the BP wave was calculated as the slope of the wave using the central differences approach:

$$f'[n] = \frac{f[n-1] - f[n+1]}{2\tau} \quad (6.2)$$

where  $f[n]$  is the BP function at the  $n^{th}$  time point and  $\tau$  is the time interval between the two pressure values. The  $\tau$  is computed as the entire heart cycle duration divided by the number of recorded pressure values (200 samples).

The CNN models were created using PyTorch library [34]. In particular, the networks were composed of four 1-D Convolutional layers, each of them followed by an activation ReLU layer. Following the four convolutional layers intercalated with the activation ReLU layers, three additional functions were used to yield the final output results. Firstly, we employed a MaxPooling layer which uses the MaxPool1d function from PyTorch framework. The MaxPooling function permits to progressively reduce the spatial size of the data for keeping only the maximum of each window while striding (kernel\_size = 3, stride = 2). The MaxPooling layer was followed by a Flatten function which flattened the output of the convolutional layers to create a single long feature vector. A Linear layer was finally applied on the output of the Flatten function, providing the final prediction of the  $E_{es}$  value. The functions are further described in the torch.nn module (Available at: <https://pytorch.org/docs/stable/generated/torch.nn>).

In order to generate our different CNN models, we made use of PyTorch Conv1D() function with different values for in\_channels and out\_channels parameters. The input data size was 200 for CNN<sub>1</sub> and 200x2 for CNN<sub>2</sub>. In addition, the kernel size of each filter was set to 5, which is a popular choice in the state of the art. Importantly, we opted for an odd-sized filter, as all the previous layer pixels would be symmetrically around the output pixel. Selecting even-sized kernel filters would require us to account for distortions across the layers. Therefore, odd-sized kernel filters were preferred for implementation simplicity. The value of stride and padding was kept constant throughout the models and equal to 2.

Table 6.3 – Number of filters per each convolutional layer for the two CNN models.

	Number of filters per channel	Total number of filters (no_filters x no_input_channels)
<b>CNN<sub>1</sub></b>		
Layer 1	2	2
Layer 2	4	8
Layer 3	8	32
Layer 4	16	128
<b>CNN<sub>2</sub></b>		
Layer 1	8	16
Layer 2	16	128
Layer 3	18	288
Layer 4	24	432

Each of the CNN model with each own input layer was characterized by the respective number of channels. Figure 6.2 illustrates the number of inputs/outputs between each convolutional layer, and the architecture of the two models. The number of filters per channel on each convolutional layer is presented in Table 6.3. The number of filters was optimized by an “error and trial” approach, and the optimal values were selected for the specific type of data.

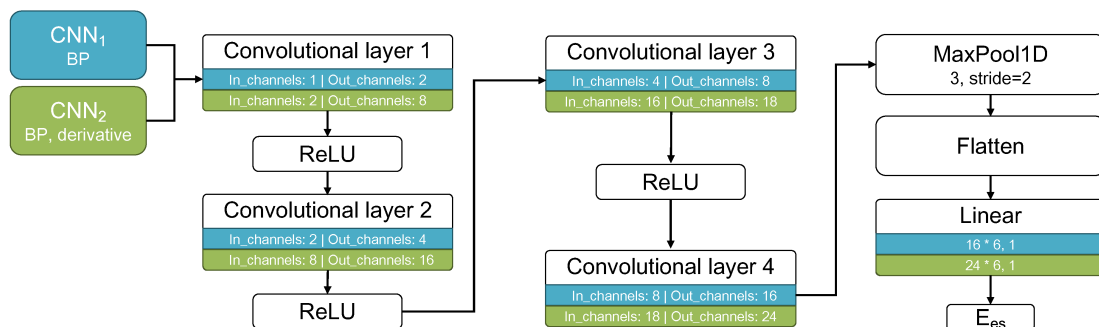


Figure 6.2 – Representation of the architecture of the CNN model configurations. The two CNN models are shown in different colors (CNN<sub>1</sub> in blue and CNN<sub>2</sub> in green) and the number of the in\_channels and out\_channels for each convolutional layer is reported. Adapted from [35].

The CNN parameters, namely the weights and biases, were optimized upon training on 60 % of the dataset. The resulting model was then applied to the validation set (20 % of the entire dataset) in order to assess the loss and the accuracy in the output. On this validation set, we performed tuning for two hyperparameters, namely the batch\_size and the number of epochs. This allowed us to ensure that no overfitting occurred. The value of learning\_rate was set equal to 0.001 and tuning was performed using the Adam optimizer [36] for batch\_size values {32, 64, 128} and epochs values within the range of [1, 400]. Adam is a versatile optimization method.

## Chapter 6. Estimation of cardiac contractility from brachial pressure waveform via deep learning

---

Given the satisfactory performance of our trained models, we did not consider evaluating additional algorithms.

The trained CNN models using the tuned hyperparameters along with the weights and biases values were applied to the test set (remaining 20 % of the data) in order to evaluate the predictive performance of the models. The tuning process was conducted with regard to the mean square error (MSE) loss function. The MSE loss function is considered as a fair selection under the inference framework of maximum likelihood when the distribution of the target variable is Gaussian-like (as in the present study). In addition, it is preferable in comparison to other methods which might be more computationally expensive (e.g. the mean absolute error method which uses modulus operator function) or might impose increased training requirements (e.g. the uber loss which involves the optimization of the hyperparameter  $\delta$  in order to maximize model accuracy).

### Sensitivity to errors

In order to investigate the impact of potential errors or adverse effects in the measurements of the BP signal, the test data were corrupted with artificial noise. White gaussian noise (WGN) was added to the BP for each subject using the `awgn()` from MATLAB (The Math Works, Inc. MATLAB. Version 2020b). The performance of the two CNN models was tested for five values of signal-to-noise ratio (SNR), i.e. 70, 60, 50, 40, and 30 dB. The metrics of agreement and accuracy were reported for each level of noise. Examples of the noise effect on the BP wave are depicted in Figure 6.3.

### Statistical analysis

The performance of the models in terms of agreement, bias and accuracy was evaluated with the use of the Pearson's correlation coefficient ( $r$ ), the normalized root mean square error (nRMSE), and the Bland-Altman analysis [37]. The computed nRMSE was based on the difference between the minimum and maximum values of the dependent variable. A  $P$ -value below 0.05 was considered as statistically significant. The statistical analysis was performed in Python (Python Software Foundation, Python Language Reference, version 3.6.8, Available at <http://www.python.org>).

## 6.3 Results

Table 6.4 presents the cardiac and vascular characteristics of the study population (3,748 cases). The CNN-derived  $E_{es}$  were compared to the reference  $E_{es}$  values, which were provided by the 1-D cardiovascular model.

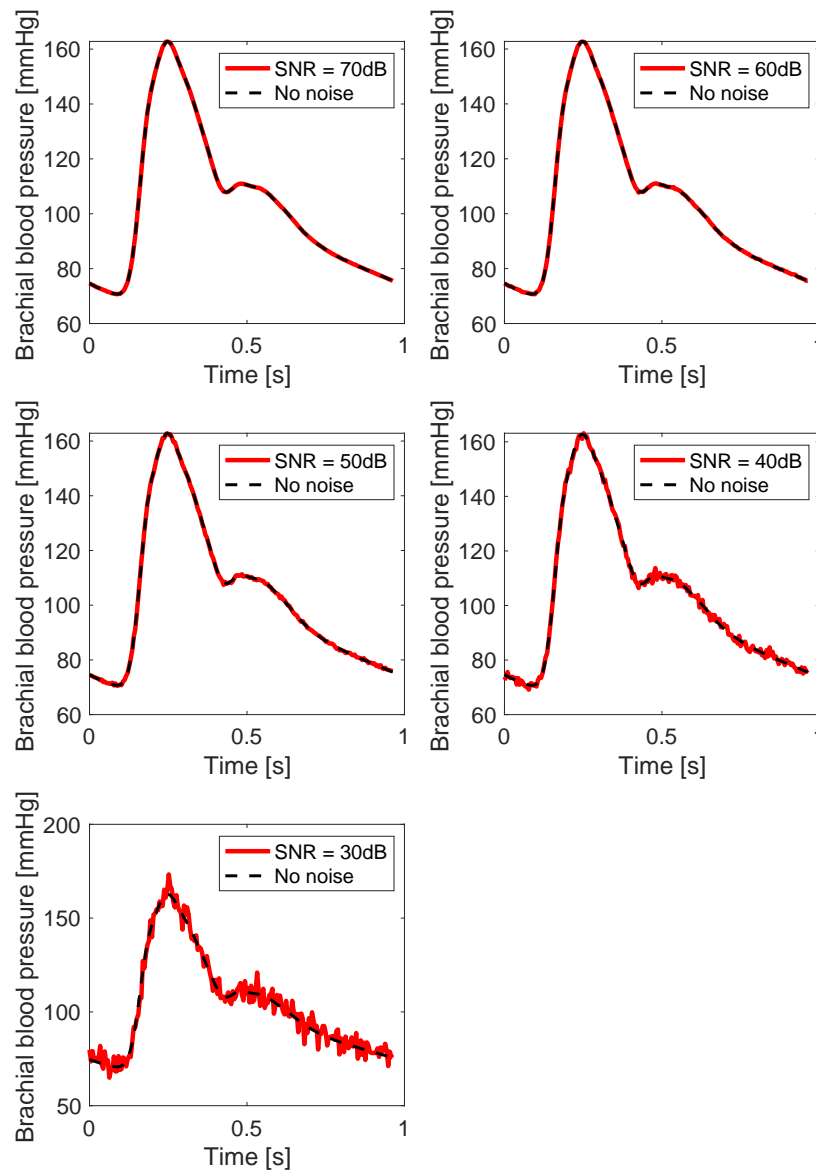


Figure 6.3 – Brachial blood pressure waves after adding artificial noise. The noisy data are presented in red solid lines and the original noise-free data in black dashed lines. Adapted from [35].

### Comparison between the CNN-predicted $E_{es}$ and the reference $E_{es}$ values

Table 6.5 summarizes the regression metrics of the statistical comparisons between the non-invasive  $E_{es}$  estimates and the reference  $E_{es}$ . The Bland-Altman analysis indicated a low bias for the estimated  $E_{es}$ . The limits of agreement (LoA) between the estimated and reference



## Chapter 6. Estimation of cardiac contractility from brachial pressure waveform via deep learning

Table 6.4 – Summary of the virtual study cohort (n = 3,748) cardiovascular characteristics.

Parameter	Value (n = 3,748)
End-systolic elastance [mmHg/mL]	2.4±0.52
End-diastolic elastance [mmHg/mL]	0.16±0.04
Filling pressure [mmHg]	16.54±3.19
Time of maximal elastance [ms]	328±23
Heart rate [bpm]	75.96±8.25
Ejection fraction [%]	47.38±6.06
Stroke volume [mL]	56.68±12.75
Aortic systolic blood pressure [mmHg]	110.62±23.13
Aortic diastolic blood pressure [mmHg]	80.93±14.79
Aortic pulse pressure [mmHg]	29.70±13.04
Mean arterial pressure [mmHg]	95.71±18.40
Brachial systolic blood pressure [mmHg]	121.64±24.07
Brachial diastolic blood pressure [mmHg]	78.71±14.44
Brachial pulse pressure [mmHg]	42.93±15.05
Pulse pressure amplification	1.49±0.11
Total peripheral resistance [mmHg.s/mL]	1.36±0.17
Total arterial compliance [mL/mmHg]	1.27±0.41

$E_{es}$  (within which 95 % of errors are expected to lie) were found to be (-0.55, 0.49) mmHg/mL and (-0.26, 0.23) mmHg/mL, for CNN<sub>1</sub> and CNN<sub>2</sub>, respectively. Figures 6.4 and 6.5 illustrate the scatterplots and the Bland-Altman plots of the estimated  $E_{es}$  against the actual  $E_{es}$  for the two CNNs. The absolute difference between the estimated  $E_{es}$  and the real  $E_{es}$  values did not exceed 0.5 mmHg/mL in 95 % of the total cases for CNN<sub>1</sub>, while all errors were found to be smaller than 0.5 mmHg/mL for CNN<sub>2</sub>. Furthermore, for the CNN<sub>2</sub> configuration, the absolute error was less than 0.05 mmHg/mL in 61 % of the test set.

The computational time required for training the models was 110 s and 115 s for CNN<sub>1</sub> and CNN<sub>2</sub>, respectively. The time required to yield the predictions for the test set was reported to be less than 1 s.

### Sensitivity to errors

The impact of potential errors or adverse effects in the measurements of the BP signal was quantified for the two CNN configurations under various noise levels (Table 6.5). The CNN<sub>1</sub> model appeared to be robust for an SNR value equal or larger than 40 dB (nRMSE < 15 %). On the other hand, the performance of CNN<sub>2</sub> remained unaffected for SNR ≥ 60 dB (nRMSE was doubled for higher values of SNR). However, when the SNR reduced to 40 dB or less, the correlation and agreement were significantly deteriorated ( $r < 0.6$  and nRMSE > 30 %).

Table 6.5 – Regression statistics between the model-predicted and the reference elastance values.

Model	SNR [dB]	Slope	Intercept [mmHg/mL]	$r$	$P$ -value	nRMSE [%]	Bias (LoA) [mmHg/mL]	Predicted $E_{es}$ [mmHg/mL]
CNN <sub>1</sub>	No noise	0.75	0.56	0.86	<0.0001	13.4	-0.03 (-0.55, 0.49)	2.36±0.45
	70	0.75	0.56	0.86		13.4	-0.03 (-0.55, 0.49)	2.36±0.45
	60	0.75	0.56	0.86		13.4	-0.03 (-0.54, 0.49)	2.36±0.45
	50	0.76	0.56	0.85		13.5	-0.02 (-0.55, 0.5)	2.36±0.45
	40	0.75	0.57	0.83		14.7	-0.03 (-0.6, 0.55)	2.36±0.46
	30	0.72	0.66	0.61		25.2	0.00 (-0.98, 0.98)	2.39±0.61
CNN <sub>2</sub>	No noise	0.94	0.12	0.97		6.4	-0.02 (-0.26, 0.23)	2.37±0.5
	70	0.94	0.12	0.97		6.5	-0.02 (-0.27, 0.23)	2.37±0.5
	60	0.94	0.11	0.96		7.3	-0.02 (-0.31, 0.26)	2.36±0.5
	50	0.93	0.12	0.88		13.5	-0.04 (-0.56, 0.47)	2.34±0.54
	40	0.88	0.47	0.59		32.9	0.2 (-1.04, 1.42)	2.57±0.77
	30	0.87	2.76	0.29		144	2.45 (-0.45, 5.6)	4.84±1.55

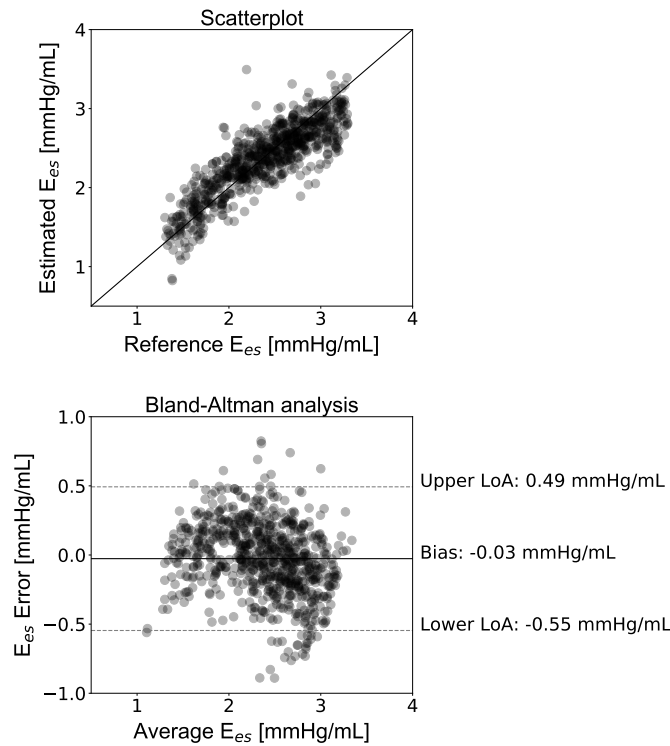


Figure 6.4 – Comparison between the predicted  $E_{es}$  and the reference  $E_{es}$  data for  $CNN_1$ . Scatterplots and Bland–Altman plots between the CNN-predicted  $E_{es}$  and the reference  $E_{es}$ . The solid line of the scatterplots represents equality. In Bland–Altman plots, limits of agreement (LoA), within which 95 % of errors are expected to lie, are defined by the two horizontal dashed lines. Adapted from [35].

## 6.4 Discussion

In the present study, we suggested that the prediction of the cardiac contractility index of  $E_{es}$  is feasible using a single brachial BP waveform. The proposed concept was appraised using an in silico dataset which was generated using a 1-D mathematical model of the cardiovascular system [20]. The results showed that the brachial BP wave may be valuable for the characterization of  $E_{es}$ . In particular, the CNN configuration combining the brachial BP wave and its time derivative provided higher precision than the precision achieved by the CNN that used only the BP signal (correlation was increased from 0.86 to 0.97).

Arterial pulse wave contains a wealth of physiological information as its morphology is influenced by the heart and the systemic circulation [9]. Quantities such as stroke volume as well as the arterial stiffness and wave reflections have a prominent impact on the arterial pulse. Furthermore, pathological changes affect the arterial pulse in different ways, including the amplitude, shape, and frequency [38]. As a result, arterial pulse waves provide abundant and reliable information about the cardiovascular function. Importantly, physiological parameters

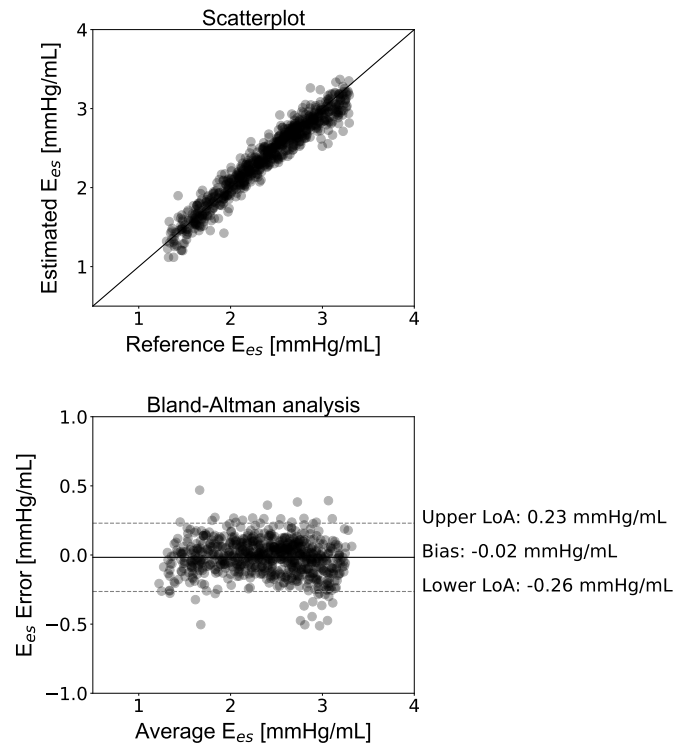


Figure 6.5 – Comparison between the predicted  $E_{es}$  and the reference  $E_{es}$  data for CNN<sub>2</sub>. Scatterplots and Bland–Altman plots between the CNN-predicted  $E_{es}$  and the reference  $E_{es}$ . The solid line of the scatterplots represents equality. In Bland–Altman plots, limits of agreement (LoA), within which 95 % of errors are expected to lie, are defined by the two horizontal dashed lines. Adapted from [35].

derived from the arterial pulse can be useful for diagnosis and clinical decision making. Arterial waves can be easily measured using non-invasive clinical devices, such as oscillometric or tonometric BP monitors. In addition, arterial waves from photoplethysmography (PPG) or other signals including the electrocardiogram (ECG), are also routinely monitored by wearable devices (e.g. smartwatches and fitness wristbands). Hence, the high accessibility of the arterial pulse waves in both clinical settings and daily life encourages further exploitation of their insights with respect to the cardiovascular function.

With the increasing availability of clinical data, signals, and images sourced from various avenues of medicine and healthcare, the application of artificial intelligence for analysis and interpretation of medical data grows rapidly. The diagnosis of the cardiovascular disease could benefit essentially from early prediction, prevention, and proactive management. Thus artificial intelligence-based methodologies could essentially contribute towards this direction. Deep learning offers a promising potential in exploring new methods for cardiac monitoring by deciphering key information from arterial waveforms. Deep learning is a class of machine learning algorithms that uses multiple layers to progressively extract higher-level features

## Chapter 6. Estimation of cardiac contractility from brachial pressure waveform via deep learning

---

from the raw input. In this study, we leveraged this exact capacity of CNN models in order to evaluate LV  $E_{es}$  from a single BP signal. Such potential can open new directives in digital health and potentially suggest new markers for cardiac monitoring purposes.

Ensuring high fidelity in the signal acquisition constitutes a critical aspect for the accurate estimation of  $E_{es}$ . Especially, caution should be paid in successfully capturing the waveform, as the measurement may be prone to errors or adverse effects which can distort the relevant information for the deep CNN prediction. In order to evaluate the effect of errors in the morphology of the input brachial BP wave, we artificially introduced simulated noise. The noise was applied only on the test set which was subsequently fed to the trained CNN models. The sensitivity analysis showed that subtle distortion in the wave shape did not significantly affect the accuracy of the CNN models. However, the performance was severely worsened when the SNR approached 30 dB. The  $CNN_1$  was found to be more robust to measurement noise when compared to the  $CNN_2$  whose estimation relies on both the pressure wave and its time derivative. This might be explained by the sensitivity of the  $CNN_2$  to two input waves. Specifically, the error may propagate through the derivative computation by directly altering the two derivative factors (i.e.  $f[n-1]$  and  $f[n+1]$ ) and, subsequently, influence to a greater extent the deep CNN prediction.

Previous methods on the estimation of  $E_{es}$  rely mainly on non-invasive single-beat measurements [39; 40; 41; 18]. These methods require the inclusion of cuff BP, stroke volume, ejection fraction or other measurements. Especially, stroke volume and ejection fraction constitute common measures of the LV systolic function and can be obtained via several cardiac imaging modalities, such as the magnetic resonance imaging, and the Simpson's method. However, these imaging techniques are tedious and require a highly trained technician. In addition, ejection fraction expresses the stroke volume as a fraction of end-diastolic volume (EDV), and, therefore, correct interpretation of ejection fraction can be achieved only with the additional knowledge of EDV. Simplification of the  $E_{es}$  approximation by using a sole BP wave recording may facilitate cardiac monitoring while reducing costs and complexity for the clinicians and the patients.

It is to be highlighted that this study aimed to address an unmet clinical need by proposing a novel methodology, dissimilar to the existing state of the art. As a result, there was not sufficient relevant literature to guide the CNN design and architecture for the research question under investigation. In particular, there did not exist previously published studies that aimed to address a similar problem and which could inform us about the selection of the model functions and parameters. Therefore, we developed and suggested an original architecture that fitted best in the specific type of data.

### Limitations

Several limitations of the present study need to be acknowledged. The current study was entirely based on simulated data and thus the results should be considered as a preliminary assessment of the theoretical concept of the proposed approach. While synthetic data can mimic numerous properties of the real clinical data, they do not copy the original content in an identical way. Future work should include the use of real clinical data that will finally verify the application of the proposed method in the clinical setting. It is likely that the models trained using the simulations are not capable for adequate predictions for real human data. Nevertheless, *in silico* trained networks could be used in transfer learning as pre-trained networks, which are subsequently fine tuned with clinical measurements. At this stage of our research, we found it reasonable to start with an *in silico* validation of our research hypothesis, instead of directly collecting measurements of  $E_{es}$  in humans. The cost and the complexity of the  $E_{es}$  measurements would make it difficult to incorporate them in the current study. In addition, the variance of the simulated EF data was reported to be low, while the average EF was equal to 47 %. Such a data distribution represents more accurately a population with heart problems. Our future *in vivo* studies will include a wider range of EF values, which will account for both diseased and healthy populations. Finally, the evaluation of the proposed framework was done using a single beat of each virtual subject. Next steps will also include the *in silico* and the *in vivo* validation of a CNN method that uses multiple heart beats from every participant. Hence, a closed-loop cardiovascular mathematical model may be adopted for achieving this goal.

### Conclusion

We showed that the use of the brachial BP waveform in conjunction with a deep CNN provided accurate estimates of  $E_{es}$ . In particular, our findings indicated that the brachial BP wave may be a promising source of information for assessing  $E_{es}$ , and its clinical utility should be emphasized. Our prediction algorithm achieved a satisfactory performance for an extensive range of LV contractility values and loading conditions. Consequently, the proposed methodological concept could be readily transferred to the bedside and potentially enhance the clinical use of  $E_{es}$  for monitoring the contractile state of the heart in the real-life medical environment.



## Bibliography

- [1] K. Sagawa, H. Suga, A. A. Shoukas, and K. M. Bakalar, "End-systolic pressure/volume ratio: a new index of ventricular contractility," *The American journal of cardiology*, vol. 40, no. 5, pp. 748–753, 1977.
- [2] H. Suga, K. Sagawa, and A. A. Shoukas, "Load independence of the instantaneous pressure-volume ratio of the canine left ventricle and effects of epinephrine and heart rate on the ratio," *Circulation research*, vol. 32, no. 3, pp. 314–322, 1973.
- [3] M. Cecconi, D. De Backer, M. Antonelli, R. Beale, J. Bakker, C. Hofer, R. Jaeschke, A. Mebazaa, M. R. Pinsky, J. L. Teboul *et al.*, "Consensus on circulatory shock and hemodynamic monitoring. task force of the european society of intensive care medicine," *Intensive care medicine*, vol. 40, no. 12, pp. 1795–1815, 2014.
- [4] H. Suga and K. Sagawa, "Instantaneous pressure-volume relationships and their ratio in the excised, supported canine left ventricle," *Circulation research*, vol. 35, no. 1, pp. 117–126, 1974.
- [5] H. Paley, I. G. McDonald, J. Blumenthal, J. Mailhot, G. W. Modin *et al.*, "The effects of posture and isoproterenol on the velocity of left ventricular contraction in man: the reciprocal relationship between left ventricular volume and myocardial wall force during ejection on mean rate of circumferential shortening," *The Journal of clinical investigation*, vol. 50, no. 11, pp. 2283–2294, 1971.
- [6] C.-H. Chen, M. Nakayama, E. Nevo, B. J. Fetts, W. L. Maughan, and D. A. Kass, "Coupled systolic-ventricular and vascular stiffening with age: implications for pressure regulation and cardiac reserve in the elderly," *Journal of the American College of Cardiology*, vol. 32, no. 5, pp. 1221–1227, 1998.
- [7] B. A. Borlaug, C. S. Lam, V. L. Roger, R. J. Rodeheffer, and M. M. Redfield, "Contractility and ventricular systolic stiffening in hypertensive heart disease: insights into the pathogenesis of heart failure with preserved ejection fraction," *Journal of the American College of Cardiology*, vol. 54, no. 5, pp. 410–418, 2009.
- [8] K. Sagawa, "The end-systolic pressure-volume relation of the ventricle: definition, modifications and clinical use." *Circulation*, vol. 63, no. 6, pp. 1223–1227, 1981.



## Bibliography

---

- [9] P. H. Charlton, J. Mariscal Harana, S. Vennin, Y. Li, P. Chowienczyk, and J. Alastruey, "Modeling arterial pulse waves in healthy aging: a database for in silico evaluation of hemodynamics and pulse wave indexes," *American Journal of Physiology-Heart and Circulatory Physiology*, vol. 317, no. 5, pp. H1062–H1085, 2019.
- [10] E. Mikulic, J. N. Cohn, and J. Franciosa, "Comparative hemodynamic effects of inotropic and vasodilator drugs in severe heart failure." *Circulation*, vol. 56, no. 4, pp. 528–533, 1977.
- [11] P. Ostadal, D. Vondrakova, A. Krüger, M. Janotka, and J. Naar, "Continual measurement of arterial dp/dt max enables minimally invasive monitoring of left ventricular contractility in patients with acute heart failure," *Critical Care*, vol. 23, no. 1, pp. 1–8, 2019.
- [12] S. G. De Hert, D. Robert, S. Cromheecke, F. Michard, J. Nijs, and I. E. Rodrigus, "Evaluation of left ventricular function in anesthetized patients using femoral artery dp/dtmax," *Journal of cardiothoracic and vascular anesthesia*, vol. 20, no. 3, pp. 325–330, 2006.
- [13] P. Morimont, B. Lambermont, T. Desaive, N. Janssen, G. Chase, and V. D'Orio, "Arterial dp/dt max accurately reflects left ventricular contractility during shock when adequate vascular filling is achieved," *BMC cardiovascular disorders*, vol. 12, no. 1, p. 13, 2012.
- [14] M. I. M. Garcia, Z. Jian, J. J. Settels, C. Hunley, M. Cecconi, F. Hatib, and M. R. Pinsky, "Performance comparison of ventricular and arterial dp/dt max for assessing left ventricular systolic function during different experimental loading and contractile conditions," *Critical Care*, vol. 22, no. 1, pp. 1–12, 2018.
- [15] J.-M. Tartiere, D. Logeart, F. Beauvais, C. Chavelas, L. Kesri, J.-Y. Tabet, and A. Cohen-solal, "Non-invasive radial pulse wave assessment for the evaluation of left ventricular systolic performance in heart failure," *European journal of heart failure*, vol. 9, no. 5, pp. 477–483, 2007.
- [16] A. Ramesh, C. Kambhampati, J. Monson, and P. Drew, "Artificial intelligence in medicine," *Annals of The Royal College of Surgeons of England*, vol. 86, no. 5, pp. 334–338, Sep. 2004.
- [17] J. M. Huttunen, L. Kärkkäinen, M. Honkala, and H. Lindholm, "Deep learning for prediction of cardiac indices from photoplethysmographic waveform: A virtual database approach," *International Journal for Numerical Methods in Biomedical Engineering*, vol. 36, no. 3, p. e3303, 2020.
- [18] V. Bikia, T. G. Papaioannou, S. Pagoulatou, G. Rovas, E. Oikonomou, G. Siasos, D. Tousoulis, and N. Stergiopoulos, "Noninvasive estimation of aortic hemodynamics and cardiac contractility using machine learning," *Scientific Reports*, vol. 10, no. 1, pp. 1–17, 2020.
- [19] V. Bikia, D. Adamopoulos, S. Pagoulatou, G. Rovas, and N. Stergiopoulos, "Ai-based estimation of end-systolic elastance from arm-pressure and systolic time intervals,"

- Frontiers in Artificial Intelligence*, vol. 4, no. 5, p. 16, 2021. [Online]. Available: <https://www.frontiersin.org/article/10.3389/frai.2021.579541>
- [20] P. Reymond, F. Merenda, F. Perren, D. Rufenacht, and N. Stergiopulos, "Validation of a one-dimensional model of the systemic arterial tree," *American Journal of Physiology-Heart and Circulatory Physiology*, vol. 297, no. 1, pp. H208–H222, 2009.
- [21] G. Langewouters, "The static elastic properties of 45 human thoracic and 20 abdominal aortas in vitro and the parameters of a new model," *J. Biomechanics*, vol. 17, no. 6, pp. 425–435, 1984.
- [22] N. Westerhof, J.-W. Lankhaar, and B. E. Westerhof, "The arterial windkessel," *Medical & biological engineering & computing*, vol. 47, no. 2, pp. 131–141, 2009.
- [23] J. Womersley, *An elastic tube theory of pulse transmission and oscillatory flow in mammalian arteries. Wright Air Development Center Technical Report*. TR 56-6114, Dayton, OH, 1957.
- [24] P. Reymond, Y. Bohraus, F. Perren, F. Lazeyras, and N. Stergiopulos, "Validation of a patient-specific one-dimensional model of the systemic arterial tree," *American Journal of Physiology-Heart and Circulatory Physiology*, vol. 301, no. 3, pp. H1173–H1182, 2011.
- [25] V. Bikia, S. Pagoulatou, B. Trachet, D. Soulis, A. D. Protogerou, T. G. Papaioannou, and N. Stergiopulos, "Noninvasive cardiac output and central systolic pressure from cuff-pressure and pulse wave velocity," *IEEE Journal of Biomedical and Health Informatics*, vol. 24, no. 7, pp. 1968–1981, 2019.
- [26] S. Z. Pagoulatou, V. Bikia, B. Trachet, T. G. Papaioannou, A. D. Protogerou, and N. Stergiopulos, "On the importance of the nonuniform aortic stiffening in the hemodynamics of physiological aging," *American Journal of Physiology-Heart and Circulatory Physiology*, vol. 317, no. 5, pp. H1125–H1133, 2019.
- [27] A. Wolak, H. Gransar, L. E. Thomson, J. D. Friedman, R. Hachamovitch, A. Gutstein, L. J. Shaw, D. Polk, N. D. Wong, R. Saouaf *et al.*, "Aortic size assessment by noncontrast cardiac computed tomography: normal limits by age, gender, and body surface area," *JACC: Cardiovascular Imaging*, vol. 1, no. 2, pp. 200–209, 2008.
- [28] C. M. McEniery, n. Yasmin, I. R. Hall, A. Qasem, I. B. Wilkinson, J. R. Cockcroft, and A. Investigators, "Normal vascular aging: differential effects on wave reflection and aortic pulse wave velocity: the anglo-cardiff collaborative trial (acct)," *Journal of the American College of Cardiology*, vol. 46, no. 9, pp. 1753–1760, 2005.
- [29] H. Senzaki, C.-H. Chen, and D. A. Kass, "Single-beat estimation of end-systolic pressure-volume relation in humans: a new method with the potential for noninvasive application," *Circulation*, vol. 94, no. 10, pp. 2497–2506, 1996.

## Bibliography

---

- [30] M. R. Starling, R. A. Walsh, L. J. Dell'Italia, G. Mancini, J. Lasher, and J. Lancaster, "The relationship of various measures of end-systole to left ventricular maximum time-varying elastance in man." *Circulation*, vol. 76, no. 1, pp. 32–43, 1987.
- [31] P. Segers, E. Rietzschel, M. De Buyzere, N. Stergiopoulos, N. Westerhof, L. Van Bortel, T. Gillebert, and P. Verdonck, "Three-and four-element windkessel models: assessment of their fitting performance in a large cohort of healthy middle-aged individuals," *Proceedings of the Institution of Mechanical Engineers, Part H: Journal of Engineering in Medicine*, vol. 222, no. 4, pp. 417–428, 2008.
- [32] A. Dogui, N. Kachenoura, F. Frouin, M. Lefort, A. De Cesare, E. Mousseaux, and A. Herment, "Consistency of aortic distensibility and pulse wave velocity estimates with respect to the Bramwell-Hill theoretical model: a cardiovascular magnetic resonance study," *Journal of Cardiovascular Magnetic Resonance*, vol. 13, no. 1, p. 11, 2011.
- [33] N. Gaddum, J. Alastruey, P. Beerbaum, P. Chowienczyk, and T. Schaeffter, "A technical assessment of pulse wave velocity algorithms applied to non-invasive arterial waveforms," *Annals of biomedical engineering*, vol. 41, no. 12, pp. 2617–2629, 2013.
- [34] A. Paszke, S. Gross, F. Massa, A. Lerer, J. Bradbury, G. Chanan, T. Killeen, Z. Lin, N. Gimelshein, L. Antiga, A. Desmaison, A. Kopf, E. Yang, Z. DeVito, M. Raison, A. Tejani, S. Chilamkurthy, B. Steiner, L. Fang, J. Bai, and S. Chintala, "Pytorch: An imperative style, high-performance deep learning library," in *Advances in Neural Information Processing Systems 32*. Curran Associates, Inc., 2019, pp. 8024–8035.
- [35] V. Bikia, M. Lazaroska, D. Scherrer Ma, M. Zhao, G. Rovas, S. Pagoulatou, and N. Stergiopoulos, "Estimation of left ventricular end-systolic elastance from peripheral pressure waveform via deep learning," *Frontiers in Bioengineering and Biotechnology*, Accepted 2021.
- [36] D. P. Kingma and J. Ba, "Adam: a method for stochastic optimization," San Diego, US, 2017. [Online]. Available: <https://arxiv.org/pdf/1412.6980.pdf>
- [37] J. M. Bland and D. G. Altman, "Statistical methods for assessing agreement between two methods of clinical measurement," *International journal of nursing studies*, vol. 47, no. 8, pp. 931–936, 2010.
- [38] N. Westerhof, N. Stergiopoulos, M. I. Noble, and B. E. Westerhof, *Snapshots of hemodynamics: an aid for clinical research and graduate education*. Springer, 2018.
- [39] C.-H. Chen, B. Fetcs, E. Nevo, C. E. Rochitte, K.-R. Chiou, P.-A. Ding, M. Kawaguchi, and D. A. Kass, "Noninvasive single-beat determination of left ventricular end-systolic elastance in humans," *Journal of the American College of Cardiology*, vol. 38, no. 7, pp. 2028–2034, 2001.

- [40] T. Shishido, K. Hayashi, K. Shigemi, T. Sato, M. Sugimachi, and K. Sunagawa, "Single-beat estimation of end-systolic elastance using bilinearly approximated time-varying elastance curve," *Circulation*, vol. 102, no. 16, pp. 1983–1989, 2000.
- [41] S. Pagoulatou, K.-P. Rommel, K.-P. Kresoja, M. von Roeder, P. Lurz, H. Thiele, V. Bikia, G. Rovas, D. Adamopoulos, and N. Stergiopoulos, "In vivo application and validation of a novel noninvasive method to estimate the end-systolic elastance," *American Journal of Physiology-Heart and Circulatory Physiology*, vol. 320, no. 4, pp. H1543–H1553, 2021.

## **Bibliography**

---

## Chapter 7

---

# Determination of aortic characteristic impedance and total arterial compliance from regional pulse wave velocities using machine learning

Vasiliki Bikia<sup>1</sup>, Georgios Rovas<sup>1</sup>, Stamatia Pagoulatou<sup>1</sup>, Nikolaos Stergiopoulos<sup>1</sup>

<sup>1</sup> *Institute of Bioengineering, École Polytechnique Fédérale de Lausanne, Switzerland*

Published in *Frontiers in Bioengineering and Biotechnology*, 2021.

### Abstract

In vivo assessment of aortic characteristic impedance ( $Z_{ao}$ ) and total arterial compliance ( $C_T$ ) has been hampered by the need for invasive methods to access simultaneous recordings of aortic pressure and flow, wall thickness, and cross-sectional area. In contrast, regional pulse wave velocity (PWV) measurements are non-invasive and clinically available. In this study, we present a non-invasive method for estimating  $Z_{ao}$  and  $C_T$  using cuff pressure, carotid-femoral PWV, and carotid-radial PWV. Regression analysis is employed for both  $Z_{ao}$  and  $C_T$ . The regression models are trained and tested using a pool of virtual subjects ( $n = 3,818$ ) generated from a previously validated in silico model. Predictions achieved an accuracy of 3.25 %,  $r = 0.98$ , and 3 %,  $r = 0.99$ , for  $Z_{ao}$ , and  $C_T$ , respectively. The proposed approach constitutes a step forward to the non-invasive screening of elastic vascular properties in humans by exploiting easily obtained measurements. This study could introduce a valuable tool for assessing arterial stiffness reducing the cost and the complexity of the required measuring techniques. Further clinical studies are required to validate the method in vivo.

## **7.1 Introduction**

Aging and vascular pathologies lead to changes in the elastic properties and the hemodynamics of the arterial network [1; 2; 3; 4]. These changes have been shown to be highly associated with increased cardiovascular risk or mortality [2; 3]. In this respect, the assessment of the arterial stiffness is increasingly used in the clinical evaluation of a patient. Proximal aortic characteristic impedance ( $Z_{ao}$ ) and total arterial compliance ( $C_T$ ) are two powerful indices for assessing the elastic properties of the proximal aorta and the entire arterial tree, respectively [5; 1].

The impedance can be defined as the ratio of the pulsatile components of pressure and flow. The impedance computed in the ascending aorta is defined as input impedance ( $Z_{in}$ ), and is a global systemic parameter, which encompasses all effects of wave travel and reflections of the arterial part which is distal to the point of measurement. For a reflectionless system  $Z_{in}$  reduces to  $Z_{ao}$ . The  $Z_{ao}$  is a cardinal parameter related to aortic stiffness and geometry. Prior art has included invasive [6; 7; 8; 9; 10; 11; 12; 13; 14] and non-invasive [13; 15; 16] techniques for estimating  $Z_{ao}$  in the frequency domain, whereby  $Z_{ao}$  is approximated as the average  $Z_{in}$  in the mid-to-high frequency range, the underlying assumption being that in those frequencies the effects of reflected waves are minimal. Other approaches have proposed time-domain calculations of the  $Z_{ao}$  based on the early systolic part of pressure and flow waveforms [17; 18; 19; 12], when reflections are considered negligible. All of the above frequency and time domain methods require simultaneous recordings of pressure and flow in the aorta, which are invasive (pressure) or inconvenient and expensive (flow).

$C_T$  is a major global elastic property of the arterial system, being a determinant of the cardiac afterload, and has significant pathophysiological relevance [20; 21; 22; 23]. It quantifies the capacity of the vessels to expand under internal pressure and store blood during systole without excessive pressure rise. Importantly,  $C_T$  is a significant determinant of central blood pressure and decrease in  $C_T$  is associated with hypertension. However, direct in vivo non-invasive measurement of  $C_T$  cannot be performed. Various methods have suggested the indirect estimation of  $C_T$  [18; 24; 25; 5] using simultaneous recordings of the proximal aortic pressure and flow or cardiac output.

Precise measurement of the  $Z_{ao}$  and  $C_T$  may increase understanding of arterial physiopathology and provide additional clinical markers for cardiovascular risk assessment. Yet, despite the significant body of research, the invasive nature or/and the complexity of the current methods have limited their applicability in every day clinical practice, while other surrogates of regional arterial stiffness have been used more often [5; 26]. Thus, a technique that offers a reliable, non-invasive, fast, and simple-to-use estimation of  $Z_{ao}$  and  $C_T$  is still highly desirable. In view of this need, this study proposes a novel methodology to evaluate  $Z_{ao}$  and  $C_T$  using machine learning.

In our previous work, we demonstrated that the combination of in silico data with machine learning modelling allows for validating a methodology to predict aortic hemodynamics and cardiac contractility [27]. This approach can be easily extended and adapted in the estimation of different cardiovascular quantities and case studies, such the one introduced in this work. In particular, this paper proposes a method which derives  $Z_{ao}$  and  $C_T$  from brachial blood pressure (cuff BP) and regional PWV measurements, while it does not require central pressure or flow data. To assess the validity of this concept, the introduced methodology was tested using an in silico population generated by a previously validated cardiovascular simulator. The schematic representation of the regression pipeline is illustrated in Figure 7.1.

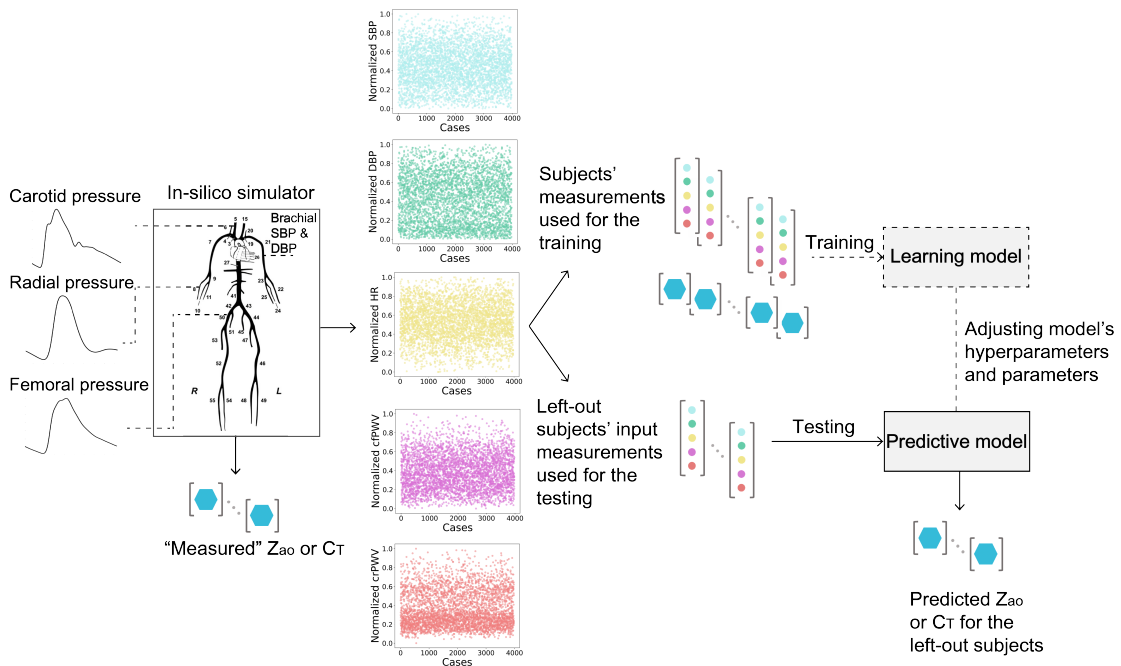


Figure 7.1 – Schematic representation of the training/testing pipeline for predicting aortic characteristic impedance ( $Z_{ao}$ ), and total arterial compliance ( $C_T$ ). SBP, systolic blood pressure; DBP, diastolic blood pressure; HR, heart rate; crPWV, carotid-femoral pulse wave velocity; crPWV, carotid-radial pulse wave velocity. Adapted from [28].

## 7.2 Methods & materials

### In silico dataset

In this study, we used a synthetic dataset which was designed to simulate various hemodynamical states. Different hemodynamic cases ( $n = 3,818$ ), representing both normotensive and hypertensive adults, were simulated by altering key cardiac and systemic parameters of a previously validated in silico cardiovascular model. The mathematical model (Figure 7.2) has been well described in the original publication [29]. Literature data are only presented in terms



## Chapter 7. Determination of aortic characteristic impedance and total arterial compliance from regional pulse wave velocities using machine learning

of mean and standard deviation or/and minimum and maximum values; thus, variation of the model's parameters was performed with random Gaussian sampling. Cardiac parameters were modified and different cardiac output values were simulated. Arterial geometry (i.e. arterial length and diameter) was modified to represent various arterial tree sizes and body types [30; 31]. Total peripheral resistance and arterial compliance were altered according to the literature [32; 33; 34]. To simulate older or hypertensive individuals, in some cases, stiffening in the aorta was considered as nonuniform and more pronounced as described in our previous works [35; 36]. For a given set of input parameters, the model provides analytical solutions of the pressure and flow at every arterial segment. The physiological validity of each subject was assessed by comparing the simulated brachial and aortic systolic BP (SBP), DBP, MAP, and pulse pressure (PP) to the reference values reported in the previously published data by McEniery [37] (normotensive cases) and Bordin Pelazza and Filho [38] (hypertensive cases). A subject was removed from the dataset if any of the BP values lied out of the 99.5 % confidence intervals ( $\text{mean} \pm 2.807 \text{ SD}$ ).

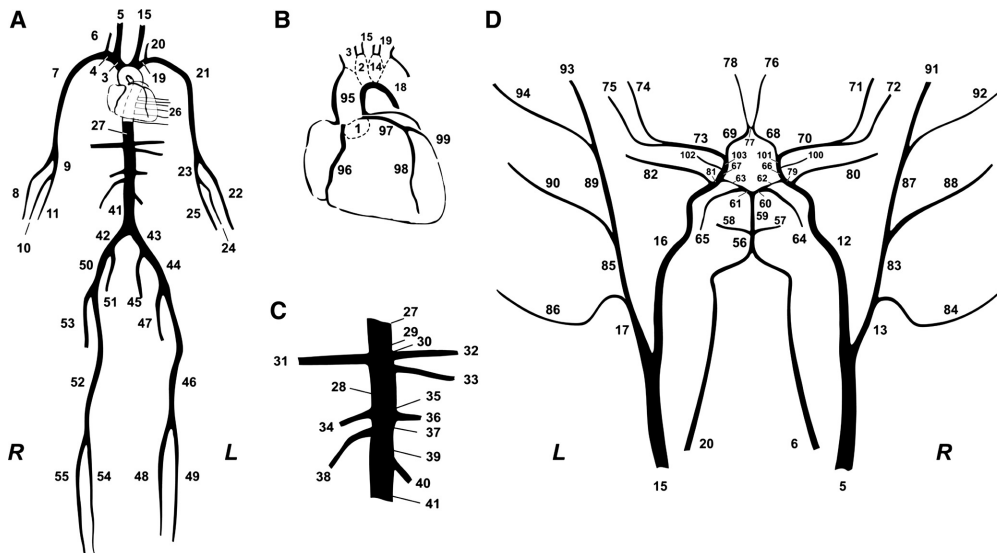


Figure 7.2 – The 1-D cardiovascular model that was used for the data generation. Adapted from [28].

### Computation of $Z_{ao}$ and $C_T$

The characteristic impedance at the root of the ascending aorta was calculated analytically using the area compliance and the geometry of the ascending aorta, namely:

$$Z_{ao} = \sqrt{\frac{\rho}{A} \frac{1}{C_A}} \quad (7.1)$$

where  $\rho$  is the blood density equal to  $1,050 \text{ kg/m}^3$ ,  $A$  is the cross-sectional area of the ascending

aorta, and  $C_A$  is the area compliance of the ascending aorta, respectively.

The  $C_T$  was computed as the sum of volume compliance ( $c_i$ ) of all the arterial segments included in the 1-D model ( $n = 103$ ) and the terminal compliances described by the terminal Windkessel models, namely:

$$C_T = \sum_i^{103} c_i. \quad (7.2)$$

### Regional PWV and BP data

The carotid-femoral pulse wave velocity (cfPWV) and carotid-radial pulse wave velocity (crPWV) were calculated by a foot-to-foot algorithm using the tangential method. Pulse transit times were computed between the two arterial sites, namely the left carotid and left femoral artery, and the left carotid and the left radial artery, respectively. Formally, the tangential method uses the intersection point of two tangents on the arterial pressure wave, i.e. the tangent passing through the systolic upstroke and the horizontal line passing through the minimum of the pressure wave as previously described [39]. The travel lengths were determined by summation of the lengths of the arterial segments within the transmission paths. Next, the value of each PWV was calculated by dividing the total travel length by the pulse transit time. Brachial systolic (brSBP) and diastolic BP (brDBP) were derived from the pressure waveform at the left brachial artery.

### Regression Analysis

The simulated data, i.e. brSBP, brDBP, heart rate (HR), cfPWV, crPWV,  $Z_{ao}$ , and  $C_T$ , were organized in pairs (inputs: brSBP, brDBP, HR, cfPWV, crPWV, and outputs:  $Z_{ao}$ ,  $C_T$ ) and were kept for the training/testing process. All the data were corrupted with artificial noise in order to simulate potential measurement errors that often occur in the respective clinical measurements. The noise allows for essentially harming the deterministic effect of the 1-D computer model. Errors in measurements were simulated with a random distribution. In particular, the error for each variable was randomly drawn from the range of  $[-15, 15]$  % (simulating a maximum absolute noise level equal to 15 %). Subsequently, each variable value was multiplied with a noise factor; for instance, for a randomly selected error of  $-6$  %, the respective variable value was multiplied with a noise factor equal to 0.94.

The data were partitioned into three subsets: (i) the train set, the set of training examples the model is trained on, (ii) the validation set, which is used to tune the hyperparameters, and (iii) the test set, which is used to test the trained model while it measures the generalization performance. In our analysis, the train/validation/test split was selected to be 60 %/20 %/20 %.

## Chapter 7. Determination of aortic characteristic impedance and total arterial compliance from regional pulse wave velocities using machine learning

---

Table 7.1 – List of the selected hyperparameters for the predictive models.

Output variable	Selected hyperparameters	
	RFR: max_depth	ANN: epochs
$Z_{ao}$	8	55
$C_T$	8	103

These percentages corresponded to 2,290/764/764 data instances, respectively. The data were normalized using `MinMaxScaler()` function from `sklearn` library. For the regression process, we used a Random Forest modelling procedure [40] and an Artificial Neural Network (ANN) to estimate the target variables of interest. The formal structure of the Random Forest Regressor (RFR) is shown in Figure 7.3. An RFR is a predictor consisting of a collection of randomized base regression trees. These random trees are combined to form the aggregated regression estimate:

$$\overline{r}_n(\mathbf{X}) = \mathbb{E}_{\Theta}[r_n(\mathbf{X}, \Theta)], \quad (7.3)$$

where  $\mathbb{E}_{\Theta}[\cdot]$  denotes expectation with respect to the random parameter, conditionally on  $\mathbf{X}$  (matrix consisting of the input features), and  $\Theta = [\Theta_1, \dots, \Theta_N]$  are independent and identically distributed (i.i.d.) random variables outputs of each tree. The estimations were provided by aggregating the individual predictions of each tree. The trees were grown by applying bootstrapping. Based on the training data, each regression tree grew for each of the bootstrap samples. Estimators were randomly sampled and the best split was chosen at each node.

A formal representation of an ANN is illustrated in Figure 7.4. Our ANN was composed of an input layer, a hidden layer, and an output layer. Typically, the input layer sequentially receives the input features as an input vector into the ANN. The hidden layer has multiple neurons connected to the input layer with weights. Each neuron is characterized by a transfer function of neuron (Figure 7.4). The training of ANN is conducted by determining the difference between the processed output of the network and the target output, namely the error. Training data are fed to the input layer and continue to the succeeding hidden layer, where they pass through the neurons' transfer functions, until they finally arrive radically transformed at the output layer. During training, the network continually adjusts its weights and thresholds until the ANN produces output which is increasingly similar to the target output (errors are minimized). In our analysis, the training set was employed to optimize the weights of neurons in the hidden and output layer using the Adam optimizer [41]. Upon tuning, the samples of the test set were used as input to the optimized ANN to obtain the estimated  $Z_{ao}$  and  $C_T$ .

A critical issue while training a machine learning model on the sample data is overfitting. For instance, when the number of epochs used to train an ANN is more than necessary, the training model learns patterns that are specific to the sample data to a great extent. In that

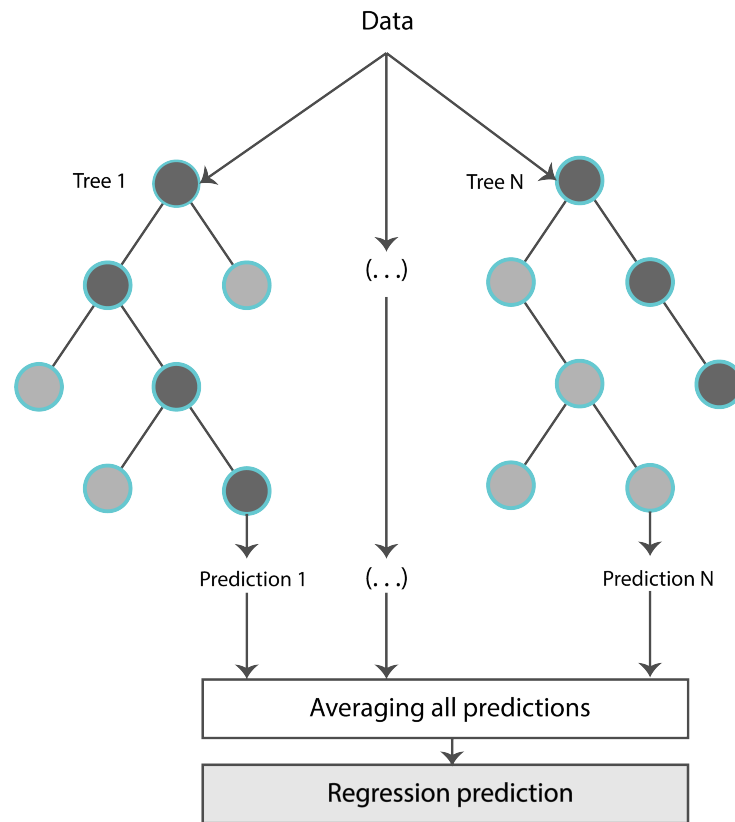


Figure 7.3 – Typical representation of a random forest regression model. Adapted from [28].

case, the model is incapable to perform well on a new dataset. In other words, the model loses generalization capacity by overfitting to the specific training data. To mitigate overfitting and to increase the generalization capacity, the model should be trained for optimal hyperparameter values.

For the RFR, we selected 100 estimators (namely the number of trees in the forest), while we decided to optimize the value for `max_depth` (the maximum depth of the tree). For the ANN, the `batch_size` (the number of samples that will be propagated through the network) was set to be equal to 10, and the number of epochs was optimized, respectively. The number of epochs is a hyperparameter that defines the number of times that the learning algorithm will work through the entire training dataset. By optimizing only one hyperparameter, we keep the complexity of the models low, and thus the models are more likely to perform well on new data and are less restricted to the peculiarities of the particular data used.

For selecting the optimal value for `max_depth`, we calculated the train score and the validation score for various values of `max_depth` in the range of [1, 10]. The score for RFR indicates the coefficient of determination  $R^2$  for the predictions. Subsequently, for each target output variable, the `max_depth` value with the maximum score was selected. In a similar manner,

## Chapter 7. Determination of aortic characteristic impedance and total arterial compliance from regional pulse wave velocities using machine learning

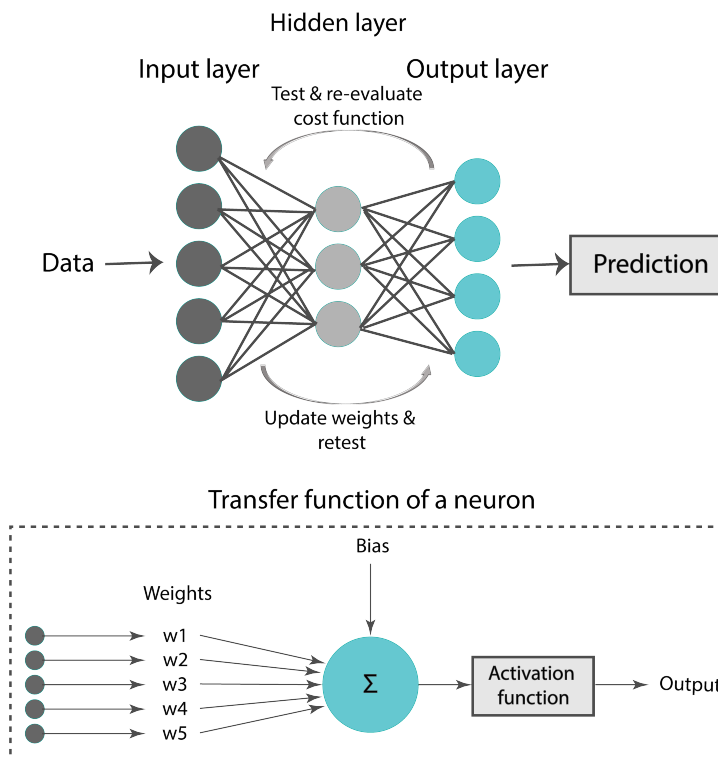


Figure 7.4 – Typical representation of an artificial neural network. Adapted from [28].

the train and validation losses [i.e. mean square error (MSE)] were calculated for the ANN. In that case, loss values can be monitored by Early stopping call back function. When there is an increment observed in loss values, training comes to halt and the respective value of epoch indicates the optimal selection. For both  $Z_{ao}$  and  $C_T$ , the highest accuracy was reported for the RFR with  $\text{max\_depth} = 8$ , whereas for ANN, training stopped at  $55^{\text{th}}$  epoch and  $103^{\text{rd}}$  epoch for  $Z_{ao}$  and  $C_T$ , respectively. Therefore, the optimal number of epochs was set to 55 and 103 for the two estimators, respectively. All optimized hyperparameters are presented in Table 7.1. Subsequently, we plotted the respective learning curves for the RFRs using the optimal hyperparameters (Figures 7.5A,B). Each learning curve was fitted using the observed accuracy [in terms of root mean square error (RMSE)] according to a given training sample size. The training size was modified from 1 to 95 % of the total number of training data instances (20 samples of training size). The training error was low, and thus the training data appear to fit well by the models (low bias). Furthermore, low variance was indicated by the small gap between the two curves. Finally, the testing set was fed into the trained RFR to estimate  $Z_{ao}$ , and  $C_T$  and the precision was evaluated.

Along with the main model configuration, which uses as inputs brSBP, brDBP, HR, cfPWV, and

crPWV (M1), we additionally evaluated three additional model configurations using different sets of inputs: (i) one which does not include HR as an input (M2), (ii) a second one that excludes HR and replaces brSBP and brDBP with MAP (M3), and (iii) a third one that uses only the PWV values (M4). The hyperparameters values were set equal to the same values as those of M1.

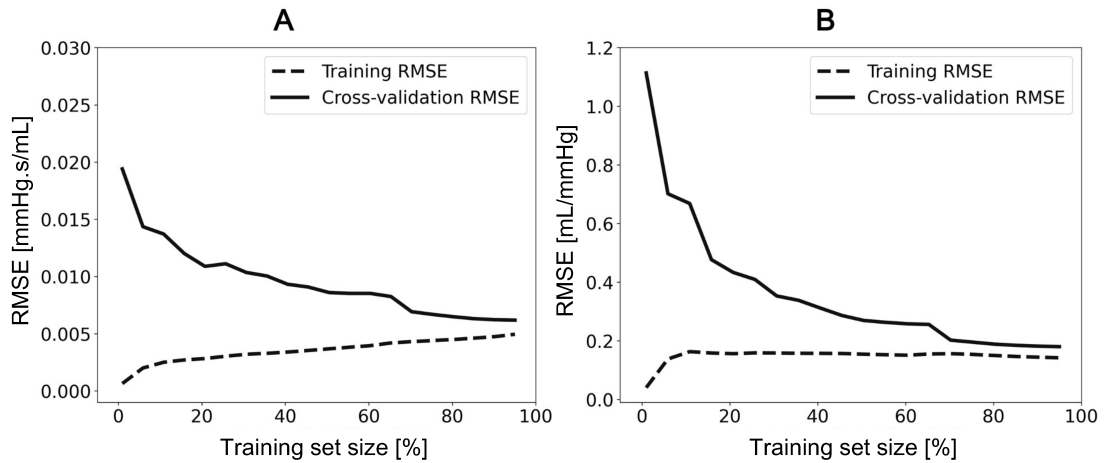


Figure 7.5 – Learning curves presenting the impact of the number of data instances on the RFR's performance for  $Z_{ao}$  (A) and  $C_T$  (B). Adapted from [28].

Furthermore, we assessed the importance of each input feature using the permutation feature importances [42] for RFR. The concept of permutation feature importances relies on measuring the importance of a feature by calculating the increase in the prediction error after permuting the feature. The permutation importances were computed by shuffling the values of each feature on the test set and by estimating the RMSE after the permutation. This process was repeated 20 times and the mean and standard deviation of the increase in RMSE were reported.

The training/testing pipeline and the post-analysis were implemented using the Scikit-learn library [43] in a Python programming environment (Python Software Foundation, Python Language Reference, version 3.6.8, Available at <http://www.python.org>). The Pandas and NumPy packages were also used [44; 45].

### Sensitivity to training data size

The number of data instances used for training, namely the training size, has a major effect on the accuracy of the model's predictions. The model's precision as a function of the number of training samples was evaluated by conducting sensitivity analysis. In this respect, the regression analysis for RFR was repeated and the RMSE was calculated after decreasing the

## Chapter 7. Determination of aortic characteristic impedance and total arterial compliance from regional pulse wave velocities using machine learning

---

training size ( $n = 2,290$ ) from 99 to 1 % of the total number of cases. The accuracy was compared using the same testing population (764 subjects).

### Comparison to prior art

We compared our RFR with prior methods that provide estimates of  $Z_{ao}$  and  $C_T$ . Application of previous methods required the central (aortic) blood pressure and flow waves. Systolic and diastolic phases were defined by the dicrotic notch from the central blood pressure waveforms and the first zero crossing for blood flow waves. Automated detection of the peaks and minima was performed using an in-house custom software in Matlab (Mathworks, Natick, Massachusetts, United States). The  $Z_{ao}$  was computed using two previously described methods:

- Time-derivative peaks method:

$$Z_{ao} = P'_{max} / Q'_{max},$$

where  $P'_{max}$  and  $Q'_{max}$  are the maximum values of the pressure and flow time derivatives, respectively [12].

- Peak flow method:

$$Z_{ao} = \frac{P_{Qmax} - aDBP}{Q_{max}},$$

where  $aDBP$  is the aortic DBP,  $Q_{max}$  is the maximum flow value, and  $P_{Qmax}$  is the aortic pressure magnitude at the maximum flow value [12].

The  $C_T$  was derived using the following previously proposed techniques:

- Decay time method: The decay time method (DTM) is based on the two-element Windkessel (WK) model of the systemic circulation. Its principle is that during diastole there is no inflow from the heart, and thus, the decrease of aortic pressure, is characterized by the decay time. This decay can be fitted monoexponentially to any portion of the diastole to yield the characteristic time or time constant, which is  $RC_T$ . The  $C_T$  can be then calculated for a known value of peripheral resistance (R) [46].
- Pulse pressure method: The pulse pressure method (PPM) [47] is based on the fact that the modulus of the input impedance of the arterial system is represented very well by the two-element WK model for the low frequencies ( $1^{st}$ - $5^{th}$  harmonic). Therefore, the pulse pressure will be similar in the true arterial system and the two-element WK model. The PPM uses an iterative process that yields the value of  $C_T$  that gives the best fit between

the measured pulse pressure and the pulse pressure predicted by the two-element WK model.

We applied the aforementioned methods on the test data ( $n = 764$ ) and compared the estimates to the machine learning-derived predictions. The reason that we did not apply the above methods to the entire dataset was to compare these methods and the machine learning model on the exact same test population. Artificial random noise of the same order of magnitude ( $\pm 15\%$ ) was also considered for the data used for the techniques above. The pressure and flow signals were uniformly multiplied by a scaling factor which was randomly selected as described in the Regression analysis section.

### Statistical analysis

Data are presented as mean and standard deviation (SD). The agreement, bias, and precision between the model predictions and the reference values were assessed by using the Pearson's correlation coefficient ( $r$ ), the RMSE, the normalized RMSE (nRMSE), and the Bland-Altman analysis [48]. The nRMSE was based on the difference between the minimum and maximum values of the dependent variable ( $y$ ) and was computed as  $\text{RMSE}/(y_{\max}-y_{\min})$ . We performed linear least squares regression for the predictions and the reference data. The slope and the intercept of the regression line were reported. Two-sided  $P$ -value for a hypothesis test whose null hypothesis is that the slope is zero, using Wald Test with  $t$ -distribution of the test statistic, was calculated. The  $P$ -value  $< 0.05$  were considered as significant. The statistical analysis was implemented in Python (Python Software Foundation, Python Language Reference, version 3.6.8, Available at <http://www.python.org>).

## 7.3 Results

The distributions of the cardiovascular parameters of the virtual study cohort are presented in Table 7.2. The correlations between the input features and the target output values are also given in Table 7.3. The highest values of Pearson's correlation coefficient were reported between  $Z_{ao}/C_T$  and the two PWV values ( $r \geq 0.84$ ).

### Comparison of model predictions to the reference values

We compared the RFR and ANN estimations to the reference data for each target output. Table 7.4 tabulates the metrics for the performance assessment of the evaluation scheme for all model configurations. The results for the RFR M1 and ANN M1, which correspond to the best-performing configurations, are visualized below. The scatterplot between the RFR-predicted and the actual  $Z_{ao}$  values is given in Figure 7.6 (top panel). The Bland-Altman plot is provided in Figure 7.6 (lower panel), in which zero bias was reported. The limits of



## Chapter 7. Determination of aortic characteristic impedance and total arterial compliance from regional pulse wave velocities using machine learning

Table 7.2 – Summary of the cardiovascular characteristics of the virtual study cohort (n = 3,818).

Variable	Value (n = 3,818)
Brachial systolic blood pressure [mmHg]	134.51±24.1
Brachial diastolic blood pressure [mmHg]	77.27±21.31
Brachial pulse pressure [mmHg]	57.24±22.58
MAP [mmHg]	94.51±20.29
Aortic systolic blood pressure [mmHg]	122.54±23.73
Aortic diastolic blood pressure [mmHg]	80.5±21.48
Aortic pulse pressure [mmHg]	42.04±19.38
Stroke volume [mL]	81.18±8.03
Heart rate [bpm]	73.26±14.9
Aortic impedance [mmHg.s/mL]	0.056±0.012
Total arterial compliance [mL/mmHg]	1.14±0.47
Total peripheral resistance [mmHg.s/mL]	0.98±0.21
Carotid-femoral PWV [m/s]	8.06±1.03
Carotid-radial PWV [m/s]	10.17±1.3

agreement (LoA), within which 95 % of errors are expected to lie, were found to be equal to  $\pm 0.012$  mmHg.s/mL. Figure 7.7 illustrates the  $C_T$  predictions in comparison to their reference values. Again, bias was close to zero ( $-0.01$  mL/mmHg), while the LoA were equal to  $\pm 0.4$  mL/mmHg. The scatterplot and Bland-Altman plot for the ANN are shown in Figures 7.8 and 7.9 for  $Z_{ao}$  and  $C_T$  respectively. For  $Z_{ao}$ , the ANN-LoA were  $(-0.013, 0.010)$  mmHg.s/mL, whereas for  $C_T$  predictions, the ANN-LoA found to be subtly narrower than the RFR and equal to  $\pm 0.3$  mL/mmHg. For both machine learning approaches, no biases were reported. The mean difference between the  $Z_{ao}$  predictions and the ground truth  $Z_{ao}$  values lied within a similar range for the two models, i.e.  $(-0.012, 0.012)$  and  $(-0.013, 0.010)$  mmHg.s/mL for RFR and ANN, respectively. The LoA of the  $C_T$ -RFR  $[(-0.39, 0.37)$  mL/mmHg] were slightly broader than the LoA of the  $C_T$ -ANN estimator  $[(-0.32, 0.33)$  mL/mmHg]. Substantially higher errors were reported when the BP information was omitted from the inputs, especially for the  $Z_{ao}$  prediction (correlation was around to 0.75). Table 7.5 presents the feature importances of the input regressors for  $Z_{ao}$  and  $C_T$ , respectively. For  $Z_{ao}$ , brDBP appeared to have the highest importance level followed by brSBP and crPWV. In the case of  $C_T$ , brDBP was reported to have the dominant importance value, followed by cfPWV and crPWV.

### Sensitivity to training data size

The nRMSEs decreased gradually with increasing training size (Figure 7.10). Errors in  $Z_{ao}$  were higher than 8 % for a training dataset with 687 subjects or less. The nRMSE of the  $C_T$  predictions exceeded 8 % when the training size was smaller than 458 data instances. It was

Table 7.3 – Correlation between the input features and the target outputs.

Parameters	<i>r</i> (n = 3,818)
brSBP/ $Z_{ao}$	0.51
brDBP/ $Z_{ao}$	-0.41
HR/ $Z_{ao}$	0.17
cfPWV/ $Z_{ao}$	0.87
crPWV/ $Z_{ao}$	0.85
brSBP/ $C_T$	-0.48
brDBP/ $C_T$	0.39
HR/ $C_T$	-0.16
cfPWV/ $C_T$	-0.87
crPWV/ $C_T$	-0.84

observed that, for both curves, addition of new data points had no significant impact on the accuracy after reaching the 20 % of the entire training population (corresponding to 458 subjects).

### Comparison to prior art

Table 7.6 presents the comparison between our proposed PWV-based machine learning models and a list of previously published methods, which, in contrast to our method, use the central aortic blood pressure and flow waveforms. The PWV-based machine learning estimators for  $Z_{ao}$  outperformed all the other methods achieving a correlation of 0.9. The peak flow method and the time-derivative peaks method demonstrated lower accuracy ( $r \leq 0.79$  and broader LoA). Estimation techniques for  $C_T$  yielded correlation coefficients equal or higher than 0.93.

## 7.4 Discussion

The  $Z_{ao}$  contributes to the pulsatile arterial load faced by heart during ejection and has been shown to be an independent predictor of LV mass index in hypertension [49]. Moreover,  $C_T$  offers a valuable assessment not only for cardiovascular (CV) risk, but also for the relationship between structural and functional changes in the arterial system with respect to its elasticity [50]. In a progressively aging population, effective monitoring of powerful biomarkers, such as  $Z_{ao}$  and  $C_T$ , is imperative. Despite the great efforts for monitoring several biomarkers for arterial stiffness, there is evidence that the prognostic value of arterial stiffness as assessed by current techniques might be compromised in the elderly or special populations [51; 52; 53; 54]. Furthermore, there are methods, such as the pulse contour techniques for minimally invasive cardiac output monitoring, which are dependent on  $C_T$  [55].

**Chapter 7. Determination of aortic characteristic impedance and total arterial compliance from regional pulse wave velocities using machine learning**

Table 7.4 – Regression statistics between model predictions and reference values.

Model	Slope	Intercept	<i>r</i>	<i>P</i> -value	RMSE	nRMSE
RFR <sub>Z<sub>ao</sub></sub> M1	0.77	0.012 mmHg.s/mL	0.89	<0.001	0.006 mmHg.s/mL	7.78 %
RFR <sub>Z<sub>ao</sub></sub> M2	0.77	0.013 mmHg.s/mL	0.89	<0.001	0.006 mmHg.s/mL	7.77 %
RFR <sub>Z<sub>ao</sub></sub> M3	0.66	0.019 mmHg.s/mL	0.81	<0.001	0.008 mmHg.s/mL	9.91 %
RFR <sub>Z<sub>ao</sub></sub> M4	0.55	0.025 mmHg.s/mL	0.75	<0.001	0.009 mmHg.s/mL	11.20 %
RFR <sub>C<sub>T</sub></sub> M1	0.81	0.21 mL/mmHg	0.93	<0.001	0.19 mL/mmHg	7.31 %
RFR <sub>C<sub>T</sub></sub> M2	0.80	0.22 mL/mmHg	0.93	<0.001	0.19 mL/mmHg	7.37 %
RFR <sub>C<sub>T</sub></sub> M3	0.73	0.31 mL/mmHg	0.88	<0.001	0.24 mL/mmHg	9.21 %
RFR <sub>C<sub>T</sub></sub> M4	0.63	0.42 mL/mmHg	0.82	<0.001	0.29 mL/mmHg	11.11 %
ANN <sub>Z<sub>ao</sub></sub> M1	0.86	0.007 mmHg.s/mL	0.90	<0.001	0.006 mmHg.s/mL	7.47 %
ANN <sub>Z<sub>ao</sub></sub> M2	0.77	0.012 mmHg.s/mL	0.90	<0.001	0.006 mmHg.s/mL	7.40 %
ANN <sub>Z<sub>ao</sub></sub> M3	0.69	0.016 mmHg.s/mL	0.83	<0.001	0.008 mmHg.s/mL	9.60 %
ANN <sub>Z<sub>ao</sub></sub> M4	0.56	0.022 mmHg.s/mL	0.76	<0.001	0.009 mmHg.s/mL	11.28 %
ANN <sub>C<sub>T</sub></sub> M1	0.88	0.14 mL/mmHg	0.95	<0.001	0.16 mL/mmHg	6.26 %
ANN <sub>C<sub>T</sub></sub> M2	0.89	0.17 mL/mmHg	0.94	<0.001	0.18 mL/mmHg	6.87 %
ANN <sub>C<sub>T</sub></sub> M3	0.75	0.29 mL/mmHg	0.88	<0.001	0.24 mL/mmHg	9.29 %
ANN <sub>C<sub>T</sub></sub> M4	0.64	0.45 mL/mmHg	0.83	<0.001	0.29 mL/mmHg	10.94 %

Table 7.5 – Feature importances for the prediction of Z<sub>ao</sub> and C<sub>T</sub> using RFR.

Feature	Permutation importance	
	Z <sub>ao</sub> [mmHg.s/mL]	C <sub>T</sub> [mL/mmHg]
Brachial SB	0.0031±0.0002	0.09±0.01
Brachial DB	0.0058±0.0002	0.21±0.01
Heart rate	0.0001±0.0000	0.01±0.00
Carotid-femoral PWV	0.0016±0.0001	0.13±0.01
Carotid-radial PWV	0.0021±0.0001	0.12±0.01

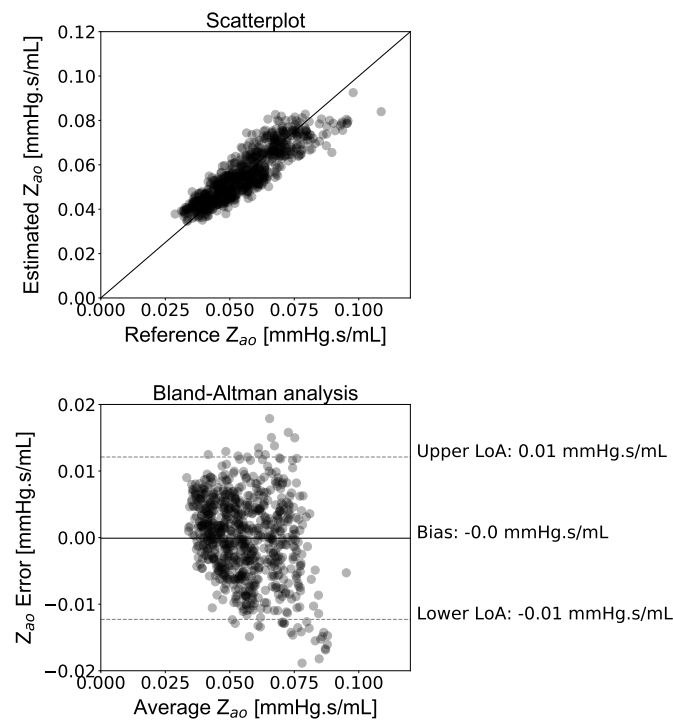


Figure 7.6 – Comparison between the estimated and the reference  $Z_{ao}$  data. Scatterplot and Bland–Altman plot between the estimated  $Z_{ao}$  and the reference  $Z_{ao}$  using the RFR. The solid line of the scatterplot represents equality. In Bland–Altman plot, limits of agreement (LoA) are defined by the two horizontal dashed lines. Adapted from [28].

Measurement of PWV can be utilized for the estimation of both local [56; 57] and regional arterial distensibility [58]. The evaluation of PWV is based on the estimation of the pulse transit time between two arterial sites, and the measurement of the distance between them. There is emerging evidence supporting that aortic PWV, i.e. cfPWV, is an independent predictor of CV risk [26; 59]. Likewise, the peripheral PWV, e.g. crPWV, has been shown to be an informative indicator of vasodilator reserve and a predictor of coronary artery disease [60]. Despite the widespread acceptance of PWV, we should not be detracted from the fact that PWV per se is still an indirect measure of the arterial properties and provides no immediate measure of the adverse effects of vascular stiffening on circulatory hemodynamics. For instance, although PWV might be often clinically relevant, it is not the sole determinant of the timing and consequences of the reflected waves [61; 62]. The  $C_T$  may be physiologically more relevant than regional or local arterial compliance surrogate (such as PWVs), in terms of modulation of cardiac load, LV function, and CV risk assessment. In particular, the  $C_T$  can have greater impact in assessing elderly population or individuals with increased vascular stiffness, where PWV appears to have limited prognostic value. Moreover,  $Z_{ao}$  has been associated with cases of increased cardiac and cerebral mortality [2; 59]. On the other hand, PWV is computed between two arterial sites, and thus cannot provide a global description of the arterial network as  $Z_{ao}$  does. Evidence reported by Segers et al. [16] presents that measurement of central

## Chapter 7. Determination of aortic characteristic impedance and total arterial compliance from regional pulse wave velocities using machine learning

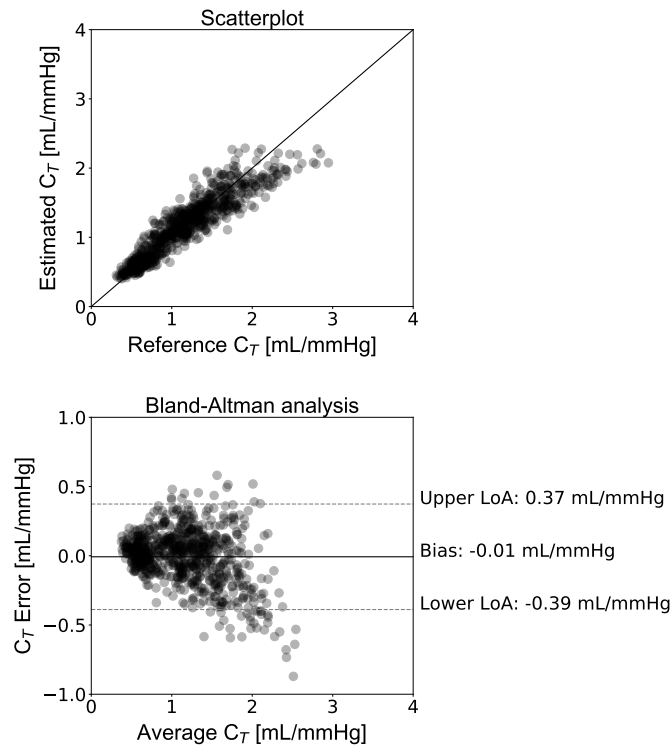


Figure 7.7 – Comparison between the estimated and the reference  $C_T$  data. Scatterplot and Bland–Altman plot between the estimated  $C_T$  and the reference  $C_T$  using the RFR. The solid line of the scatterplot represents equality. In Bland–Altman plot, limits of agreement (LoA) are defined by the two horizontal dashed lines. Adapted from [28].

pressure and flow for the evaluation of global arterial parameters is more relevant and provides major mechanistic information that it should be also considered when the more frequently acquired PWV is evaluated.

Knowledge of  $Z_{ao}$  and  $C_T$  might have additional diagnostic impact as well as additive prognostic value beyond PWV. Estimation of the  $Z_{ao}$  and  $C_T$  is, however, difficult in clinical practice, as it requires concomitant recordings of pressure and flow waveforms in the proximal aorta [63; 12; 47; 15]. The methodological complexity and lack of validation have prohibited their application in the everyday clinical practice. For this reason, capitalization of the regional PWV measurements for estimating  $Z_{ao}$  and  $C_T$  may permit their clinical assessment in a simple and cost-efficient way.

The present study suggested a machine learning predictive tool for  $Z_{ao}$  and  $C_T$  by using regional PWV measurements and cuff BP. The cfPWV is a measure of central arterial stiffness, whereas the crPWV expresses a mix of central and peripheral stiffness of the arterial tree. The principle of this concept is that the combined information embedded in the two indicators of regional elasticity can lead to an improved characterization of  $Z_{ao}$  and  $C_T$ . The results indicated that the suggested framework appears to apply well over a wide range of simulated

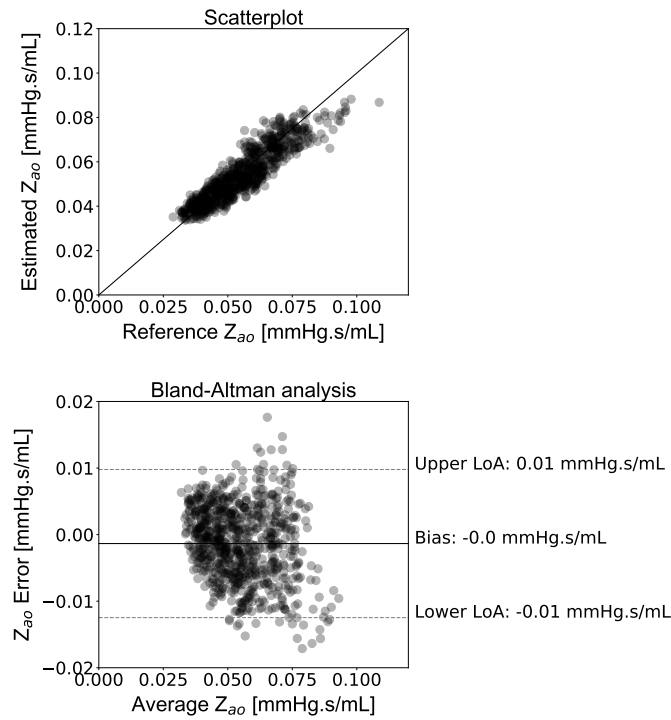


Figure 7.8 – Comparison between the estimated and the reference  $Z_{ao}$  data. Scatterplot and Bland–Altman plot between the estimated  $Z_{ao}$  and the reference  $Z_{ao}$  using the ANN. The solid line of the scatterplot represents equality. In Bland–Altman plot, limits of agreement (LoA) are defined by the two horizontal dashed lines. Adapted from [28].

physiological conditions. The methodology was appraised by testing two different machine learning models which, with proper hyperparameters' selection, achieved a similar predictive precision. This may also suggest that there is no high dependency on the nature of the machine learning approach, while it can provide preliminary evidence of the validity of the proposed framework.

Our methodology seems to offer a competitive advantage in comparison to prior methods. More specifically, it does not require central pressure and flow waves, for which the gold standard measurements are invasive. The invasive nature of the central BP wave's acquisition has been addressed either by the use of the carotid BP which is considered a good surrogate of aortic BP and can be easily acquired via tonometry, or by the use of devices that provide an approximation of the central BP wave via transformation of the radial BP wave [64; 65]. Measurement of central flow has been feasible by non-invasive techniques (e.g. ultrasound or magnetic resonance imaging) which are, however, expensive and rather dependent on operator skills. Yet, the results of this study showed that it outperformed some of the existing estimators. Previous methods for estimating  $Z_{ao}$  had significantly wider LoA when compared to our PWV-based machine learning estimators, while all current methods were also found to have high biases ( $> 0.01$  mmHg.s/mL). For  $C_T$ , PWV-based ANN had a similar performance

## Chapter 7. Determination of aortic characteristic impedance and total arterial compliance from regional pulse wave velocities using machine learning

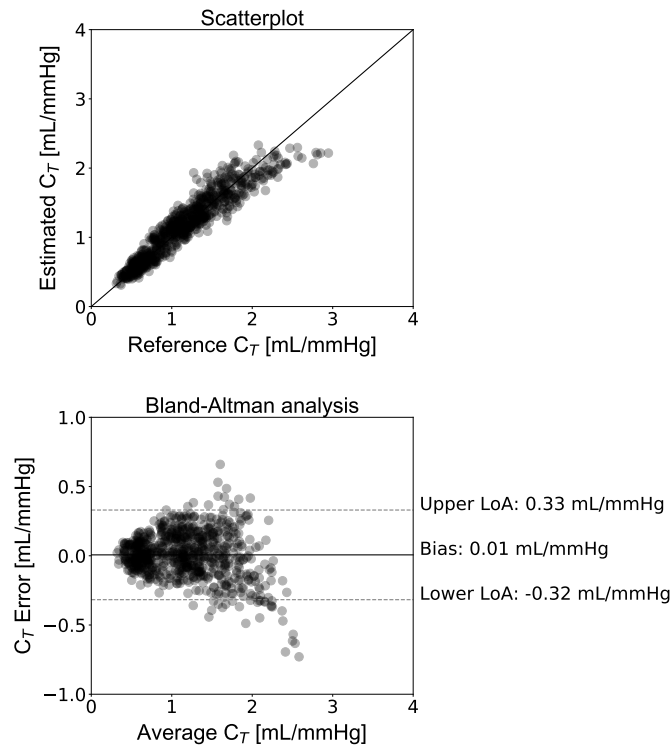


Figure 7.9 – Comparison between the estimated and the reference  $C_T$  data. Scatterplot and Bland–Altman plot between the estimated  $C_T$  and the reference  $C_T$  using the ANN. The solid line of the scatterplot represents equality. In Bland–Altman plot, limits of agreement (LoA) are defined by the two horizontal dashed lines. Adapted from [28].

to the PPM estimator, while the DTM yielded a lower precision. It is to be stressed that the comparison of the PWV-based machine learning estimators with the prior art cannot be direct and absolute, due to two main reasons: (i) the different nature of the required inputs, and (ii) the simplified simulation of the measurement error in the time signals. Specifically, although the previously published techniques are non-invasive, they require simultaneous measurement of the central blood pressure and flow, which are more difficult to acquire compared to the measurement required for the proposed machine learning estimator. In our experiments, the testing of these methods was done using the simulated aortic blood pressure which is the gold standard; in a real clinical setting, invasive aortic blood pressure is rarely available. Regarding the noise simulation, the artificial errors added to the signals were simplified; a random scaling factor was selected and multiplied with the entire signal. Hence, the error did not vary during the entire beat, and, as a result, the shape of the wave, to which the computational algorithms are highly dependent, remained unaffected.

The main advantage of our proposed method pertains to its simplicity and convenience (for both the patient and the physician) rather than its increased accuracy in comparison to the state of the art. The existing techniques require non-invasive, yet expensive and complex, flow

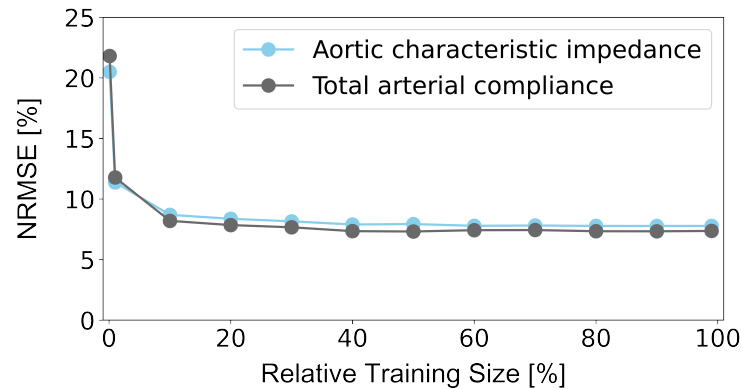


Figure 7.10 – Sensitivity of precision in terms of nRMSE to the number of the training data. The 100 % of the training size corresponds to 2,290 cases. Adapted from [28].

or velocity measurements for evaluating  $Z_{ao}$  and  $C_T$ . It is undeniable that previous studies have shown that current non-invasive techniques provide high accuracy and reliability for both  $Z_{ao}$  and  $C_T$  when compared with the invasive ground truth [13; 16]. However, being able to assess  $Z_{ao}$  and  $C_T$  from PWVs alone could be very valuable given that such an approach eliminates the need for flow measurement which requires magnetic resonance imaging or echocardiographic procedures. Undoubtedly, both techniques are not as accessible as tonometry, are much more expensive in comparison to the simple tonometric recordings, and render necessary the presence of well-trained personnel to handle the required equipment.

Following a regression analysis' concept, in a previous *in silico* study, Vardoulis et al. [66] demonstrated that  $C_T$  could be effectively derived using only cfPWV. They provided a simple equation that directly relates the cfPWV measurement to  $C_T$ . The results hypothesized that solely cfPWV should be sufficient for accurately estimating  $C_T$ . Further light upon the significance of including more features to the regression method can be provided by assessing the features' importance levels. As per the feature importances of our study, indeed cfPWV appeared to be among the most significant parameter for estimating  $C_T$ . In order to further verify the necessity of including additional features to cfPWV (namely cuff BP and crPWV), we predicted  $C_T$  using only cfPWV. Following a similar approach with Vardoulis et al. yielded a lower prediction precision with an nRMSE = 12.4 %, a zero bias, while LoA were reported to be  $\pm 0.64$  mL/mmHg. This error is approximately two times higher than the error provided by the machine learning model of this study (6.26 % from ANN estimator). Although the cfPWV-based estimator performed adequately, we may deduce that inclusion of both cfPWV and crPWV improves the precision in  $C_T$  estimation. Importantly, this apparently slight improvement might be rather necessary when performing the analysis on an *in vivo* population. Yet, the regression analysis, which uses both PWV values might provide a more clinically relevant estimation of  $C_T$ , as it combines both a proximal and a distal approximation of arterial stiffness, and thus a



**Chapter 7. Determination of aortic characteristic impedance and total arterial compliance from regional pulse wave velocities using machine learning**

Table 7.6 – Comparison of the proposed machine learning-based  $Z_{ao}$  and  $C_T$  estimators to prior art.

Method	Estimated $Z_{ao}$ [mmHg.s/mL]	Reference $Z_{ao}$ [mmHg.s/mL]	Error [%]	$r$	Bland-Altman bias (LoA) [mmHg.s/mL]
Time-derivative peaks method*	0.044±0.008	0.056±0.014	Min: -55 Max: -20	0.66	-0.011 (-0.030, 0.007)
Peak flow method*	0.071±0.018		Min: -14 Max: 107	0.79	0.016 (-0.007, 0.038)
PWV-based RFR	0.056±0.013		Min: -27, Max: 34	0.89	-0.000 (-0.012, 0.012)
PWV-based ANN	0.056±0.012		Min: -21, Max: 37	0.90	-0.000 (-0.013, 0.010)
	Estimated $C_T$ [mL/mmHg]	Reference $C_T$ [mL/mmHg]	Errors [%]	$r$	Bland-Altman bias (LoA) [mL/mmHg]
Decay time method*	1.60±0.71	1.16±0.51	Min: -10, Max: 152	0.93	0.44 (-0.16, 1.05)
Pulse pressure method*	1.23±0.48		Min: -24, Max: 58	0.94	0.07 (-0.27, 0.41)
PWV-based RFR	1.16±0.45		Min: -36, Max: 62	0.93	-0.01 (-0.39, 0.37)
PWV-based ANN	1.18±0.48		Min: -28, Max: 57	0.95	0.01 [-0.32, 0.33]
Errors are expressed as $100 \times (X_{est} - X_{actual}) / X_{actual}$ , where X is the target output under test (i.e. $Z_{ao}$ or $C_T$ ).					
Limits of agreement are defined as (bias + 1.96 SD, bias - 1.96 SD).					
*These methods utilize both the central blood pressure and flow waves for estimating $Z_{ao}$ and $C_T$ .					

more complete description of the arterial tree's elasticity.

This study further explored and quantified the importance of every input for the predictive performance. Diastolic pressure had the most significant contribution to the estimations. This is to be expected given that both  $Z_{ao}$  and  $C_T$  are strong determinants of mean pressure and by extension the brDBP. Furthermore, most of the arterial compliance is contained in the aorta. This could explain why the permutation importance of cfPWV (namely aortic PWV) was found to be slightly higher compared to crPWV (Table 7.5). Yet, the two PWV inputs presented similar, high importance levels. It is highly possible that the bulk of the required information for  $Z_{ao}$  and  $C_T$  is contained in the common arterial path included in both cfPWV and crPWV; namely the arterial segments which are closer to the aorta. Hence, the inclusion of both is important

to detect and reveal this joint information. Attention must be paid to the fact that this study uses synthetic data produced by a simulator and, hence, there is a direct deterministic relation between the input and the outputs. This relation may lead to an increased accuracy in the predictions. The results regarding the importance of each feature would be of benefit if they are considered in a qualitative way.

We additionally evaluated the models' sensitivity to the inputs by training and testing the models using different sets of features. Given that the HR has been shown to have a pressure-independent impact on PWV [67], we decided to include it in our experiments in order to consider its independent contribution and to enhance the clinical relevance of our results. Nevertheless, it was shown that exclusion of HR from the input vector did not harm the accuracy. Moreover, both RFR and ANN performed adequately when brSBP and brDBP were replaced by MAP. However, when only the PWV values were fed to the models, the precision was deteriorated for both  $Z_{ao}$  and  $C_T$ . This may be explained due to the BP-dependency of PWV which has been shown to have implications for the clinical use of arterial stiffness measurements, both in risk classification and in treatment monitoring of individual patients [68].

Recent advancements in Artificial Intelligence (AI) have led to new research possibilities and methodologies for novel cardiovascular modelling and predictive tools for clinical use [69]. The present study is in line with this direction that introduces AI to the field of clinical medicine. There have been several novel works toward this path, including estimation of PWV or central BP [70; 71; 72]. Machine learning modelling allows for enhancing monitoring of vascular biomarkers via the analysis of complex datasets, signals and/or images. The availability of large clinical datasets and powerful computing systems further encourage the application of machine learning-based concepts. In addition, nowadays, vascular parameters or arterial pulse signals can also be obtained using unobtrusive devices such as smartphones and smartwatches, providing a plethora of available data.

### Limitations

The main limitation of the present study is that the data used in the analysis have been derived from a computer simulator rather than a real human population. A machine learning model which is trained/tested using *in silico* data, it is likely that it will not be capable of making accurate predictions for a real patient. Yet, the *in silico* data allow us for performing an initial validation of the proposed methodology, whose results will allow to proceed with the clinical validation. Previous works have used a similar approach to validate machine learning-based techniques using virtual patients when real clinical data were not available [73; 74; 27]. Hence, the present study proposes the methodology rather than the model *per se*. *Stricto sensu*, based on the findings from an *in silico* population, we may only deduce that the proposed machine learning-based methodology could also work using real human data for both the

## **Chapter 7. Determination of aortic characteristic impedance and total arterial compliance from regional pulse wave velocities using machine learning**

---

training and testing procedures. The latter hypothesis remains to be verified *in vivo*. Future work will be done toward this direction. Nevertheless, synthetic data can sufficiently simulate the content of the real clinical measurements, while they allow for controlling the distribution of rare but relevant conditions or events. It is also to be mentioned that the *in silico* data allow us for appraising this concept using the actual  $Z_{ao}$  and  $C_T$ , which are derived analytically from the computer simulator and would not have been available *in vivo*. Future work should also include validation of the method on populations with pathologies or special populations.

Finally, a major consideration with respect to the application of machine learning in healthcare is generalizability, i.e. the ability of a model to predict accurately on data sources which are not included in the dataset of the specific study. Dexter et al. [75] demonstrated that studies showing high-performance machine learning models may not perform well when applied to data from other holdout systems. Each modelling strategy is limited by assumptions and data collection is dependent on several factors, including clinical context, local factors (e.g. physician preferences, local care standards), medication selection or other clinical decisions which influence the model development [76]. Therefore, direct validation of a machine learning algorithm to a new dataset should not assume model's strong performance under all conditions; even when the model is trained using real clinical data. The above limitations underline the need to consider more inclusive training approaches for machine learning models which could encourage the practical application of machine learning in healthcare.

### **Conclusion**

This paper introduces a non-invasive simple-to-use estimator for two valuable hemodynamic quantities, namely the  $Z_{ao}$  and  $C_T$ . The proposed approach incorporates cuff BP and regional PWV data, along with a versatile and scalable machine learning pipeline. Our findings provide evidence that data related to regional arterial stiffness can be rather informative for obtaining a global description of arterial elasticity. Further validation of the proposed methodology on a large human cohort remains to be conducted. Upon successful clinical validation, this framework may provide a reliable method to inform the clinicians about arterial stiffness, leading to an improved diagnosis and patients' treatment management.

## Bibliography

- [1] S. Laurent, P. Boutouyrie, R. Asmar, I. Gautier, B. Laloux, L. Guize, P. Ducimetiere, and A. Benetos, "Aortic stiffness is an independent predictor of all-cause and cardiovascular mortality in hypertensive patients," *Hypertension*, vol. 37, no. 5, pp. 1236–1241, May 2001. [Online]. Available: <https://www.ahajournals.org/doi/10.1161/01.HYP.37.5.1236>
- [2] G. F. Mitchell, S.-J. Hwang, R. S. Vasan, M. G. Larson, M. J. Pencina, N. M. Hamburg, J. A. Vita, D. Levy, and E. J. Benjamin, "Arterial stiffness and cardiovascular events: the Framingham heart study," *Circulation*, vol. 121, no. 4, pp. 505–511, Feb. 2010. [Online]. Available: <https://www.ahajournals.org/doi/10.1161/CIRCULATIONAHA.109.886655>
- [3] C. Vlachopoulos, K. Aznaouridis, and C. Stefanadis, "Prediction of cardiovascular events and all-cause mortality with arterial stiffness," *Journal of the American College of Cardiology*, vol. 55, no. 13, pp. 1318–1327, Mar. 2010. [Online]. Available: <https://linkinghub.elsevier.com/retrieve/pii/S0735109710002809>
- [4] A. Redheuil, W.-C. Yu, E. Mousseaux, A. A. Harouni, N. Kachenoura, C. O. Wu, D. Bluemke, and J. A. Lima, "Age-related changes in aortic arch geometry," *Journal of the American College of Cardiology*, vol. 58, no. 12, pp. 1262–1270, Sep. 2011. [Online]. Available: <https://linkinghub.elsevier.com/retrieve/pii/S0735109711022789>
- [5] I. S. Mackenzie, I. B. Wilkinson, and J. R. Cockcroft, "Assessment of arterial stiffness in clinical practice," *QJM: monthly journal of the Association of Physicians*, vol. 95, no. 2, pp. 67–74, Feb. 2002.
- [6] W. W. Nichols, C. R. Conti, W. E. Walker, and W. R. Milnor, "Input impedance of the systemic circulation in man." *Circulation Research*, vol. 40, no. 5, pp. 451–458, May 1977. [Online]. Available: <https://www.ahajournals.org/doi/10.1161/01.RES.40.5.451>
- [7] C. J. Pepine, W. W. Nichols, and C. R. Conti, "Aortic input impedance in heart failure," *Circulation*, vol. 58, no. 3, pp. 460–465, Sep. 1978. [Online]. Available: <https://www.ahajournals.org/doi/10.1161/01.CIR.58.3.460>
- [8] J. P. Murgo, N. Westerhof, J. P. Giolma, and S. A. Altobelli, "Aortic input impedance in normal man: relationship to pressure wave forms," *Circulation*, vol. 62, no. 1, pp. 105–116, Jul. 1980. [Online]. Available: <https://www.ahajournals.org/doi/10.1161/01.CIR.62.1.105>

## Bibliography

---

- [9] W. Gundel, G. Cherry, B. Rajagopalan, L. B. Tan, G. Lee, and D. Schultz, "Aortic input impedance in man: acute response to vasodilator drugs," *Circulation*, vol. 63, no. 6, pp. 1305–1314, Jun. 1981. [Online]. Available: <https://www.ahajournals.org/doi/10.1161/01.CIR.63.6.1305>
- [10] J. Merillon, G. Fontenier, J. Lerallut, M. Jaffrin, J. Chastre, P. Assayag, G. Motte, and R. Gourgon, "Aortic input impedance in heart failure: comparison with normal subjects and its changes during vasodilator therapy\*," *European Heart Journal*, vol. 5, no. 6, pp. 447–455, Jun. 1984. [Online]. Available: <https://academic.oup.com/eurheartj/article-lookup/doi/10.1093/oxfordjournals.eurheartj.a061690>
- [11] C. T. Ting, K. P. Brin, S. J. Lin, S. P. Wang, M. S. Chang, B. N. Chiang, and F. C. Yin, "Arterial hemodynamics in human hypertension," *Journal of Clinical Investigation*, vol. 78, no. 6, pp. 1462–1471, Dec. 1986. [Online]. Available: <http://www.jci.org/articles/view/112737>
- [12] C. Lucas, B. Wilcox, B. Ha, and G. Henry, "Comparison of time domain algorithms for estimating aortic characteristic impedance in humans," *IEEE Transactions on Biomedical Engineering*, vol. 35, no. 1, pp. 62–68, Jan. 1988. [Online]. Available: <http://ieeexplore.ieee.org/document/1337/>
- [13] R. Kelly and D. Fitchett, "Noninvasive determination of aortic input impedance and external left ventricular power output: a validation and repeatability study of a new technique," *Journal of the American College of Cardiology*, vol. 20, no. 4, pp. 952–963, Oct. 1992. [Online]. Available: <https://linkinghub.elsevier.com/retrieve/pii/073510979290198V>
- [14] E. P. Kromer, D. Eisner, S. R. Holmer, A. Muntze, and G. A. J. Riegger, "Aortic input impedance and neurohormonal activation in patients with mild to moderate chronic congestive heart failure," *Cardiovascular Research*, vol. 26, no. 3, pp. 265–272, Mar. 1992. [Online]. Available: <https://academic.oup.com/cvr/article-lookup/doi/10.1093/cvr/26.3.265>
- [15] G. F. Mitchell, J.-C. Tardif, J. M. O. Arnold, G. Marchiori, T. X. O'Brien, M. E. Dunlap, and M. A. Pfeffer, "Pulsatile hemodynamics in congestive heart failure," *Hypertension*, vol. 38, no. 6, pp. 1433–1439, Dec. 2001. [Online]. Available: <https://www.ahajournals.org/doi/10.1161/hy1201.098298>
- [16] P. Segers, E. R. Rietzschel, M. L. De Buyzere, S. J. Vermeersch, D. De Bacquer, L. M. Van Bortel, G. De Backer, T. C. Gillebert, and P. R. Verdonck, "Noninvasive (input) impedance, pulse wave velocity, and wave reflection in healthy middle-aged men and women," *Hypertension*, vol. 49, no. 6, pp. 1248–1255, Jun. 2007. [Online]. Available: <https://www.ahajournals.org/doi/10.1161/HYPERTENSIONAHA.106.085480>

- [17] J.-P. L. Dujardin and D. N. Stone, "Characteristic impedance of the proximal aorta determined in the time and frequency domain: a comparison," *Medical & Biological Engineering & Computing*, vol. 19, no. 5, pp. 565–568, Sep. 1981. [Online]. Available: <http://link.springer.com/10.1007/BF02442770>
- [18] Z. Liu, K. P. Brin, and F. C. Yin, "Estimation of total arterial compliance: an improved method and evaluation of current methods," *American Journal of Physiology-Heart and Circulatory Physiology*, vol. 251, no. 3, pp. H588–H600, Sep. 1986. [Online]. Available: <http://www.physiology.org/doi/10.1152/ajpheart.1986.251.3.H588>
- [19] B. I. Levy, D. Babalis, P. Lacolley, P. Poitevin, and M. E. Safar, "Cardiac hypertrophy and characteristic impedance in spontaneously hypertensive rats," *Journal of Hypertension*, vol. 6, no. 4, pp. S110–111, Dec. 1988. [Online]. Available: <http://journals.lww.com/00004872-198812040-00031>
- [20] M. E. Safar and G. M. London, "Arterial and venous compliance in sustained essential hypertension," *Hypertension*, vol. 10, no. 2, pp. 133–139, Aug. 1987. [Online]. Available: <https://www.ahajournals.org/doi/10.1161/01.HYP.10.2.133>
- [21] D. Chemla, I. Antony, Y. Lecarpentier, and A. Nitenberg, "Contribution of systemic vascular resistance and total arterial compliance to effective arterial elastance in humans," *American Journal of Physiology-Heart and Circulatory Physiology*, vol. 285, no. 2, pp. H614–H620, Aug. 2003. [Online]. Available: <https://www.physiology.org/doi/10.1152/ajpheart.00823.2002>
- [22] B. Haluska, K. Matthys, R. Fathi, E. Rozis, S. Carlier, and T. Marwick, "Influence of arterial compliance on presence and extent of ischaemia during stress echocardiography," *Heart*, vol. 92, no. 1, pp. 40–43, 2006.
- [23] B. A. Haluska, L. Jeffriess, M. Downey, S. G. Carlier, and T. H. Marwick, "Influence of cardiovascular risk factors on total arterial compliance," *Journal of the American Society of Echocardiography*, vol. 21, no. 2, pp. 123–128, Feb. 2008. [Online]. Available: <https://linkinghub.elsevier.com/retrieve/pii/S0894731707004713>
- [24] P. Segers, P. Verdonck, Y. Deryck, S. Brimiouille, R. Naeije, S. Carlier, and N. Stergiopoulos, "Pulse pressure method and the area method for the estimation of total arterial compliance in dogs: sensitivity to wave reflection intensity," *Annals of Biomedical Engineering*, vol. 27, no. 4, pp. 480–485, Aug. 1999.
- [25] N. Stergiopoulos, P. Segers, and N. Westerhof, "Use of pulse pressure method for estimating total arterial compliance in vivo," *The American Journal of Physiology*, vol. 276, no. 2 Pt 2, pp. H424–428, Feb. 1999.

## Bibliography

---

- [26] S. Sakuragi and W. P. Abhayaratna, "Arterial stiffness: methods of measurement, physiologic determinants and prediction of cardiovascular outcomes," *International Journal of Cardiology*, vol. 138, no. 2, pp. 112–118, Jan. 2010.
- [27] V. Bikia, S. Pagoulatou, B. Trachet, D. Soulis, A. D. Protogerou, T. G. Papaioannou, and N. Stergiopulos, "Noninvasive cardiac output and central systolic pressure from cuff-pressure and pulse wave velocity," *IEEE Journal of Biomedical and Health Informatics*, vol. 24, no. 7, pp. 1968–1981, Jul. 2020. [Online]. Available: <https://ieeexplore.ieee.org/document/8918060/>
- [28] V. Bikia, G. Rovas, S. Pagoulatou, and N. Stergiopulos, "Determination of aortic characteristic impedance and total arterial compliance from regional pulse wave velocities using machine learning: An in-silico study," *Frontiers in Bioengineering and Biotechnology*, vol. 9, p. 345, 2021.
- [29] P. Reymond, F. Merenda, F. Perren, D. Rüfenacht, and N. Stergiopulos, "Validation of a one-dimensional model of the systemic arterial tree," *American Journal of Physiology. Heart and Circulatory Physiology*, vol. 297, no. 1, pp. H208–222, Jul. 2009.
- [30] A. Wolak, H. Gransar, L. E. J. Thomson, J. D. Friedman, R. Hachamovitch, A. Gutstein, L. J. Shaw, D. Polk, N. D. Wong, R. Saouaf, S. W. Hayes, A. Rozanski, P. J. Slomka, G. Germano, and D. S. Berman, "Aortic size assessment by noncontrast cardiac computed tomography: normal limits by age, gender, and body surface area," *JACC. Cardiovascular imaging*, vol. 1, no. 2, pp. 200–209, Mar. 2008.
- [31] R. B. Devereux, G. de Simone, D. K. Arnett, L. G. Best, E. Boerwinkle, B. V. Howard, D. Kitzman, E. T. Lee, T. H. Mosley, A. Weder, and M. J. Roman, "Normal limits in relation to age, body size and gender of two-dimensional echocardiographic aortic root dimensions in persons  $\geq 15$  years of age," *The American Journal of Cardiology*, vol. 110, no. 8, pp. 1189–1194, Oct. 2012. [Online]. Available: <https://linkinghub.elsevier.com/retrieve/pii/S0002914912015342>
- [32] G. Langewouters, *Visco-elasticity of the human aorta in vitro in relation to pressure and age (Ph.D. thesis)*. Amsterdam: Free University of Amsterdam: Krips Repro, 1982. [Online]. Available: <https://books.google.gr/books?id=qvSrHAAACAAJ>
- [33] Z. Lu and R. Mukkamala, "Continuous cardiac output monitoring in humans by invasive and noninvasive peripheral blood pressure waveform analysis," *Journal of Applied Physiology*, vol. 101, no. 2, pp. 598–608, Aug. 2006. [Online]. Available: <https://www.physiology.org/doi/10.1152/jappphysiol.01488.2005>
- [34] P. Segers et al., "Three- and four-element Windkessel models: assessment of their fitting performance in a large cohort of healthy middle-aged individuals," *Proceedings of the Institution of Mechanical Engineers, Part H: Journal of Engineering in Medicine*, 2008.

- [35] S. Z. Pagouladou, V. Bikia, B. Trachet, T. G. Papaioannou, A. D. Protogerou, and N. Stergiopoulos, "On the importance of the nonuniform aortic stiffening in the hemodynamics of physiological aging," *American Journal of Physiology-Heart and Circulatory Physiology*, vol. 317, no. 5, pp. H1125–H1133, Nov. 2019. [Online]. Available: <https://www.physiology.org/doi/10.1152/ajpheart.00193.2019>
- [36] V. Bikia, T. G. Papaioannou, S. Pagouladou, G. Rovas, E. Oikonomou, G. Siasos, D. Tousoulis, and N. Stergiopoulos, "Noninvasive estimation of aortic hemodynamics and cardiac contractility using machine learning," *Scientific Reports*, vol. 10, no. 1, p. 15015, Dec. 2020. [Online]. Available: <http://www.nature.com/articles/s41598-020-72147-8>
- [37] C. M. McEniery, n. Yasmin, I. R. Hall, A. Qasem, I. B. Wilkinson, J. R. Cockcroft, and ACCT Investigators, "Normal vascular aging: differential effects on wave reflection and aortic pulse wave velocity: the Anglo-Cardiff Collaborative Trial (ACCT)," *Journal of the American College of Cardiology*, vol. 46, no. 9, pp. 1753–1760, Nov. 2005.
- [38] B. Bordin Pelazza and S. R. F. Filho, "Comparison between central and brachial blood pressure in hypertensive elderly women and men," *International Journal of Hypertension*, vol. 2017, p. 6265823, Sep. 2017, publisher: Hindawi. [Online]. Available: <https://doi.org/10.1155/2017/6265823>
- [39] O. Vardoulis, T. G. Papaioannou, and N. Stergiopoulos, "Validation of a novel and existing algorithms for the estimation of pulse transit time: advancing the accuracy in pulse wave velocity measurement," *American Journal of Physiology-Heart and Circulatory Physiology*, vol. 304, no. 11, pp. H1558–H1567, Jun. 2013. [Online]. Available: <http://www.physiology.org/doi/10.1152/ajpheart.00963.2012>
- [40] A. Liaw and M. Wiener, "Classification and regression by randomForest," *R News*, vol. 2, no. 3, pp. 18–22, 2002. [Online]. Available: <http://CRAN.R-project.org/doc/Rnews/>
- [41] D. P. Kingma and J. Ba, "Adam: a method for stochastic optimization," San Diego, US, 2017. [Online]. Available: <https://arxiv.org/pdf/1412.6980.pdf>
- [42] L. Breiman, "Random forests," *Machine Learning*, vol. 45, no. 1, pp. 5–32, 2001. [Online]. Available: <http://link.springer.com/10.1023/A:1010933404324>
- [43] F. Pedregosa, G. Varoquaux, A. Gramfort, V. Michel, B. Thirion, O. Grisel, M. Blondel, P. Prettenhofer, R. Weiss, V. Dubourg, J. Vanderplas, A. Passos, D. Cournapeau, M. Brucher, M. Perrot, and E. Duchesnay, "Scikit-learn: machine learning in Python," vol. 12, pp. 2825–2830, 2011.
- [44] T. E. Oliphant, "A guide to NumPy." Trelgol Publishing USA, 2006, vol. 1.
- [45] W. McKinney, "Data structures for statistical computing in Python," in *Proceedings of the 9th Python in Science Conference*, 2010, pp. 51–56, doi: 10.25080/Majora-92bf1922-00a.



## Bibliography

---

- [46] N. Stergiopoulos, J. Meister, and N. Westerhof, "Evaluation of methods for estimation of total arterial compliance," *American Journal of Physiology-Heart and Circulatory Physiology*, vol. 268, no. 4, pp. H1540–H1548, Apr. 1995. [Online]. Available: <https://www.physiology.org/doi/10.1152/ajpheart.1995.268.4.H1540>
- [47] N. Stergiopoulos, J.-J. Meister, and N. Westerhof, "Simple and accurate way for estimating total and segmental arterial compliance: the pulse pressure method," *Annals of Biomedical Engineering*, vol. 22, no. 4, pp. 392–397, 1994.
- [48] J. M. Bland and D. G. Altman, "Statistical methods for assessing agreement between two methods of clinical measurement," *Lancet (London, England)*, vol. 1, no. 8476, pp. 307–310, Feb. 1986.
- [49] J. A. Chirinos, P. Segers, A. Raina, H. Saif, A. Swillens, A. K. Gupta, R. Townsend, A. G. Emmi, J. N. Kirkpatrick, M. G. Keane, V. A. Ferrari, S. E. Wiegers, and M. G. St. John Sutton, "Arterial pulsatile hemodynamic load induced by isometric exercise strongly predicts left ventricular mass in hypertension," *American Journal of Physiology-Heart and Circulatory Physiology*, vol. 298, no. 2, pp. H320–H330, Feb. 2010. [Online]. Available: <https://www.physiology.org/doi/10.1152/ajpheart.00334.2009>
- [50] M. I. Mendonça, R. P. Reis, A. C. Sousa, S. Gomes, P. Faria, A. Pereira, B. Silva, M. Serrão, N. Santos, F. S. Sousa, J. A. Silva, J. Sousa, I. Ornelas, S. Freitas, A. Cardoso, and J. J. Araújo, "Pulse wave velocity and coronary risk stratification," *Revista Portuguesa De Cardiologia: Orgao Oficial Da Sociedade Portuguesa De Cardiologia = Portuguese Journal of Cardiology: An Official Journal of the Portuguese Society of Cardiology*, vol. 28, no. 2, pp. 155–171, Feb. 2009.
- [51] J. Megnien, "Aortic stiffening does not predict coronary and extracoronary atherosclerosis in asymptomatic men at risk for cardiovascular disease," *American Journal of Hypertension*, vol. 11, no. 3, pp. 293–301, Mar. 1998. [Online]. Available: [https://academic.oup.com/ajh/article-lookup/doi/10.1016/S0895-7061\(97\)00477-9](https://academic.oup.com/ajh/article-lookup/doi/10.1016/S0895-7061(97)00477-9)
- [52] S. Meaume, A. Benetos, O. Henry, A. Rudnichi, and M. Safar, "Aortic pulse wave velocity predicts cardiovascular mortality in subjects >70 years of age," *Arteriosclerosis, Thrombosis, and Vascular Biology*, vol. 21, no. 12, pp. 2046–2050, Dec. 2001. [Online]. Available: <https://www.ahajournals.org/doi/10.1161/hq1201.100226>
- [53] A. D. Protogerou, M. E. Safar, P. Iaria, H. Safar, K. Le Dudal, J. Filipovsky, O. Henry, P. Ducimetière, and J. Blacher, "Diastolic blood pressure and mortality in the elderly with cardiovascular disease," *Hypertension*, vol. 50, no. 1, pp. 172–180, Jul. 2007. [Online]. Available: <https://www.ahajournals.org/doi/10.1161/HYPERTENSIONAHA.107.089797>
- [54] G. C. Verwoert, S. E. Elias-Smale, D. Rizopoulos, M. T. Koller, E. W. Steyerberg, A. Hofman, M. Kavousi, E. J. G. Sijbrands, A. P. G. Hoeks, R. S. Reneman, F. U. S. Mattace-Raso,

- and J. C. M. Witteman, "Does aortic stiffness improve the prediction of coronary heart disease in elderly? The Rotterdam Study," *Journal of Human Hypertension*, vol. 26, no. 1, pp. 28–34, Jan. 2012. [Online]. Available: <https://doi.org/10.1038/jhh.2010.124>
- [55] R. B. P. de Wilde, J. J. Schreuder, P. C. M. van den Berg, and J. R. C. Jansen, "An evaluation of cardiac output by five arterial pulse contour techniques during cardiac surgery," *Anaesthesia*, vol. 62, no. 8, pp. 760–768, Aug. 2007.
- [56] S. I. Rabben, N. Stergiopoulos, L. R. Hellevik, O. A. Smiseth, S. Slørdahl, S. Urheim, and B. Angelsen, "An ultrasound-based method for determining pulse wave velocity in superficial arteries," *Journal of Biomechanics*, vol. 37, no. 10, pp. 1615–1622, Oct. 2004. [Online]. Available: <https://linkinghub.elsevier.com/retrieve/pii/S0021929004000107>
- [57] A. Borlotti, S. Vermeersch, E. Rietzschel, P. Segers, and A. W. Khir, "A comparison between local wave speed in the carotid and femoral arteries in healthy humans: application of a new method," in *2010 Annual International Conference of the IEEE Engineering in Medicine and Biology*. Buenos Aires: IEEE, Aug. 2010, pp. 2857–2860. [Online]. Available: <http://ieeexplore.ieee.org/document/5626348/>
- [58] S. Laurent, J. Cockcroft, L. Van Bortel, P. Boutouyrie, C. Giannattasio, D. Hayoz, B. Pannier, C. Vlachopoulos, I. Wilkinson, H. Struijker-Boudier, and on behalf of the European Network for Non-invasive Investigation of Large Arteries, "Expert consensus document on arterial stiffness: methodological issues and clinical applications," *European Heart Journal*, vol. 27, no. 21, pp. 2588–2605, Sep. 2006. [Online]. Available: <https://academic.oup.com/eurheartj/article-lookup/doi/10.1093/eurheartj/ehl254>
- [59] C. Vlachopoulos, K. Aznaouridis, D. Terentes-Printzios, N. Ioakeimidis, and C. Stefanadis, "Prediction of cardiovascular events and all-cause mortality with brachial-ankle elasticity index: a systematic review and meta-analysis," *Hypertension*, vol. 60, no. 2, pp. 556–562, Aug. 2012. [Online]. Available: <https://www.ahajournals.org/doi/10.1161/HYPERTENSIONAHA.112.194779>
- [60] Y.-S. Lee, K.-S. Kim, C.-W. Nam, S.-W. Han, S.-H. Hur, Y.-N. Kim, K.-B. Kim, and J.-B. Lee, "Clinical implication of carotid-radial pulse wave velocity for patients with coronary artery disease," *Korean Circulation Journal*, vol. 36, no. 8, p. 565, 2006. [Online]. Available: <https://e-kcj.org/DOIx.php?id=10.4070/kcj.2006.36.8.565>
- [61] R. G. Asmar, G. M. London, M. E. O'Rourke, M. E. Safar, and for the REASON Project coordinators and investigators, "Improvement in blood pressure, arterial stiffness and wave reflections with a very-low-dose perindopril/indapamide combination in hypertensive patient: a comparison with atenolol," *Hypertension*, vol. 38, no. 4, pp. 922–926, Oct. 2001. [Online]. Available: <https://www.ahajournals.org/doi/10.1161/hy1001.095774>

## Bibliography

---

- [62] The CAFE Investigators, CAFE Steering Committee and Writing Committee, B. Williams, P. S. Lacy, S. M. Thom, K. Cruickshank, A. Stanton, D. Collier, A. D. Hughes, H. Thurston, and M. O'Rourke, "Differential impact of blood pressure-lowering drugs on central aortic pressure and clinical outcomes: principal results of the conduit artery function evaluation (CAFE) study," *Circulation*, vol. 113, no. 9, pp. 1213–1225, Mar. 2006. [Online]. Available: <https://www.ahajournals.org/doi/10.1161/CIRCULATIONAHA.105.595496>
- [63] O. S. Randall, M. D. Esler, R. V. Calfee, G. F. Bulloch, A. S. Maisel, and B. Culp, "Arterial compliance in hypertension," *Australian and New Zealand Journal of Medicine*, vol. 6, pp. 49–59, Jun. 1976. [Online]. Available: <http://doi.wiley.com/10.1111/j.1445-5994.1976.tb03323.x>
- [64] W. Weiss, C. Gohlisch, C. Harsch-Gladisch, M. Tölle, W. Zidek, and M. van der Giet, "Oscillometric estimation of central blood pressure: validation of the Mobil-O-Graph in comparison with the SphygmoCor device," *Blood Pressure Monitoring*, vol. 17, no. 3, pp. 128–131, Jun. 2012.
- [65] T. Shoji, A. Nakagomi, S. Okada, Y. Ohno, and Y. Kobayashi, "Invasive validation of a novel brachial cuff-based oscillometric device (SphygmoCor XCEL) for measuring central blood pressure," *Journal of Hypertension*, vol. 35, no. 1, pp. 69–75, 2017.
- [66] O. Vardoulis, T. G. Papaioannou, and N. Stergiopoulos, "On the estimation of total arterial compliance from aortic pulse wave velocity," *Annals of Biomedical Engineering*, vol. 40, no. 12, pp. 2619–2626, Dec. 2012.
- [67] V. Bikia, N. Stergiopoulos, G. Rovas, S. Pagoulatou, and T. G. Papaioannou, "The impact of heart rate on pulse wave velocity: an in-silico evaluation," *Journal of Hypertension*, vol. 38, no. 12, pp. 2451–2458, 2020.
- [68] B. Spronck, M. H. Heusinkveld, F. H. Vanmolkot, J. Op't Roodt, E. Hermeling, T. Delhaas, A. A. Kroon, and K. D. Reesink, "Pressure-dependence of arterial stiffness: potential clinical implications," *Journal of hypertension*, vol. 33, no. 2, pp. 330–338, 2015.
- [69] A. Ramesh, C. Kambhampati, J. Monson, and P. Drew, "Artificial intelligence in medicine," *Annals of The Royal College of Surgeons of England*, vol. 86, no. 5, pp. 334–338, Sep. 2004. [Online]. Available: <http://www.ingentaselect.com/rpsv/cgi-bin/cgi?ini=xref&body=linker&reqdoi=10.1308/147870804290>
- [70] S. V. Greve, M. K. Blicher, R. Kruger, T. Sehestedt, E. Gram-Kampmann, S. Rasmussen, J. K. Vishram, P. Boutouyrie, S. Laurent, and M. H. Olsen, "Estimated carotid-femoral pulse wave velocity has similar predictive value as measured carotid-femoral pulse wave velocity," *Journal of Hypertension*, vol. 34, no. 7, pp. 1279–1289, Jul. 2016. [Online]. Available: <http://journals.lww.com/00004872-201607000-00009>

- 
- [71] H. Xiao, A. Qasem, M. Butlin, and A. Avolio, "Estimation of aortic systolic blood pressure from radial systolic and diastolic blood pressures alone using artificial neural networks," *Journal of Hypertension*, vol. 35, no. 8, pp. 1577–1585, Aug. 2017.
- [72] P. Tavallali, M. Razavi, and N. M. Pahlevan, "Artificial intelligence estimation of carotid-femoral pulse wave velocity using carotid waveform," *Scientific Reports*, vol. 8, no. 1, p. 1014, Dec. 2018. [Online]. Available: <http://www.nature.com/articles/s41598-018-19457-0>
- [73] J. M. J. Huttunen, L. Kärkkäinen, and H. Lindholm, "Pulse transit time estimation of aortic pulse wave velocity and blood pressure using machine learning and simulated training data," *PLOS Computational Biology*, vol. 15, no. 8, p. e1007259, Aug. 2019. [Online]. Available: <http://dx.plos.org/10.1371/journal.pcbi.1007259>
- [74] J. M. Huttunen, L. Kärkkäinen, M. Honkala, and H. Lindholm, "Deep learning for prediction of cardiac indices from photoplethysmographic waveform: a virtual database approach," *International Journal for Numerical Methods in Biomedical Engineering*, vol. 36, no. 3, Mar. 2020. [Online]. Available: <https://onlinelibrary.wiley.com/doi/abs/10.1002/cnm.3303>
- [75] G. P. Dexter, S. J. Grannis, B. E. Dixon, and S. N. Kasthurirathne, "Generalization of machine learning approaches to identify notifiable conditions from a statewide health information exchange," *AMIA Joint Summits on Translational Science proceedings. AMIA Joint Summits on Translational Science*, vol. 2020, pp. 152–161, 2020.
- [76] K. Shameer, K. W. Johnson, B. S. Glicksberg, J. T. Dudley, and P. P. Sengupta, "Machine learning in cardiovascular medicine: are we there yet?" *Heart*, vol. 104, no. 14, pp. 1156–1164, Jul. 2018. [Online]. Available: <https://heart.bmj.com/lookup/doi/10.1136/heartjnl-2017-311198>

## **Bibliography**

---

## Chapter 8

---

# On the assessment of arterial compliance from carotid pressure waveform

Vasiliki Bikia<sup>1</sup>, Patrick Segers<sup>2</sup>, Georgios Rovas<sup>1</sup>, Stamatia Pagoulatou<sup>1</sup>, Nikolaos Stergiopoulos<sup>1</sup>

<sup>1</sup> *Institute of Bioengineering, École Polytechnique Fédérale de Lausanne, Switzerland*

<sup>2</sup> *IBiTech, University of Ghent, Belgium*

Published in AJP-Heart and Circulatory Physiology, 2021.

### Abstract

In a progressively aging population, it is of utmost importance to develop reliable, non-invasive, and cost-effective tools to estimate biomarkers that can be indicative of cardiovascular risk. Various pathophysiological conditions are associated with changes in the total arterial compliance ( $C_T$ ), and thus its estimation via an accurate and simple method is valuable. Direct non-invasive measurement of  $C_T$  is not feasible in clinical practice. Previous methods exist for indirect estimation of  $C_T$ , which, however, require non-invasive, yet complex and expensive, recordings of the central pressure and flow. Here, we introduce a novel, non-invasive method for estimating  $C_T$  from a single carotid waveform measurement using regression analysis. Features were extracted from the carotid wave and are combined with demographic data. A prediction pipeline is adopted for estimating  $C_T$  using, firstly, feature-based regression analysis and, secondly, the raw carotid pulse wave. The proposed methodology was appraised using the large human cohort ( $n = 2,256$ ) of the Asklepios study. Accurate estimates of  $C_T$  were yielded for both prediction schemes; namely  $r = 0.83$  and normalized-RMSE = 9.58 % for the feature-based model, and  $r = 0.83$  and normalized-RMSE = 9.67 % for the model which

## **Chapter 8. On the assessment of arterial compliance from carotid pressure waveform**

---

used the raw signal. The major advantage of this method pertains to the simplification of the technique offering easily applicable and convenient  $C_T$  monitoring. Such an approach could offer promising applications, ranging from fast and cost-efficient hemodynamical monitoring by the physician to integration in wearable technologies.

## 8.1 Introduction

In a progressively aging population, it is of utmost importance to develop reliable, non-invasive, and cost-effective tools for estimating relevant biomarkers which can be indicative of cardiovascular risk. Numerous invasive and non-invasive markers have been researched, but there is still the need for additional structural and functional parameters that would be able to assess cardiovascular risk [1]. The total arterial compliance ( $C_T$ ) is a biomechanical property of the arterial tree with great physiological and pathological importance [2; 3; 4].  $C_T$  and peripheral resistance constitute a major part of the arterial load on the heart [5]. Arterial compliance expresses the ability of the arterial system to store blood during systole without excessive pressure rise, and influences central blood pressure [6] and stroke volume [7]. The  $C_T$  is becoming a promising parameter for evaluating the relationship between structural and functional changes in the vascular system with respect to its elasticity and capacity [8; 9]. Alterations in arterial compliance are associated to various physiological (aging) [10] or pathological (hypertension) conditions [11], which cannot be necessarily assessed by current biomarkers. Importantly,  $C_T$  has been found to be superior over traditional evaluation techniques including pulse pressure and echocardiography [9; 11]. In addition, other studies have shown that  $C_T$  was proven capable of differentiating among diseased, elderly, and health individuals [10; 11; 12]. In view of the emerging evidence on the importance of  $C_T$  [8], the development of an accurate and simple method for its estimation may be valuable.

Direct non-invasive measurement of  $C_T$  is not feasible in the clinical practice. Several methods have been proposed for indirect estimation of  $C_T$  [13; 14; 15; 16]. Most commonly, these methods require simultaneous recordings of the proximal aortic pressure and flow waves. Some of the most reliable and accurate techniques include the decay time method (DTM), the area method (AM), and the pulse pressure method (PPM), [15; 17]. The principle of the DTM is that during diastole there is no inflow from the heart, and thus, the decrease of aortic pressure, is characterized by the decay time. This decay can be fitted mono-exponentially to any portion of the diastole to yield the characteristic time or time constant, which is  $RC_T$ , where  $R$  is a known value of peripheral resistance [18]. The AM was introduced by Randall [19] and it essentially represents an integral variation of the exponential decay method. Compliance is calculated from

$$RC_T = \int_{t_1}^{t_2} P dx / (P_1 - P_2),$$

where  $P_1$  and  $P_2$  are diastolic pressure at time points  $t_1$  and  $t_2$ , respectively. The PPM is based on the fact that the modulus of the input impedance of the arterial system is represented very well by the two-element Windkessel model for the low frequencies 1<sup>st</sup> to 5<sup>th</sup> harmonic). Therefore, the pulse pressure will be similar in the true arterial system and the two-element Windkessel model. The PPM uses an iterative process that yields the value of  $C_T$  that gives the best fit between the measured pulse pressure and the pulse pressure predicted by the



two-element Windkessel model.

Yet, the invasive nature, lack of convenience or high cost of the required measurements have limited the assessment of  $C_T$ , namely the inverse of arterial stiffness, in every day clinical practice, while surrogates of local or regional arterial stiffness have been applied more often [16; 20]. In particular, the carotid-femoral pulse wave velocity (cfPWV) is now considered as the gold standard to evaluate arterial stiffness [21].

Recent advances in machine learning have expanded the areas and the opportunities in developing novel modelling and predictive methods for clinical use [22]. In a previous study, Tavallali et al. proposed and validated a method for estimating cfPWV from the carotid waveform and clinical parameters using neural networks [23]. Their results showed that this approach can provide accurate estimates of cfPWV, offering an advancement in the assessment of arterial stiffness via cfPWV.

In view of these nascent opportunities, the present study introduces a novel, non-invasive, cost-efficient method for estimating  $C_T$  from a single carotid waveform using regression analysis. The proposed methodology uses an uncalibrated carotid blood pressure waveform which is subsequently calibrated using the brachial blood pressure values. Features are extracted from the carotid wave and are combined with readily available clinical parameters such as age, gender, height, and weight. A prediction pipeline is adopted for estimating  $C_T$  using, firstly, a feature-based regression analysis and, secondly, the raw carotid pulse wave. A main advantage of this method pertains to the avoidance of aortic blood flow recording which is commonly required by prior  $C_T$  estimators. Given that accurate values of  $C_T$  are cumbersome to obtain in the intact organism, in this study, the accuracy of the predictive model was evaluated by comparing the predictions against the  $C_T$  values which were derived using the precise and extensively validated PPM [18; 14; 15].

## 8.2 Methods & materials

### Asklepios database

Human data were available from the Asklepios study, a broad prospective longitudinal study with the aim of assessing the development and progression of cardiovascular disease [24]. A total of 2,404 subjects were found eligible to be included in the study. The participants underwent a non-invasive evaluation of central hemodynamics, including recordings of carotid blood pressure and aortic blood flow waveforms. The inclusion and exclusion criteria are listed in Table 8.1. The study protocol was approved by the ethical committee of Ghent University Hospital and informed consent of participation was given by all subjects. A comprehensive description of the Asklepios data can be found in the original publication [24].

Table 8.1 – Asklepios study inclusion and exclusion criteria.

<b>Inclusion criteria</b>
1 Male and female volunteers aged 35–55 years at study initiation, living in the communities of Erpe–Mere or Nieuwerkerken.
<b>Exclusion criteria</b>
1 Clinical presence of atherosclerosis/atherothrombosis (a) Atherosclerosis: symptomatic or hemodynamically significant (> 50 % stenosis) presence of atherosclerosis in any major vascular bed. (b) Atherothrombosis: acute coronary syndromes, cerebrovascular thrombosis. (c) Previous or planned revascularization procedure (carotid, coronary, lower limb).
2 Major concomitant illness (a) Cardiac: cardiomyopathy/heart failure, significant valvular disease, previous cardiac surgery, (complex) congenital heart disease, heart transplant. (b) Organ failure: end-stage renal disease, hepatic insufficiency, previous organ transplant. (c) Malignant tumours (recently diagnosed or currently treated, with < 3 years tumour-free follow-up or tumours that are metastatic or initial treatment was not curative). (d) Other conditions in which the screening physician expected a life expectancy < 5 years.
3 Diabetes mellitus (a) Diabetes mellitus type 1. (b) Diabetes mellitus type 2 if confirmed macrovasculopathy (see exclusion criterion 1) or significant renal impairment [see exclusion criterion 2(b)].
4 Specific conditions precluding accurate hemodynamic assessment. (a) Continually irregular cardiac cycle: atrial fibrillation. (b) State of hyperdynamic activity: pregnancy (in the preceding 6 months).
5 Inability to provide informed consent.

## **Chapter 8. On the assessment of arterial compliance from carotid pressure waveform**

---

### **Measurement of pressure and flow waves**

Blood pressure recordings were performed at the left common carotid artery via applanation tonometry using a Millar pen-type tonometer (SPT 301; Millar Instruments, Houston, Texas, USA). The measurement set-up, processing, and calibration procedure (based on sphygmomanometer systolic and diastolic blood pressure and applanation tonometry at the brachial artery) were previously described in detail [24; 25].

The carotid pressure was derived as a "mean" waveform of multiple beats from a 20-second recording [6]. Pressure data were recorded in continuous sequences of 20 seconds. The postprocessing included signal filtering (Savitsky-Golay filter, Matlab, The Mathworks Inc.). Subsequently, identification of individual cycles, detrending (i.e. linearly smoothing out eventual differences in the numerical value of the start and end of the cycle), and averaging were performed. The cycles with a cycle length shorter or longer than 20 % of the mean cycle duration were automatically deselected. The same applied for cycles with a shape surpassing the "envelope" curves, which were constructed from the average  $\pm$  (two times the standard deviation). The process was repeated iteratively until all cycles were within the "envelope" curves. As an arbitrary quality criterion, data were accepted only if minimally 10 cycles were retained. The average of these cycles was considered as the tonometry recording for the carotid artery. The carotid waveform was calibrated by assuming that diastolic and mean BP values remain fairly constant for the major arteries.

Flow at the aorta was measured using ultrasound (VIVID 7; GE Vingmed Ultrasound, Horten, Norway) from the cross-sectional area and blood velocities in the left ventricular outflow tract (LVOT). The internal diameter of the LVOT was measured in the parasternal long-axis view at the valve annulus, and LVOT area was calculated assuming a circular cross-section. Flow velocities were obtained in the LVOT via pulsed wave Doppler in the apical 5-chamber view. Images were exported in raw DICOM format and processed off-line within a dedicated software interface in Matlab (The Mathworks, Natick, MA). For each cardiac cycle, the onset and end of systolic ejection were visually delineated with two cursors, after which the contours in the systolic phase were automatically traced using the transition in pixel intensity above a user-defined threshold value. Two to three cycles were averaged, and the average cycle sub-sampled to 500 sample points and smoothed using a Savitsky-Golay filter (order 3, frame width 31). The maximal velocities were multiplied with the LVOT cross-sectional area to obtain the aorta flow waveform (assuming a flat velocity profile in the LVOT). This approach yielded physiologically relevant values of stroke volume and cardiac output [2].

The heart rate (HR) was calculated from the average duration of pressure and flow signals. The time vectors of the two signals were normalized, synchronized and then denormalized, rendering the heart cycle length equal to the average length of the pressure and flow waveform.

### Derivation of the reference compliance

Measurement of the real  $C_T$  values in a human cohort is not feasible. In the present study, the PPM was used as the ground truth value for compliance [18]. The PPM is based on the fact that the modulus of the input impedance of the arterial system is represented very well by the two-element Windkessel model for the low frequencies (1<sup>st</sup> to 5<sup>th</sup> harmonic). Therefore, the pulse pressure will be similar in the true arterial system and the two-element Windkessel model. From the ratio of mean pressure over mean flow we derive peripheral resistance. Then, using measured flow as input to the two-element Windkessel, the predicted pulse pressure is fit to the actual pulse pressure by adjusting compliance. Compliance adjustment is done by a simple "trial and error" type of approach knowing that lower compliance yields larger pulse pressures. Following an iterative process, the value of the compliance ( $C_T$ ) that gives the best fit of the measured pulse pressure provides the estimate of the compliance. The method has been thoroughly validated using both in silico [18; 17] and in vivo data [14], and it has been proven to be capable of accurately estimating arterial compliance.

### Features extraction from the carotid pressure wave

Features were extracted from the carotid pressure signal and its time derivative (Figure 8.1). The features included the systolic blood pressure (SBP), the diastolic blood pressure (DBP), the dicrotic notch pressure point ( $P_{DN}$ ), the dicrotic notch time point ( $t_{DN}$ ), the upstroke systolic area ( $A_{upstroke}$ ), the total systolic area ( $A_{systolic}$ ), the diastolic area ( $A_{diastolic}$ ), the peak of time derivative ( $dP/dt_{max}$ ), the time point that peak derivative occurs ( $tdP/dt_{max}$ ), and the HR.

### Regression analysis

The extracted features, i.e. SBP, DBP, MAP, PP,  $P_{DN}$ ,  $t_{DN}$ ,  $A_{upstroke}$ ,  $A_{systolic}$ ,  $A_{diastolic}$ ,  $dP/dt_{max}$ ,  $tdP/dt_{max}$ , HR, as well as the demographic data including age, gender, height, weight were used as the input features to the machine learning model. The  $C_T$  (as derived from PPM) was set to be the target output variable. The data were organized in pairs (inputs-outputs) and were kept for the training/testing process. For the regression process, we used an artificial neural network (ANN) and a linear regressor (LR) to estimate the target variable of interest. Furthermore, the performance of a predictive model including cardiac output (CO) as an additional input feature was assessed. It should be noted that the models including the CO feature are not considered as the main focus of the present study. We, however, decided to include them in the analysis for investigating the importance of CO in the estimations. For the ANN, a fixed one-hidden layer structure was selected and the "Adam" optimizer was used [27]. In addition, the ANN was trained/tested using as input the entire raw carotid waveform, as well as demographic data. The carotid BP waveforms were sampled at 100 data points per

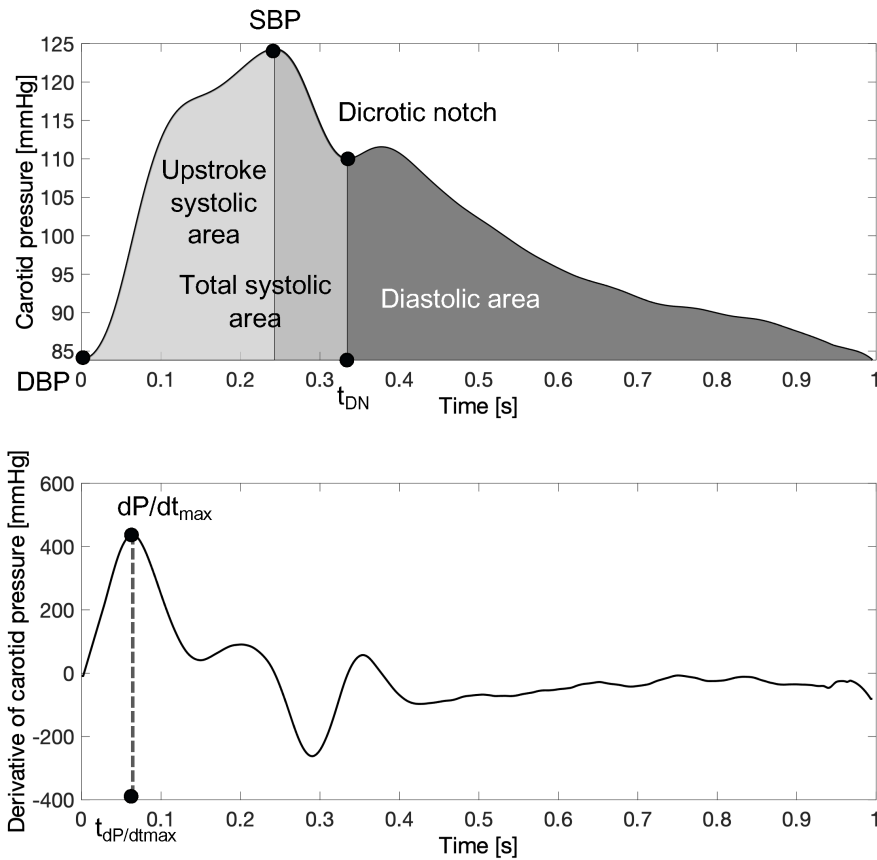


Figure 8.1 – Indication of features on the carotid pressure waveform and the time-derivative. Adapted from [26].

cycle. The predictive models are summarized in Table 8.2.

One-hundred forty eight out of the 2,404 participants were excluded due to missing or erroneously measured data. Their exclusion led to a final population of 2,256 participants. The data were randomly split into three sets: a training set (80 % of the total dataset), a validation set (10 %) and a test set (10 %). Therefore, out of the entire cohort, 1,796 subjects were used for the training, 223 data instances were used as validation for the hyperparameter selection and 237 subjects were kept for the testing. To mitigate overfitting and to increase the generalization capacity, the model should be trained for optimal hyperparameter values. For the ANN, the `batch_size` (defines the number of samples that will be propagated through the network) was set to be equal to 200, while the number of epochs was optimized. The number of epochs defines the number of times that the learning algorithm works through the entire training dataset. For selecting the optimal value for epochs, we computed the train loss and the validation loss for various values of epochs. Here, the loss corresponds to the mean square error (MSE). Loss values were monitored by Early stopping call back function. When an increment is observed in the loss values, training comes to halt and the respective value of epoch indicates

Table 8.2 – Summary of all the machine learning models trained/tested in this study.

Model	Inputs	Input vector size
LR1	SBP, DBP, MAP, PP, $P_{DN}$ , $t_{DN}$ , $A_{upstroke}$ , $A_{systolic}$ , $A_{diastolic}$ , $dP/dt_{max}$ , $tdP/dt_{max}$ , HR, age, gender, height, weight	16 inputs
LR2	SBP, DBP, MAP, PP, $P_{DN}$ , $t_{DN}$ , $A_{upstroke}$ , $A_{systolic}$ , $A_{diastolic}$ , $dP/dt_{max}$ , $tdP/dt_{max}$ , HR, age, gender, height, weight, CO	17 inputs
ANN1	SBP, DBP, MAP, PP, $P_{DN}$ , $t_{DN}$ , $A_{upstroke}$ , $A_{systolic}$ , $A_{diastolic}$ , $dP/dt_{max}$ , $tdP/dt_{max}$ , HR, age, gender, height, weight	16 inputs
ANN2	SBP, DBP, MAP, PP, $P_{DN}$ , $t_{DN}$ , $A_{upstroke}$ , $A_{systolic}$ , $A_{diastolic}$ , $dP/dt_{max}$ , $tdP/dt_{max}$ , HR, age, gender, height, weight, CO	17 inputs
ANN3	Entire raw carotid pressure waveform, HR, age, gender, height, weight	105 inputs
ANN4	Entire raw carotid pressure waveform, HR	101 inputs
ANN5	PP, SBP, $A_{diastolic}$ , $A_{systolic}$ , weight (Most important features)	5 inputs

Table 8.3 – Optimal number of epochs for every ANN configuration.

$C_T$ models	Epochs
ANN1	118
ANN2	380
ANN3	187
ANN4	212
ANN5	101

the optimal selection. All the yielded optimized hyperparameters are aggregated in Table 8.3. Subsequently, the test set was fed into the trained models to predict  $C_T$  and the precision was evaluated.

The current study aimed to evaluate the importance of each input feature for the  $C_T$  prediction. The importance was quantified by the use of the permutation feature importances [28]. The concept of permutation feature importances relies on measuring the importance of a feature by calculating the increase in the prediction error after permuting the feature. The permutation importances were computed by shuffling the values of each feature on the test set and by estimating the RMSE after the permutation. This process was repeated 20 times and the mean and standard deviation of the increase in RMSE were reported. Subsequently, an additional ANN was trained/tested using the 5 most important features yielded by the aforementioned analysis. The training/testing pipeline as well as the pre- and post-analyses were implemented

## Chapter 8. On the assessment of arterial compliance from carotid pressure waveform

---

using the Scikit-learn library [29] in a Python programming environment. The Pandas and Numpy packages were also used [30; 31].

### Sensitivity to noise and variations in the wave morphology

We further evaluated the robustness of the method in the case of measurement noise or variations in the morphology of the wave. The evaluation was done following two controlled experiments. Firstly, errors were considered for the extraction of the wave-based features for ANN1 model. Especially, errors in features were simulated with a random distribution. The error for each variable was randomly drawn from the range of  $[-5, 5]$  % (simulating a maximum absolute noise level equal to 5 %). Subsequently, each variable value was multiplied with a noise factor; for instance, for a randomly selected error of  $-4$  %, the respective variable value was multiplied with a noise factor equal to 0.96. The process was repeated for the noise ranges of  $\pm 7$  and  $\pm 10$  %. Secondly, we wished to simulate adverse effects for the ANN3 by distorting the shape of the input pressure wave. This was achieved by adding white Gaussian noise assuming three signal-to-ratio (SNR) values, i.e. 40, 35, and 30 dB. Selection of the SNR values was done experimentally so that an obvious distortion in the wave morphology is achieved that could render the model incapable of making a correct prediction. A lower SNR value would lead to an unrealistically signal variation which would be inappropriate to use and thus would be discarded. A higher SNR value would make it easy for the model to yield a precise estimation.

### Statistical analysis

All data are presented as means and standard deviation (SD). The statistical analysis was performed in Python (Python Software Foundation, Python Language Reference, version 3.6.8, available at <http://www.python.org>). The accuracy between the estimates and the reference values were evaluated using the Pearson's correlation coefficient ( $r$ ) and the normalized root mean square error (nRMSE). Bias and limits of agreement (LoA) (where the 95 % of errors are expected to lie) were calculated using the Bland-Altman analysis [32]. The computed nRMSE was based on the difference between the minimum and maximum values of the dependent variable  $y$  and was computed as  $RMSE/(y_{max}-y_{min})$ . Level of statistical significance was set equal to 0.05.

## 8.3 Results

The population consisted of 1,087 (48 %) male participants and 1,169 (52 %) female participants. The distributions of the cardiovascular parameters of the study cohort ( $n = 2,256$ ) are presented in Table 8.4.

Table 8.4 – Description of the cardiovascular characteristics and parameters of the study cohort (n = 2,256).

<b>Variable</b>	<b>mean±SD (n = 2,256)</b>
Age [years]	45.91±5.98
Height [cm]	169.18±8.82
Weight [kg]	73.65±14.45
Carotid SBP [mmHg]	130.96±10.90
Carotid DBP [mmHg]	77.36±16.83
Carotid PP [mmHg]	53.59±11.82
Mean arterial pressure [mmHg]	99.60±12.04
Cardiac output [L/min]	4.95±1.16
Heart rate [bpm]	60.35±8.94
Total arterial compliance [mL/mmHg]	1.00±0.32
Total peripheral resistance [mmHg.s/mL]	1.27±0.34
$P_{DN}$ [mmHg]	110.38±13.50
$t_{DN}$ [s]	0.38±0.05
$A_{upstroke}$ [mmHg.s]	26.21±7.00
$A_{systolic}$ [mmHg.s]	43.38±8.03
$A_{diastolic}$ [mmHg.s]	58.58±13.00
$dP/dt_{max}$ [mmHg/s]	657.07±160.08
$tdP/dt_{max}$ [s]	0.068±0.014

Table 8.5 – Regression statistics between the model-predicted and the reference  $C_T$  data.

<b>Model</b>	<b>Slope</b>	<b>Intercept [mL/mmHg]</b>	<b><math>r</math></b>	<b><math>P</math>-value</b>	<b>nRMSE [%]</b>	<b>Bias (LoA) [mL/mmHg]</b>
LR1	0.71	0.29	0.81	<0.001	10.63	-0.00 (-0.35,0.35)
LR2	0.93	0.07	0.93	<0.001	6.13	0.01 (-0.21,0.22)
ANN1	0.77	0.24	0.83	<0.001	9.58	0.01 (-0.33, 0.34)
ANN2	0.97	0.05	0.96	<0.001	4.8	0.01 (-0.15, 0.18)
ANN3	0.73	0.28	0.83	<0.001	9.67	0.02 (-0.32, 0.36)
ANN4	0.68	0.28	0.77	<0.001	11.26	-0.04 (-0.43, 0.35)
ANN5	0.74	0.26	0.82	<0.001	9.9	0.01 (-0.34, 0.36)

Two-sided  $P$ -value for a hypothesis test whose null hypothesis is that the slope is zero, using Wald Test with  $t$ -distribution of the test statistic.



## Chapter 8. On the assessment of arterial compliance from carotid pressure waveform

Table 8.6 – Permutation feature importances for the ANN1.

Feature	+ $\delta$ RMSE [mL/mmHg]	Feature	+ $\delta$ RMSE [mL/mmHg]
PP	0.31±0.04	$P_{DN}$	0.04±0.01
SBP	0.28±0.02	MAP	0.03±0.01
$A_{diastolic}$	0.24±0.02	$dP/dt_{max}$	0.02±0.00
$A_{systolic}$	0.14±0.02	HR	0.02±0.01
Weight	0.11±0.01	$t_{dP/dt_{max}}$	0.02±0.01
DBP	0.07±0.01	Age	0.02±0.00
Height	0.05±0.01	$t_{DN}$	0.01±0.00
Gender	0.04±0.01	$A_{upstroke}$	0.01±0.01

### Comparison between the model-predicted and reference data

The scatterplots and the Bland–Altman plots of the estimated  $C_T$  for each of the models against the ground truth are shown in Figures 8.2 and 8.3. Regression metrics for the agreement, precision, and bias are aggregated in Table 8.5. The regression slopes were similar for the LR1, ANN1, and ANN3 in which the demographic data were considered as inputs. Accuracy was significantly increased for the models which used CO as an input feature ( $r \geq 0.94$ ). Variability of the absolute errors between predicted and actual compliance values was low for the LR1, ANN1, and ANN3. In all models, LoA were narrow and biases were reported to be close to zero. Table 8.6 presents the feature importances of the input regressors for  $C_T$ , respectively. Among the inputs, PP, SBP, and  $A_{diastolic}$  appeared to have the highest importance levels (error increase was more than 0.20 mL/mmHg). On the other hand,  $P_{DN}$  and  $A_{upstroke}$  had the lowest importance levels (error increased by 0.01 mL/mmHg). The ANN5 using only the 5 top-contributing features had a satisfactory performance similar to the one of ANN1 which used all the extracted wave-based features and the performance of ANN3 which was fed with the entire waveform and the demographical data (nRMSE was found to be close to 10 % and correlation equal to 0.82).

### Sensitivity to noise and variations in the wave morphology

An input carotid pressure wave with the simulated artificial noise is illustrated in Figure 8.5. The addition of artificial noise affected the wave's shape, harming the smoothness of the curve and leading to variations in the peaks. We can observe that for an SNR = 30 dB, it begins to become difficult to clearly distinguish the shape. As anticipated, the agreement and correlation between the estimated  $C_T$  and the reference  $C_T$  decreased with the increase in the noise level. Table 8.7 reports the correlation coefficients and normalized RMSE values as a function of the noise levels for the two simulated experimental settings.

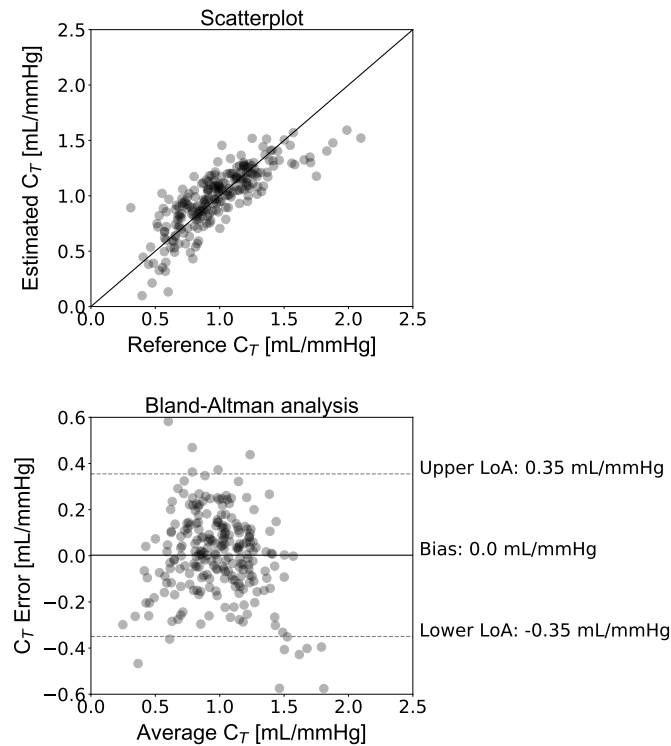


Figure 8.2 – Comparison between the predicted and the reference  $C_T$  data using LR1. Scatterplot and Bland–Altman plot between the predicted  $C_T$  and the reference  $C_T$  using the LR1 model. The solid line of the scatterplot represents equality. In Bland–Altman plot, limits of agreement (LoA) are defined by the two horizontal dashed lines. Adapted from [26].

## 8.4 Discussion

This paper introduces a novel machine learning method for estimating  $C_T$ . The findings indicated that arterial compliance can be accurately predicted by exploiting the carotid blood pressure waveform. This method relies on the raw information hidden in the carotid pulse wave that can be unveiled via the sophisticated machine learning capacity. In addition, the present study introduces an ANN estimator which is based on features extracted from the carotid wave. These features appeared to be powerful predictors of  $C_T$ . The major advantage of a method for estimating  $C_T$  from a single carotid pressure waveform is that it eliminates the need for a flow or velocity recording which require complex and expensive echocardiographic or magnetic resonance imaging procedures. Consequently, it provides a faster and more convenient way for monitoring arterial compliance.

The  $C_T$  together with the total vascular resistance are the two major parameters that describe the global biomechanical properties of the arterial system. Modelling vasculature and hemodynamical responses often require the estimation of  $C_T$ , while other methods for minimally invasive cardiac output monitoring (namely pulse contour analysis) are also dependent on  $C_T$

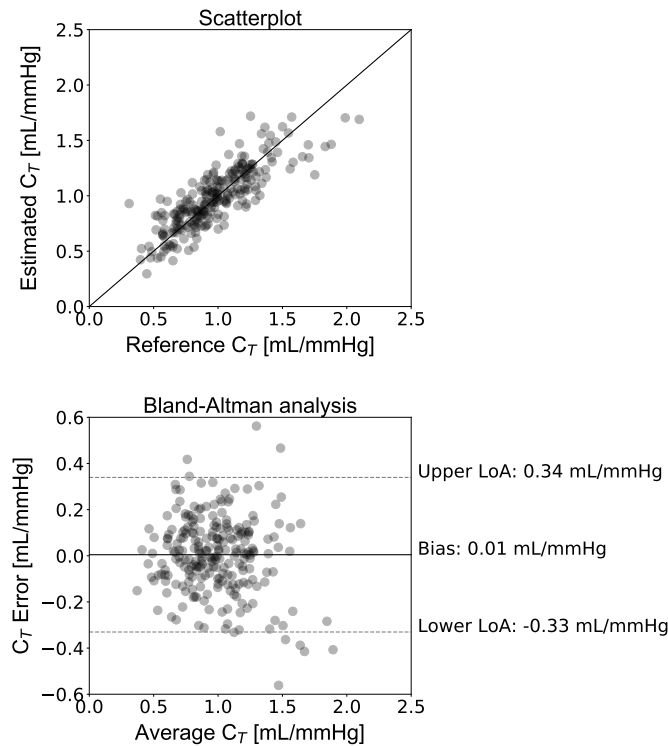


Figure 8.3 – Comparison between the predicted and the reference  $C_T$  data using ANN1. Scatterplot and Bland–Altman plot between the predicted  $C_T$  and the reference  $C_T$  using the ANN1 model. The solid line of the scatterplot represents equality. In Bland–Altman plot, limits of agreement (LoA) are defined by the two horizontal dashed lines. Adapted from [26].

values [33]. Yet, despite the additional clinical utility of  $C_T$ , current techniques for  $C_T$  have not entered the everyday clinical practice. This is mainly attributed to inherent limitations, including methodological complexity and expensiveness.

Moreover, the lack of a common basis and guidelines has hampered the establishment of  $C_T$  as an outcome predictor. However, several studies have demonstrated that assessment of  $C_T$  is valuable not only for cardiovascular risk evaluation but also for assessment of the relationship between structural and functional changes in the vascular system with respect to its elasticity [14; 34]. Moreover, Haluska et al. stressed that derivation of  $C_T$  adds incremental benefit to Framingham risk scores in patients with intermediate cardiovascular risk [9]. Hence,  $C_T$  is becoming a valuable parameter in the clinical setting by providing additive value in conjunction with other vascular characteristics [12] or by acting as a superior predictor over current traditional techniques [9]. The suggested method could potentially facilitate the further elucidation of the clinical utility of  $C_T$  as a risk predictor.

The current study trained and tested two machine learning models of different nature, namely a typical linear regressor, and an artificial neural network. There was not a significant variability in the errors among the two models for the feature-based configurations, i.e. LR1

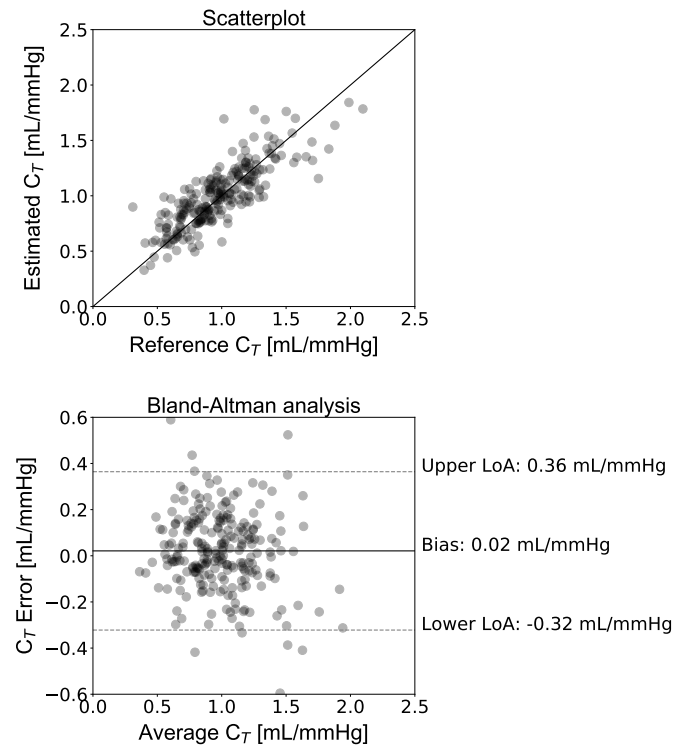


Figure 8.4 – Comparison between the predicted and the reference  $C_T$  data using ANN3. Scatterplot and Bland–Altman plot between the predicted  $C_T$  and the reference  $C_T$  using the ANN3 model. The solid line of the scatterplot represents equality. In Bland–Altman plot, limits of agreement (LoA) are defined by the two horizontal dashed lines. Adapted from [26].

and ANN1, (LoA were (-0.35,0.35) and (-0.33, 0.34) mL/mmHg). However, the LR1 could not account for the nonlinear relationships between the inputs and the compliance and this led to curvilinearity in the results' plots. Importantly, there is much additive value offered by the ANN estimator which has been proven capable of accurately predicting  $C_T$  from the raw blood pressure waveform. This approach could introduce a greatly promising method for the medical community by reducing the cost and the complexity in assessing  $C_T$ . Moreover, as anticipated, the inclusion of CO in the input vector essentially increased the precision of the results. Compliance is a measure of volume change against unit pressure change. Hence, the two parameters are highly interdependent. The dependency in conjunction to the blood pressure information allows for computing the one from the other. This is a principal applied by several existing methods. In addition, providing that the PPM (used to derive the reference  $C_T$ ) utilizes the aortic flow for the  $C_T$  calculation, introducing the aortic flow information to the machine learning model would inarguably reduce the error. Nevertheless, our study's objective is to provide estimates of  $C_T$  without the need for the aortic flow or velocity recording (and thus CO).

It is of importance to recognize the contribution of each input to the prediction of  $C_T$ . The PP

## Chapter 8. On the assessment of arterial compliance from carotid pressure waveform

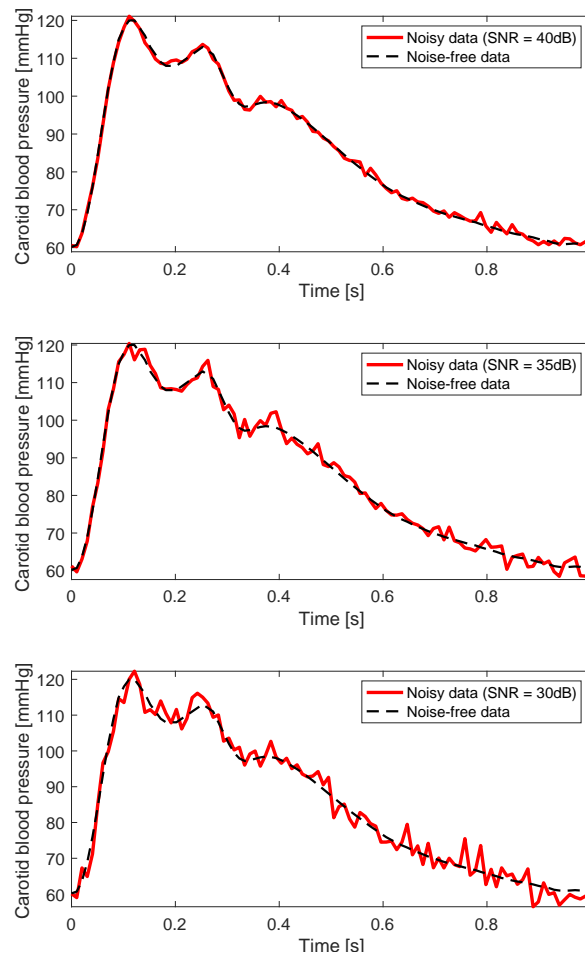


Figure 8.5 – Carotid blood pressure waves after adding artificial noise. The noisy data are presented in red solid lines and the original noise-free data in black dashed lines. Adapted from [26].

was found to have the highest influence on the prediction error, namely  $0.31 \pm 0.04$  mL/mmHg for  $C_T$  values within a range of 0.3-2.1 mL/mmHg. This is highly anticipated given that PP is essentially determined by the elastic properties of the aorta [35]. Due to the topological proximity of the carotid artery to the aorta, the carotid PP constitutes a fair surrogate of the aortic PP. Hence, the strong interdependence between the PP and  $C_T$  is also in effect for the carotid pressure. Moreover, one should not ignore the fact that the PPM, which was applied for acquiring the compliance values, relies on an iterative process that yields the  $C_T$  with the best fit in terms of PP. The SBP also appeared to impact the accuracy of the estimation by an error increase of  $0.28 \pm 0.02$  mL/mmHg. The PP and SBP were followed by  $A_{diastolic}$  and  $A_{systolic}$ . The combination of the latter yields the entire area under the curve whose measurement is involved in the arterial pulse contour analysis for CO estimation [33]; knowledge of MAP and a notion of CO allows for approximating arterial compliance. Moreover, the substantial contribution of the  $A_{diastolic}$  may be attributed to its association to the decay

Table 8.7 – Correlation coefficients and nRMSE values as a function of the artificial noise level in the distorted carotid pressure waves for the ANN1 and ANN3.

Model		$r$	nRMSE [%]
	<b>Noise level [%]</b>		
ANN1	±5	0.79	10.73
	±7	0.78	11.11
	±10	0.71	13.51
	<b>SNR [dB]</b>		
ANN3	40	0.8	10.34
	35	0.79	10.76
	30	0.75	12.36

time constant ( $\tau = RC_T$ ) whose concept it is employed by the AM for estimating compliance. The demographic information, and in particular weight, had a high importance level for the  $C_T$  estimator. This was also observed from the reduced precision of the predictive model which excluded the individual's demographic data from the input vector (ANN4) where correlation was decreased to 0.77. Arterial compliance has been shown to be highly dependent on arterial geometry which is determined by the body size, and thus weight and height. When only the most importance features were used in ANN5 (permutation importance higher than 0.1 mL/mmHg), the accuracy was remained similarly high as the one of the ANNs which used either all the extracted features (ANN1) or all the wave points (ANN3). Therefore, it should not be necessary to use a higher number of input features for the  $C_T$  predictive models. Finally, the lower importance levels of some inputs might be explained by the fact that the information embedded in their values may be contained already in other inputs with higher importance levels.

Estimation of cfPWV using the proposed methodology would yield a correlation equal to 0.6 between the estimated and the reference values (data not shown). It is likely that the lower correlation is attributed to the fact that the method uses as input a waveform from a single arterial site, while measurement of the foot-to-foot cfPWV requires waves from two arterial locations. Nevertheless, cfPWV can be measured in an easy and non-invasive way with satisfactory reproducibility, and hence further simplification of its acquisition would not add tremendously to the current state of the art. In contrast, fast, convenient, and cost-efficient determination of  $C_T$  is still missing.

In this study, we chose to use a single carotid pressure waveform for estimating arterial compliance. The rationale behind the use of a single wave relies on the current function of the existing devices. The current commercial devices (e.g. SphygmoCor) collect multiple recordings of the pressure wave for a specific time window and then yield an average blood pressure wave for the subject under consideration. Ideally, our algorithm could be embedded into such a device and provide the additional approximation of arterial compliance. In such

## **Chapter 8. On the assessment of arterial compliance from carotid pressure waveform**

---

a setting, a single carotid waveform would be sufficient. However, as variations may occur across several beats of measurement, it is possible that the  $C_T$  prediction is influenced. Yet, the sensitivity analysis demonstrated that small alterations in the wave's morphology due to noise do not affect significantly the predictions for an SNR equal to 40 dB. Validation of the methodology using multiple beats of carotid pressure remains to be conducted in order to quantify the effect of such variations in vivo.

The BP waveform has been shown to be crucial for assessing the vascular state in the human. It provides outstanding information on central hemodynamics, micro- and macrocirculation crosstalk, as well as arterial stiffness, [2; 3; 9; 36; 37]. Moreover, signal processing techniques are rapidly advancing allowing for creating a gold mine of physiological information hidden in pressure blood waveform. In this study, we evaluated the performance of machine learning models on revealing the hidden information related to arterial compliance in commonly used pressure wave features. Furthermore, we tested the unveiling capacity of an ANN which was fed with the raw pressure signal and received no guidance regarding the input features to use for the training/testing process. Interestingly, the algorithm performed very satisfactorily when the raw carotid waveform was prescribed to the ANN input layer. These findings indicate the beginning of a new era where the machine learning algorithms are capable of revealing more sophisticated piece of vascular information through learning by itself from the available clinical data.

Undoubtedly, non-invasive health monitoring technology is on the frontiers of modern healthcare and it is bound to expand inside and beyond the clinical environment. Concurrently, the rapid advance of wearable technologies is transforming the healthcare system on a global scale. Blood pressure sensing devices aim to be essentially miniaturized whereas their function will be highly assisted by pressure wave analysis techniques. In this context, reducing the required measurements to only a single waveform in conjunction with the greatly promising potential of signal processing techniques creates a unique opportunity for future use in the market. In addition, medical consultation is expected to become available remotely at all times by connecting to the data cloud where specialized clinicians will be interpreting the available parameters.

### **Limitations**

A main limitation of this study is that the values for  $C_T$ , which were used as the ground truth, were derived using the PPM. Unarguably, this value does not correspond to the actual arterial compliance. Nonetheless, acquisition of the real arterial compliance would not be feasible in an intact organism. In addition, the PPM has been shown to provide reliable compliance estimations and, therefore, it constitutes a trustworthy alternative for validating our method [14; 15; 18]. Another limitation is that the study population included individuals free of cardiovascular disease or pathology. It is not guaranteed that the developed models will be capable

of making predictions for patients with, for instance, aortic valve stenosis, arrhythmias or other pathologies. In future work, we aim to validate the proposed methodological framework using such populations. Finally, it is well established that healthy aging and cardiovascular diseases, such as hypertension and heart failure, are associated with increased arterial stiffness [38; 39]. Therefore, a method which is capable of differentiating between healthy and disease is highly desirable. At this initial stage, we demonstrated that accurate estimations of  $C_T$  can be yielded using our machine learning-based approach. Given that  $C_T$  has been found to be capable of differentiating between hypertensive, elderly and healthy individuals [10; 11; 12], as a next step, we envision to evaluate the robustness of the proposed method for classifying high-risk populations and finally verify its clinical significance in terms of risk stratification.

### Conclusion

This paper introduces a novel artificial intelligence method to estimate the  $C_T$ . The method relies on exploiting the information provided by the carotid blood pressure waveform as well as typical clinical variables (such as demographic data). Our results demonstrated that accurate estimates of  $C_T$  can be obtained following our methodology. The importance of the method is based on the simplification of the technique offering easily applicable and convenient monitoring of  $C_T$ . Such an approach could provide promising applications which may be integrated in wearable technologies and smartphones. Finally, the study further supports the importance of arterial pulse waves in the assessment of cardiovascular health and suggests the potentiality of machine learning in advancing the detection of clinical biomarkers in medicine.



## **Chapter 8. On the assessment of arterial compliance from carotid pressure waveform**

---

## Bibliography

- [1] W. Koenig, "Update on integrated biomarkers for assessment of long-term risk of cardiovascular complications in initially healthy subjects and patients with manifest atherosclerosis," *Annals of Medicine*, vol. 41, no. 5, pp. 332–343, Jan. 2009.
- [2] M. E. Safar and G. M. London, "Arterial and venous compliance in sustained essential hypertension." *Hypertension*, vol. 10, no. 2, pp. 133–139, Aug. 1987.
- [3] D. Chemla, I. Antony, Y. Lecarpentier, and A. Nitenberg, "Contribution of systemic vascular resistance and total arterial compliance to effective arterial elastance in humans," *American Journal of Physiology-Heart and Circulatory Physiology*, vol. 285, no. 2, pp. H614–H620, Aug. 2003.
- [4] B. A. Haluska, L. Jeffriess, M. Downey, S. G. Carlier, and T. H. Marwick, "Influence of cardiovascular risk factors on total arterial compliance," *Journal of the American Society of Echocardiography*, vol. 21, no. 2, pp. 123–128, Feb. 2008.
- [5] G. Elzinga and N. Westerhof, "Pressure and flow generated by the left ventricle against different impedances," *Circulation Research*, vol. 32, no. 2, pp. 178–186, Feb. 1973.
- [6] P. Segers, E. R. Rietzschel, M. L. De Buyzere, S. J. Vermeersch, D. De Bacquer, L. M. Van Bortel, G. De Backer, T. C. Gillebert, and P. R. Verdonck, "Noninvasive (input) impedance, pulse wave velocity, and wave reflection in healthy middle-aged men and women," *Hypertension*, vol. 49, no. 6, pp. 1248–1255, Jun. 2007.
- [7] N. Stergiopoulos, J. J. Meister, and N. Westerhof, "Determinants of stroke volume and systolic and diastolic aortic pressure," *American Journal of Physiology-Heart and Circulatory Physiology*, vol. 270, no. 6, pp. H2050–H2059, Jun. 1996.
- [8] R. Heitmar, "Total arterial compliance: the future of cardiovascular risk assessment?" *Journal of Human Hypertension*, vol. 24, no. 4, pp. 227–229, Apr. 2010.
- [9] B. A. Haluska, L. Jeffries, S. Carlier, and T. H. Marwick, "Measurement of arterial distensibility and compliance to assess prognosis," *Atherosclerosis*, vol. 209, no. 2, pp. 474–480, Apr. 2010, PMID: 19896128.

## Bibliography

---

- [10] L. Van Bortel and J. Spek, "Influence of aging on arterial compliance," *Journal of Human Hypertension*, vol. 12, no. 9, pp. 583–586, Sep. 1998.
- [11] A. Beltran, "Arterial compliance abnormalities in isolated systolic hypertension," *American Journal of Hypertension*, vol. 14, no. 10, pp. 1007–1011, Oct. 2001.
- [12] L. Lind, "Arterial compliance and endothelium-dependent vasodilation are independently related to coronary risk in the elderly: the prospective investigation of the vasculature in uppsala seniors (pivus) study," *Clinical Physiology and Functional Imaging*, vol. 28, no. 6, pp. 373–377, Nov. 2008.
- [13] Z. Liu, K. P. Brin, and F. C. Yin, "Estimation of total arterial compliance: an improved method and evaluation of current methods," *American Journal of Physiology-Heart and Circulatory Physiology*, vol. 251, no. 3, pp. H588–H600, Sep. 1986.
- [14] N. Stergiopulos, P. Segers, and N. Westerhof, "Use of pulse pressure method for estimating total arterial compliance in vivo," *The American Journal of Physiology*, vol. 276, no. 2 Pt 2, pp. H424–428, Feb. 1999, PMID: 9950841.
- [15] P. Segers, P. Verdonck, Y. Deryck, S. Brimiouille, R. Naeije, S. Carlier, and N. Stergiopulos, "Pulse pressure method and the area method for the estimation of total arterial compliance in dogs: sensitivity to wave reflection intensity," *Annals of Biomedical Engineering*, vol. 27, no. 4, pp. 480–485, Aug. 1999, PMID: 10468232.
- [16] I. S. Mackenzie, I. B. Wilkinson, and J. R. Cockcroft, "Assessment of arterial stiffness in clinical practice," *QJM: monthly journal of the Association of Physicians*, vol. 95, no. 2, pp. 67–74, Feb. 2002, PMID: 11861952.
- [17] N. Stergiopulos, J. J. Meister, and N. Westerhof, "Evaluation of methods for estimation of total arterial compliance," *American Journal of Physiology-Heart and Circulatory Physiology*, vol. 268, no. 4, pp. H1540–H1548, Apr. 1995.
- [18] M. Stergiopulos and Westerhof, "Simple and accurate way for estimating total and segmental arterial compliance: the pulse pressure method," *Annals of Biomedical Engineering*, vol. 22, no. 4, pp. 392–397, Aug. 1994, PMID: 7998684.
- [19] O. S. Randall, M. D. Esler, R. V. Calfee, G. F. Bulloch, A. S. Maisel, and B. Culp, "Arterial compliance in hypertension," *Australian and New Zealand Journal of Medicine*, vol. 6, pp. 49–59, Jun. 1976.
- [20] S. Sakuragi and W. P. Abhayaratna, "Arterial stiffness: methods of measurement, physiologic determinants and prediction of cardiovascular outcomes," *International Journal of Cardiology*, vol. 138, no. 2, pp. 112–118, Jan. 2010, PMID: 19473713.

- [21] S. Laurent, J. Cockcroft, L. Van Bortel, P. Boutouyrie, C. Giannattasio, D. Hayoz, B. Pannier, C. Vlachopoulos, I. Wilkinson, H. Struijker-Boudier, and on behalf of the European Network for Non-invasive Investigation of Large Arteries, “Expert consensus document on arterial stiffness: methodological issues and clinical applications,” *European Heart Journal*, vol. 27, no. 21, pp. 2588–2605, Sep. 2006.
- [22] K. Shameer, K. W. Johnson, B. S. Glicksberg, J. T. Dudley, and P. P. Sengupta, “Machine learning in cardiovascular medicine: are we there yet?” *Heart*, vol. 104, no. 14, pp. 1156–1164, Jul. 2018.
- [23] P. Tavallali, M. Razavi, and N. M. Pahlevan, “Artificial intelligence estimation of carotid-femoral pulse wave velocity using carotid waveform,” *Scientific Reports*, vol. 8, no. 1, p. 1014, Dec. 2018.
- [24] E.-R. Rietzschel, M. L. De Buyzere, S. Bekaert, P. Segers, D. De Bacquer, L. Cooman, P. Van Damme, P. Cassiman, M. Langlois, P. van Oostveldt *et al.*, “Rationale, design, methods and baseline characteristics of the asklepios study,” *European Journal of Preventive Cardiology*, vol. 14, no. 2, pp. 179–191, 2007.
- [25] P. Segers, E. Rietzschel, S. Heireman, M. Debuyzere, T. Gillebert, P. Verdonck, and L. Vanbortel, “Carotid tonometry versus synthesized aorta pressure waves for the estimation of central systolic blood pressure and augmentation index,” *American Journal of Hypertension*, vol. 18, no. 9, pp. 1168–1173, Sep. 2005.
- [26] V. Bikia, P. Segers, G. Rovas, S. Pagoulatou, and N. Stergiopoulos, “On the assessment of arterial compliance from carotid pressure waveform,” *American Journal of Physiology-Heart and Circulatory Physiology*, vol. 321, no. 2, pp. H424–H434, 2021.
- [27] D. P. Kingma and J. Ba, “Adam: a method for stochastic optimization.” San Diego, US: 3rd International Conference for Learning Representations, 2017. [Online]. Available: <https://arxiv.org/pdf/1412.6980.pdf>
- [28] L. Breiman, “Random forests,” *Machine Learning*, vol. 45, no. 1, pp. 5–32, 2001.
- [29] F. Pedregosa, G. Varoquaux, A. Gramfort, V. Michel, B. Thirion, O. Grisel, M. Blondel, P. Prettenhofer, R. Weiss, V. Dubourg, J. Vanderplas, A. Passos, D. Cournapeau, M. Brucher, M. Perrot, and E. Duchesnay, “Scikit-learn: machine learning in python,” vol. 12, pp. 2825–2830, 2011.
- [30] W. McKinney, “Data structures for statistical computing in python,” in *Proceedings of the 9th Python in Science Conference*, 2010, pp. 51–56, doi: 10.25080/Majora-92bf1922-00a.
- [31] T. E. Oliphant, “A guide to numpy.” Trelgol Publishing USA, 2006, vol. 1.

## Bibliography

---

- [32] J. M. Bland and D. G. Altman, "Statistical methods for assessing agreement between two methods of clinical measurement," *Lancet (London, England)*, vol. 1, no. 8476, pp. 307–310, Feb. 1986, PMID: 2868172.
- [33] E. Litton\* and M. Morgan, "The picco monitor: A review," *Anaesthesia and Intensive Care*, vol. 40, no. 3, pp. 393–408, May 2012.
- [34] J. D. Cameron, G. L. Jennings, and A. M. Dart, "Systemic arterial compliance is decreased in newly-diagnosed patients with coronary heart disease: implications for prediction of risk," *Journal of Cardiovascular Risk*, vol. 3, no. 6, pp. 495–500, Dec. 1996, PMID: 9100084.
- [35] N. Stergiopoulos and N. Westerhof, "Determinants of pulse pressure," *Hypertension*, vol. 32, no. 3, pp. 556–559, Sep. 1998.
- [36] B. A. Haluska, "Influence of arterial compliance on presence and extent of ischaemia during stress echocardiography," *Heart*, vol. 92, no. 1, pp. 40–43, Jan. 2006.
- [37] P. Bruinsma, T. Arts, J. Dankelman, and J. A. E. Spaan, "Model of the coronary circulation based on pressure dependence of coronary resistance and compliance," *Basic Research in Cardiology*, vol. 83, no. 5, pp. 510–524, Sep. 1988.
- [38] G. F. Mitchell, "Arterial stiffness and hypertension: Chicken or egg?" *Hypertension*, vol. 64, no. 2, pp. 210–214, Aug. 2014.
- [39] J. A. Chirinos, P. Segers, T. Hughes, and R. Townsend, "Large-artery stiffness in health and disease," *Journal of the American College of Cardiology*, vol. 74, no. 9, pp. 1237–1263, Sep. 2019.

## Chapter 9

---

# The impact of heart rate on pulse wave velocity: an in silico evaluation

Vasiliki Bikia<sup>1</sup>, Nikolaos Stergiopoulos<sup>1</sup>, Georgios Rovas<sup>1</sup>, Stamatia Pagoulatou<sup>1</sup>, Theodore G. Papaioannou<sup>2</sup>

<sup>1</sup> *Institute of Bioengineering, École Polytechnique Fédérale de Lausanne, Switzerland*

<sup>2</sup> *Biomedical Engineering Unit, 1<sup>st</sup> Department of Cardiology, “Hippokration” Hospital, Medical School, National and Kapodistrian University of Athens, Greece*

Published in Journal of Hypertension, 2020.

### Abstract

Clinical and experimental evidence regarding the influence of HR on arterial stiffness and its surrogate marker carotid-femoral pulse wave velocity (cfPWV) is conflicting. We aimed to evaluate the effect of HR on cfPWV measurement under controlled hemodynamic conditions and especially with respect to blood pressure (BP) that is a strong determinant of arterial stiffness. Fifty-nine simulated cases were created using a previously validated in silico model. For each case, cfPWV was measured at five HR values, 60, 70, 80, 90, and 100 bpm. With increasing HR, we assessed cfPWV under two scenarios: with BP free to vary in response to HR increase, and with aortic DBP (aDBP) fixed to its baseline value at 60 bpm, by modifying total peripheral resistance accordingly. Further, we quantified the importance of arterial compliance ( $C_T$ ) on cfPWV changes caused by increasing HR. When BP was left free to vary with HR, a significant HR-effect on cfPWV ( $0.66 \pm 0.24$  m/s per 10 bpm,  $P$ -value  $< 0.001$ ) was observed. This effect was reduced to  $0.21 \pm 0.14$  m/s per 10 bpm ( $P$ -value = 0.048) when aDBP was maintained fixed with increasing HR. The HR-effect on the BP-corrected cfPWV was higher

## **Chapter 9. The impact of heart rate on pulse wave velocity: an in silico evaluation**

---

in the case of low  $C_T = 0.8 \pm 0.3$  mL/mmHg ( $0.26 \pm 0.15$  m/s per 10 bpm,  $P$ -value = 0.014) than the case of higher  $C_T = 1.7 \pm 0.5$  mL/mmHg ( $0.16 \pm 0.07$  m/s per 10 bpm,  $P$ -value = 0.045). Our findings demonstrated that relatively small HR changes may only slightly affect the cfPWV. Nevertheless, in cases wherein HR might vary to a greater extent, a more clinically significant impact on cfPWV should be considered.

## 9.1 Introduction

Pulse wave velocity (PWV), defined as the propagation speed of the pulse wave through the circulatory system, constitutes a significant and clinically pertinent index of arterial stiffness [1]. A huge body of clinical evidence, using simple and reproducible non-invasive techniques [2], indicates that arterial stiffness (as assessed via PWV measurement) is a strong, independent predictor of cardiovascular morbidity and mortality in several populations [1; 3; 4; 5]. Measurement of carotid-femoral PWV (cfPWV) is considered as the gold-standard non-invasive method for the assessment of aortic stiffness [6], and can be readily performed by several non-invasive techniques and devices.

An increased variation in sequential cfPWV measurements may be often observed [7], due to inherent physiological vascular and hemodynamic variations or/and measurement errors. A parameter that has been questioned for affecting cfPWV is the heart rate (HR). Cross-sectional population studies have demonstrated either no significant correlation [8] or a positive correlation between cfPWV and resting HR [9; 10]. Albaladejo et al. [8] reported that there is no significant rise in cfPWV when HR is increased. On the contrary, Lantelme et al. [10] demonstrated that HR is an important factor of the intra-patient cfPWV changes in the elderly. Nevertheless, those studies have investigated the potential effect of HR on cfPWV without isolating the effect of the concurrent increase in blood pressure (BP) with increasing HR. In addition, results from existing acute experimental studies have been also inconclusive [10]. Therefore, it is of utmost importance to investigate more thoroughly the BP-independent cfPWV-HR relation; especially, now, that the clinical use of cfPWV is increasing [11; 12; 13]. The main objective of the present study was to evaluate and quantify the influence of HR on cfPWV measurement, and determine potential hemodynamic conditions that modulate the HR- cfPWV association. Furthermore, we aimed to quantify the potential impact of arterial compliance on cfPWV changes caused by increasing HR.

## 9.2 Methods & materials

We used a dataset of virtual individuals with a variety of cardiovascular characteristics. Specifically, 59 virtual individuals were created using a generic 1-D model of the human cardiovascular system [14]. For every individual, the HR was increased at five levels, that is, 60, 70, 80, 90, 100 bpm and PWV was determined at each of them. BP at the ascending aorta and brachial artery was also determined at each HR level. Finally, we calculated the stroke volume (SV) and the mean aortic flow (cardiac output).

We performed two experiment series: with BP free to vary when HR was increased, and with BP fixed to its baseline value (at 60 bpm). For this purpose, the aortic DBP (aDBP) was maintained constant by altering the total peripheral resistance (TPR). Adjusting TPR compensated for the HR-related changes in cardiac output and allowed us to maintain the pressure level constant.



## Chapter 9. The impact of heart rate on pulse wave velocity: an in silico evaluation

---

This was done to ensure that potential changes in cfPWV were the result of the change in HR alone and not due to the expected BP increase.

### Generation of the in silico population

We simulated 59 hemodynamic cases by running an in silico model of the cardiovascular system using arbitrary sets of input parameters. The values' ranges of the input parameters were selected based on physiological data published in the literature (Table 9.1) [15; 16; 17; 18; 19; 20; 21; 22; 23]. The model that was adopted in the present study has been previously described and validated against in vivo measurements [14; 24].

It comprises the main arteries of the systemic circulation, including a network of the cerebral circulation and the coronary circulation. The governing equations of the model are acquired by integration of the longitudinal momentum and continuity equations over the arterial cross-section. Flow and pressure waves are obtained at an arterial segment-level by solving the governing equations using an implicit finite-difference scheme. Concretely, the simulated flow and pressure waveforms are provided in the form of a vector with respect to the time duration of the cardiac cycle. The arteries are considered as long tapered tubes, and their compliance is defined as a nonlinear function of pressure and location [15]. Nonlinearity and more importantly for the purpose of this study viscoelasticity of the arterial wall is considered following Holenstein et al. [25]. Distal vessels are terminated with three-element Windkessel models to consider the resistance of the peripheral vasculature. Contractility of the left ventricle is simulated with a time-varying elastance model [26; 27]. The HR is prescribed as an input parameter to the model of the left ventricle. It should be noted that the model also captures the variation of the ratio of systolic and diastolic duration in the presence of HR changes. Namely, an increase in HR will result to an increase in the systole/diastole duration ratio [28]. The dead volume ( $V_d$ ) and the time of maximal elastance were kept unchanged and equal to the average values of  $V_d = 15$  mL and  $t_{max} = 340$  ms as reported previously [14; 29]. Arterial geometry was changed by adapting the height of the arterial tree, as well as the diameter of the arterial segments in order to simulate different body types. The cardiovascular parameters of the entire virtual study population are reported in Table 9.1.

### Data analysis

The values of HR varied between 60 and 100bpm for each of the virtual cases. At an individual-level at each HR level, cfPWV, BP (aortic and brachial), SV and mean aortic blood flow were computed. The 'measurements' were performed for both scenarios, namely free-varying pressure and fixed aortic BP.

The cfPWV was calculated by a foot-to-foot algorithm using the tangential method [30]. Pulse transit time was computed between the carotid artery and the femoral artery. The method

Table 9.1 – Cardiovascular parameters of the virtual study population (n = 59).

Parameter	Value (n = 59)				Reference
	min	max	mean	SD	
Height [cm]	150.00	200.00	170.00	13.50	[22]
End-systolic elastance [mmHg/mL]	1.14	3.48	2.24	0.60	[16; 17; 18]
End-diastolic elastance [mmHg/mL]	0.05	0.19	0.11	0.03	
Venous pressure [mmHg]	9.46	22.57	16.17	3.29	[19]
Aortic diameter [cm]	1.91	3.98	2.74	1.44	[20; 21]
*Aortic distensibility [ $10^{-3}$ /mmHg]	1.00	8.05	4.53	1.90	[22; 15]
*Brachial distensibility [ $10^{-3}$ /mmHg]	0.40	3.23	1.82	0.76	
TPR [mmHg.s/mL]	0.62	1.55	1.13	0.24	[23]
*The arterial wall distensibility and the respective lumen radius correspond to a reference transmural pressure of 100 mmHg.					

uses the intersection point of two tangents on the arterial pressure wave, that is the tangent passing through the systolic upstroke and the horizontal line passing through the minimum of the pressure wave. The travel length was determined by summation of the lengths of the arterial segments within the transmission path, that is the relevant carotid-femoral path. Then, the value of cfPWV was calculated by dividing the total travel length by the pulse transit time.

In addition, aortic SBP, DBP, mean arterial pressure (MAP) and pulse pressure (PP) were derived from the pressure waveform at the aortic root. Brachial SBP, DBP, MAP and PP were obtained by computing the pressure at the left brachial artery. SV was calculated from the area under the curve of the aortic flow waveform. Mean aortic flow was derived from the mean value of the flow waveform at the aortic root.

### Blood pressure correction method

To isolate the direct HR effect on PWV from any consequent BP influence, we employed a method to correct for BP; namely, to maintain constant the aortic DBP (aDBP). The aDBP was chosen instead of MAP, as cfPWV was computed using the foot-to-foot method and thus, using the diastolic points of the pulse wave (this point is further elaborated in the Discussion). In this respect, the individual- specific TPR was adjusted. This was achieved by multiplying the TPR with a scaling factor. A gradient-based optimization algorithm was employed to derive the adjusted TPR. With increasing HR (from 60 to 100 bpm) in every individual, the optimization algorithm estimated the optimal TPR that would allow aDBP to remain constant (equal to its baseline value at 60 bpm) eliminating the expected rise in pressure. The tolerated error for capturing aDBP was set to 0.01 %. Figure 9.1 provides the schematic representation of the optimization process used to correct cfPWV measurement for BP changes. Once the algorithm provided the corrected TPR, the 1-D model ran and produced the flow and pressure waves for

## Chapter 9. The impact of heart rate on pulse wave velocity: an in silico evaluation

every segment of the arterial tree. From the solution, we were able to obtain the quantities of interest, including the corrected cfPWV.

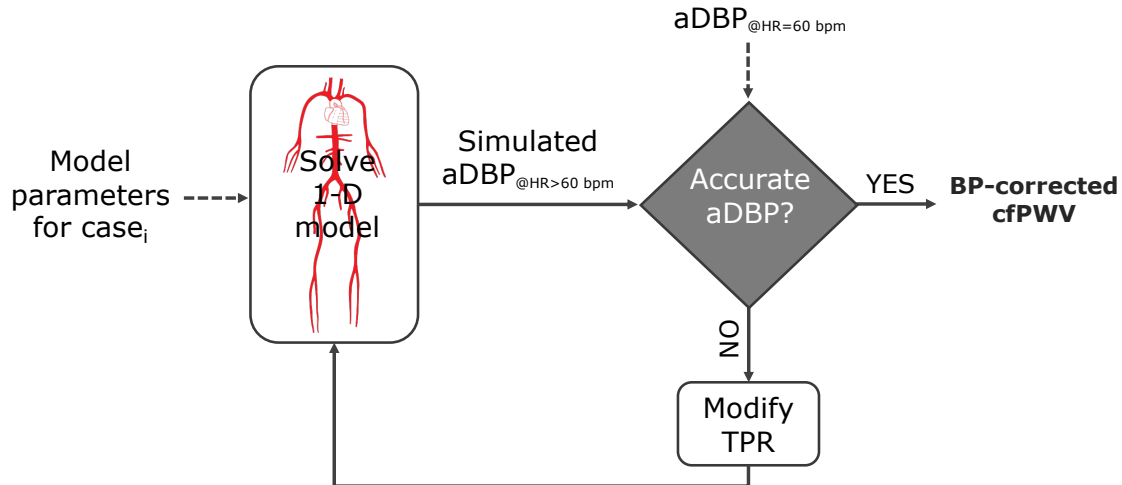


Figure 9.1 – Schematic representation of the optimization algorithm that corrects blood pressure. aDBP, aortic DBP; BP, blood pressure; cfPWV, carotid-femoral pulse wave velocity; TPR, total peripheral resistance. Adapted from [31].

### Compliance-dependency of pulse wave velocity response to increasing heart rate

Further investigation was performed to quantify the importance of arterial compliance on the cfPWV changes caused by increasing HR. The effect of HR on cfPWV was assessed for two different levels of arterial stiffness. In this respect, the entire sample was divided into two groups based on the total arterial compliance ( $C_T$ ) to represent two different levels of arterial stiffness, that is a more elastic tree ( $C_T > 2.00$  mL/mmHg) and a stiffer tree ( $C_T < 2.00$  mL/mmHg). The hemodynamical parameters of the two groups at baseline conditions, that is 60 bpm, are presented in Table 9.2. With increasing HR, the variable characteristics of the two groups were assessed and compared.

### Statistical analysis

The statistical analysis was performed in Python (Python Software Foundation, Python Language Reference, version 3.6.8; <http://www.python.org>). One-way analysis of variance (ANOVA) for repeated measures was used to determine the effect of HR levels on cfPWV, SBP, DBP, MAP, SV and cardiac output (CO). Values were reported as mean±SD. Statistically significant difference was set at the level of  $P$ -value value less than 0.05.

Table 9.2 – Hemodynamical parameters of the two groups with different levels of compliance at baseline (HR = 60 bpm).

<b>Variable@60bpm</b>	<b>Low arterial stiffness</b> $C_T = 1.7 \pm 0.5 \text{ mL/mmHg}$ $(n_1 = 28)$	<b>High arterial stiffness</b> $C_T = 0.8 \pm 0.3 \text{ mL/mmHg}$ $(n_2 = 31)$
cfPWV [m/s]	8.28±0.78	10.67±1.27
Aortic SBP [mmHg]	116.12±24.24	138.05±29.92
Aortic DBP [mmHg]	79.66±14.61	74.69±20.73
Aortic PP [mmHg]	36.45±14.95	63.36±20.56
MAP [mmHg]	91.81±16.98	95.81±22.16
Brachial SBP [mmHg]	129.67±26.61	152.28±28.21
Brachial DBP [mmHg]	76.85±14.42	72.07±20.1
Brachial PP [mmHg]	52.82±19.49	80.22±19.35
Aorto-brachial PP amplification	1.47±0.08	1.3±0.13
Mean aortic flow [L/min]	5.29±1.72	5.05±1.2
Stroke volume [mL]	87.09±28.36	83.13±19.73

### 9.3 Results

The changes of the measured hemodynamical parameters of the entire population at the five HR values are reported in Table 9.3.

Under free-varying pressure conditions, a gradual rise in cfPWV with respect to the HR increase was observed (Figure 9.2, solid line). The values of cfPWV were reported to be equal to  $9.54 \pm 1.60$ ,  $10.20 \pm 1.69$ ,  $10.83 \pm 1.84$ ,  $11.50 \pm 1.96$  and  $12.17 \pm 2.07$  m/s at 60, 70, 80, 90 and 100 bpm, respectively. The difference between cfPWV<sub>@60bpm</sub> and cfPWV<sub>@100bpm</sub> was  $2.64 \pm 0.70$  m/s ( $27.73 \pm 6.26$  % with respect to the baseline cfPWV<sub>@60bpm</sub>). When correction for aDBP was performed, the cfPWV<sub>BPcorrected</sub> increase was reduced to  $9.54 \pm 1.60$ ,  $9.66 \pm 1.60$ ,  $9.92 \pm 1.69$ ,  $10.14 \pm 1.75$  and  $10.37 \pm 1.81$  m/s ( $P$ -value = 0.048) at 60, 70, 80, 90 and 100 bpm, respectively (Figure 9.2, dashed line). The respective differences between the BP-corrected cfPWV<sub>@60bpm</sub> and the corrected cfPWV<sub>@100bpm</sub> was  $0.84 \pm 0.36$  m/s ( $8.71 \pm 3.12$  % with respect to the baseline cfPWV<sub>@60bpm</sub>).

The concomitant HR-related changes on MAP were reported as  $93.91 \pm 19.80$ ,  $102.21 \pm 21.51$ ,  $110.08 \pm 22.98$ ,  $118.17 \pm 24.52$  and  $126.00 \pm 26.10$  mmHg for the five HR values (from 60 to 100 bpm), respectively. A significant effect of HR changes on MAP was observed, with a total average increase in MAP equal to  $32.09 \pm 7.73$  mmHg ( $P$ -value < 0.001) for a total increase in HR by 40 bpm. Aortic SBP and DBP were increased with the increase in HR from 60 to 100bpm by  $23.90 \pm 7.40$  mmHg ( $P$ -value < 0.001) and  $36.18 \pm 9.13$  ( $P$ -value < 0.001) mmHg, respectively. The increase in aDBP was markedly higher resulting to a decrease in aortic PP [by  $12.28 \pm 7.93$  mmHg ( $P$ -value = 0.015)]. Similar response was observed in the brachial BP with a less significant effect on the PP decrease (by  $11.11 \pm 6.64$  mmHg,  $P$ -value = 0.041). Consequently, PP

**Chapter 9. The impact of heart rate on pulse wave velocity: an in silico evaluation**

Table 9.3 – Hemodynamical characteristics of the entire population with increasing heart rate (from 60 to 100 bpm).

Variable (with no correction for BP)	Value (n = 59) mean±SD					P-value
	HR = 60 bpm	HR = 70 bpm	HR = 80 bpm	HR = 90 bpm	HR = 100 bpm	
*cfPWV [m/s]	9.54±1.6	10.2±1.69	10.83±1.84	11.5±1.96	12.17±2.07	<0.001
Aortic SBP [mmHg]	127.64±29.3	133.93±29.89	139.85±30.11	145.87±30.46	151.54±30.89	<0.001
Aortic DBP [mmHg]	77.05±18.11	86.35±20.12	95.2±21.99	104.31±23.93	113.23±25.92	<0.001
Aortic PP [mmHg]	50.59±22.5	47.57±21.74	44.64±20.82	41.56±20.09	38.31±19.53	0.015
MAP [mmHg]	93.91±19.8	102.21±21.51	110.08±22.98	118.17±24.52	126±26.1	<0.001
Brachial SBP [mmHg]	141.55±29.51	148.14±30.16	153.74±30.46	159.61±30.88	165.26±31.42	<0.001
Brachial DBP [mmHg]	74.34±17.65	83.06±19.6	91.66±21.4	100.53±23.25	109.15±25.18	<0.001
Brachial PP [mmHg]	67.21±23.69	65.07±22.52	62.08±21.49	59.08±20.57	56.11±19.76	0.041
Aorto-brachial PP amplification	1.38±0.14	1.44±0.16	1.47±0.18	1.51±0.21	1.58±0.28	<0.001
Mean aortic flow [L/min]	5.17±1.46	5.68±1.64	6.11±1.79	6.44±1.9	6.68±2.01	<0.001
Stroke volume [mL]	85.01±24.08	80.07±23.16	75.33±22.03	70.86±20.95	66.16±19.92	<0.001
*The cfPWV was calculated from the free-varying pressure experiment.						

Table 9.4 – Relative changes in hemodynamical variables at 100 bpm with respect to their baseline values at 60 bpm for the two groups with different levels of arterial compliance.

Variable	Low arterial stiffness $C_T = 1.7 \pm 0.5$ mL/mmHg ( $n_1 = 28$ )	High arterial stiffness $C_T = 0.8 \pm 0.3$ mL/mmHg ( $n_2 = 31$ )
* $\delta$ (cfPWV) [m/s]	2.32 $\pm$ 0.53	2.92 $\pm$ 0.72
† $\delta$ (cfPWV <sub>corrected</sub> ) [m/s]	0.64 $\pm$ 0.19	1.02 $\pm$ 0.38
$\delta$ (aSBP) [mmHg]	26.51 $\pm$ 6.45	21.54 $\pm$ 7.5
$\delta$ (aDBP) [mmHg]	36.21 $\pm$ 8.76	36.16 $\pm$ 9.59
$\delta$ (aPP) [mmHg]	-9.7 $\pm$ 4.78	-14.61 $\pm$ 9.44
$\delta$ (MAP) [mmHg]	32.97 $\pm$ 7.74	31.28 $\pm$ 7.77
$\delta$ (brSBP) [mmHg]	26.62 $\pm$ 6.27	21.09 $\pm$ 8.04
$\delta$ (brDBP) [mmHg]	35.69 $\pm$ 8.37	34.03 $\pm$ 9.21
$\delta$ (brPP) [mmHg]	-9.07 $\pm$ 6.07	-12.95 $\pm$ 6.69
$\delta$ (a-brPPampl)	0.26 $\pm$ 0.25	0.14 $\pm$ 0.13
$\delta$ (CO) [L/min]	1.63 $\pm$ 0.78	1.42 $\pm$ 0.45
$\delta$ (SV) [mL]	-18.62 $\pm$ 4.66	-19.07 $\pm$ 6.71
*For free-varying blood pressure; †For fixed aortic diastolic blood pressure.		

amplification from the aorta to the brachial artery was increased by 14.15 $\pm$ 13.67 % ( $P$ -value < 0.001) for the 40-bpm increase in HR. Finally, SV was decreased by 18.85 $\pm$ 5.78 mL ( $P$ -value < 0.001), whereas mean aortic flow was increased by 1.52 $\pm$ 0.63 L/min ( $P$ -value < 0.001) due to the 40-bpm total increase in HR.

### Influence of arterial stiffness on the heart rate induced changes in carotid-femoral pulse wave velocity and blood pressure

Table 9.4 summarizes the total net change between the maximal HR (100 bpm) and the baseline HR (60bpm) in every variable for the two groups of arterial stiffness. For the group with higher values of arterial compliance, the effect of HR on cfPWV was found to be equal to 0.58 $\pm$ 0.18 m/s per 10bpm ( $P$ -value < 0.001) and 0.16 $\pm$ 0.07 m/s per 10bpm ( $P$ -value = 0.045), under the free-varying pressure scenario and the fixed aDBP scenario, respectively. When the group with stiffer arterial system was assessed, the corresponding quantified effects were reported to be 0.73 $\pm$ 0.25 m/s per 10bpm ( $P$ -value < 0.001) and 0.26 $\pm$ 0.15 m/s per 10 bpm ( $P$ -value = 0.014) for the free-varying pressure and the fixed DBP scenarios, respectively. It appeared that the increase in HR had a greater effect on PP at the lower than higher arterial compliance level (Table 9.4). Particularly, a 10-bpm increase in HR resulted to a decrease in PP by 2.42 $\pm$ 1.22 mmHg ( $P$ -value = 0.077) at  $C_T = 1.7 \pm 0.5$  mL/mmHg (group with low arterial stiffness). The same HR increase led to a PP reduction equal to 3.65 $\pm$ 2.39mmHg ( $P$ -value = 0.034) at  $C_T = 0.8 \pm 0.3$  mL/mmHg (group with high arterial stiffness). Similar response was reported for the brachial PP (Table 9.4). SV was reduced at a slightly greater extend at the low

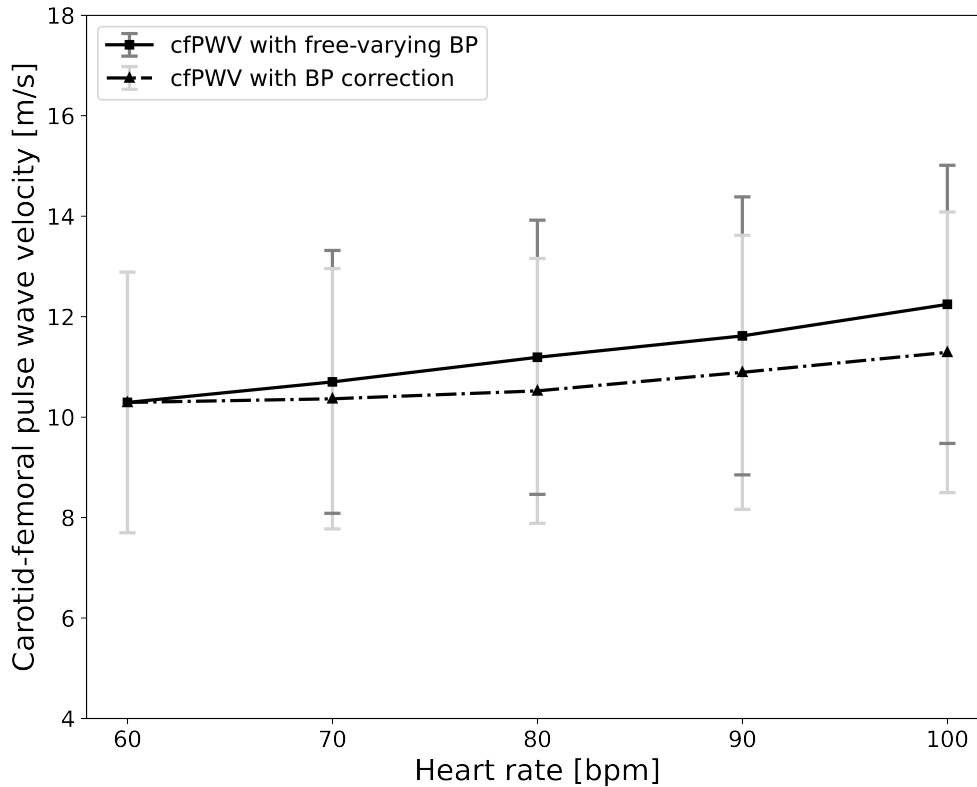


Figure 9.2 – Changes in the carotid-femoral pulse wave velocity with increasing heart rate under two scenarios: (1) with free-varying blood pressure (solid line) and (2) with fixed DBP (dashed line). Adapted from [31].

compliance group in comparison to the higher compliance group; this had as a result that CO experienced a smaller increase in the case of high than the case of low arterial stiffness.

## 9.4 Discussion

The present study evaluated the influence of HR on cfPWV on 59 in silico individuals. We leveraged the simulation capacity of a previously validated mathematical model of the cardiovascular system in order to create a complete hemodynamical dataset accessing information that is not easily obtained in a real clinical setting. Mathematical modelling allowed for isolating the inherent HR effect independent of any HR-induced systemic variations, that is BP changes. It was demonstrated that a 10-bpm increase in HR imposes a minimal direct effect on cfPWV in the total sample. However, in cases of higher HR increase, the accumulative effect may lead to a clinically significant change in cfPWV measurements. These HR effects on cfPWV were amplified in cases with increased arterial stiffness.

Despite previous works that investigated the effect of HR on cfPWV, the inherent mechanisms

that are responsible for the variation in arterial stiffness with HR are yet to be elucidated. A possible explanation for the alteration in the arterial stiffness with HR has been related mostly to the concomitant changes in BP with increasing HR and in a lesser degree to the viscoelastic properties of the arterial walls. Previous studies have suggested that it is the HR-induced rise in BP that incites cfPWV to increase, rather than a direct influence from the HR per se [8; 32]. Here, we achieved to isolate the BP-dependency on the cfPWV changes by employing a correction technique that maintained aDBP constant (while HR increased). The rationale for choosing the aDBP to be controlled is due to the fact that measurement of cfPWV using the foot-to-foot method is associated with the vicinity of the diastolic foot, and thus aDBP. This choice is further supported both theoretically and empirically by previous studies [33; 34; 35].

On the basis of our findings, the HR effect on cfPWV was reported to be equal to  $0.66 \pm 0.24$  m/s per 10 bpm in the presence of BP-free response. When the BP correction method was employed to derive the corrected cfPWV, the respective effect was reported to be  $0.21 \pm 0.14$  m/s per 10 bpm. This effect was found to be in accordance with previously published data from the work of Tan et al. [36], wherein they also reported an effect equal to approximately 0.20 m/s per 10bpm ( $P$ -value  $< 0.001$ ). We also performed our analysis by keeping the aortic SBP (aSBP) constant. In this case, the effect of HR on cfPWV was equal to 0.40 m/s per 10 bpm instead of 0.21 m/s per 10 bpm when the aDBP was maintained constant. This is rather expected if we consider that the increase in aSBP is smaller than the increase in aDBP with increased HR, and, as a result, the BP correction is greater when we choose to maintain fixed aDBP.

Increased HR was associated with increased MAP and decreased aortic and peripheral PP (brachial PP), as expected. The decrease in central PP was found to be greater in magnitude than the decrease in brachial PP, and thus, an increase in PP amplification was observed. These observations have also been acknowledged in previous studies [8]. It was also noted that the increase in DBP, especially, lead to the PP reduction. Nevertheless, in our data, the increase of PP amplification was less prominent (approximately 14 %,  $P$ -value  $< 0.001$ ). According to Pichler et al. [37], PP amplification is related to BP level; the higher the BP, the lower the BP amplification. In our study, BP was relatively higher than other published data [8; 38] in which a higher increase in PP amplification was observed. Moreover, increasing HR led to a decrease in SV, which was rather expected considering that SV is a major determinant of PP. In contrast, CO was increased due to the large increases in HR.

The correction methodology that was employed in the current study interferes with the TPR, which is the main systemic determinant of aDBP [39]. An increase in TPR leads to an increase in BP level, and thus to increased arterial stiffness based on the nonlinear pressure-compliance relationship. By employing a correction technique, it is exactly this BP increase that we wish to control. In practice, by decreasing BP, we expect that TPR will also decrease, and vice versa. In our in silico model, the modification of TPR allows us to achieve the control of BP per



## Chapter 9. The impact of heart rate on pulse wave velocity: an in silico evaluation

---

se. Importantly, a prominent element of our approach is that our manoeuvre is not applied directly to the aorta. On the contrary, we only modify locally the peripheral sites (resistances) without imposing any intervention on the properties of the global arterial tree. Possible interference due to the influence of TPR on cfPWV (using the foot-to-foot method) has been evaluated by previous studies demonstrating low correlations between the two quantities [40; 41].

It should be noted that, although our study population presented a concurrent increase in BP with increased HR, this observation is not systematic in the literature. In studies wherein HR was changed acutely through pacing, despite the fact that some scientists reported a rise in cfPWV in the presence of a significant parallel increase in BP [9; 10], others observed no BP rise with increased HR [8; 42; 43; 44]. This existing inconsistency makes it hard to determine whether HR, additionally, contributed to the increase in cfPWV independently of BP. Our objective was to precisely quantify the part of cfPWV increase that is caused intrinsically due to the HR changes, and to isolate the cfPWV increase due to the BP increase. Thus, we simulated and compared the two different phenotypes, namely where BP was deliberately allowed to vary in response to HR changes that physiologically occur in some individuals, and where BP was controlled so that it remains unchanged when HR varies, which is also apparent in some humans.

It is undeniable that the effect of HR on cfPWV measurement has been a subject of high controversy. In a previous study, Albaladejo et al. [8] have showed that increased HR (introduced acutely by pacing) leads to a rise in cfPWV accompanied with an increase in BP. The authors also reported an increase in PP amplification that was not, however, associated with a change in aortic stiffness. The cfPWV change was rather attributed to the interaction between reduced SV and modified wave reflection sites. Nevertheless, their study includes only 11 individuals, whereas the cfPWV was evaluated under only three averaged levels (low, medium, high), which were not predetermined.

On the contrary, Lantelme et al. [10] have claimed that HR changes exert a significant effect on cfPWV measurement in an elderly population ( $n = 22$ ) in the absence of BP changes. However, concerns have been raised [45] against the Complior technique [46], which was employed to measure cfPWV in this study. It is likely that increasing HR can affect the shape of the pressure waveform. The sensitivity of the cfPWV estimation method (Complior apparatus) on the waveform characteristics may explain the discrepancies between their findings and other clinical investigations, as already suggested by Hayward et al. [45]. These discrepancies do not allow us to derive a clear understanding on the HR impact on arterial stiffness measurement. Furthermore, evidence from the aforementioned studies was based on cross-sectional population data in which the intrinsic effect of HR on cfPWV cannot be isolated.

Of particular interest is the study by Tan et al. [36] in which the HR effect on cfPWV was evaluated by isolating the corresponding influence of BP. The cfPWV measurement was corrected for

BP using three methods: a statistical method, an empirical formula and a model-based technique. This study was the first one to assess the HR-related changes in cfPWV regardless of BP variation. Following a similar principle to the one adopted in our study, they quantified the HR effect on cfPWV by assuming a constant aDBP. The authors performed the correction method on a study population of 52 individuals and calculated an effect equal to 0.2 m/s per 10bpm. In another study, Tan et al. [47] reviewed and analysed the findings of several published experimental studies investigating the acute effects of HR changes on PWV measurements. They found that the average HR dependency of cfPWV, weighted by study sample size, was 0.30 m/s per 10bpm (or 0.03 m/s/bpm) [47], which is in line with our findings. Furthermore, in that study, it was revealed that epidemiological studies exploring the association between resting HR and cfPWV regardless of BP levels have failed to converge, with approximately just half of the examined studies reporting a significant BP-independent association between HR and cfPWV [47]. In this respect, our study provides additional evidence showing that HR is a relevant factor that should be considered when arterial stiffness is assessed via the cfPWV measurement.

In addition to the quantification of the HR effect on cfPWV, our study investigated the HR dependency on cfPWV for different levels of arterial stiffness. Our results showed that the cfPWV increase was 40 % higher for stiffer ( $C_T = 0.8 \pm 0.3$  mL/mmHg) than more compliant arteries ( $C_T = 1.7 \pm 0.5$  mL/mmHg). This is rather expected if we consider that a more compliant artery will present a lower increase in pressure due to a volume rise than the increase presented by a stiffer artery. At the same time, aorto-brachial PP amplification was lower in the group of high stiffness (1.9 times smaller than the group of low stiffness). Evidence from previous work [48; 49] have demonstrated that, in general, central PP appears to be lower (more compliant aorta) than peripheral PP (stiffer periphery). This PP difference often disappears with ageing and hypertension, wherein the arterial tree and especially the elastic arteries (i.e. proximal aorta) becomes stiffer [50].

Moreover, it must be highlighted that, for the total increase in HR by 40 bpm, the consequent increase in cfPWV (under constant BP levels) by approximately 0.64 and 1.02 m/s for low and high arterial stiffness levels, respectively, is remarkable and clinically relevant. Even more impressive is the respective increase in cfPWV per 40 bpm increase under free BP-response (which is a more realistic scenario), namely by 2.32 m/s for low and 2.92 m/s for high arterial stiffness levels, respectively. This is mostly based on existing evidence relating these cfPWV changes with the corresponding theoretical increase in the cardiovascular (CV) and mortality-risk, as predicted by published prospective, longitudinal, studies. Specifically, a previous meta-analysis exploring the predictive value of cfPWV demonstrated that an increase in aortic PWV by 1.0 m/s corresponds to an age, sex and risk factor adjusted risk increase of 14, 15 and 15 % in total CV events, CV mortality and all-cause mortality, respectively [5]. Finally, our findings provide additional evidence in support of the scientific statement from the American Heart Association [51] recommending that HR should be recorded at the time of an arterial

## **Chapter 9. The impact of heart rate on pulse wave velocity: an in silico evaluation**

---

stiffness measurement and taken into consideration in analyses involving PWV.

Furthermore, correction of the cfPWV measurement for resting HR may have significant clinical implications in the occurrence of pharmacologically induced changes in cardiac rhythm. Concretely, several patients suffering from high resting HR are in need for antiarrhythmic drugs to restore a normal heart beat. Assessment of the cardiovascular state in these patients is crucial [52; 53]. However, the medication targeting on HR decrease is likely to affect arterial stiffness and thus, lower the measured cfPWV value. A lower HR would appear concurrently with a lower cfPWV value, thus hiding the potential cardiovascular risk associated with arterial stiffness. Employment of a correction method would allow for the corrected characterization of arterial stiffness by isolating the potential pharmacologically induced changes in HR and thus optimizing the accuracy of cardiovascular risk assessment and the predictive value of cfPWV.

### **Limitations**

A few study limitations should be acknowledged. Nevertheless, synthetic data can be representative of the properties of the real clinical measurements, while they allow for controlling the distribution of rare but relevant conditions or events. Translation of the results from any in silico study to real conditions and patients cannot be direct, and the extrapolation and application of the theoretical results to clinical practice should be made with great caution. On the contrary, in silico models allow the control of specific parameters in highly multifactorial problems, which is impossible to be achieved under in vivo conditions. Finally, the in silico model that was used in this study has been thoroughly validated against in vivo data and provides realistic representations of the physiological signals.

### **Conclusion**

In conclusion, the present study estimated the direct effect of HR on cfPWV independently of the concomitant BP variations. Overall, the BP-independent effect of HR on cfPWV was estimated to be approximately 0.16 m/s per 10 bpm and 0.26 per 10 bpm in cases with decreased and increased arterial stiffness, respectively. Although small variations in HR appear to have a minimal effect on the cfPWV measurement, a larger increase in HR may lead to a more significant physiological change in cfPWV and, hence, to a higher cardiovascular risk. In this respect, our study provided a strong and clinically relevant background for the establishment of cfPWV correction for HR changes (especially for individuals with increased arterial stiffness) and also for further examination of the combined predictive role of both cfPWV and HR.

## Bibliography

- [1] S. Laurent, P. Boutouyrie, R. Asmar, I. Gautier, B. Laloux, L. Guize, P. Ducimetiere, and A. Benetos, "Aortic stiffness is an independent predictor of all-cause and cardiovascular mortality in hypertensive patients," *Hypertension*, vol. 37, no. 5, pp. 1236–1241, May 2001.
- [2] S. Laurent, J. Cockcroft, L. Van Bortel, P. Boutouyrie, C. Giannattasio, D. Hayoz, B. Pannier, C. Vlachopoulos, I. Wilkinson, H. Struijker-Boudier, and on behalf of the European Network for Non-invasive Investigation of Large Arteries, "Expert consensus document on arterial stiffness: methodological issues and clinical applications," *European Heart Journal*, vol. 27, no. 21, pp. 2588–2605, Sep. 2006.
- [3] B. Pannier, A. P. Guérin, S. J. Marchais, M. E. Safar, and G. M. London, "Stiffness of capacitive and conduit arteries: prognostic significance for end-stage renal disease patients," *Hypertension*, vol. 45, no. 4, pp. 592–596, Apr. 2005.
- [4] G. F. Mitchell, S.-J. Hwang, R. S. Vasan, M. G. Larson, M. J. Pencina, N. M. Hamburg, J. A. Vita, D. Levy, and E. J. Benjamin, "Arterial stiffness and cardiovascular events: the Framingham heart study," *Circulation*, vol. 121, no. 4, pp. 505–511, Feb. 2010.
- [5] C. Vlachopoulos, K. Aznaouridis, D. Terentes-Printzios, N. Ioakeimidis, and C. Stefanadis, "Prediction of cardiovascular events and all-cause mortality with brachial-ankle elasticity index: a systematic review and meta-analysis," *Hypertension*, vol. 60, no. 2, pp. 556–562, Aug. 2012.
- [6] S. A. Huybrechts, D. G. Devos, S. J. Vermeersch, D. Mahieu, E. Achten, T. L. de Backer, P. Segers, and L. M. van Bortel, "Carotid to femoral pulse wave velocity: a comparison of real travelled aortic path lengths determined by MRI and superficial measurements," *Journal of Hypertension*, vol. 29, no. 8, pp. 1577–1582, Aug. 2011.
- [7] T. G. Papaioannou, A. D. Protogerou, E. G. Nasothimiou, D. Tzamouranis, N. Skliros, A. Achimastos, D. Papadogiannis, and C. I. Stefanadis, "Assessment of differences between repeated pulse wave velocity measurements in terms of 'bias' in the extrapolated cardiovascular risk and the classification of aortic stiffness: Is a single PWV measurement enough?" *Journal of Human Hypertension*, vol. 26, no. 10, pp. 594–602, Oct. 2012.

## Bibliography

---

- [8] P. Albaladejo, X. Copie, P. Boutouyrie, B. Laloux, A. D. Déclère, H. Smulyan, and A. Bénétos, "Heart rate, arterial stiffness, and wave reflections in paced patients," *Hypertension*, vol. 38, no. 4, pp. 949–952, Oct. 2001.
- [9] E. Haesler, X. Lyon, E. Pruvot, L. Kappenberger, and D. Hayoz, "Confounding effects of heart rate on pulse wave velocity in paced patients with a low degree of atherosclerosis," *Journal of Hypertension*, vol. 22, no. 7, pp. 1317–1322, Jul. 2004.
- [10] P. Lantelme, C. Mestre, M. Lievre, A. Gressard, and H. Milon, "Heart rate: an important confounder of pulse wave velocity assessment," *Hypertension*, vol. 39, no. 6, pp. 1083–1087, Jun. 2002.
- [11] M. L. Muiesan, M. Salvetti, A. Paini, C. Monteduro, C. A. Rosei, C. Aggiusti, E. Belotti, F. Bertacchini, G. Galbassini, D. Stassaldi, M. Castellano, and E. A. Rosei, "Pulse wave velocity and cardiovascular risk stratification in a general population: the Vobarno study," *Journal of Hypertension*, vol. 28, no. 9, pp. 1935–1943, Sep. 2010.
- [12] H. J. Joo, S.-A. Cho, J.-Y. Cho, J. H. Park, S. J. Hong, C. W. Yu, and D.-S. Lim, "The relationship between pulse wave velocity and coronary artery stenosis and percutaneous coronary intervention: a retrospective observational study," *BMC Cardiovascular Disorders*, vol. 17, no. 1, Dec. 2017.
- [13] A. R. Khoshdel, S. L. Carney, B. R. Nair, and A. Gillies, "Better management of cardiovascular diseases by pulse wave velocity: combining clinical practice with clinical research using evidence-based medicine," *Clinical Medicine and Research*, vol. 5, no. 1, pp. 45–52, Mar. 2007.
- [14] P. Reymond, F. Merenda, F. Perren, D. Rüfenacht, and N. Stergiopoulos, "Validation of a one-dimensional model of the systemic arterial tree," *American Journal of Physiology. Heart and Circulatory Physiology*, vol. 297, no. 1, pp. H208–222, Jul. 2009.
- [15] G. Langewouters, *Visco-elasticity of the human aorta in vitro in relation to pressure and age (Ph.D. thesis)*. Amsterdam: Free University of Amsterdam: Krips Repro, 1982.
- [16] C.-H. Chen, M. Nakayama, E. Nevo, B. J. Fetts, W. Maughan, and D. A. Kass, "Coupled systolic-ventricular and vascular stiffening with age," *Journal of the American College of Cardiology*, vol. 32, no. 5, pp. 1221–1227, Nov. 1998.
- [17] P. H. Pak, W. L. Maughan, K. L. Baughman, R. S. Kieval, and D. A. Kass, "Mechanism of acute mechanical benefit from vdd pacing in hypertrophied heart: similarity of responses in hypertrophic cardiomyopathy and hypertensive heart disease," *Circulation*, vol. 98, no. 3, pp. 242–248, Jul. 1998.
- [18] M. D. Feldman, P. H. Pak, C. C. Wu, H. L. Haber, C. M. Heesch, J. D. Bergin, E. R. Powers, T. D. Cowart, W. Johnson, A. M. Feldman, and D. A. Kass, "Acute cardiovascular effects of

- OPC-18790 in patients with congestive heart failure: time- and dose-dependence analysis based on pressure-volume relations," *Circulation*, vol. 93, no. 3, pp. 474–483, Feb. 1996.
- [19] H. Senzaki, C.-H. Chen, and D. A. Kass, "Single-beat estimation of end-systolic pressure-volume relation in humans: a new method with the potential for noninvasive application," *Circulation*, vol. 94, no. 10, pp. 2497–2506, Nov. 1996.
- [20] A. Wolak, H. Gransar, L. E. J. Thomson, J. D. Friedman, R. Hachamovitch, A. Gutstein, L. J. Shaw, D. Polk, N. D. Wong, R. Saouaf, S. W. Hayes, A. Rozanski, P. J. Slomka, G. Germano, and D. S. Berman, "Aortic size assessment by noncontrast cardiac computed tomography: normal limits by age, gender, and body surface area," *JACC. Cardiovascular imaging*, vol. 1, no. 2, pp. 200–209, Mar. 2008.
- [21] R. B. Devereux, G. de Simone, D. K. Arnett, L. G. Best, E. Boerwinkle, B. V. Howard, D. Kitzman, E. T. Lee, T. H. Mosley, A. Weder, and M. J. Roman, "Normal limits in relation to age, body size and gender of two-dimensional echocardiographic aortic root dimensions in persons  $\geq 15$  years of age," *The American Journal of Cardiology*, vol. 110, no. 8, pp. 1189–1194, Oct. 2012.
- [22] P. Segers et al., "Three- and four-element Windkessel models: assessment of their fitting performance in a large cohort of healthy middle-aged individuals," *Proceedings of the Institution of Mechanical Engineers, Part H: Journal of Engineering in Medicine*, 2008.
- [23] Z. Lu and R. Mukkamala, "Continuous cardiac output monitoring in humans by invasive and noninvasive peripheral blood pressure waveform analysis," *Journal of Applied Physiology*, vol. 101, no. 2, pp. 598–608, Aug. 2006.
- [24] P. Reymond, Y. Bohraus, F. Perren, F. Lazeyras, and N. Stergiopoulos, "Validation of a patient-specific one-dimensional model of the systemic arterial tree," *American Journal of Physiology. Heart and Circulatory Physiology*, vol. 301, no. 3, pp. H1173–1182, Sep. 2011.
- [25] R. Holenstein, P. Niederer, and M. Anliker, "A viscoelastic model for use in predicting arterial pulse waves," *Journal of Biomechanical Engineering*, vol. 102, no. 4, pp. 318–325, Nov. 1980.
- [26] K. Sagawa, H. Suga, A. A. Shoukas, and K. M. Bakalar, "End-systolic pressure/volume ratio: a new index of ventricular contractility," *The American Journal of Cardiology*, vol. 40, no. 5, pp. 748–753, Nov. 1977.
- [27] Suga Hiroyuki and Sagawa Kiichi, "Instantaneous pressure-volume relationships and their ratio in the excised, supported canine left ventricle," *Circulation Research*, vol. 35, no. 1, pp. 117–126, Jul. 1974.
- [28] T. Bombardini, V. Gemignani, E. Bianchini, L. Venneri, C. Petersen, E. Pisanisi, L. Pratali, D. Alonso-Rodriguez, M. Pianelli, F. Faita, M. Giannoni, G. Arpesella, and E. Picano,

## Bibliography

---

- “Diastolic time – frequency relation in the stress echo lab: filling timing and flow at different heart rates,” *Cardiovascular Ultrasound*, vol. 6, no. 1, p. 15, Apr. 2008.
- [29] M. R. Starling, R. A. Walsh, L. J. Dell’Italia, G. B. Mancini, J. C. Lasher, and J. L. Lancaster, “The relationship of various measures of end-systole to left ventricular maximum time-varying elastance in man.” *Circulation*, vol. 76, no. 1, pp. 32–43, Jul. 1987.
- [30] O. Vardoulis, T. G. Papaioannou, and N. Stergiopoulos, “Validation of a novel and existing algorithms for the estimation of pulse transit time: advancing the accuracy in pulse wave velocity measurement,” *American Journal of Physiology-Heart and Circulatory Physiology*, vol. 304, no. 11, pp. H1558–H1567, Jun. 2013.
- [31] V. Bikia, N. Stergiopoulos, G. Rovas, S. Pagoulatou, and T. G. Papaioannou, “The impact of heart rate on pulse wave velocity: an in-silico evaluation,” *Journal of Hypertension*, vol. 38, no. 12, pp. 2451–2458, 2020.
- [32] I. B. Wilkinson, N. H. Mohammad, S. Tyrrell, I. R. Hall, D. J. Webb, V. E. Paul, T. Levy, and J. R. Cockcroft, “Heart rate dependency of pulse pressure amplification and arterial stiffness,” *American Journal of Hypertension*, vol. 15, no. 1, pp. 24–30, Jan. 2002.
- [33] W. W. Nichols, M. F. O’Rourke, and C. Vlachopoulos, *McDonald’s blood flow In arteries*, 6th ed. London: Arnold, 2011.
- [34] E. R. Nye, “The effect of blood pressure alteration on the pulse wave velocity,” *Heart*, vol. 26, no. 2, pp. 261–265, Mar. 1964.
- [35] M. Gao, H.-M. Cheng, S.-H. Sung, C.-H. Chen, N. B. Olivier, and R. Mukkamala, “Estimation of pulse transit time as a function of blood pressure using a nonlinear arterial tube-load model,” *IEEE Transactions on Biomedical Engineering*, vol. 64, no. 7, pp. 1524–1534, Jul. 2017.
- [36] I. Tan, B. Spronck, H. Kiat, E. Barin, K. D. Reesink, T. Delhaas, A. P. Avolio, and M. Butlin, “Heart rate dependency of large artery stiffness,” *Hypertension*, vol. 68, no. 1, pp. 236–242, Jul. 2016.
- [37] G. Pichler, F. Martinez, A. Vicente, E. Solaz, O. Calaforra, and J. Redon, “Pulse pressure amplification and its determinants,” *Blood Pressure*, vol. 25, no. 1, pp. 21–27, Jan. 2016.
- [38] T. G. Papaioannou, A. Protogerou, C. Papamichael, D. Mathioulakis, S. Tsangaris, E. Karatzis, S. Toumanidis, N. Zakopoulos, and J. Lekakis, “Experimental and clinical study of the combined effect of arterial stiffness and heart rate on pulse pressure: differences between central and peripheral arteries,” *Clinical and Experimental Pharmacology and Physiology*, vol. 32, no. 3, pp. 210–217, Mar. 2005.

- [39] N. Stergiopoulos, J. J. Meister, and N. Westerhof, "Determinants of stroke volume and systolic and diastolic aortic pressure," *American Journal of Physiology-Heart and Circulatory Physiology*, vol. 270, no. 6, pp. H2050–H2059, Jun. 1996.
- [40] H. Xiao, M. Butlin, I. Tan, and A. Avolio, "Effects of cardiac timing and peripheral resistance on measurement of pulse wave velocity for assessment of arterial stiffness," *Scientific Reports*, vol. 7, no. 1, p. 5990, Dec. 2017.
- [41] C. Ye, Y. Pan, X. Xu, S. Su, H. Snieder, F. Treiber, G. Kapuku, and X. Wang, "Pulse wave velocity in elastic and muscular arteries: tracking stability and association with anthropometric and hemodynamic measurements," *Hypertension Research*, vol. 39, no. 11, pp. 786–791, Nov. 2016.
- [42] S. C. Millasseau, A. D. Stewart, S. J. Patel, S. R. Redwood, and P. J. Chowienczyk, "Evaluation of carotid-femoral pulse wave velocity: influence of timing algorithm and heart rate," *Hypertension*, vol. 45, no. 2, pp. 222–226, Feb. 2005.
- [43] Y.-L. Liang, C. D. Gatzka, X.-J. Du, J. D. Cameron, and B. A. Kingwell, "Effects of heart rate on arterial compliance in men," *Clinical and Experimental Pharmacology and Physiology*, vol. 26, no. 4, pp. 342–346, Apr. 1999.
- [44] I. B. Wilkinson, H. MacCallum, L. Flint, J. R. Cockcroft, D. E. Newby, and D. J. Webb, "The influence of heart rate on augmentation index and central arterial pressure in humans," *The Journal of Physiology*, vol. 525, no. 1, pp. 263–270, May 2000.
- [45] C. S. Hayward, A. P. Avolio, and M. F. O'Rourke, "Arterial pulse wave velocity and heart rate," *Hypertension*, vol. 40, no. 6, Dec. 2002.
- [46] F. Stea, E. Bozec, S. Millasseau, H. Khettab, P. Boutouyrie, and S. Laurent, "Comparison of the Complior Analyse device with Sphygmocor and Complior SP for pulse wave velocity and central pressure assessment," *Journal of Hypertension*, vol. 32, no. 4, pp. 873–880, Apr. 2014.
- [47] I. Tan, M. Butlin, B. Spronck, H. Xiao, and A. Avolio, "Effect of heart rate on arterial stiffness as assessed by pulse wave velocity," *Current Hypertension Reviews*, vol. 13, Jul. 2017.
- [48] C. H. Chen, E. Nevo, B. Fetcs, P. H. Pak, F. C. Yin, W. L. Maughan, and D. A. Kass, "Estimation of central aortic pressure waveform by mathematical transformation of radial tonometry pressure: validation of generalized transfer function," *Circulation*, vol. 95, no. 7, pp. 1827–1836, Apr. 1997.
- [49] M. F. O'Rourke, "Influence of ventricular ejection on the relationship between central aortic and brachial pressure pulse in man," *Cardiovascular Research*, vol. 4, no. 3, pp. 291–300, Jul. 1970.



## Bibliography

---

- [50] P. Reymond, N. Westerhof, and N. Stergiopulos, "Systolic hypertension mechanisms: effect of global and local proximal aorta stiffening on pulse pressure," *Annals of Biomedical Engineering*, vol. 40, no. 3, pp. 742–749, Mar. 2012.
- [51] R. R. Townsend, I. B. Wilkinson, E. L. Schiffrin, A. P. Avolio, J. A. Chirinos, J. R. Cockcroft, K. S. Heffernan, E. G. Lakatta, C. M. McEniery, G. F. Mitchell, S. S. Najjar, W. W. Nichols, E. M. Urbina, and T. Weber, "Recommendations for improving and standardizing vascular research on arterial stiffness: a scientific statement from the american heart association," *Hypertension*, vol. 66, no. 3, pp. 698–722, Sep. 2015.
- [52] S. E. Kjeldsen and P. M. Okin, "High resting heart rate predicts mortality, disability, and cognitive decline in patients after ischaemic stroke: time for additional selective I(f) channel inhibitor trials?" *European Heart Journal*, vol. 33, no. 22, pp. 2761–2763, Nov. 2012.
- [53] A. Kohler, S. Muzzarelli, G. Leibundgut, J. Müller-Brand, M. Brinkert, and M. Zellweger, "Relationship between the resting heart rate and the extent of coronary artery disease as assessed by myocardial perfusion SPECT," *Swiss Medical Weekly*, Aug. 2012.

# Chapter 10

---

## Conclusions

### 10.1 Summary of thesis achievements

The aim of this thesis was to develop and assess the performance of techniques for monitoring key cardiovascular parameters, and more precisely aortic systolic blood pressure (aSBP), cardiac output (CO) or stroke volume (SV), end-systolic elastance ( $E_{es}$ ), total arterial compliance ( $C_T$ ), and aortic characteristic impedance ( $Z_{ao}$ ). Chapters 2 to 8 presented original methodologies to address this aim. Finally, Chapter 9 reported evidence on the influence of heart rate (HR) on the assessment of arterial stiffness. The achievements of the thesis are summarised in the following paragraphs.

#### 10.1.1 Non-invasive estimation of aortic hemodynamics from readily available clinical data

Estimation of aortic hemodynamics is key in disease diagnosis and effective patient management [31; 6]. Chapter 2 introduced a novel inverse problem-solving method for estimating aSBP and CO using non-invasive, easily obtained clinical measurements. The method relied on the partial adjustment of a generic one-dimensional (1-D) arterial model using the non-invasive brachial systolic and diastolic blood pressures and carotid-femoral pulse wave velocity, which are easily obtained in a clinical setting. The 1-D model of the arterial tree, which was adopted, has been thoroughly validated in vivo and provides realistic flow and pressure waveforms. Identifiability analysis allowed for identifying the most sensitive parameters that drove the variability in the model outputs. Subsequently, the fusion of the physics-based model and the measured data was achieved via an optimization process. In particular, the arterial 1-D model parameters were adjusted so that the model-simulated data fit the measured

## Chapter 10. Conclusions

---

data and thus render the generic model closer to a patient-specific model. After describing the concept and processes undertaken to develop the algorithm, the method was tested on twenty healthy adults for the purposes of this thesis. Doppler ultrasound-derived CO was used as ground truth for validating the accuracy of the proposed methodology. The in vivo evaluation suggested that this novel method predicts aSBP and CO with good accuracy and agreement with the reference values ( $r = 0.98$ , RMSE = 2.46 mmHg and  $r = 0.91$ , RMSE = 0.36 L/min, respectively).

In Chapter 3, the inverse method, which was presented and described in Chapter 2, was validated using a larger dataset ( $n=144$ ) from the Anglo-Cardiff Collaborative Trial [37]. This allowed for an extensive validation of the proposed method across a wide range of age groups. The ground truth for the aortic flow data was derived from phase-contrast magnetic resonance imaging (PC-MRI), which is the gold-standard non-invasive method for measuring flow. Following the promising results of the study described in Chapter 2, the validity and accuracy of the inverse method in estimating SV was anew verified, achieving again a satisfactory correlation and accuracy ( $r = 0.83$ , RMSE = 16 mL). Furthermore, we investigated whether the performance of the inverse method for SV estimation was superior to the traditional statistical approach of multilinear regression. The inverse method achieved higher accuracy in comparison to the traditional linear regression approach ( $r = 0.72$ , RMSE = 14 mL), highlighting the importance of physics-based mathematical modelling in developing predictive tools for hemodynamical monitoring. Overall, this work demonstrated that creating a version of the generalized arterial tree model closer to each individual's standards can potentially enhance the performance of aSBP and CO (or SV) prediction.

Addressing the same aim, a part of Chapter 4 presented another method for predicting central hemodynamics (i.e. aSBP and CO) from non-invasive brachial (cuff) blood pressure and cfPWV, but this time using a machine learning regression pipeline. Different regression models were trained and tested using an in silico dataset which was generated using the previously validated 1-D cardiovascular model. An extensive range of hemodynamical conditions was simulated by varying the model's parameters. The results indicated that the use of non-invasive arm cuff pressure and PWV alone allows for the precise estimation of aSBP and CO ( $r = 0.99$ , RMSE = 3.13 mmHg, and  $r = 0.92$ , RMSE = 0.34 L/min, respectively). Moreover, model-derived aSBP compared to in vivo data in a large human cohort ( $n = 783$ ) and achieved high precision ( $r = 0.97$ , RMSE = 3.53 mmHg). Finally, transfer learning was performed for the aSBP estimator and yielded accurate estimates of aSBP ( $r = 0.94$ , RMSE = 5.34 mmHg), meeting the international standards of the European Society of Hypertension International Protocol [62]. In summary, the findings of this study indicated that this novel machine learning-based methodology has potential for improving the non-invasive monitoring of aortic hemodynamics using unintrusive, readily available, standard clinical measurements.

### 10.1.2 Machine learning for the prediction of left ventricular contractility

Assessment of left ventricular (LV) contractility via measuring  $E_{es}$  has been shown to be valuable in physiological studies and clinical practice. This thesis introduced three original methods for estimating LV  $E_{es}$ . The selection of the method in estimating  $E_{es}$  may be dictated by the scope and the available data and apparatus of the specific setting.

Chapter 4 proposed a machine learning regression method for predicting cardiac  $E_{es}$  from readily available clinical data. The training and testing of the models was conducted using *in silico* data. The findings demonstrated that the use of non-invasive arm cuff pressure and PWV is not sufficient for a precise  $E_{es}$  prediction. The estimated  $E_{es}$  can be greatly improved when ejection fraction (EF) is used as an additional input in the prediction model ( $r = 0.91$ , RMSE = 0.15 mmHg/mL). Nonetheless, accurate interpretation of EF renders essential the additional knowledge of physical determinants of myocardial contraction, namely, the preload and afterload [12; 13]. As a result, the inclusion of EF may compromise the clinical relevance of the estimated  $E_{es}$ .

In an effort to discard the EF measurement from the required inputs, we formulated the research question whether EF could be replaced by other cardiac functional parameters, e.g. electrical or acoustic signals of cardiac events, that are related to the LV contractility in a direct or indirect manner. In this respect, Chapter 5 presented an alternative, novel artificial intelligence method for estimating  $E_{es}$ , which utilized systolic time intervals. Results from our *in silico* study provided evidence that accurate estimates of  $E_{es}$  could be yielded from arm cuff pressure data and contractility-related timing parameters using a scalable data-driven approach. The regression results showed that cuff pressure in conjunction with systolic time intervals achieved a low test error and can capture the left ventricular  $E_{es}$  value with sufficient accuracy ( $r = 0.92$ , RMSE = 0.3 mmHg/mL). The systolic time intervals appeared to be a promising source of information for assessing  $E_{es}$  and their usefulness should be emphasized. Interestingly, this methodology could easily be turned into a useful clinical application, where systolic time intervals could be easily obtained using ECG and a precise electronic stethoscope. This finding creates a rather promising proof-of-evidence towards the non-invasive estimation of  $E_{es}$  reducing the complexity and the cost of the technique for acquiring the necessary measurements. The proposed methodological concept could be easily integrated in a medical device such as a smart stethoscope.

The final proposed methodology suggested in Chapter 6, pertains to the prediction of the cardiac contractility index of  $E_{es}$  from a sole pressure waveform that can be measured, for instance, at the brachial artery. The performance of the trained neural networks was tested using an independent set of the virtual population. The results demonstrated that neural networks are promising for predicting cardiac contractility. Specifically, we found that the arterial pulse wave alone may be informative for the characterization of  $E_{es}$  ( $r = 0.86$  and RMSE = 0.27 mmHg/mL). In particular, the CNN configuration combining the peripheral pressure

wave and its time derivative provided higher precision ( $r = 0.97$  and  $\text{RMSE} = 0.13$  mmHg/mL). With the increasing availability of clinical data, signals and images sourced from various avenues of medicine and healthcare, the application of artificial intelligence for analysis and interpretation of medical data grows rapidly. Deep learning offers a promising potential in exploring new methods for cardiac monitoring by deciphering key information from arterial pulse waves. In this study, we leveraged the capacity of CNN models in order to evaluate LV  $E_{es}$  from a single arterial pulse wave. Such potential can open new directives in digital health and potentially suggest new markers for cardiac monitoring purposes.

### 10.1.3 Can machine learning improve the assessment of arterial elasticity?

Chapter 7 presented a non-invasive simple-to-use machine learning estimator for predicting  $C_T$  and  $Z_{ao}$ . The proposed approach incorporates cuff blood pressure and regional pulse wave velocity data, along with a versatile and scalable machine learning pipeline. Our findings provide evidence that data related to regional arterial stiffness can be rather informative for obtaining a global description of arterial elasticity. In particular, it was observed that the machine learning approach achieved significantly higher accuracy ( $r = 0.95$  and  $\text{RMSE} = 0.16$  mL/mmHg for  $C_T$  and  $r = 0.9$  and  $\text{RMSE} = 0.006$  mmHg.s/mL for  $Z_{ao}$ , respectively) in comparison to prior methods, especially for  $Z_{ao}$ . However, the main advantage of the proposed method pertains to its simplicity and convenience (for both the patient and the physician). The existing techniques require non-invasive, yet expensive and complex, flow or velocity measurements for evaluating  $Z_{ao}$  and  $C_T$ . The proposed approach constitutes a step forward to the non-invasive screening of elastic vascular properties in humans by exploiting easily obtained measurements. This study could introduce a valuable tool for assessing arterial stiffness reducing the cost and the complexity of the required measuring techniques.

Chapter 8 takes a step further and explores the possibility of deriving  $C_T$  from a single carotid blood pressure wave. The method relies on exploiting the information provided by the carotid blood pressure waveform as well as typical clinical variables (such as demographical data). Our results demonstrated that accurate estimates of  $C_T$  can be obtained following our methodology ( $r = 0.83$  and  $\text{RMSE} = 0.17$  mL/mmHg). The importance of the method is based on the simplification of the technique offering easily applicable and convenient monitoring of  $C_T$ . Importantly, it was evidenced that  $C_T$ , which is usually estimated using both pressure and flow waveforms, can be accurately derived by the use of the pressure wave alone. Such an approach could offer promising applications which may be integrated into wearable technologies and smartphones and could potentially facilitate easily applicable and convenient monitoring of  $C_T$ . Finally, the study further supported the importance of arterial pulse waves in the assessment of cardiovascular health and suggested the potentiality of machine learning in advancing the detection of clinical biomarkers in medicine.

**10.1.4 Disentangling the mystery behind heart rate's effect on pulse wave velocity measurement**

Chapter 9 presented a study investigating the direct effect of HR on carotid-femoral pulse wave velocity (cfPWV) independently of the concomitant blood pressure variations. Overall, the blood pressure-independent effect of HR on cfPWV was estimated to be approximately 0.16 m/s per 10 bpm and 0.26 per 10 bpm in cases with decreased and increased arterial stiffness, respectively. Although small variations in HR appear to have a minimal effect on the cfPWV measurement, a larger increase in HR may lead to a more significant physiological change in cfPWV. Precisely, it must be highlighted that, for the total increase in HR by 40 bpm, the consequent increase in cfPWV (under constant BP levels) by approximately 0.64 and 1.02 m/s for low and high arterial stiffness levels, respectively, is remarkable and potentially clinically relevant. Even more impressive is the respective increase in cfPWV per 40 bpm increase under free BP-response (which is a more realistic scenario), namely by 2.32 m/s for low and 2.92 m/s for high arterial stiffness levels, respectively. Consequently, our findings recommended that HR should be recorded at the time of an arterial stiffness measurement and taken into consideration in analyses involving PWV. In this respect, our study provided a strong and clinically relevant background for the establishment of cfPWV correction for HR changes (especially for individuals with increased arterial stiffness) and also for further examination of the combined predictive role of both cfPWV and HR.

**10.2 Future perspectives**

The inverse problem-solving method provides a non-invasive, reliable, and cost-efficient way to assess central hemodynamics, without the need for population-based transfer functions (aortic blood pressure) or invasive calibration techniques (mean aortic blood flow). The estimates of aSBP and CO or SV have been successfully validated against reference data from existing commercial central blood pressure monitors, e.g. Mobil-O-Graph and SphygmoCor, and both an ultrasound and PC-MRI protocol (CO or SV), respectively. Further clinical validation against gold standards measurements remains to be performed in order to verify that the proposed technique may be employed for non-invasive aSBP and CO monitoring in the real clinical setting. In addition, an interesting extension to our study would be the additional implementation of the method for assessing the inter-patient variability of CO in critically ill and hemodynamically unstable patients. This would also require the incorporation of a closed-loop model of the cardiovascular system. Finally, future work could investigate the age- and gender-related variation of the aortic flow wave morphology. Further personalization of the generic aortic flow waveform could potentially improve the performance and clinical relevance of the method.

In this thesis, the initial goal was to provide evidence on the utility of machine learning in as-

## Chapter 10. Conclusions

---

sessing vascular ageing. Due to the inherent limitations in collecting large datasets of invasive gold-standard data, some of the proposed machine learning methodologies were evaluated *in silico*. Following validation on *in vivo* data, the proposed computational tools may provide valuable alternative techniques for the non-invasive prediction of aortic hemodynamics and LV  $E_{es}$  using easily obtained clinical measurements. In addition, *in vivo* validation of the artificial intelligence-based estimation method for  $E_{es}$  (presented in Chapter 5) will be followed by the development of a prototype device for implementing the acquisition of the systolic time intervals, namely a smart stethoscope.

Similarly, a regression pipeline was introduced for predicting  $Z_{ao}$  and  $C_T$  from commonly acquired surrogates of arterial stiffness (i.e. regional PWV measurements). Although the *in silico* validation allows for comparing the estimated data to the actual values of  $Z_{ao}$  and  $C_T$ , the proposed concept should be validated using clinical data over a wide range of age groups and across different populations.

The waveform-based estimator (Chapter 8) has been proven capable of providing accurate estimates of  $C_T$  in a large human cohort ( $n = 2,256$ ). A main limitation of this study is that the study population included individuals free of cardiovascular disease or pathology. In future work, we aim to validate the methodology against patients with cardiovascular disease. It is well established that healthy aging and cardiovascular diseases, such as hypertension and heart failure, are associated with increased arterial stiffness [39]. Hence, it is critically important that our method is capable of differentiating between healthy and diseased patient groups. As a next step, we envision to evaluate the robustness of the method for classifying high-risk populations and finally verify its clinical significance in terms of risk stratification.

Finally, the influence of HR on PWV is especially relevant to people with pathologies or diseases. For instance, people with diabetes are confronted with accelerated vascular ageing. More specifically, there is a unique diabetic complication interfering with neural control of the cardiovascular system that is cardiac autonomic neuropathy (CAN). Cardinal feature of CAN is decreased HR variability at the early stages leading ultimately to resting tachycardia. Current absence of the CAN model poses an intrinsic limitation in simulating this condition. Complementary analysis using a model simulating CAN could provide valuable insights into this area of research.

### Closing remarks

In this dissertation, physics-based modelling and machine learning provided pertinent examples of the value of engineering in the non-invasive cardiovascular monitoring. Rapid advancements in m-Health suggest the expansion of health monitoring beyond the clinical environment and, hence, render indispensable the employment of the available engineering apparatus. The human interaction via smartphones and wearable devices is steadily grow-

ing, transforming the healthcare scheme across the world. The greatest leap forward in the estimation of cardiovascular parameters will be made with the advent of future wearable technologies, which may capture and harness multi-modal sensorial data, which in turn will allow for remote screening on an everyday basis. The use of consumer devices to assess vascular health presents several opportunities [148]: these devices can be used away from the clinical setting, and may facilitate assessment in a range of additional situations (e.g. after exercise, whilst asleep, and during potentially stressful daily activities). Importantly, consumer devices can be used remotely, an important consideration in the light of COVID-19. A critical stepping stone for the establishment of the developed methodologies is the proper and inclusive design of clinical trials on large human cohorts, which may permit their standardization and, finally, lead to their adoption in the real world.



# VASILIKI BIKIA

@ vasiliki.bikia@epfl.ch    ☎ +41 78 640 09 80    ✉ Avenue de Sévelin 4B, CH-1007 Lausanne  
in <https://www.linkedin.com/in/vasiliki-bikia-131107102/>

## EDUCATION

---

### Researcher, Ph.D. Candidate

École Polytechnique Fédérale de Lausanne

📅 Sep 2017 – Sep 2021

📍 Switzerland

- Researched novel tools for cardiovascular monitoring and early assessment of disease. Invented cardiac output estimator (error < 7 %, reducing costs by 50 %, PCT/IB2020/057656).
- Developed grant proposals. Holder of Innossuisse grant ("A novel noninvasive device for cardiac output monitoring", 56211.1 IP-LS) and SNF grant ("Hemodynamics of physiological ageing", SNF205321/197234).
- Performed conceptualization, feasibility study, end-to-end project design, model selection and application with Python (Numpy, Pandas, Scikit-learn, Matplotlib), MATLAB.
- Built predictive analytic models (gradient descent, gradient boosting, random forest, support vector machines) for estimating aortic hemodynamics and cardiac contractility. Research published in top-tiered journals.
- Implemented business model/market analyses for grants.
- Mentored students to solve engineering problems, empowering them to become more complete engineers and get inspired by real-world queries.

---

### Diploma in Electrical Engineering & Computer Science (5-year Bachelor & Master joint degree)

Aristotle University of Thessaloniki

📅 Sep 2011 – Jul 2017

📍 Greece

**GPA:** 8.5/10, graduation with highest honors.

**Major:** Telecommunications/Signal Processing

**Core Courses:** Calculus, Algorithms, Statistics, Pattern Recognition, Signal Processing, Telecommunication Systems.

---

### Internship

École Polytechnique Fédérale de Lausanne

📅 Sep 2016 – Jan 2017

📍 Switzerland

**Master Thesis:** "Implantable Bio-sensing Microsystem for Aortic Blood Pressure Monitoring in Small Animals using BluetoothLe Protocol".

- Designed and prototyped (mechanical design and telecommunication system) to detect changes in arterial blood pressure. Developed Android app (Java) for data visualization.
- Programmed data transfer and communication between the embedded sensor and the terminal.

---

### High School Diploma

2<sup>nd</sup> Experimental High School of Thessaloniki

📅 Sep 2005 – Jun 2011

📍 Greece

- Graduation with highest honors (top 1 % of class for all consecutive years).

## EXPERIENCE

---

### Researcher, Ph.D. Candidate

École Polytechnique Fédérale de Lausanne

📅 Sep 2017 – Sep 2021

📍 Switzerland

- Supervised semester and master projects.
- Teaching assistant in the following courses of the EPFL Curriculum:
  - Fluid Mechanics (Bachelor, 4<sup>th</sup> semester).
  - Biomechanics of the cardiovascular system (Master, 2<sup>nd</sup> semester).
- Teaching duties within EPFL doctoral program (349 hours of teaching certified).  
*Doctoral program's required amount: 300 hrs. Hours included preparation, exercise solving, organization of simulation labs and seminars, answering students' questions, holding revision sessions.*

---

### Co-founder & Engineer

Prognosis

📅 Jan 2015 – Sept 2017

📍 Greece

- Designed and prototyped a mobile application for early detection of Parkinson's Disease.
- Pilot tested supportive solutions with patients and clinicians for meeting users' requirements and optimizing customer adoption.
- Analyzed natural speech and typing data, and trained/tested Machine Learning classifiers.
- Attained 1<sup>st</sup> worldwide place in MICROSOFT ImagineCup (300,000+ competitors).
- Designed and implemented business plan and presentations to investors resulted in total cash flow of 27k €.
- Pitched scientific concepts to non-experts and VCs.

## EXTRACURRICULAR ACTIVITIES

---

### Management Committee Member

CA18216 Network for Research in Vascular Ageing

📅 Nov 2019 – Present

📍 European Cooperation

- Leading publications for vascular ageing in order to improve clinical practice and raise awareness for vascular disease.
- Facilitating collaborations and knowledge transfer among research labs and industry via networking sessions, increasing engagement between industry and A\*STAR researchers.

---

### Co-founder & Vice President

IEEE Engineering in Medicine & Biology

📅 Jan 2016 – Apr 2017

📍 Greece

- Founded the 1<sup>st</sup> Greek University branch. Coordinated activities and meetings of a 10-member team.
- Promoted education and knowledge transfer for undergraduate students via seminars and workshops.
- Administered communication with the international community and other chapters.

## SKILLS

---

Machine learning Algorithms Signal processing Statistics Computational modelling  
Medical devices Python MATLAB Scikit-learn Python NumPy TensorFlow  
Pandas PyTorch Project management Public speaking Creative thinking

## LANGUAGES

---

Greek  
English  
French  
Spanish



## HONORS

---

- 1 Keynote talk for #MakeWhatsNext, "Woman in S.T.E.M.", MICROSOFT Europe, 2016.
- 2 Keynote talk for Girls in Tech, "From Engineering to Entrepreneurship", MICROSOFT, 2016.
- 3 Aristotle University of Thessaloniki Excellency Award, 2016.
- 4 National Bank of Greece, Seeds Innovation and Technology Competition, 4<sup>th</sup> place, 2016.
- 5 MICROSOFT ImagineCup (300,000+ competitors), Ability Award, 1<sup>st</sup> place, 2015.
- 6 MICROSOFT ImagineCup (300,000+ competitors), World Citizenship, 3<sup>rd</sup> place, 2015.
- 7 National Hellenic Math Competition Finalist, 2010.

## List of publications

1. **V. Bikia**, S. Pagoulatou, B. Trachet, D. Soulis, A. D. Protogerou, T. G. Papaioannou, and N. Stergiopoulos, "Non-invasive cardiac output and central systolic pressure from cuff-pressure and pulse wave velocity," *IEEE Journal of Biomedical and Health Informatics*, vol. 24, no. 7, pp. 1968–1981, Jul. 2020, doi: 10.1109/JBHI.2019.2956604.
2. **V. Bikia**, T. G. Papaioannou, S. Pagoulatou, G. Rovas, E. Oikonomou, G. Siasos, D. Tousoulis, and N. Stergiopoulos, "Non-invasive estimation of aortic hemodynamics and cardiac contractility using machine learning," *Scientific Reports*, vol. 10, no. 1, p. 15015, Dec. 2020, doi: 10.1038/s41598-020-72147-8.
3. **V. Bikia**, N. Stergiopoulos, G. Rovas, S. Pagoulatou, and T. G. Papaioannou, "The impact of heart rate on pulse wave velocity: an in silico evaluation," *Journal of Hypertension*, vol. 38, no. 12, pp. 2451–2458, Dec. 2020, doi: 10.1097/HJH.0000000000002583.
4. **V. Bikia**, D. Adamopoulos, S. Pagoulatou, G. Rovas, and N. Stergiopoulos, "AI-based estimation of end-systolic elastance from arm-pressure and systolic time intervals," *Frontiers in Artificial Intelligence*, vol. 4, p. 16, 2021, doi: 10.3389/frai.2021.579541.
5. **V. Bikia**, G. Rovas, S. Pagoulatou, and N. Stergiopoulos, "Determination of aortic characteristic impedance and total arterial compliance from regional pulse wave velocities using machine learning: an in silico study," *Frontiers in Bioengineering and Biotechnology*, vol. 9, p. 649866, May 2021, doi: 10.3389/fbioe.2021.649866.
6. **V. Bikia**, P. Segers, G. Rovas, S. Pagoulatou, and N. Stergiopoulos, "On the assessment of arterial compliance from carotid pressure waveform," *American Journal of Physiology - Heart and Circulatory Physiology*, vol. 321, no. 2, pp. H424–H434, Aug. 2021, doi: 10.1152/ajpheart.00241.2021.
7. **V. Bikia**, C. McEniery, E.M. Roussel, G. Rovas, S. Pagoulatou, I. Wilkinson, and N. Stergiopoulos, "Validation of a non-invasive inverse problem-solving method for stroke volume: do physics-based models add to the traditional statistical approaches?" (Under review)
8. **V. Bikia**, M. Lazaroska, D. Scherrer, M. Zhao, G. Rovas, S. Pagoulatou, and N. Stergiopoulos, "Estimation of left ventricular end-systolic elastance from peripheral pressure waveform

## List of publications

---

- via deep learning", *Frontiers in Bioengineering and Biotechnology*, Accepted 2021, doi: 10.3389/fbioe.2021.754003.
9. **V. Bikia**, T. Fong, R. E. Climie, R. M. Bruno, B. Hametner, C. Mayer, D. Terentes-Printzios, P. H. Charlton, "Leveraging the potential of machine learning for assessing vascular ageing: state-of-the-art and future research", *European Heart Journal - Digital Health*, Accepted 2021.
  10. H. Obeid, **V. Bikia**, C. Fortier, M. Pare , P. Segers, N. Stergiopoulos, M. Agharazii, "Assessment of large and small arteries stiffness in end-stage renal disease patients: a numerical study" (Under review)
  11. S. Pagoulatou, **V. Bikia**, B. Trachet, T. G. Papaioannou, A. D. Protogerou, and N. Stergiopoulos, "On the importance of the nonuniform aortic stiffening in the hemodynamics of physiological aging," *American Journal of Physiology - Heart and Circulatory Physiology*, vol. 317, no. 5, pp. H1125–H1133, Nov. 2019, doi: 10.1152/ajpheart.00193.2019.
  12. S. Pagoulatou, M. Ferraro, B. Trachet, **V. Bikia**, G. Rovas, L. A. Crowe, J.P. Vallée, D. Adamopoulos, and N. Stergiopoulos, "The effect of the elongation of the proximal aorta on the estimation of the aortic wall distensibility," *Biomechanics and Modeling in Mechanobiology*, vol. 20, no. 1, pp. 107–119, Feb. 2021, doi: 10.1007/s10237-020-01371-y.
  13. K. Kadry, S. Pagoulatou, Q. Mercier, G. Rovas, **V. Bikia**, H. Müller, D. Adamopoulos, and N. Stergiopoulos, "Biomechanics of diastolic dysfunction: a one-dimensional computational modeling approach," *American Journal of Physiology-Heart and Circulatory Physiology*, vol. 319, no. 4, pp. H882–H892, Oct. 2020, doi: 10.1152/ajpheart.00172.2020.
  14. S. Pagoulatou, K.P. Rommel, K.P. Kresoja, M. von Roeder, P. Lurz, H. Thiele, **V. Bikia**, G. Rovas, D. Adamopoulos, and N. Stergiopoulos, "In vivo application and validation of a novel non-invasive method to estimate the end-systolic elastance," *American Journal of Physiology - Heart and Circulatory Physiology*, vol. 320, no. 4, pp. H1554–H1564, Apr. 2021, doi: 10.1152/ajpheart.00703.2020.
  15. S. Pagoulatou, N. Stergiopoulos, **V. Bikia**, G. Rovas, M.J. Licker, H. Müller, S. Noble, and D. Adamopoulos, "Acute effects of transcatheter aortic valve replacement on the ventricular-aortic interaction," *American Journal of Physiology - Heart and Circulatory Physiology*, vol. 319, no. 6, pp. H1451–H1458, Dec. 2020, doi: 10.1152/ajpheart.00451.2020.
  16. S. Pagoulatou, D. Adamopoulos, G. Rovas, **V. Bikia**, and N. Stergiopoulos, "Acute and long-term effects of aortic compliance decrease on central hemodynamics: a modeling analysis," *Frontiers in Physiology*, vol. 12, p. 701154, Jul. 2021, doi: 10.3389/fphys.2021.701154.

17. S. Pagoulatou, D. Adamopoulos, G. Rovas, **V. Bikia**, and N. Stergiopoulos, "The effect of left ventricular contractility on arterial hemodynamics: a model-based investigation," *PLoS ONE*, vol. 16, no. 8, p. e0255561, Aug. 2021, doi: 10.1371/journal.pone.0255561.
18. S. Pagoulatou, D. Adamopoulos, Y. Niu, N. Stergiopoulos, **V. Bikia**, G. Rovas, J.P. Vallée, and L. Crowe, "Assessing regional aortic pulse wave velocity with compressed-sensing accelerated 4D MRI: a clinical comparison with 2D MRI" (Under review)
19. S. Pagoulatou, D. Adamopoulos, N. Stergiopoulos, **V. Bikia**, G. Rovas, "The role of arterial wave reflection in the evaluation of aortic stenosis" (Under review)

## List of publications

---